



**GEOLOGICAL SURVEY OF CANADA
OPEN FILE 7109**

Logs of piston cores, deep-water Labrador margin

**F. Saint-Ange, D.J.W. Piper, K. Mackillop, K.A. Jarrett, J. Higgins,
S. Ledger-Piercey**

2013



Natural Resources
Canada

Ressources naturelles
Canada

Canada



**GEOLOGICAL SURVEY OF CANADA
OPEN FILE 7109**

Logs of piston cores, deep-water Labrador margin

**F. Saint-Ange, D.J.W. Piper, K. Mackillop, K.A. Jarrett, J. Higgins,
S. Ledger**

Geological Survey of Canada (Atlantic), Bedford Institute of Oceanography, Dartmouth, NS, Canada
B2Y 4A2

2013

©Her Majesty the Queen in Right of Canada 2013

doi:10.4095/292579

This publication is available for free download through GEOSCAN (<http://geoscan.ess.nrcan.gc.ca/>).

Recommended citation

Saint-Ange, F., Piper, D.J.W., Mackillop, K., Jarrett, K.A., Higgins, J., and Ledger, S., 2013. Logs of piston cores, deep-water Labrador margin: Geological Survey of Canada, Open File 7109, 193 p.
doi:10.4095/292579

Publications in this series have not been edited; they are released as submitted by the author.

PREFACE

This Open File Report presents cores and related ultra-high resolution seismic-reflection profiles from the Labrador Margin, offshore northeastern Canada. These data support geohazard interpretations by the Geological Survey of Canada within this area of active petroleum exploration. The Labrador Margin is also an important area for understanding ice-margin sedimentation in deep water and the relationship between ice margins and ocean circulation.

Acknowledgements: Data were collected by our colleagues David Mosher and Calvin Campbell. We are grateful to the ship's personnel and GSC staff who assisted in data acquisition. Core processing was managed by Kate Jarrett and Jenna Higgins and assisted by numerous Co-op students. Advanced geotechnical testing was carried out by Kevin Mackillop, assisted by Co-op students. This work was funded by the Geological Survey of Canada and the Program for Energy R & D. We are grateful to Gordon Cameron who internally reviewed the report.

Table of contents

Introduction	6
1. Data set	7
2. Geological framework	11
3. Lithostratigraphy and sedimentary facies	12
3.1 Stratigraphy	12
3.2 Sediment facies	14
4. Geohazards	19
4.1 Recent failures and characteristics	19
4.2 Advanced geotechnical analysis	23
4.2.1 Consolidation testing	23
4.2.2 Triaxial Testing	24
4.2.3 Slope Stability	25
4.2.4 Stress history	28
Bibliography	31
Appendix	34

Introduction

In spite of gas discoveries on the central Labrador Shelf in the 1970s, difficulties in bringing product to market meant that offshore exploration was quickly dropped and as a consequence, the Labrador Margin is poorly documented compared to many other hydrocarbon bearing basins. But the abrupt increase in oil prices from 2004 to 2008 renewed interest in exploration on northern latitude continental margins. This renewed interest has allowed the Geological Survey of Canada to conduct a regional survey to improve understanding of geohazards and related sedimentary processes, with a particular focus on late Quaternary deposits. This focus is justified by the fact that a significant number of Holocene and latest Pleistocene landslides have been documented in other areas of the Canadian margin (Campbell, 2005; Tripsanas et al., 2008), and that the nature and stability of surficial sediments can represent a significant threat or constraint during offshore exploratory drilling and subsequent seafloor installations.

Three expeditions were conducted from 2005 to 2008 on board the Canadian research ship CCGS *Hudson* (expeditions 2005033B, 2006040 and 2008027). The objectives of the cruises were principally focused on conducting regional assessment of Quaternary geology and geohazards on the deep water Labrador margin. Objectives were met by acquiring regional high- (air gun) and ultra-high- (Huntec) resolution seismic reflection data, sediment cores and camera stations. Additional multibeam bathymetry has been collected by John Hughes-Clarke (University of New Brunswick) on CCGS *Amundsen*.

Expedition 2005033B carried out work in Orphan Basin and on the southern part of the Labrador Margin, and has produced several open file reports and publications (Campbell, 2005; Goss, 2006; Mosher et al., 2008; Tripsanas et al., 2007). Expeditions 2006040 and 2008027 were focused on the central and northern Labrador Margin. Preliminary interpretations of deeper geohazards and constraints to exploratory drilling have been published by Deptuck et al. (2007).

This report presents a compilation of all cores collected during expeditions 2006040 and 2008027, and summarizes preliminary interpretation of the shallow sediment cover derived from piston core analysis, multibeam and Huntec data. We start with a short presentation of the available data set, including newly acquired radiocarbon dates. This is

followed by a summary of the geological framework of the margin, followed by a synthesis of the main sediment facies observed and their significance in term of glacial environments. Finally, a preliminary geotechnical and geohazard assessment is presented. The Appendix consists of a section on the procedure used for acquisition and laboratory analysis of cores followed by all the data related to the cores.

1. Data set

Cruise 2006040 acquired 2542 line-km of seismic reflection data, 415 line-km of sidescan sonar, 31 piston cores, 15 camera stations and 14 grab samples (Figure 1A). Cruise 2008027 acquired 1135 line-km of seismic reflection data, 12 piston cores, 1 short gravity core and 4 camera stations (Figure 1B).

At the time of this report, a total of 26 C-14 dates are available (Table 1). The dates were obtained on *N. pachyderma* (*s*) for deep water cores and benthic foraminifers and mollusc shells from cores from the shelf. A total of 19 samples were sent to Keck Carbon Cycle AMS Facility at the University of California Irvine, and seven dates were sent to the former IsoTrace Radiocarbon Laboratory at the University of Toronto; in both labs, ages were determined using accelerator mass spectrometry (AMS). The ages were then calibrated using Calib 6.0 (<http://calib.qub.ac.uk/calib/>) by using a reservoir correction of 144 ± 38 yrs, based on 26 measurements from McNeely et al. (2006). For the Holocene interval, an additional reservoir correction has to be done in order to take in account the impact of seasonal sea ice cover on the shelf (Lewis et al., 2012). Stratigraphic correlations are made with two reference cores (97048 0016 and MD99-2233) located on the northern part of the Labrador margin. These two cores have been intensively studied (Rashid et al., 2003c; Rashid and Piper, 2007; Thomas et al., 2003) and no less than 17 C-14 dates are available from these cores.

Information on core			Information on dated sample				Laboratory number			Conventional radiocarbon age		Calibrated radiocarbon age
Expedition number	Station number	Core type	water depth (m)	depth (cm)	Material dated	Species where known	Laboratory code	Lab No	age (radiocarbon years BP)	standard deviation	age (calibrated years BP)	$\pm 2 \sigma$
2006040	36	PC	358	50.5	F	<i>N labradorica</i>	UCIAMS	68903	9100	20	4560	47
2006040	36	PC	358	154	F	<i>Islandiella</i> spp.	UCIAMS	58043	9300	25	4662.5	67
2006040	36	PC	358	405	Shell	<i>Yoldia</i>	UCIAMS	45389	10350	20	5185	87.5
2006040	36	PC	358	425	Shell	<i>Yoldia</i>	UCIAMS	45369	10490	25	5257.5	32.75
2006040	36	PC	358	441	Shell	bivalve	UCIAMS	45370	10475	20	5247.5	33.5
2006040	36	PC	358	494	Shell	<i>Nuculana</i>	UCIAMS	45371	10925	25	5475	107.5
2006040	36	PC	358	848	Shell	bivalve frags.	UCIAMS	58049	32260	200	16230	318.5
2006040	40	PC	203	26.5	F	benthic forams	UCIAMS	45219	1390	15	794	71
2006040	40	PC	203	28	F	benthic forams	UCIAMS	45218	1350	20	763	68
2006040	40	PC	203	108	Shell	bivalve frags.	TO	13470	5010	60	5142	64
2006040	40	PC	203	252	Shell	bivalves	TO	13408	6380	70	6682	275.5
2006040	40	PC	203	455	Shell	gastropod	TO	13409	7550	70	7686	224
2006040	40	PC	203	630	Shell	bivalve frags.	TO	13471	7620	70	7751	230.5
2006040	40	PC	203	869	Shell	bivalve frags.	TO	13410	8310	60	8440	287
2006040	40	PC	203	959.5	F	benthic forams	UCIAMS	54039	8800	20	9098	291.5
2006040	45	PC	1589	380.5	F	<i>N. Pachyderma</i> s	TO	13447	12580	90	13863	219
2006040	45	PC	189	580.5	F	<i>N. Pachyderma</i> s	TO	13448	20350	140	23649	467.5
2006040	46	PC	1214	279	F	<i>N. Pachyderma</i> s	UCIAMS	89053	20870	80	24241	295
2006040	46	PC	1214	327	F	<i>N. Pachyderma</i> s	UCIAMS	74201	26310	140	30704	636
2006040	47	PC	2049	72	F	<i>N. Pachyderma</i> s	UCIAMS	74197	12015	25	13419	77
2006040	47	PC	2049	235	F	<i>N. Pachyderma</i> s	UCIAMS	74198	17555	45	20348	138
2006040	55	PC	1443	534.5	F	<i>N. Pachyderma</i> s	UCIAMS	68908	23990	90	28196	328
2006040	56	PC	1020	740.5	F	<i>N. Pachyderma</i> s	UCIAMS	68909	11710	40	13033	190.5
2006040	57	PC	1539	246.5	F	<i>N. Pachyderma</i> s	UCIAMS	68910	9395	20	10089	135.5
2008027	21	PC	1223	63	F	<i>N. Pachyderma</i> s	UCIAMS	74199	8485	20	9099	205
2008027	21	PC	1223	221	F	<i>N. Pachyderma</i> s	UCIAMS	74200	21175	30	24762	521

Table1: C14 dates available on cores recently collected (at the time of the report).

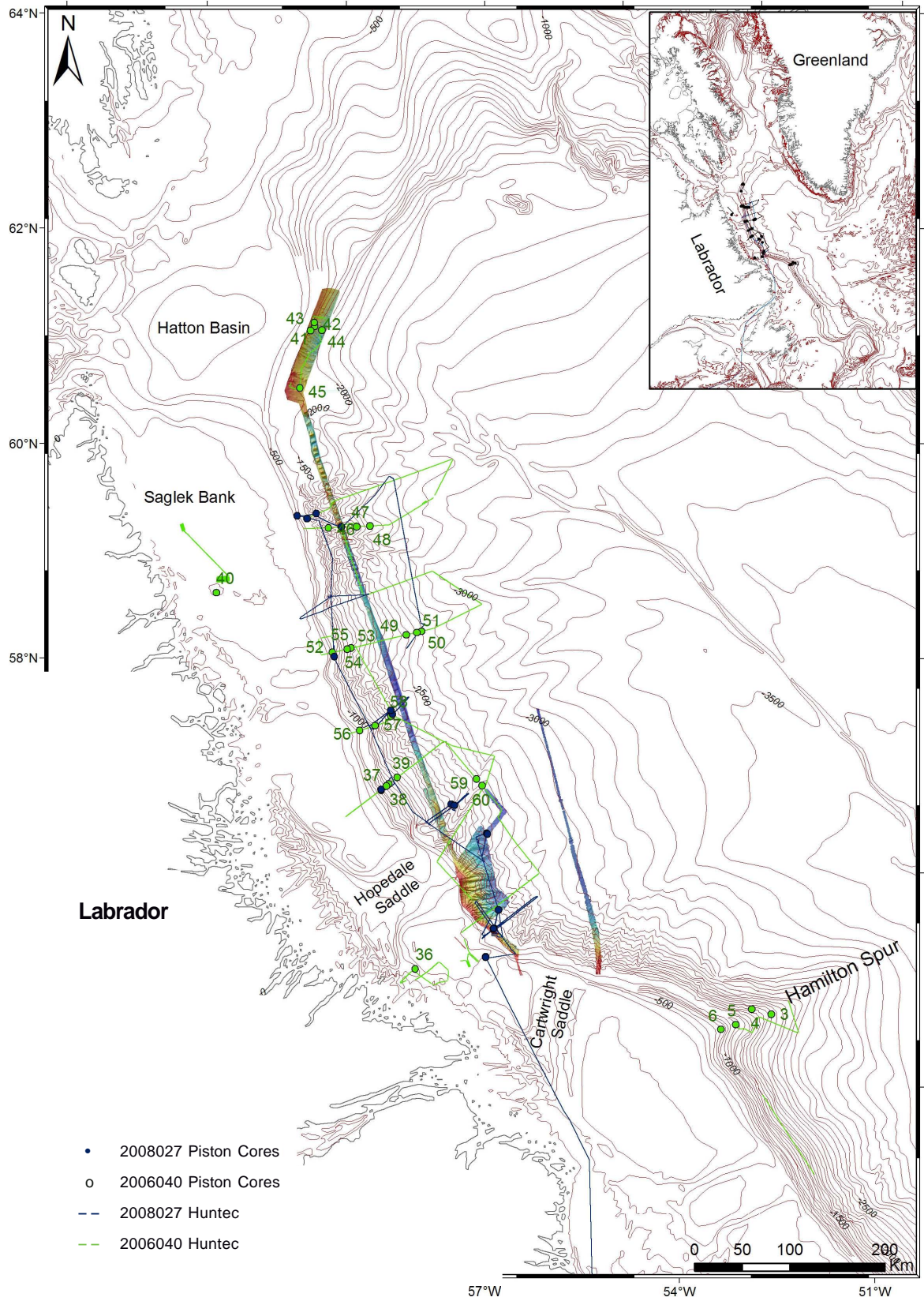


Figure 1A: Geographic location of the data collected during expeditions 2006040 and 2008027. Only cores from 2006040 are labelled.

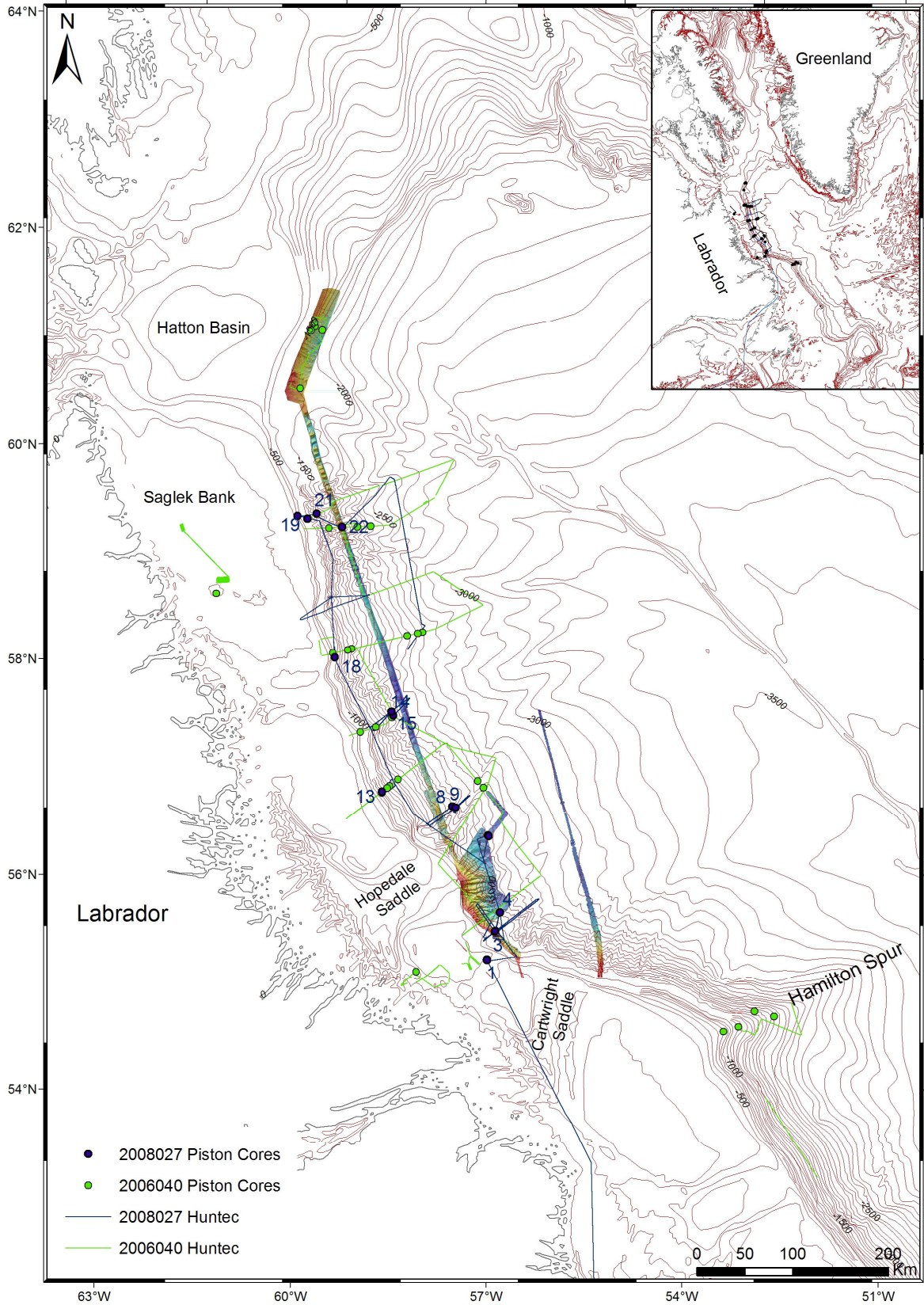


Figure 1B: Geographic location of the data collected during expeditions 2006040 and 2008027. Only cores from 2008027 are labelled.

2. Geological framework

The Labrador Margin is a rifted margin created during the opening of the Labrador Sea in the Cretaceous (Dickie et al., 2011; Roest and Srivastava, 1989). During the Quaternary, the entire continental shelf was glaciated several times (Josenhans et al., 1986; Piper, 2005). This resulted in the formation of transverse troughs, marginal troughs, till banks and Quaternary glacially dominated sedimentation (Figure 2, left panel). The different troughs result directly from the presence of ice streams during glaciated periods and their morphology is a good indication of the size of the different ice streams. Ice streams represent the main erosion/transport process during the Quaternary, and as a consequence, large ice streams are correlated with wide outlets and significant sediment input to the slopes (Figure 2).

The Quaternary geology of the Labrador Shelf was widely studied during the 1980s (Josenhans et al., 1986, 1989; Hall et al., 1999). The regional distribution of glacial and postglacial sediments was mapped to the continental shelf edge at about 600 m water depth. On the shelf, the sediment cover consists essentially of a succession of tills overlain by a deglacial sequence of glaciomarine silts and postglacial muds. Till deposits are observed from north to south along the Labrador Margin down to 600 m of water depth on average, but the maximum accumulation occurs at the mouth of transverse troughs where the shelf edge has prograded (Deptuck et al., 2007). There, tills eventually evolve into glacial debris flows forming wide bulged glacial fans by stacking downslope (Benetti, 2006; Rashid and Piper, 2007). Trough mouth fans (TMFs) built of glacial debris flow deposits are not necessarily preserved or observed off troughs (Piper et al., 2012). TMFs tend to be preserved on slopes with low gradients ($<4^\circ$ for the upper 1 km) (Piper et al., 2012).

Huntec seismic profiles and detailed multibeam data along the slopes of Labrador Margin show a high density of valleys and gullies. Overall, the degree of dissection decreases southward, with wide, flat-bottomed valleys off Saglek Bank to narrow gullies off Cartwright Bank. The degree of dissection off troughs is more variable and depends on the local dynamics of ice streams. Valleys and gullies merge around 3000 m water depth to form single wide channels that eventually connect to the NAMOC. Development of such a

network is mostly controlled by large-scale meltwater discharges that cyclically occurred during the past glacial cycles (Piper et al., 2007, 2012). Published data on regional sedimentation shows that during the Pleistocene, the sediment cover on the main slopes consists principally of graded sediments related to proglacial plume fall-out (Hesse et al., 1997). Coarse grained sediments other than ice rafted detritus (IRD) essentially by-pass the upper and mid slopes and are transported downslope to the continental rise (Hesse et al., 2001).

Preliminary assessment on geohazards along the Labrador Margin (Deptuck et al., 2007) has shown that mass failures were widespread during the Plio-Pleistocene, with some areas showing higher failure recurrence than others. This is the case for Hopedale – Makkovik area (Figure 2), where a large scale complex failure has been identified (Deptuck et al., 2007). This failure complex comprises at least four separate failures showing blocks up to 6 km across, with some elevated by 350 m above the seafloor.

3. Lithostratigraphy and sedimentary facies

3.1 Stratigraphy

Late Quaternary stratigraphy and sediment provenance along the Labrador Margin and in the Labrador Basin were actively studied during the 1990s and early 2000s, following the identification of Hudson Strait as the main source for Heinrich events in North Atlantic (Heinrich, 1988; Andrews and MacLean, 2003; Hesse et al., 1999; Hemming, 2004). Heinrich Events *sensu stricto* are identified by a sudden increase in the coarse lithic fraction rich in detrital carbonate grains from the LIS, a dominance of the polar planktonic foraminifer *N. pachyderma* (s), and a lowering of inferred sea-surface salinity (Heinrich, 1988; Bond et al., 1992). In this report, we tie our stratigraphy to cores 97048-016pc and MD99-2233 (Figure 3), for both of which an age model is well established to MIS 4 (Rashid et al., 2003b; Rashid and Piper, 2007). These two piston cores consist mostly of 1 to 4 m thick beds with high detrital carbonate interbedded with thin bioturbated intervals of mud with IRD (Figure 3). The detrital carbonate beds are correlated with the standard sequence of Heinrich events in the Labrador Sea with the support of radiocarbon dates back to 45 cal. ka (Rashid et al., 2003b; Rashid and Piper, 2007).

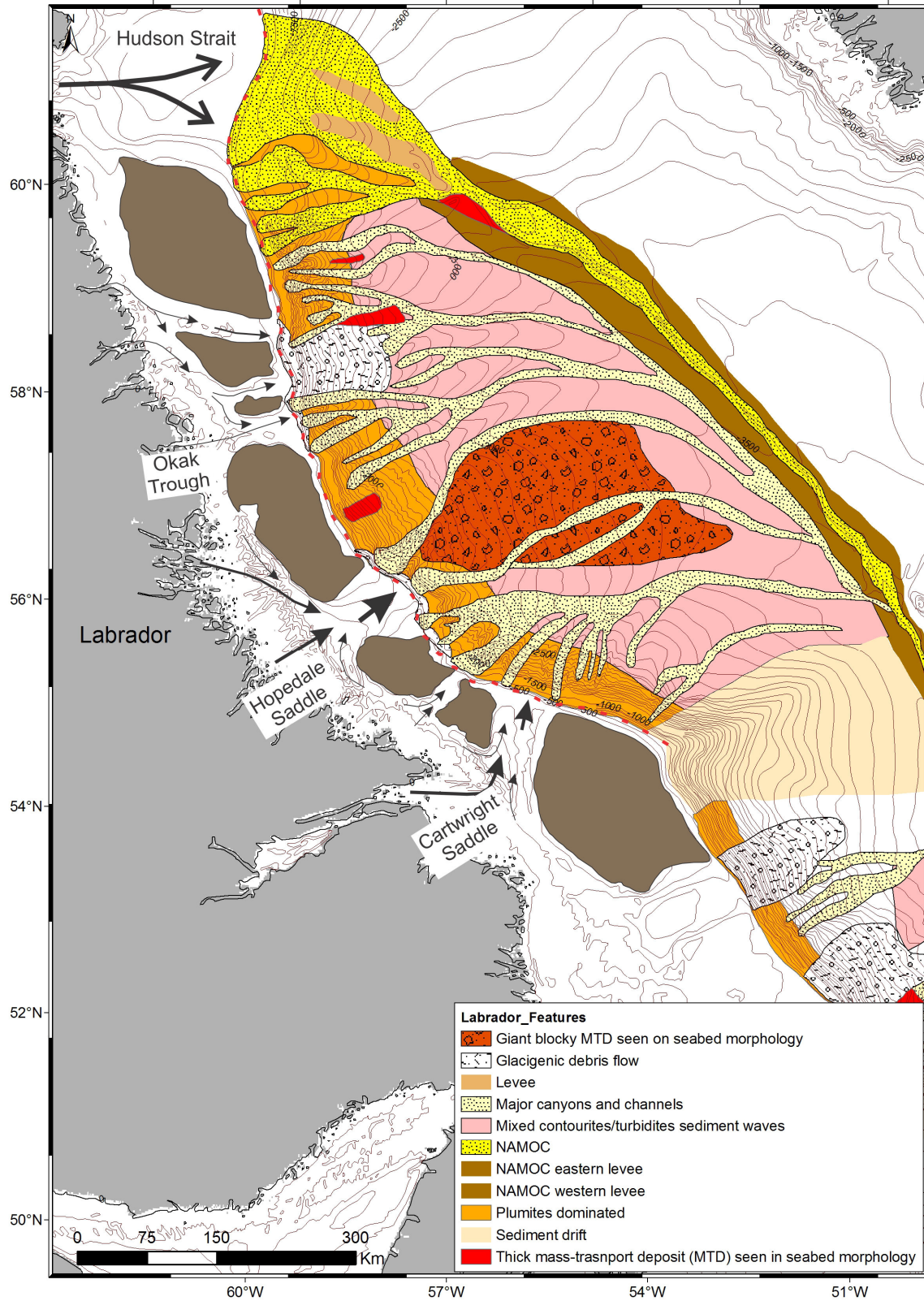


Figure 2: Simplified map showing the main sedimentary features along the Labrador Margin. Arrows indicate the location of paleo-ice streams; Till banks on the shelf are shown in brown. Modified from Hesse and Khodabakhsh (2006).

3.2 Sediment facies

Facies distribution and changes are related to processes in sedimentation occurring in a given environment. On glacial margins, sedimentation processes are directly controlled by the dynamic of glaciers and ice streams, e.g. in the case of the Labrador Margin by the Laurentide Ice Sheet (LIS) (Andrews and Tedesco, 1992; Hesse and Khodabakhsh, 2006; Shaw et al., 2006; Rashid and Piper, 2007). Thus, for each observed facies, a sediment transport pathway, a sedimentary process and an environment of deposition can be inferred (Figure 4).

The proposed facies classification is based only on texture, structure and apparent grain size, as seen in split core face and X-radiographs of half cores. Sediment colour is not used because the colour is not related to a sediment transport-deposition process, but rather related to a source or to in situ diagenesis. Colour is used with core description for detailed work in which variations in source may be important.

Nine major facies have been identified in cores from the Labrador Margin (Figure 4):

- Homogeneous mud with IRD
- Homogeneous mud
- Varve-like facies
- Turbidites
- Turbidites with IRD
- Massive gravelly mud bed
- Debris flow deposits
- Diamicton
- Complex diamicton

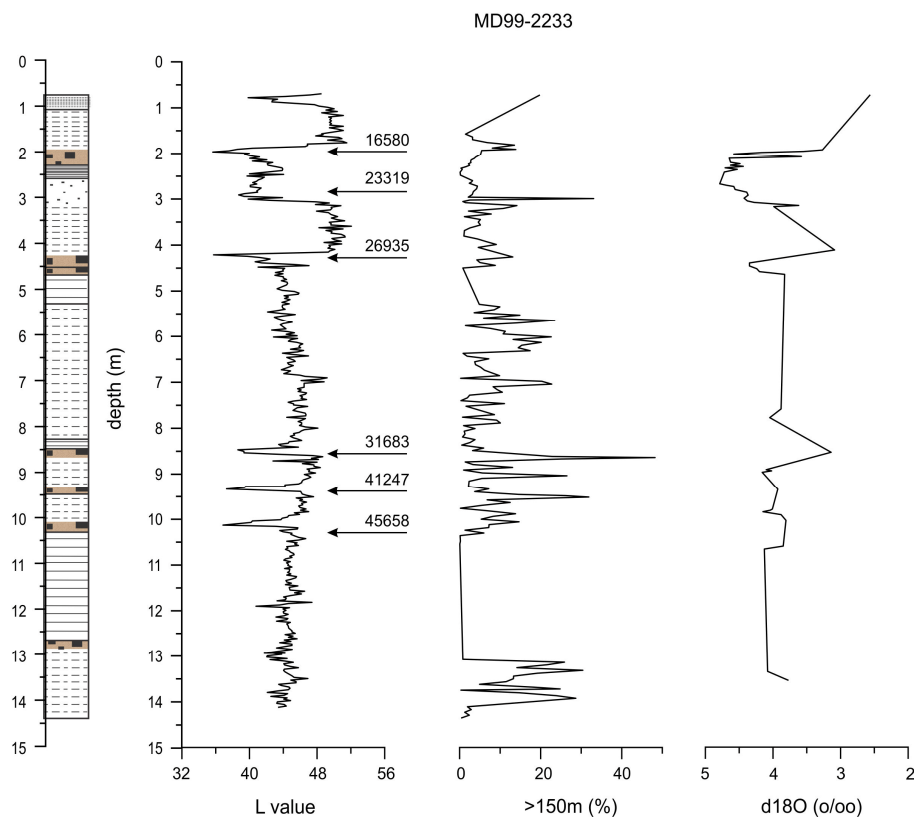
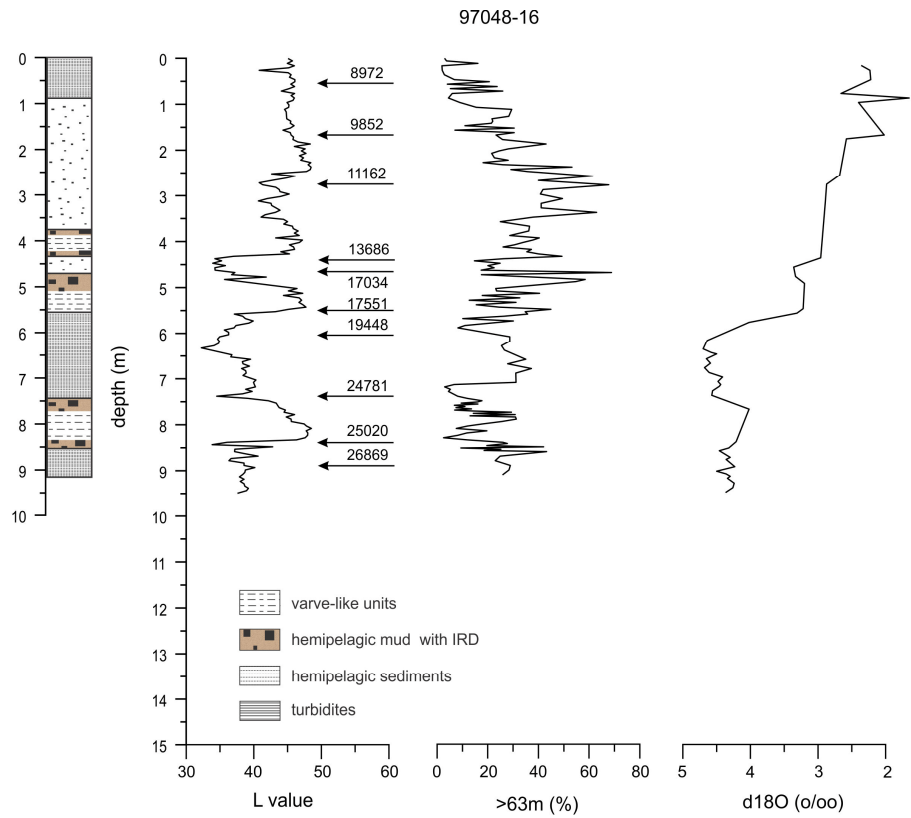


Figure 3: Cores used for stratigraphic reference (See Rashid et al., 2003 a,b, for more details)

Homogeneous mud with IRD usually corresponds to hemipelagic sediments (biogenic oozes and terrigenous clays-silts) mixed with ice rafted detritus (IRD). This facies is common in all cores from the shelf to deep water and represent slow deposition processes. These units do not show any sedimentary structures and IRD ranges from coarse sands to pebbles and locally cobbles.

Homogeneous mud usually corresponds to thick units of fine grained sediments without any sedimentary structures. Few scattered small IRD can be found locally, but are not characteristic of the facies. This type of facies is most likely to be observed on the shelf and upper slopes and corresponds to plumite deposits related to meltwater events (Piper et al., 1994; Lewis et al., 2012;) which implies high sedimentation rates. These facies are mostly observed during the Holocene in the northern part of the Labrador Margin, and post LGM south of Cartwright Saddle.

Turbidites and turbidites with IRD are a rhythmic succession of laminated to cross laminated sediments. The grain size ranges from mud turbidites to sand turbidites. Turbidites along the Labrador margin are mostly related to meltwater events generating hyperpycnal flows with occasional landslides. Presence of IRD is not common but observed in some units suggesting the presence of drifting icebergs during the depositional event.

Massive gravelly mud beds consist of gravels, coarse sands and mud. These facies are commonly found within channel floors. This type of deposit may be related to debris flows or to the basal part of turbidites.

Debris flow deposits are observed all along the margin. They are identified by their folded sedimentary structures with poorly preserved internal structures. In most cases they are associated with slopes instabilities.

Diamicton (or diamict) is defined as non-sorted to poorly sorted matrix-supported sediment showing a till-like appearance (Flint et al., 1960a, b). Diamicton is a major facies off troughs and in trough mouth fans, and is usually referred to as glacial debris flow deposits but differs in its characteristic from “classic” debris flow deposits (Figures 4 and 7).

Complex diamicton is weakly to moderately stratified diamict in which distinct fine grained sediment laminae are observed. This facies is common along the slopes of the Labrador margin and indicates proximal glaciers or a high concentration of icebergs.

The varve-like facies is composed of couplets that in X-radiographs comprise light (fine grained) and dark (coarse grained) laminated sediment. Typical varves are defined as a seasonal or annual variation in deposition responsible for contrasting layers within one year (De Geer, 1940) and are known from both lacustrine and marine environments (Edwards, 1986; Miller, 1996; Talbot and Allen, 1996). The “varve-like” facies was previously described as nepheloid layers by Hesse and Khodabakhsh (1998) to differentiate the fine component from mud turbidites. Although we do not question the general process defined by Hesse and Khodabakhsh, we considered the nomenclature inadequate as it introduces confusion with the common definition of nepheloid layers. A nepheloid layer is defined as a plume or cloud of suspended particulate matter observed on the bottom of the ocean (bottom nepheloid layer) or in the intermediate water column (intermediate nepheloid layer) (Biscaye and Eitrem, 1977; Ewing and Thorndike, 1965; Pak et al., 1980). Nepheloid layers are not restricted to glacial environments and thus are not necessarily related to glacial processes like meltwater plumes. The fine component (i.e. clay and silt) of this facies cannot be considered separately from the coarse component (sand/IRD), as they are organized as couplets and not in a simple rhythmic succession like turbidites. The presence of IRD rich layers is characteristic of iceberg calving, whereas fine grained deposits are linked to injection of meltwater. The distinct but gradual separation between the two layers (and the related processes) is similar to what has been described for a typical glacial varve.

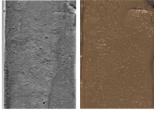

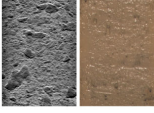
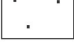
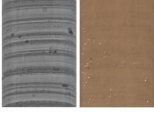
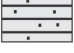
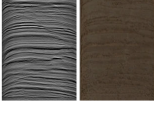
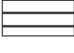
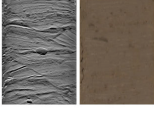
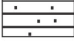
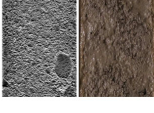
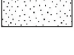
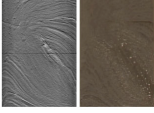

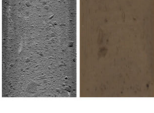

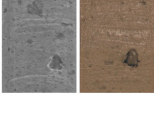
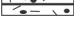
Xray Photo	Facies	Symbol	Sedimentary structures	Environment and processes
	Homogeneous mud		No sedimentary structures. Sometimes bioturbated. In some cases, few scattered IRD can be found.	More likely to be found on the shelf or shelf edge. Deposits related to meltwater event. Usually plumites.
	Homogeneous mud with IRD		No sedimentary structures. May be bioturbated. IRD are observed (few to high amount).	Often mix of clay and biogenic oozes with Ice Rafted Debris. Open water condition. Sedimentation rates for these intervals are usually low.
	Varves type		Laminated structures. Complex and cyclic interstratification of mud layers, IRD layers and sandy layers.	Glacial facies related to seasonal subglacial meltwater discharge. Mix of sediment gravity flows, underflows, suspension settling, overflow plume.
	Turbidites		Laminated to cross bedded structures. Well sorted sediment. Grain size from clays to sands.	Sediment gravity flows, essentially hyperpycnal flows related to meltwater events. In some cases can be related to submarine instabilities.
	Turbidites with IRD		Same as classic turbidites, but scattered IRD are observed.	Sediment gravity flows, essentially hyperpycnal flows related to meltwater events. IRD are related to rapid drifting/melting of iceberg.
	Massive gravelly rich mud layer		Grain supported matrix. Tractional structures composed of gravels to coarse sands mixed with mud. Can be graded.	Sediment gravity flows. Non to semi-cohesive debris flow or basal part of coarse grain turbidity currents. Characteristic of canyon and channel floors.
	Debris Flow		Folded sedimentary structures, with poorly preserved internal structures.	Sediment gravity flows. Cohesive debris flow mostly observed on trough mouth fan, but can be observed anywhere on the Labrador slopes.
	Diamicton		Coarse grain sediments (can be larger than 2 mm) set in a matrix of fine grains. Sediment poorly sorted.	Glacial facies characteristic of trough mouth fan area. Related to proximal Glaciers or Ice Streams. Interpreted as Glaciogenic debris flows.
	Complex Diamicton		Similar to Diamicton structures, but weakly to moderately stratified.	Glacial facies related to proximal Glaciers or Ice Streams. Subglacial meltwater related to late glacial/early deglacial condition. Rapid deposition of mud and drop stones from iceberg drifting/melting.

Figure 4: Summary table of main sedimentary facies observed in cores along the Labrador Margin.

4. Geohazards

4.1. Recent failures and characteristics

Geohazards include a wide range of geological processes from iceberg scours to deepwater slope failures. Here we focus only on what is observable in the cores, which is the distribution and timing of small mass transport deposits (MTD) (Figures 5 to 7).

Few failures have been recognized in preliminary examination of cores. The most recent regional failure occurred off Saglek Bank within the past few thousand years (Figure 5 and 6).

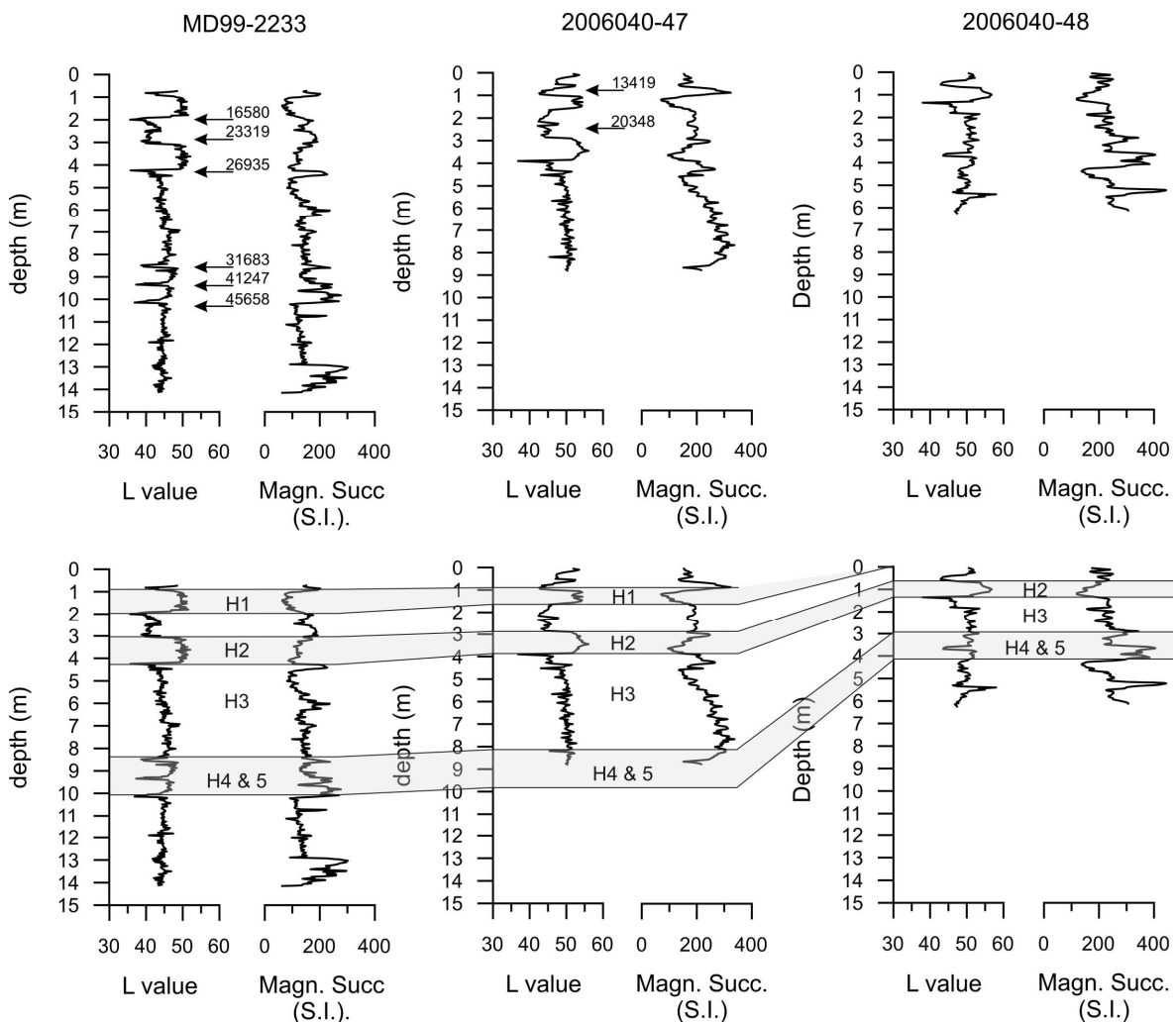


Figure 5: Correlation between cores on Saglek slope showing evidence of early Holocene unconformity. The unconformity is observed on core 48 where the last 15 ka of sediment deposits are missing.

Near surface failures have been also observed off Okak Trough and north of Hopedale Saddle (Figure 7). Mass transport deposits or unconformities in cores have been identified by recognition of unconformities through physical properties record, age control and correlation with the reference cores (Figure 5 to 7).

As elsewhere on the eastern Canadian margin, submarine failures and related MTDs are spatially widespread and may create unusual shallow drilling conditions. Larger regional failures occur in multiple valley systems and are therefore likely triggered by large earthquakes (Piper et al. 2012). The estimated frequency of large failures on the Labrador margin, although preliminary, may be a little less frequent than elsewhere off eastern Canada (Piper, 2005).

The shear strength (S_u) is an important parameter measured from cores that gives the magnitude of the maximum shear stress that the sediment can sustain before failure. By normalizing the shear strength, we are able to identify the state of consolidation of the sediment (overconsolidate vs underconsolidate), which help us to define the susceptibility of the sediment to fail and to identify past failures within the cores (Figure 6).

The normalized shear strength S_u/σ_v' ratio is about 0.30 for the tests done on the sediments from the Labrador Slope. Therefore for normally consolidated sediment:

$$S_u = \sigma_v' * 0.30$$

Where σ_v' is the vertical effective overburden pressure in kPa and is found by:

$$\sigma_v' = (\rho_{sat} - \rho_{sea\ water}) * 9.81 * \text{depth below sea bed}$$

Where ρ_{sat} = saturated bulk density of sediment

Typical profiles are shown in Figure 6 for cores 2008027-21, 2006040-46 and 2006040-48. The normal consolidation curve shows zones of overconsolidation and underconsolidation of the sediment. Cores 21 and 46 show underconsolidated sediment for the bottom meter or so of the core. The underconsolidation here is related to coring disturbance, confirmed by X-radiography and visual observations (see Appendix). Underconsolidated sediments are also observed on the upper part of cores 21 and 46, respectively above 200 cm and 250 cm (Figure 6 and appendix). X-radiography and visual observations, as well as carbon dates,

reveal that this drop in the apparent consolidation corresponds to an unconformity. Core 48 shows overconsolidated sediments. X-ray and visual observation show that core 48 is strongly disturbed. Correlation with other cores in the area and Hunttec data suggest that core 48 was taken in a failure area and probably sampled a rotated block (Figure 7). Locally, the consolidation is biased because of the presence of drop stones, which explain some large variations in the shear strength signal.

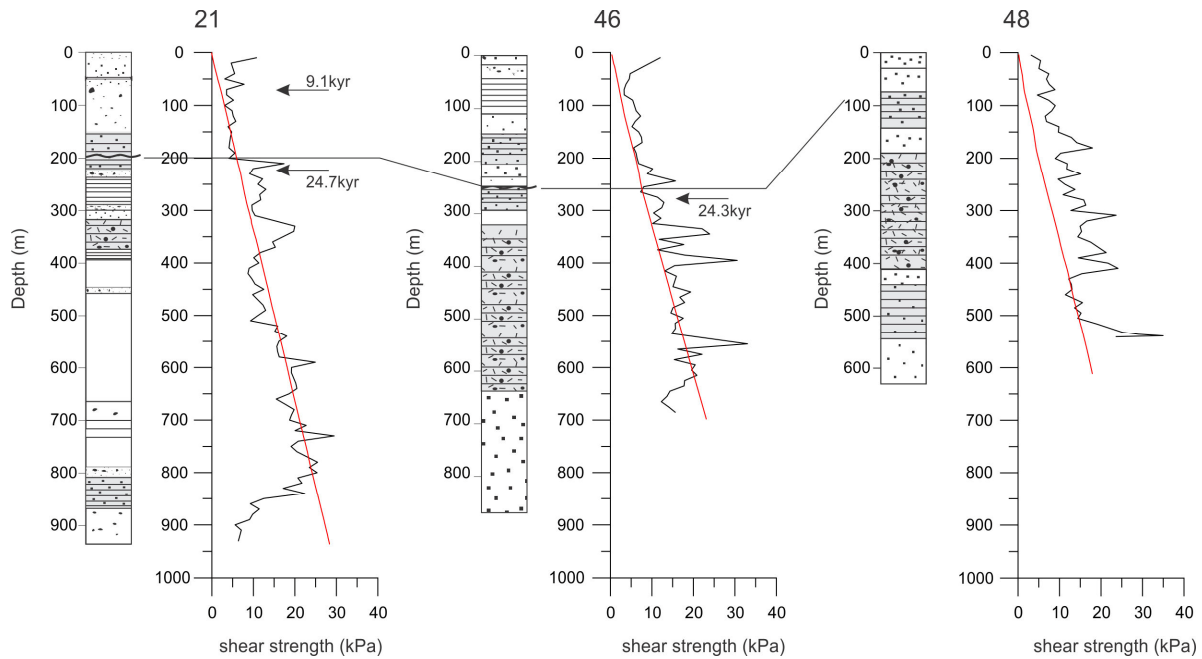


Figure 6: Core transect on Saglek slope. The red curve represents normal consolidation (S_u).

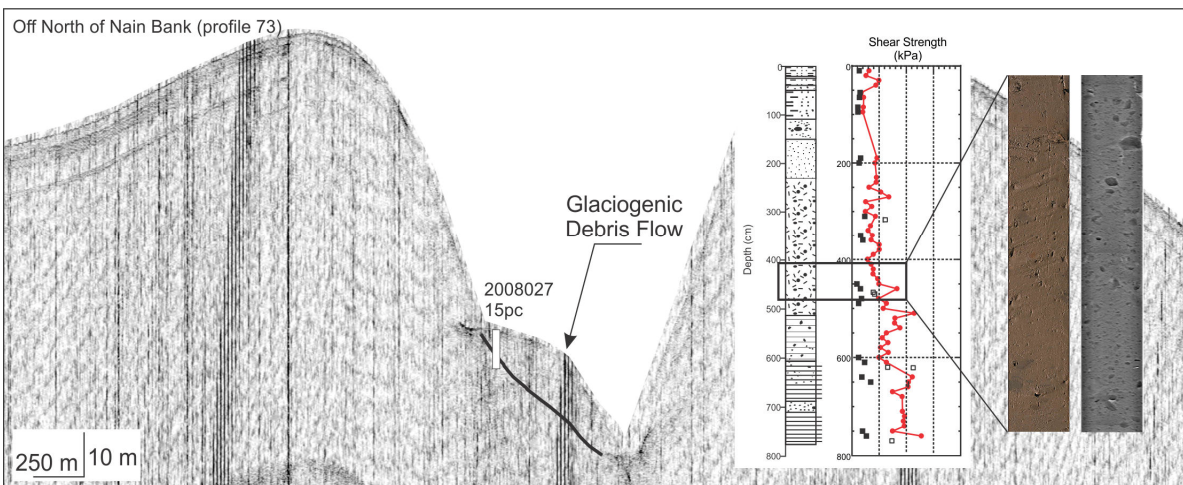
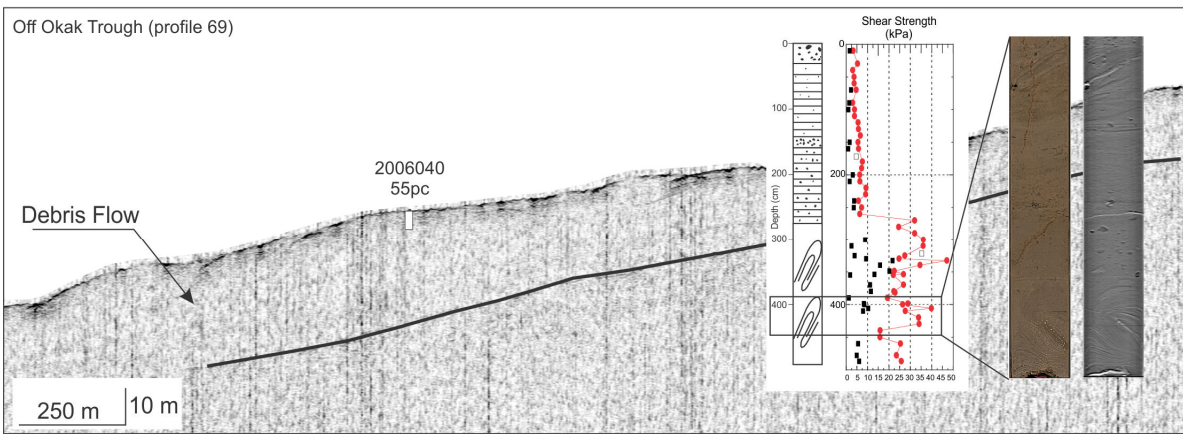
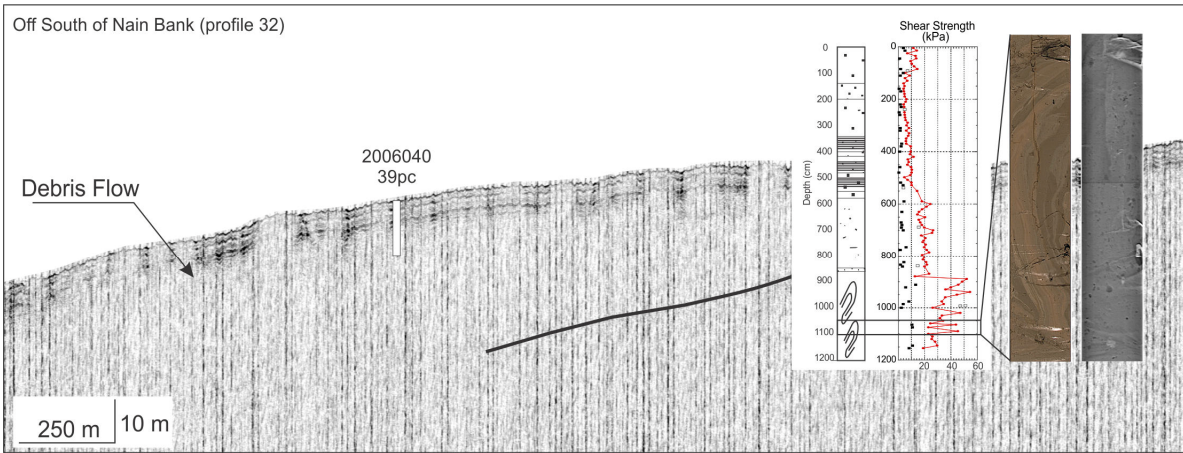


Figure 7: Three Huntex seismic profiles showing examples of two debris flows (top two profiles) and a glaciogenic debris flow (bottom profile) and their sedimentary facies. See figure 4 for the symbols. Note the differences in shear strength values and sediment structures between the “classic” debris flow and the glaciogenic debris flows.

4.2 Advanced geotechnical analysis

4.2.1 Consolidation testing

The compressibility of the sediments was measured using standard incremental loading tests with a load increment ratio of 0.5. The samples were back pressured to 290 kPa to ensure full saturation. The effective overburden pressure used to determine the overconsolidation ratio (OCR) values calculated using the multi-sensor logger density values. Loads were then applied until the samples were in a state of normal consolidation and the virgin compression line (VCL) was established.

The consolidation tests were conducted using a modified GeoTest back pressured system consisting of a consolidometer, linear displacement transducer, two digiquartz pressure transducers for measuring back and loading pressures and a DAQ system. The samples were extruded from a 10 cm whole round core sample using a thin-walled sampling tube (4 cm long, 6.25 cm ID) with a sharp cutting edge. The sample is trimmed using a push block to ensure uniformity of samples and allow for accurate sample height measurements. Initial measurements of dimensions, weights and water contents were taken after the sample was trimmed.

Variables, such as void ratios, square root times, and consolidation coefficients, were calculated from the test data using Microsoft Excel. The void ratios used to generate the e - $\log p'$ curve were determined from the time vs. displacement relationship at the end of primary consolidation. Taylor's square root of time method was used to determine the consolidation coefficients (C_v). The preconsolidation pressure (P'_c) was determined as an average of Casagrande's, Work's and Silva's methods. The results of the consolidation tests are presented in Table 2.

Station (cruise 2006040)	Depth (cm)	ρ_{sat} (g/cm^3)	W (%)	LL (%)	PL (%)	σ'_v (kPa)	P'_c (kPa)	C_c	C_r	OCR	Classification
3	575	1.69	58.6	40.16	22.1	51.6	49	0.56	0.055	0.95	CL
3	1033	2.08	21.71	22.39	13.7	91.4	59	0.14	0.012	0.65	CL
4	425	1.71	55.29	41.07	21.6	40.5	51	0.56	0.055	1.26	CL
5	622	1.81	39.8	37.6	19.7	57.8	107	0.36	0.027	1.85	CL
58	573	1.57	70.1	58.8	25.9	53.2	50	0.64	0.046	0.94	CH

Table 2: Summary of consolidation test results.

4.2.2 Triaxial Testing

Multi-stage isotropically consolidated, undrained (CIU) triaxial tests were conducted on 4 undisturbed marine sediment samples collected on cruise 2006040. The samples were from piston cores 0003, 004 and 0005. The tests were performed at the GSC-A geomechanical laboratory.

The triaxial testing system is a GDS computer controlled hydraulic triaxial testing system consisting of a 38mm Bishop & Wesley triaxial cell, three 2000 kPa pressure/volume controllers, a 5 KN submersible load cell, a pore pressure transducer, linear displacement transducer, differential pressure transducer and GDS software. The GDS software can perform CU, UU, CC, K_0 and extension triaxial tests

A thin-walled sampling tube (10 cm, 3.8 cm ID) with a sharp cutting edge was pushed into the core and then extruded with the sediment from the core liner. The samples were trimmed with a wire saw and initial measurements of dimensions, weights and water contents were taken after the sample was trimmed. The samples were extruded from the sampling tube into a rubber membrane attached to a split form placed on the base pedestal. The samples were backpressured to 240 kPa to ensure 100% saturation. A “B” check was conducted to measure the degree of saturation. A minimum B value of 0.95 was assumed to indicate 100% saturation. The samples were isotropically consolidated to 3 different confining pressures. The samples were sheared at a rate of 0.04 mm/min after each consolidation stage. The axial loading stages were stopped when the stress-strain curve began to level off. Continuously measured and derived values included: effective average mean stress (s), maximum shear stress (t) and Skempton’s A_f value. The failure envelopes for each tests were defined and the cohesion (C') and effective friction angle (ϕ') were determined.

A continuous profile of the normalized undrained shear strength was calculated using the Mohr-Coulomb relationship

$$\frac{S_u}{\sigma'_{v0}} = \frac{[K_0 + A_f(1 - K_0)] \sin \phi' + \frac{c'}{\sigma'_{v0} \cos \phi'}}{1 + (2A_f - 1) \sin \phi'} \quad [1]$$

where σ'_{vo} is the effective overburden stress and the coefficient of lateral earth pressure at rest (K_o) was calculated with the equation $K_o = 1 - \sin\phi'$. The normalized shear strengths from the CIU triaxial tests were also used to obtain profiles of undrained shear strength using the Stress History and Normalized Soil Engineering Properties (SHANSEP) procedure (Ladd and Foot 1974). The results of the triaxial tests are presented in Table 3.

Station	Depth (cm)	ρ_{sat} (g/cm ³)	W (%)	ϕ' (°)	C' (kPa)	S_u/σ'_v	A_f	Classification
3	578	1.69	59.5	29.5	2.8	0.28	0.63	CL
3	1035	2.06	25.64	31.1	7.3	0.47	0.64	CL
4	429	1.74	53.26	30.9	1.0	0.26	0.57	CL
5	624	1.56	39.8	33.0	1.3	0.40	0.28	CL

Table 3: Summary of triaxial tests results.

4.2.3 Slope Stability

Methods of slope stability assessment traditionally rely on limit equilibrium analysis. The simplest of the limit equilibrium methods is the infinite slope method which uses force equilibrium theory to evaluate both the resisting and stress of the overlying sediment or load on an assumed sliding surface.

The Factor of Safety (FOS) for a potential failure plane is defined as

$$FOS = \frac{\text{AvailableShearStrength}}{\text{DrivingForce}}$$

Instability occurs when the stress of the overlying sediments is greater than the strength of the soil. Sediments are considered to be unstable if the FOS is equal to or less than 1. A factor of safety can be calculated if the physical properties and the undrained shear strength of the sediment are known. The factor of safety due to gravitational loading was calculated using

$$FOS = \frac{S_u}{\gamma' H \cos \beta \sin \beta} \quad [3]$$

where S_u is miniature laboratory vane peak undrained shear strength (MV), γ' is the sediment submerged unit weight, H is the depth below seafloor and β is the seabed slope angle. Miniature shear vane measurements taken in disturbed core sections and obvious erroneous measurements were not included.

An earthquake is assumed to produce a horizontal acceleration, k , as a fraction of gravity that adds a horizontal force. The equation for the factor of safety becomes

$$FOS = \frac{\tau_f}{\gamma' H \cos \beta \sin \beta + k \gamma H \cos^2 \beta} \quad [4]$$

The critical pseudo-static acceleration (k_c) to cause failure can be estimated by setting the FOS to one (Equation 2)

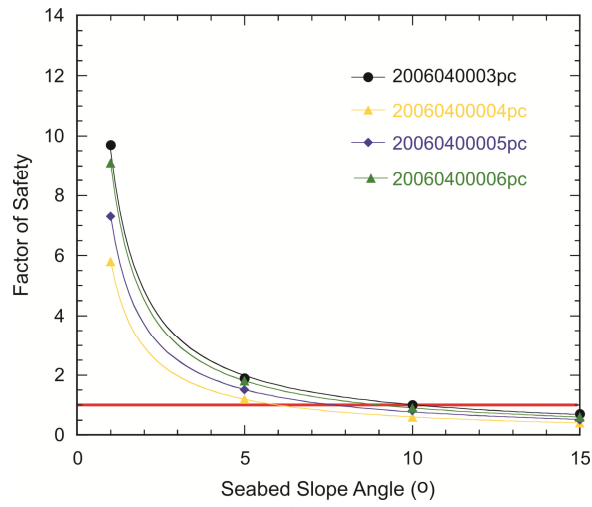
$$k_c = \frac{\gamma'}{\gamma} \left[\frac{S_u}{\sigma'_v} (OCR)^m - \sin \beta \right] \quad [5]$$

The critical seabed angle (β_c), and the critical slope thickness H_c , can be calculated by solving eq. 1 for β and H when the factor of safety is unity. Table 3 is a summary of the slope analysis.

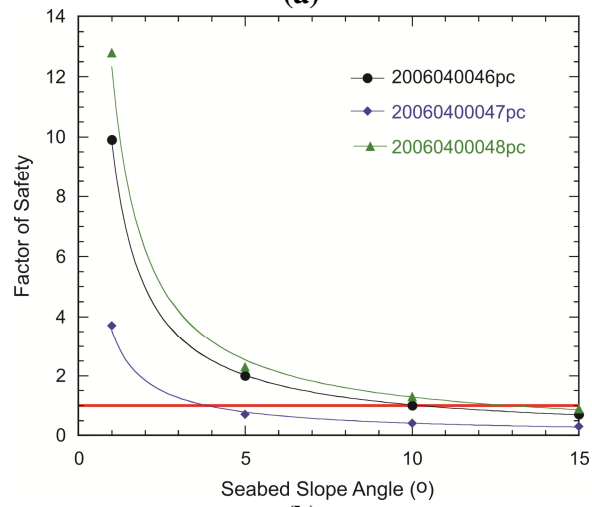
The slope angles for the various cores are very low with the largest slope angle being 1.9° at site 2006040_057PC. The FOS was calculated for slope angles of 1° , 5° , 10° and 15° for the 7 locations are presented in figures 1, 2 and 3. With the exception of 2006040_047PC the cores sites are stable with slope angles $< 5^\circ$. At site 2006040_057PC however the critical slope angle is $< 4^\circ$.

Station	Slope Angle ($^\circ$)	FOS	K_c	β_c ($^\circ$)	H_c (m)
3	1.4	6.9	0.16	9.9	5.48
4	0.8	7.2	0.09	5.8	8.72
5	0.9	8.1	0.11	7.4	4.98
6	0.8	11.4	0.15	9.3	7.55
46	1.4	6.4	0.13	8.8	8.15
47	1.2	3.2	0.04	3.7	12.07
48	0.1	21.3	0.016	13.2	4.40
56	2.2	4.5	0.13	10.1	3.69
57	1.9	4.9	0.13	9.6	3.23
58	1.4	5.5	0.11	7.7	6.85

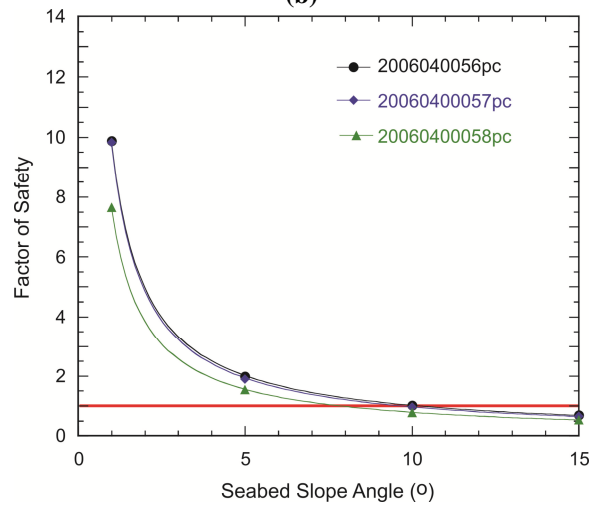
Table 4: Summary of slope stability analysis



(a)



(b)



(c)

Figure 8: Factor of Safety for various seabed slopes for: (a) cores 2006040_3, 4, 5 and 6; (b) cores 2006040_46, 47 and 48; (c) cores 2006040_56, 57, and 58.

4.2.4 Stress History

The sediment stress history can be determined using the OCR ratio determined from the consolidation tests and also by comparing the MV values to the calculated normalized shear strength profiles using the Mohr-Coulomb equation Eq. 1 and the SHANSEP analysis. The SHANSEP normalized shear strength profiles show good agreement with the MV data and also the stress state inferred from the OCR values. The SHANSEP normalized strength values obtained from CIU tests ranged from 0.28 to as high as 0.47. The shear strength profiles that were calculated using the modified Mohr-Coulomb equation Eq. 1, yielded trends that were consistent with the MV data but were usually on the high side of the MV strengths.

At site 2006040_003 (Figure 9) normalized strength values of 0.28 and 0.47 were used for the SHANSEP normalized shear strength profile and accounts for the offset in the profile at 7 m. This change corresponds to a change in lithology from a marine silt and clay sequence to a glacial marine till. The change in lithology is also reflected by a change in Plasticity Index from 18.1 to 8.7. The data suggest that the sediment is normally consolidated from 2 m to 7 meters and is then mostly underconsolidated. The drop off in shear strength at 10 m may be a result of coring disturbance. The higher than normal shear strengths in the upper 1 to 2 m is considered to be a result of apparent overconsolidation which is typical in marine sediments. The OCRs from 2 consolidation tests appear to confirm the normal stress state at 5.78 m and the underconsolidated stress state at 10.33m.

At Site 2006040_004 (Figure 10) the normalized strength value of 0.29 was used for the SHANSEP normalized shear strength profile. The normalized strength and MV data suggests that the sediments are normally consolidated from 1 to 8 m. The sediments are mostly underconsolidated below 8 m and may result from coring disturbance. The upper 1 m is overconsolidated and may be due to apparent overconsolidation. The OCR value of 1.26 at 429 cm correlates well with the shear strength analysis.

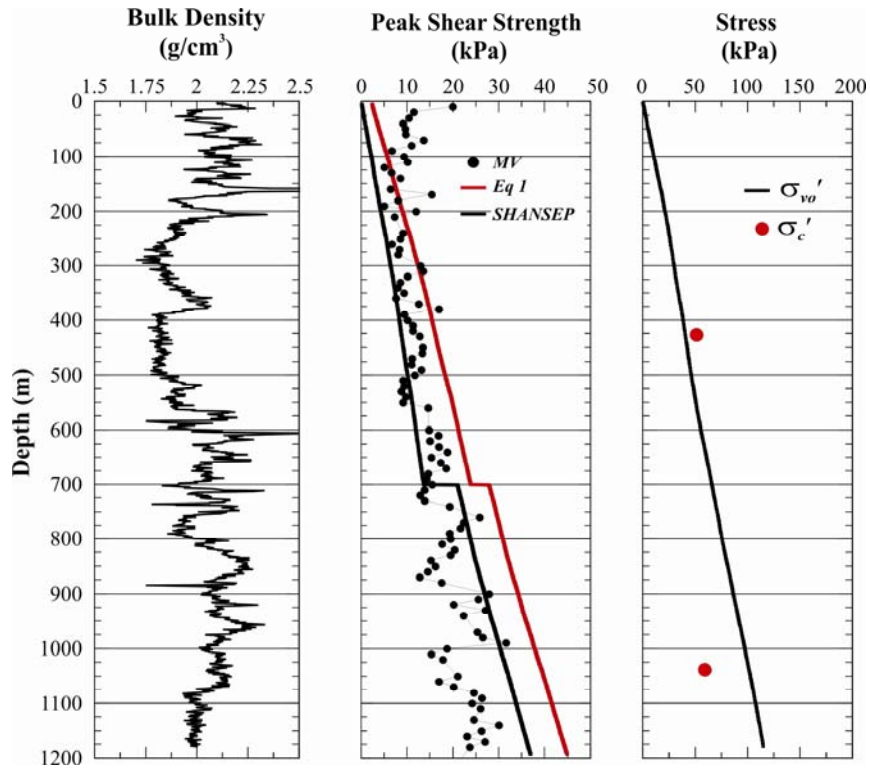


Figure 9: Geotechnical data from core 2006040_003pc

At Site 2006040_005 (Figure 11) the normalized strength value of 0.34 was used for the SHANSEP normalized shear strength profile. The normalized strength and MV data suggests that the sediments are normally to overconsolidated from the surface to 8 m. Below 8 m the sediments are underconsolidated and may result from coring disturbance. The OCR value of 1.85 indicates that the sediments are overconsolidated at a depth of 622 cm.

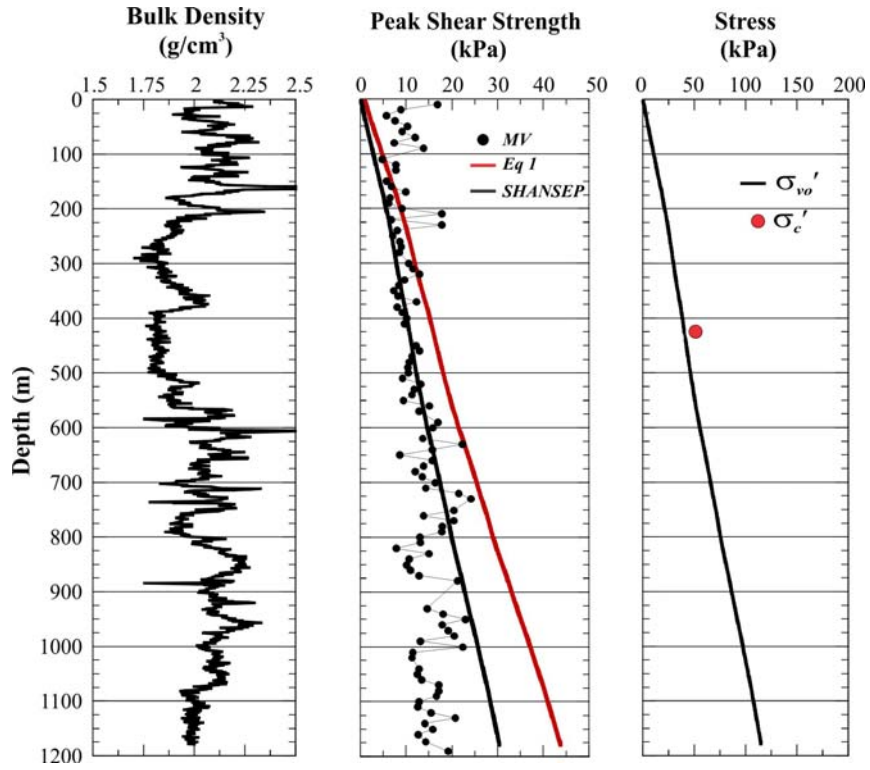


Figure 10: Geotechnical data from core 2006040_004pc

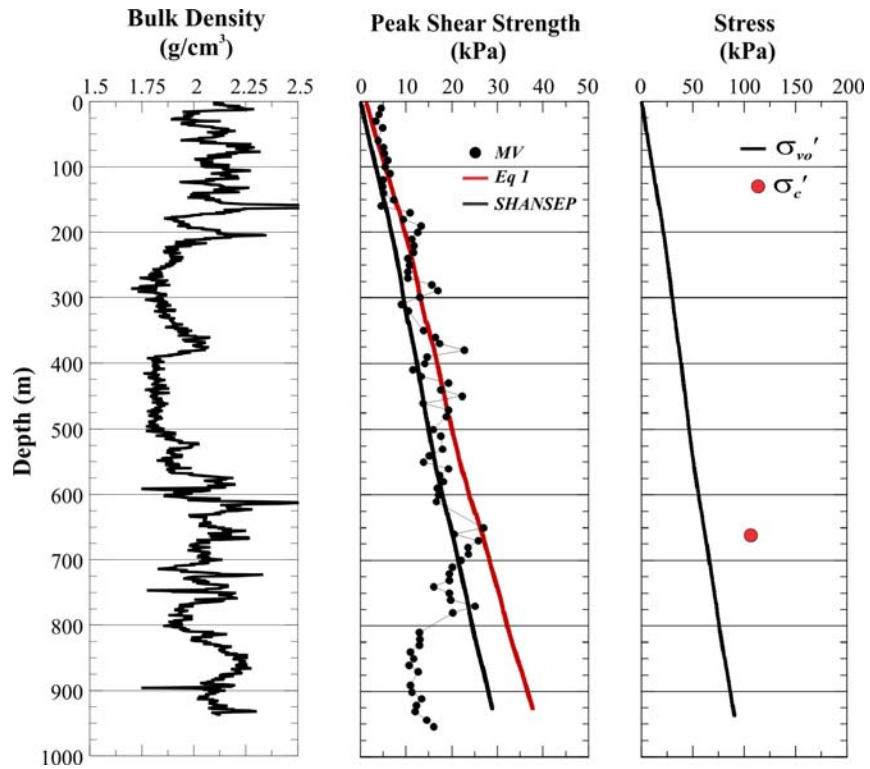


Figure 11: Geotechnical data from core 2006040_005pc

References

- Andrews, J.T., MacLean, B., 2003. Hudson Strait ice streams: a review of stratigraphy, chronology and links with North Atlantic Heinrich events. *Boreas* 32, 4-17.
- Andrews, J.T., Tedesco, K., 1992. Detrital carbonate-rich sediments, northwestern Labrador Sea: Implications for ice-sheet dynamics and iceberg rafting (Heinrich) events in the North Atlantic. *Geology* 20, 1087-1090.
- Benetti, S., 2006. Late Quaternary sedimentary processes along the western North Atlantic margin. School of Ocean and Earth Sciences, University of Southampton, p. 188.
- Biscaye, P.E., Eitrem, S.L., 1977. Suspended particulate loads and transports in the nepheloid layer of the abyssal Atlantic Ocean. *Marine Geology* 23, 155-172.
- Bond, G., Heinrich, H., Broecker, W., Labeyrie, L., McManus, J., Andrews, J., Huon, S., Jantschik, R., Clasen, S., Simet, C., Tedesco, K., Klas, M., Bonani, G., Ivy, S., 1992. Evidence for massive discharges of icebergs into the North Atlantic ocean during the last glacial period. *Nature* 360, 245-249.
- Campbell, D.C., 2005. Major Quaternary mass-transport deposits in southern Orphan Basin, offshore Newfoundland and Labrador. Geological Survey of Canada, pp. 1-10.
- De Geer, G., 1940, *Geochronologia Suecica* principles: Kungl. Svenska Vetenskapsakademiens Handlingar, Tredje Series, Band 18, no. 6, 357 p. and Atlas of plates.
- Deptuck, M.E., Mosher, D.C., Campbell, D.C., Hughes-Clarke, J.E., Noseworthy, D., 2007. Along slope variations in mass failures and relationships to major plio-pleistocene morphological elements, SW Labrador Sea, In: Lykousis, V., Sakellariou, D., Locat, J. (Eds.), 3rd International Symposium on Submarine Mass Movements and Their Consequences. Springer, Santorini, GREECE, pp. 37-45.
- Dickie, K., Keen, C.E., Williams, G.L., Dehler, S.A., 2011. Tectonostratigraphic evolution of the Labrador margin, Atlantic Canada. *Marine and Petroleum Geology* 28, 1663-1675.
- Edwards, M., 1986. Glacial Environments, In: Reading, H.G. (Ed.), *Sedimentary Environments and Facies*, 2nd Edition ed. Blackwell, Oxford, pp. 445-470.
- Ewing, M., Thorndike, E.M., 1965. Suspended Matter in Deep Ocean Water. *Science* 147, 1291-1294.
- Flint, R.F., Sanders, J.E., Rodgers, J., 1960a. Diamictite, a substitute term for symmictite. *Geological Society of America Bulletin* 71, 1809-1810.
- Flint, R.F., Sanders, J.E., Rodgers, J., 1960b. Symmictite: a name for nonsorted terrigenous sedimentary rocks that contain a wide range of particle sizes. *Geological Society of America Bulletin* 71, 507-510.
- Goss, S.J., 2006. Quaternary seismic stratigraphy of the Hamilton Spur: A sediment drift in the Labrador continental slope, Department of Earth Sciences. Dalhousie, Halifax, p. 56.

- Hall, F.R., Andrews, J.T., Jennings, A., Vilks, G., Moran, K., 1999. Late Quaternary sediments and chronology of the northeast Labrador Shelf (Karlsefni Trough, Saglek Bank): Links to glacial history. *Geological Society of America Bulletin* 111, 1700-1713.
- Heinrich, H., 1988. Origin and consequences of cyclic ice rafting in the Northeast Atlantic Ocean during the past 130,000 years. *Quaternary Research* 29, 142-152.
- Hemming, S.R., 2004. Heinrich events: Massive late Pleistocene detritus layers of the North Atlantic and their global climate imprint. *Rev. Geophys.* 42, RG1005.
- Hesse, R., Khodabakhsh, S., 1998. Depositional facies of late Pleistocene Heinrich events in the Labrador Sea. *Geology* 26, 103-106.
- Hesse, R., Khodabakhsh, S., 2006. Significance of fine-grained sediment lofting from melt-water generated turbidity currents for the timing of glaciomarine sediment transport into the deep sea. *Sedimentary Geology* 186, 1-11.
- Hesse, R., Khodabakhsh, S., Klaucke, I., Ryan, W.B.F., 1997. Asymmetrical turbid surface-plume deposition near ice-outlets of the Pleistocene Laurentide ice sheet in the Labrador Sea. *Geo-Marine Letters* 17, 179-187.
- Hesse, R., Klauck, I., Khodabakhsh, S., Piper, D., 1999. Continental slope sedimentation adjacent to an ice margin. III. The upper Labrador Slope. *Marine Geology* 155, 249-276.
- Hesse, R., Klaucke, I., Khodabakhsh, S., Piper, D.J.W., Ryan, W.B.F., Group, N.S., 2001. Sandy Submarine Braid Plains: Potential Deep-Water Reservoirs. *Aapg Bulletin* 85, 1499-1521.
- Josenhans, H.W., Zevenhuizen, J., Klassen, R.A., 1986. The Quaternary geology of the Labrador Shelf. *Canadian Journal of Earth Sciences* 23, 1190-1213.
- Josenhans, H.W. and Barrie, V. 1989. Submersible observations on the Labrador Shelf, Hudson Strait and Baffin Shelf. *GSC Paper* 88-20, 41-56.
- Ladd, C.C and Foote, R 1974. New Design procedure for stability of soft clays. *Journal of the Geotechnical Engineering and Foundation Division, ASCE, GT7, July, 763-785.*
- Lewis, C.F.M., Miller, A.A.L., Levac, E., Piper, D.J.W., Sonnichsen, G.V., 2012. Lake Agassiz outburst age and routing by Labrador Current and the 8.2 cal ka cold event. *Quaternary International* 260, 83-97. 10.1016/j.quaint.2011.08.023.
- McNeely, R., Dyke, A.S., Southon, J.R., 2006. Canadianmarine reservoir ages, preliminary data assessment. *Geological Survey of Canada, 3 (Open File 5049, CD-ROM).*
- Miller, J.M.G., 1996. Glacial sediments, In: Reading, H.G. (Ed.), *Sedimentary Environments: Processes, Facies and Stratigraphy*. Blackwell, Oxford, pp. 455-484.
- Mosher, D.C., Sonnichsen, G.V., Tremblay, L., 2008. CCGS Hudson 2005033B Cruise Report Grand Banks, Orphan Basin and Labrador Sea, St. John's to Halifax. *Geological Survey of Canada.*
- Pak, H., Zaneveld, J.R.V., Kitchen, J., 1980. Intermediate Nepheloid Layers Observed off Oregon and Washington. *J. Geophys. Res.* 85, 6697-6708.

- Piper, D.J.W., 2005. Late Cenozoic evolution of the continental margin of eastern Canada. *Norwegian Journal of Geology* 85, 305-318.
- Piper, D.J.W., Deptuck, M.E., Mosher, D.C., Clarke, J.E.H., Migeon, S., 2012. Erosional and depositional features of glacial meltwater discharges on the Eastern Canadian continental margin, In: Prather, B.E., Deptuck, M.E., Mohrig, D.C., van Hoorn, B., Wynn, R.B. (Eds.), *Application of seismic geomorphology principles to continental slope and Base-of-slope systems: Case studies from seafloor and near-seafloor analogues*. Tulsa, Society of Sedimentary Research.
- Piper, D.J.W., Mudie, P.J., Aksu, A.E., Skene, K.I., 1994. A 1 Ma record of sediment flux south of the grand banks used to infer the development of glaciation in southeastern Canada. *Quaternary Science Reviews* 13, 23-37.
- Piper, D.J.W., Shaw, J., Skene, K.I., 2007. Stratigraphic and sedimentological evidence for late Wisconsinan sub-glacial outburst floods to Laurentian Fan. *Palaeogeography, Palaeoclimatology, Palaeoecology* 246, 101-119.
- Rashid, H., Hesse, R., Piper, D.J.W., 2003a. Distribution, thickness and origin of Heinrich layer 3 in the Labrador Sea. *Earth and Planetary Science Letters* 205, 281-293.
- Rashid, H., Hesse, R., Piper, D.J.W., 2003b. Evidence for an additional Heinrich event between H5 and H6 in the Labrador Sea. *Paleoceanography* 18, 1077.
- Rashid, H., Hesse, R., Piper, D.J.W., 2003c. Origin of unusually thick Heinrich layers in ice-proximal regions of the northwest Labrador Sea. *Earth and Planetary Science Letters* 208, 319-336.
- Rashid, H., Piper, D.J.W., 2007. The extent of ice on the continental shelf off Hudson Strait during Heinrich events 1-3. *Canadian Journal of Earth Sciences* 44, 1537-1549.
- Roest, W.R., Srivastava, S.P., 1989. Sea-floor spreading in the Labrador Sea: A new reconstruction. *Geology* 17, 1000-1003.
- Shaw, J., Piper, D.J.W., Fader, G.B.J., King, E.L., Todd, B.J., Bell, T., Batterson, M.J., Liverman, D.G.E., 2006. A conceptual model of the deglaciation of Atlantic Canada. *Quaternary Science Reviews* 25, 2059-2081.
- Talbot, M.R., Allen, P.A., 1996. Lakes, In: Reading, H.G. (Ed.), *Sedimentary Environments: Processes, Facies and Stratigraphy*. Blackwell, Oxford, pp. 83-124.
- Thomas, F.C., Hardy, I.A., Rashid, H., 2003. Bryozoan-rich layers in surficial Labrador Slope sediments, eastern Canadian Arctic. *Canadian Journal of Earth Sciences* 40, 337-350.
- Tripsanas, E.K., Piper, D.J.W., Campbell, D.C., 2008. Evolution and depositional structure of earthquake-induced mass movements and gravity flows: Southwest Orphan Basin, Labrador Sea. *Marine and Petroleum Geology* 25, 645-662.
- Tripsanas, E.K., Piper, D.J.W., Jarrett, K.A., 2007. Logs of piston cores and interpreted ultra-high-resolution seismic profiles, Orphan Basin. *Geological Survey of Canada*, pp. 1-339.

Appendix

Acquisition and laboratory analysis of cores

Shipboard equipment and procedures

The piston coring system used was the AGC Long Piston Corer, which consists of a weighted core head combined with coupled barrel sections to produce a desired coring length. The 909 kg core head is 3 m long, 0.6m diameter and provides the initial stable downward force. Additional core barrels add substantially to this force. A single core barrel is comprised of a 300 cm length of 108 mm ID, 127 mm OD extra heavy seamless steel BI pipe with double grooves at each end. These barrels are butt-joined using bevelled edge sleeve couplings 46 cm long with sixteen 3/4"NC cup point Gr. 8 Allen setscrews (4 each opposed at 90 degrees). The setscrews fasten securely into the barrel grooves. The cores are collected in 300 cm sections of extruded CAB clear plastic liners slid inside the barrels and end joined with clear 50 mm packing tape. The liner section is held in place at the bottom by a core catcher (used at all coring sites to prevent the sediment from being sucked out by the vacuum created by the receding piston during retrieval). An externally tapered cutter (designed to initially penetrate the sea floor) slides over the last core barrel and is secured by the same setscrew/groove combination. The piston core is activated by a separate pilot core or trigger weight core (TWC). The TWC is supported by a trip arm connected to a 108 mm diameter gravity pilot corer with a 136 kg weighted head, a single 183 cm barrel, catcher and liner. It is calibrated to hang 15.25 m below the tip of the piston core. When the TWC contacts the bottom sediment, a trip arm releases the piston core in a controlled free fall to the seabed sediment.

The ship's crew rig, position, deploy and raise cores using the Pengo winch in combination with a hoist boom and block extended outboard of the ship's starboard. Sounding and hoist wire meter blocks measure water depth. The Pengo winch uses 3/4" dia 6 x 19 IWRC cable and a 316 SS swivel head. Upon surfacing, piston cores were safely secured and stabilized by the core handling system which included the rotating core-head cradle, swivelling outboard support brackets, an overhead monorail transport system with chain hoists and brake, and a processing half-height sea going container complete with a pendant controlled hydraulic boom crane and manually controlled hydraulic core extruder. From here the cores were taken to the GP lab for on board processing as described below.

The piston corer used the following dimensions for a 12 m core: head 2.74 m, scope, barrels and cutter 1250 cm; trip arm dip 91 cm, 15.75 m wire rope, trigger weight core 3.81 m. The scope is appropriate for 1.83 m penetration of the trigger weight core. All cores are identified alphabetically by section at the time of dismantling individual 10 ft core barrels from the bottom to the top, commencing with the bottommost core barrel and proceeding to the upper-most barrel containing sediment. Onboard shear strength measurements and constant volume samples are taken from the top and base of each whole core section prior to it being sealed and waxed. The core sections are stored upright in a refrigerated container maintained at 4°C onboard the Hudson.

Core processing at BIO

The initial steps in core processing at the GSC-A Core Processing Laboratory are the non-destructive measurements of whole core X-Ray and Multi Sensor Track (MST). Whole core X-Ray allows for evaluation of the core quality and semi-quantitative assessment of sediment structure and composition. The core is brought to ambient room temperature after X-Ray is completed and run through the MST for measurement of whole core sediment physical properties at a standard 1 cm down-core resolution. Following whole core analysis the plastic liner is cut longitudinally using the GSC-A Duits splitter. The sediment core is then split longitudinally by pulling a piece of fine wire through the sediment along the cuts in the plastic core liner. The two core halves designated archive and working, are temporarily covered with saran wrap. Each half is labelled with an up arrow, cruise number, sample number and section information.

Metre tape is placed along the length of the split core section to indicate down-core depth. The archive half is photographed, measured for colour reflectance, and described visually. The working half is immediately measured for physical properties (velocity, shear strength, bulk density and water content) that change as the core dries. Additional samples are taken depending on the specific core site objectives. The core halves are re-covered with plastic wrap, sealed in labeled plastic core sleeving, placed in labelled plastic D-tubes and stored at 4°C in the GSC-A Core Repository.

Multi Sensor Track (MST)

The MST measures compressional (P) wave velocity in a transverse direction, bulk density and magnetic susceptibility. The MST consists of a conveyor system, a central unit assembly, a microprocessor and a PC computer. The conveyor system consists of two track sections, mounted and aligned on either side of the central unit, and a 1.54 m core boat. The core boat is driven in either direction by a stepper motor and gear box assembly. The central unit assembly incorporates a compressional wave (p-wave) logger, a gamma ray attenuation logger and a magnetic susceptibility loop. The p-wave logger system is located at the right hand end of the unit. The gamma ray attenuation logger and magnetic susceptibility loop are offset to the left of the p-wave logger at 14 and 48 cm respectively.

Each whole core section is placed in the core boat to the right of the p-wave logger and travels incrementally past the p-wave logger, gamma ray attenuation logger and through the magnetic susceptibility coil. Measurements from each sensor are taken after each increment of travel. A piece of plastic core liner filled with distilled water is run through the MST every four or five sections of core as a quality check of the MST system.

The quality of the bulk density and velocity values is dependent on: 1) an accurate measure of sediment thickness; 2) degree of sediment saturation; and 3) the presence of air voids between sediment and plastic core liner. The magnitude of magnetic susceptibility values is dependent on the type of sediment and the volume of material within the coil. Identical cores containing the same sediment but of varying diameters will give different magnetic susceptibility values but will show the same down-core profile.

Compressional Wave Velocity (PWL)

The P-wave logger system consists of two spring loaded compressional wave transducers (PWT) and two rectilinear displacement transducers attached to the PWT mountings. The PWTs are pushed against either side of the core as it moves between the transducers. A short 500 kHz compressional wave pulse is produced at the transmitting transducer at a repetition rate of 1 kHz. This wave pulse travels through the core and is detected by the receiving transducer and the time of flight of the wave pulse is measured. The two rectilinear displacement transducers measure the displacement of the active faces of the PWT transducers. The diameter of the sediment core is calculated by subtracting the liner

thickness from the measured distance between the displacement transducers. This calculation assumes that the core liner is full with sediment. The P-wave travel time delay caused by the core liner and the electronics of the system is calculated using a distilled water standard of known diameter and temperature. The measured sediment P-wave travel time is corrected for the P-wave travel time delay. The sediment P-wave velocity is calculated as the sediment diameter/corrected P-wave travel time.

Gamma Ray Attenuation (GRA)

The GRA unit measures the bulk density of the sediment. It comprises a 10 millicurie ¹³⁷Cesium capsule housed in a 150 mm diameter primary lead shield with 2.5 and 5 mm collimators and a sodium iodide scintillation detector housed in a 100 mm diameter collimated lead shielding. The source and detector are mounted on opposite sides of the core as it moves through the central unit assembly. A narrow (pencil size) beam of gamma rays with energies principally at 0.662 MeV is emitted from the ¹³⁷Cesium source and passes through the diameter of the sediment core. At these energy levels Compton scattering is the primary mechanism for the attenuation of the gamma rays in most sedimentary material. The incident photons are scattered by collision with electrons encountered in the core and there is a partial energy loss. The attenuated gamma-ray beam is measured by the scintillation detector. The Compton scattering of the photons is directly related to the number of electrons in the path of the gamma ray beam. A two-phase model representing the mineral and interstitial water of fully saturated marine sediment is assumed for the MST GRA calibration. Aluminum is assumed to have an attenuation coefficient similar to common minerals found in marine sediments and represents the mineral phase. Distilled water represents the interstitial water phase. A calibration standard consisting of different thicknesses of aluminum and distilled water is used to calibrate the GRA. The measure of density of the sediments assumes that the marine sediment is fully saturated and completely fills the core liner. The diameter of the sediment is determined using the measured displacement between the rectilinear displacement transducers and the thickness of the liner. Sediment density is calculated using the calibration coefficients and the measured diameter of the sediment.

Magnetic Susceptibility Logger (MSL)

A Bartington loop sensor (MS2B) measures the magnetic susceptibility of the sediment. It is mounted to minimize the affects of magnetic or metallic components of the MST system. An oscillator circuit in the sensor loop produces a low intensity non-saturating, alternating magnetic field. Changes in the oscillator frequency caused by material that has a magnetic susceptibility is measured and converted into magnetic susceptibility values. Air measurements taken at the beginning and end of each section are used to correct the measurements for drift of the equipment during each section run.

Core Photography

The archive half of the core is photographed using a Nikon D100 six megapixel digital camera. Overlapping digital photographs are taken at two scales. The first is a close up image covering a 30 cm interval, and the second is a long shot image covering a 90cm interval. The images are saved in raw, tiff and jpg formats.

Reflectance Spectrophotometry

High accuracy measurements of spectral reflectance of split core are made over wavelengths of 400 to 700 nm using the Minolta Spectrophotometer CM 2002. Tristimulus values X, Y and Z are derived from the colour reflectance spectra according to the Commission Internationale d'Eclairage (CIE) method. The $L^*a^*b^*$ system (CIELAB) represents coordinates in 3 dimensional space where the L^* is the vertical axis representing lightness and a^* b^* are horizontal radii representing chromaticity. The L^* value ranges from zero (black) to 100 (white). The a^* value represents green (-) to red (+) and the b^* value represents blue (-) to yellow (+). Munsell colour is calculated and output but there is no international standard for converting Tristimulus values to Munsell HVC notation.

A zero calibration is performed to compensate for the effects of any change in the optical system and changes in ambient and internal temperature. White calibration is done using a white ceramic calibration cap and sets the maximum reflectance to 100%. Zero calibrations are performed daily and white calibrations are performed routinely at the beginning of each section. Prior to spectral reflectance measurements the archive half of the core is carefully

covered with Saran Wrap taking care to minimize the presence of air bubbles between the sediment and the wrap. Measurements are taken at 5 cm intervals where possible.

Sample Description

The written laboratory descriptions for the sediment cores includes: 1) condition of sample (e.g. cracks, disturbance, oxidation), 2) consistency of sample (e.g. soft, hard, firm, 3) reaction to hydrochloric acid which indicates the presence of calcium carbonate, 4) colour based on the Munsell soil colour charts and 5) visual core description consisting of colour, texture, grain size, bedding, contacts, bedforms, structures, presence of organic material, bioturbation and any other visible feature.

Discrete Velocity

The split core p-wave logger system has four transducer probes that are carefully inserted into the split core section and measure compressional wave velocity in the longitudinal and transverse directions to the axis of the core. There is a P-wave travel time delay caused by the electronics of the system. It is calculated for each set of transducers by measuring the distance between the transducers and measuring the travel time in distilled water at a known temperature. The measured sediment p-wave travel time is corrected for the P-wave travel time delay. The sediment P wave velocity is calculated as the sediment diameter/corrected P wave travel time. Longitudinal and transverse velocity measurements are taken at a standard 10 cm interval.

Discrete Shear Strength

Split core undrained shear strength measurements are made using a motorized miniature vane shear apparatus. A four bladed vane is inserted into soft sediment split core to a constant depth and rotated at a constant rate of 90°/min until sediment failure.

The difference in rotational strain between the top and bottom of a linear spring (deflection angle) is measured and the torque required to shear the cylindrical surface around the vane is calculated. Routine calibration of the system is not necessary. Each vane has a vane blade constant dependant on the geometry of the blade, and each spring has a spring constant that relates the deflection angle to the torque. Peak and remoulded shear strength values are calculated according to ASTM Method D 4648. Peak shear strength measurements are taken

at a standard 10cm interval. Two to three measurements of remoulded shear strength are taken per section. Onboard measurements of whole core peak shear strength are taken from the top and base of each whole core section using a hand-held Torvane.

Constant volume sampling

Constant volume samples are taken using a stainless steel cylinder of known volume. The cylinder is gently introduced into the sediment at a constant rate. The cylinder is then carefully removed from the core and trimmed using a wire saw. The sediment is extruded from the cylinder, weighed, dried at 105 °C for 24 hrs and weighed again. Bulk density and water content values are calculated according to ASTM Method D2216-98.

Data compilation

The MST, spectral reflectance, shear strength and constant volume data for individual cores are compiled as Excel workbooks. Each workbook consists of individual worksheets containing the original unedited physical property datasets and a worksheet of the compiled physical property dataset. The compiled dataset is imported into Kaleidagraph and poor quality data is masked. The edited good quality data is saved as a tab delimited text file and plotted. The graphic lithology, MST, spectral reflectance, and discrete onboard and laboratory physical property data plots are compiled in a Coreldraw letter size core plot summary file.

Consolidation Plots

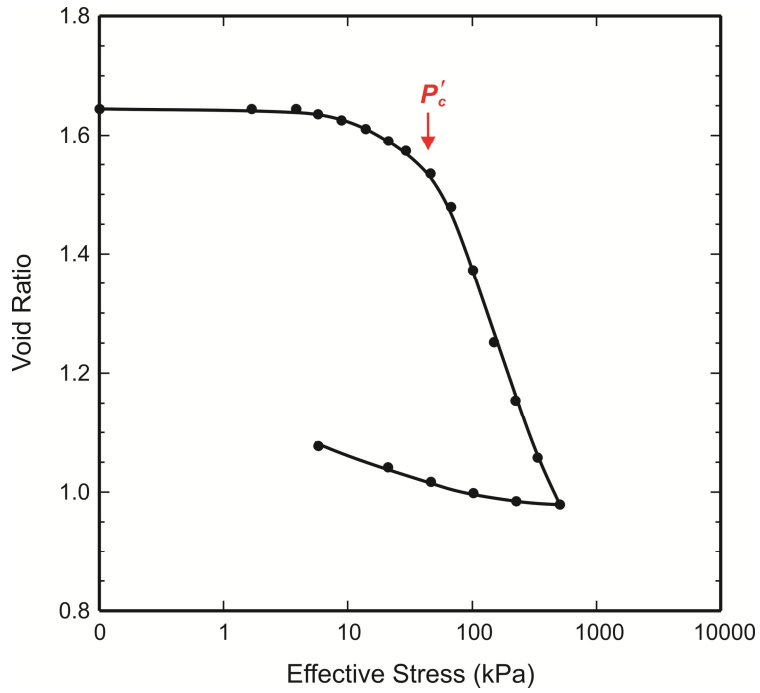


Figure 1 Consolidation plot for sample 2006040_003 575 cm.

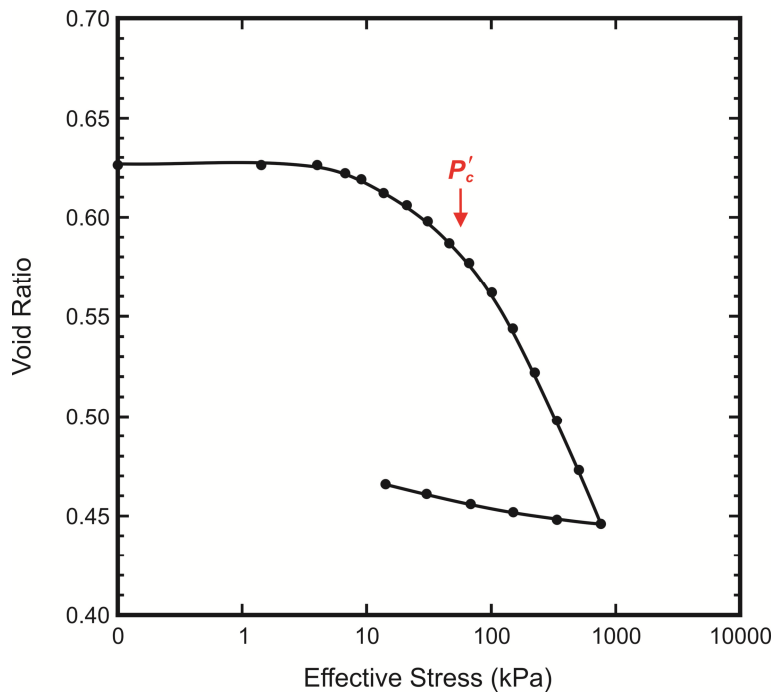


Figure 2 Consolidation Plot for sample 2006040_003 1033 cm.

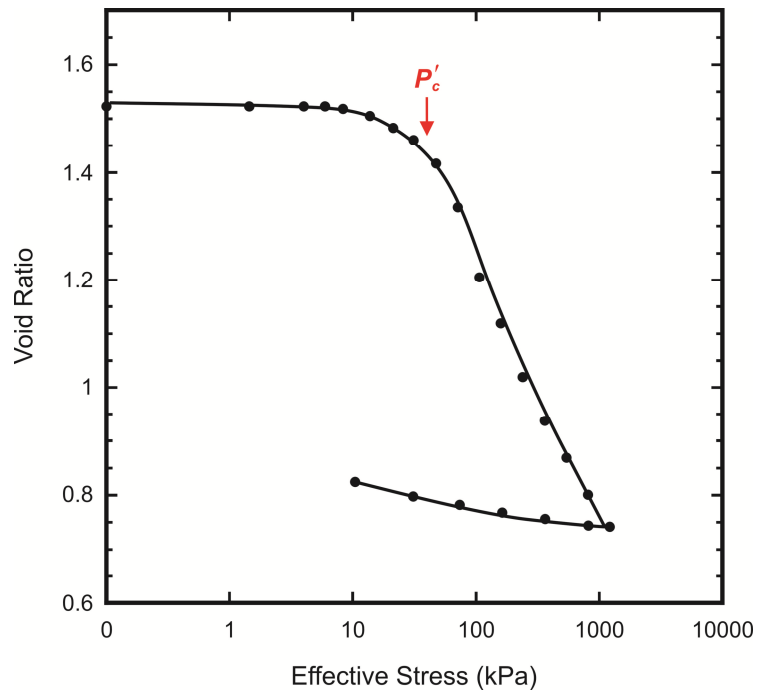


Figure 3 Consolidation Plot for sample 2006040_004 425 cm.

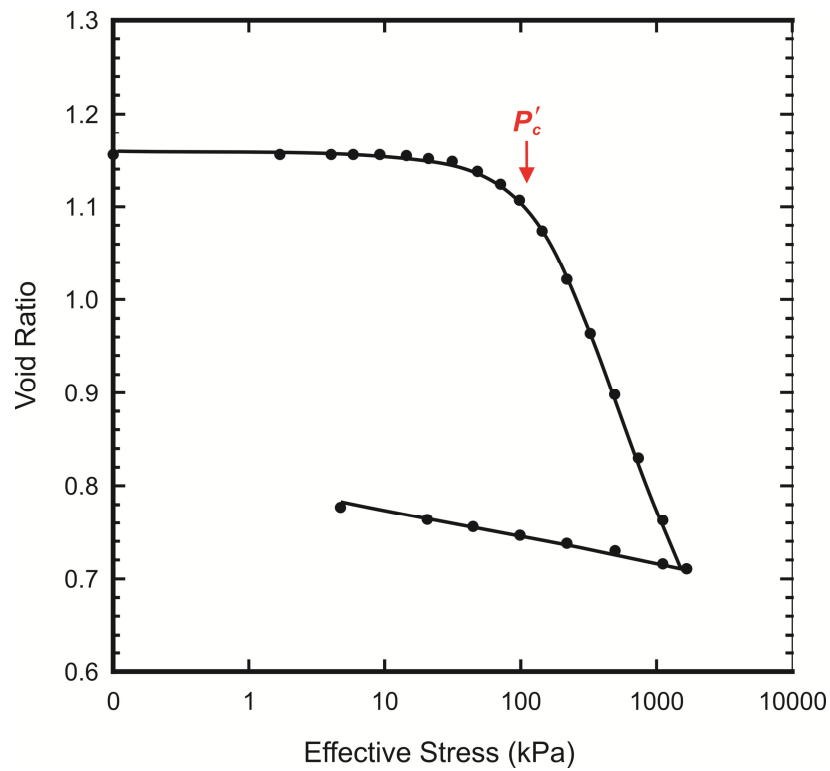


Figure 4 Consolidation Plot for sample 2006040_005 622 cm.

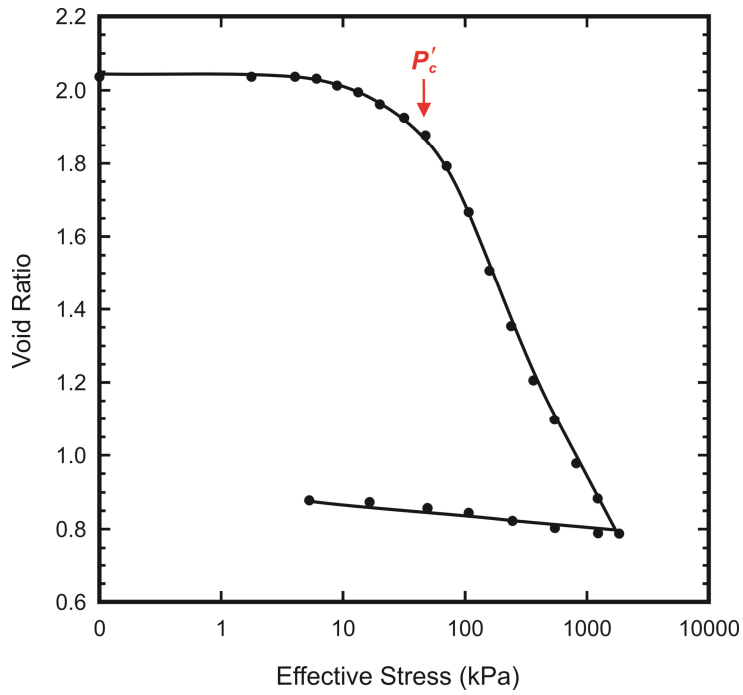


Figure 5 Consolidation Plot for sample 2006040_058 573 cm.

Triaxial Failure Envelope Plots

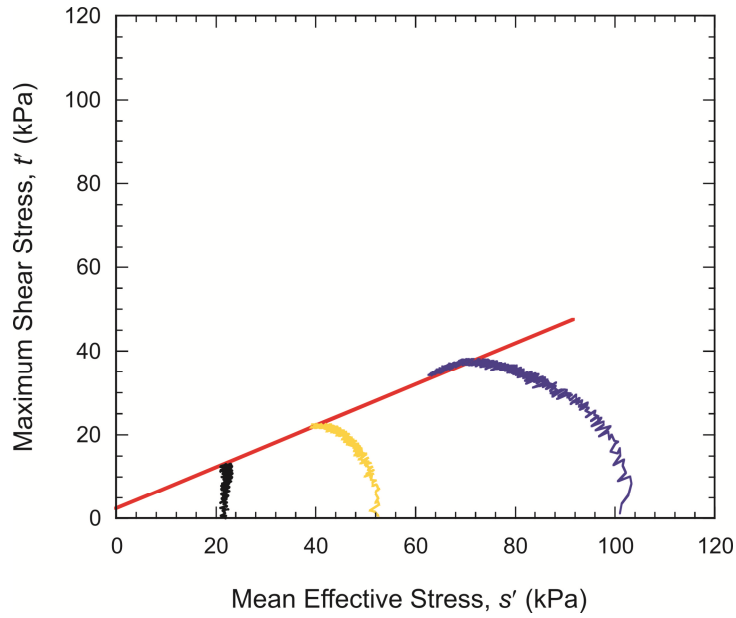


Figure 1 Stress paths for multistage triaxial (CIU) test for sample 2006040_003 578 cm.

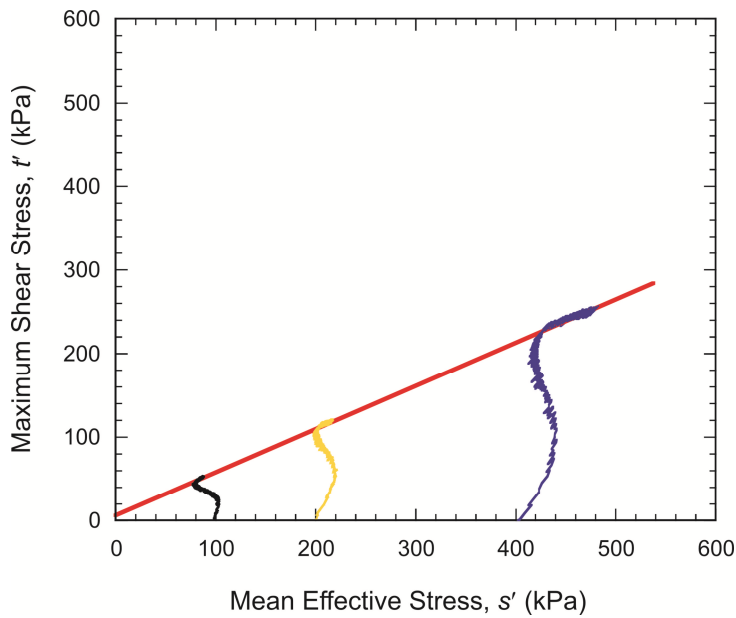


Figure 2 Stress paths for multistage triaxial (CIU) test for sample 2006040_003 1035 cm.

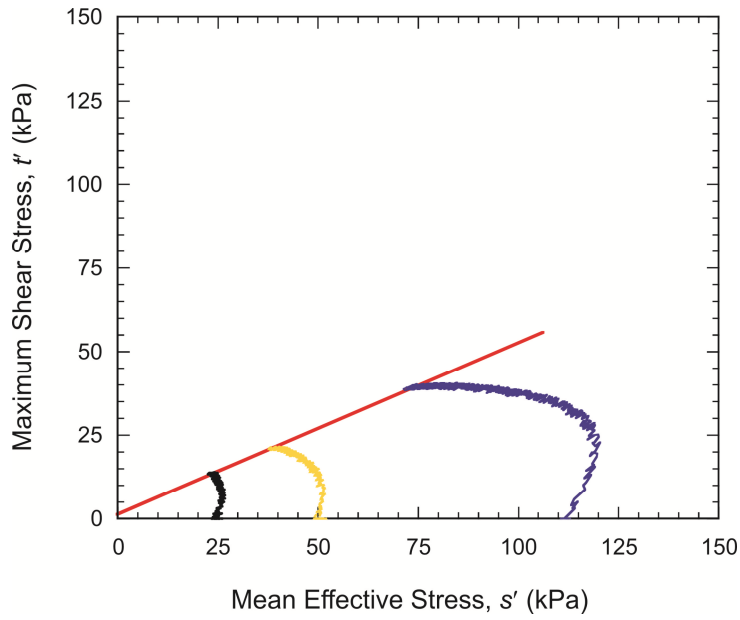


Figure 3 Stress paths for multistage triaxial (CIU) test for sample 2006040_004 429 cm.

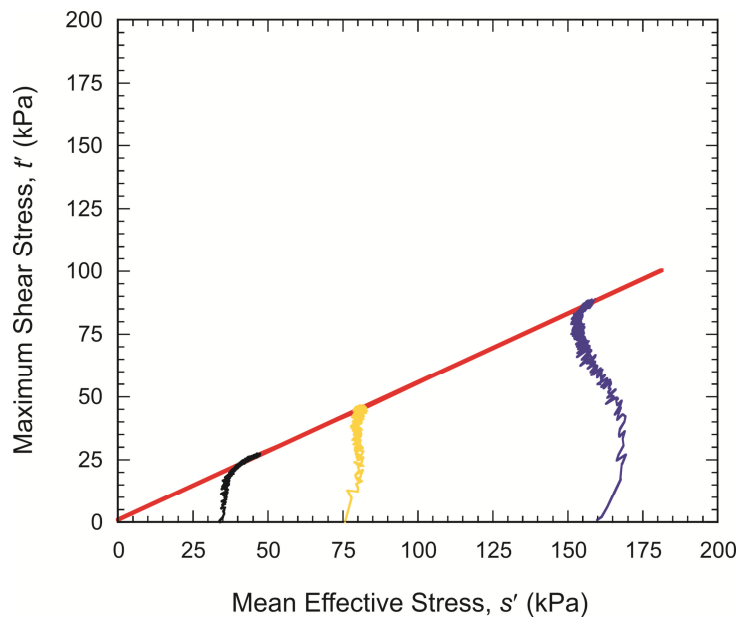
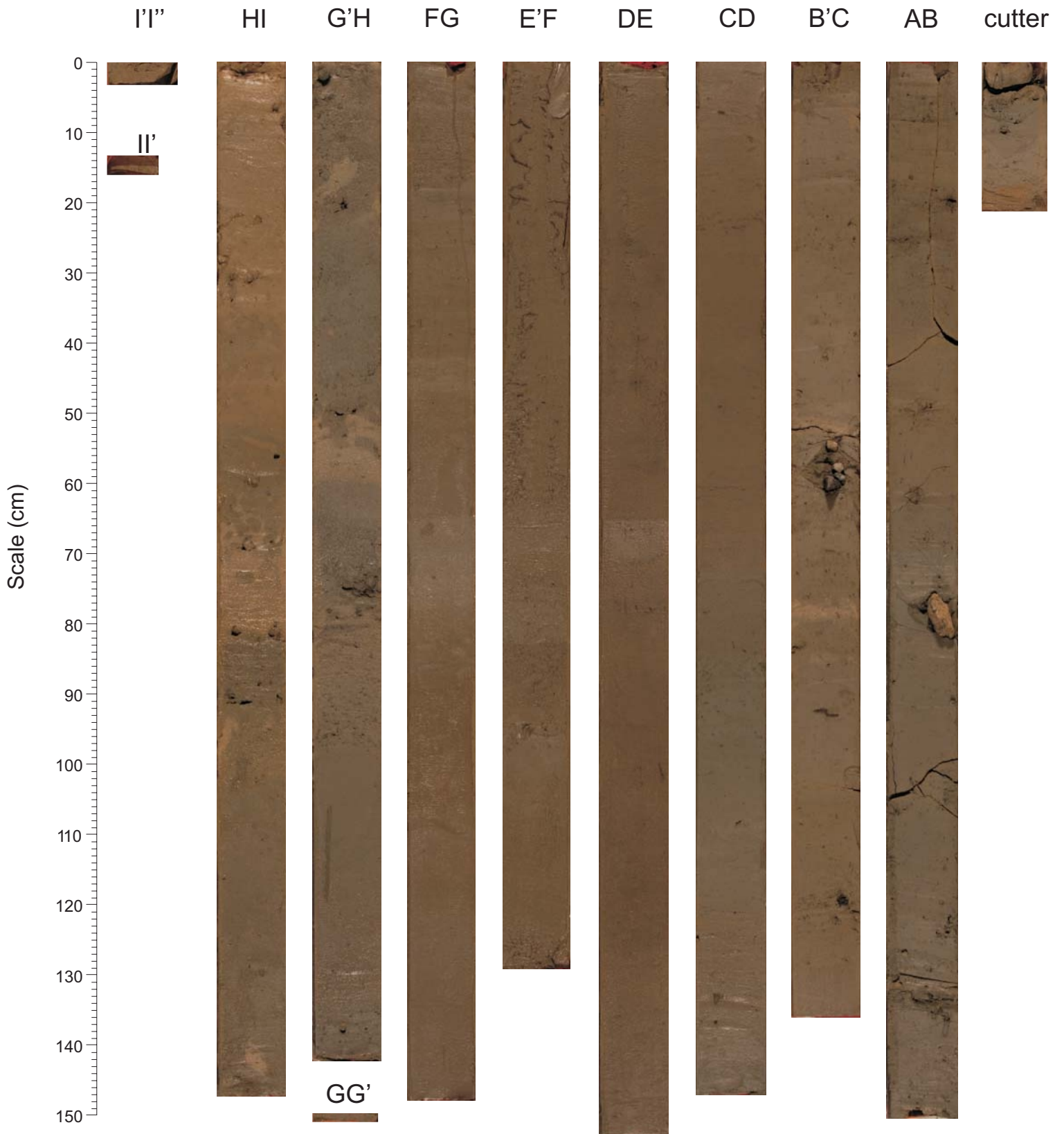


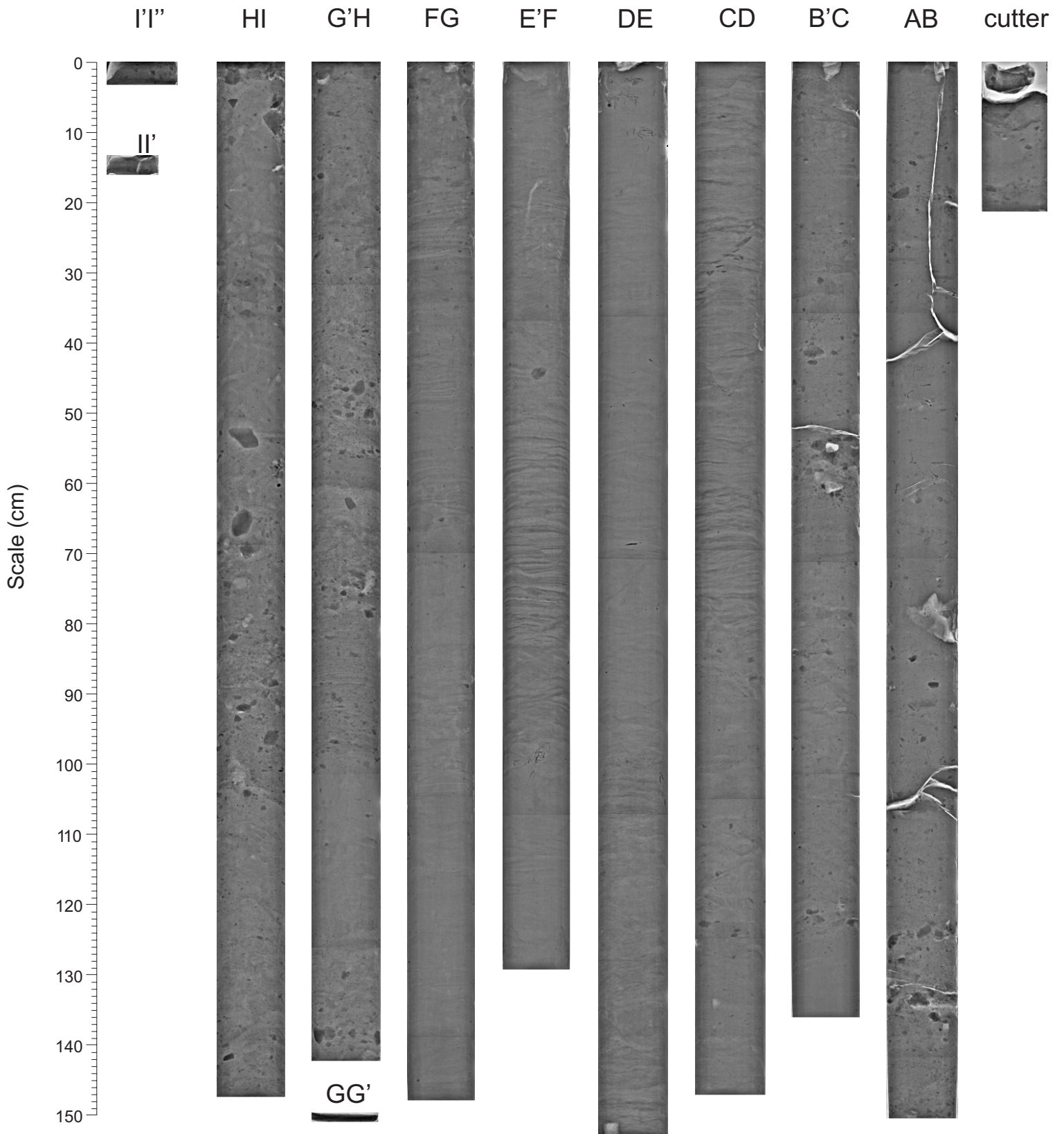
Figure 4 Stress paths for multistage triaxial (CIU) test for sample 2006040_005 624 cm.

Logs of piston cores

2006040 0003 Piston Core



2006040 0003 Piston Core



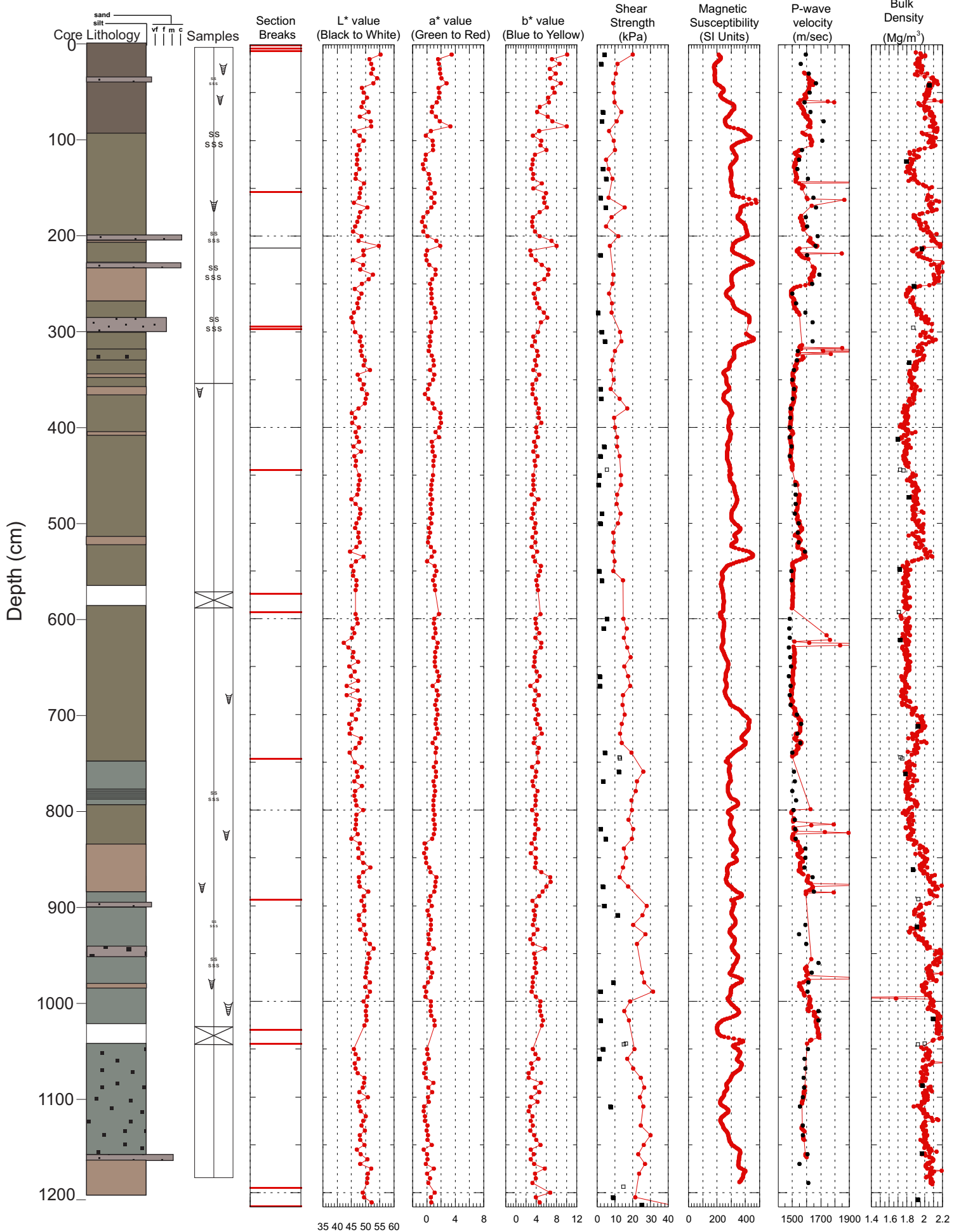
Hudson 2006040 Piston Core 0003

TD 1215 cm 54.794818° N -52.321300° W Water depth 2002 m

- Peak
- Remoulded
- Peak Torvane
- Peak penetrometer

- MST
- Discrete
- Longitudinal
- Discrete
- Transverse

- MST
- Discrete cv
- Discrete cv onboard

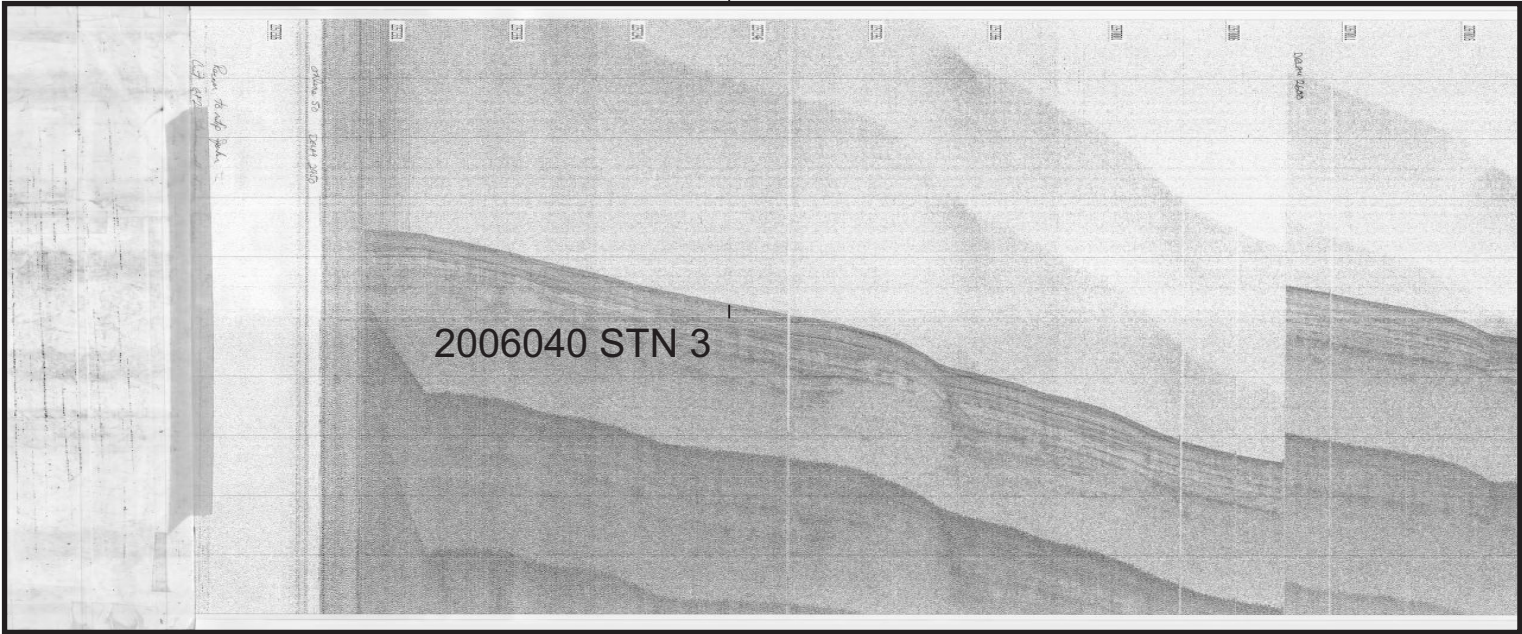


2006040-0003PC Hunttec Figure

225/2345

SW

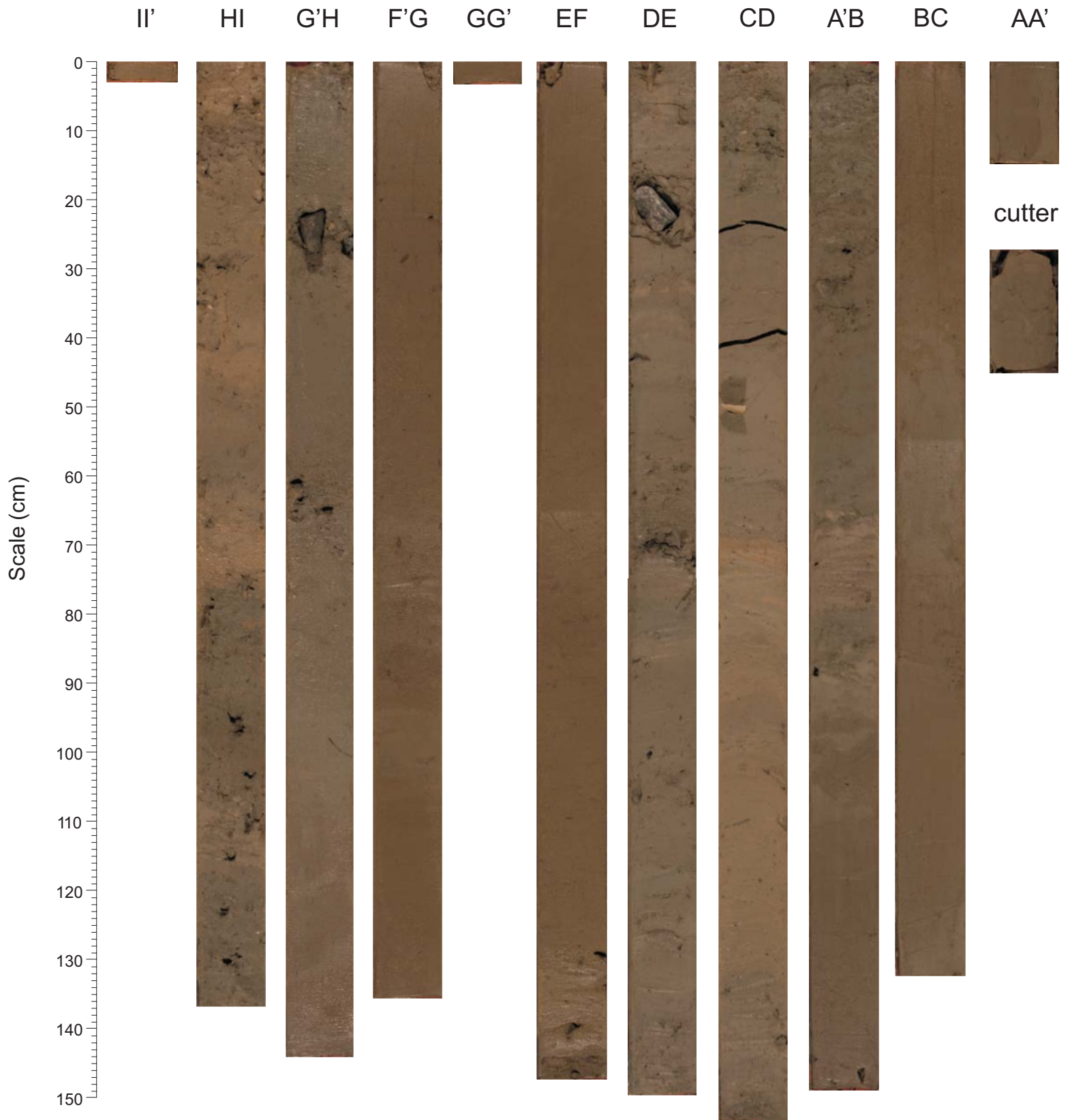
NE



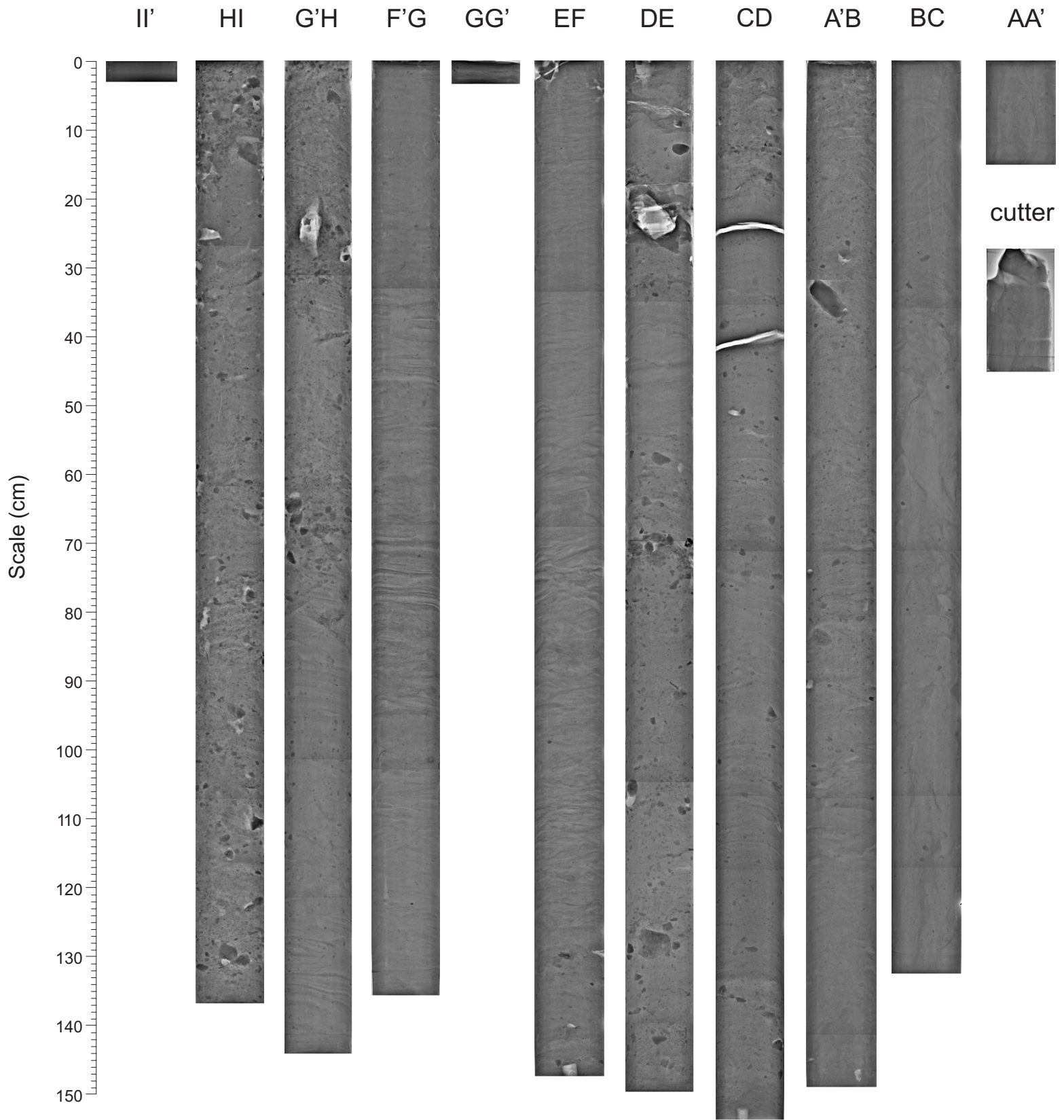
225/2326

226/0016

2006040 0004 Piston Core



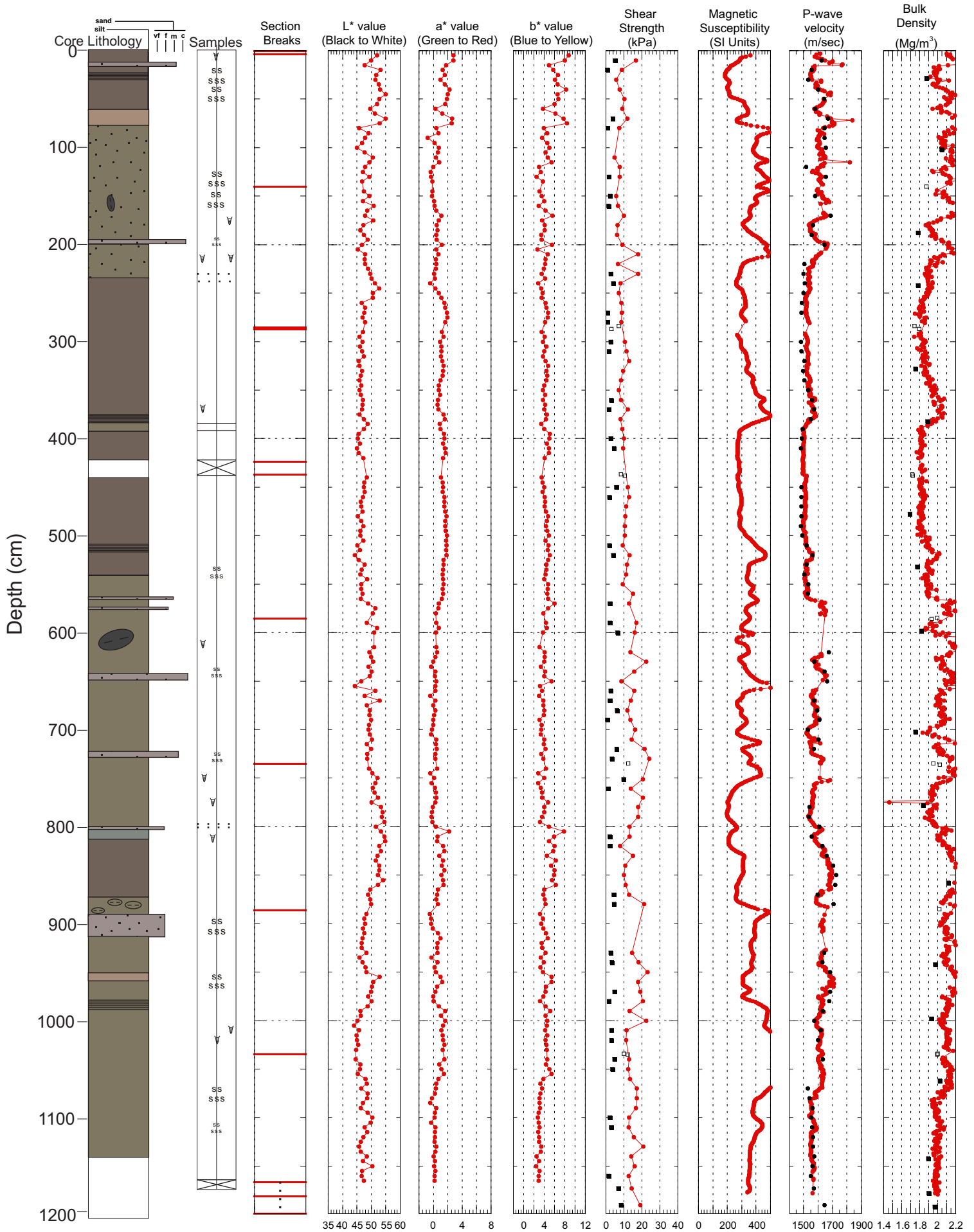
2006040 0004 Piston Core



Hudson 2006040 Piston Core 0004

TD 1199 cm 54.854578° N -52.636661° W Water depth 1770 m

- Peak
- Remoulded
- Peak Torvane
- Peak penetrometer
- MST
- Discrete
- Longitudinal
- Discrete Transverse
- Discrete cv
- Discrete cv onbord

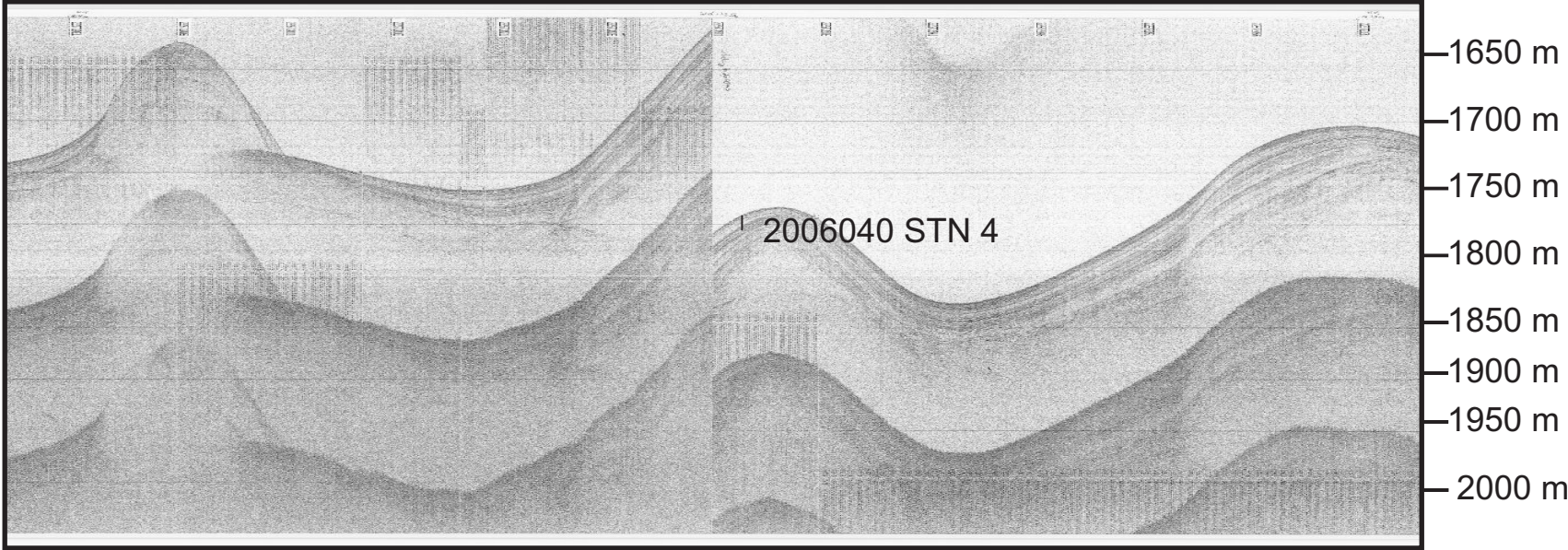


2006040-0004PC Hunttec Figure

NW

225/2032

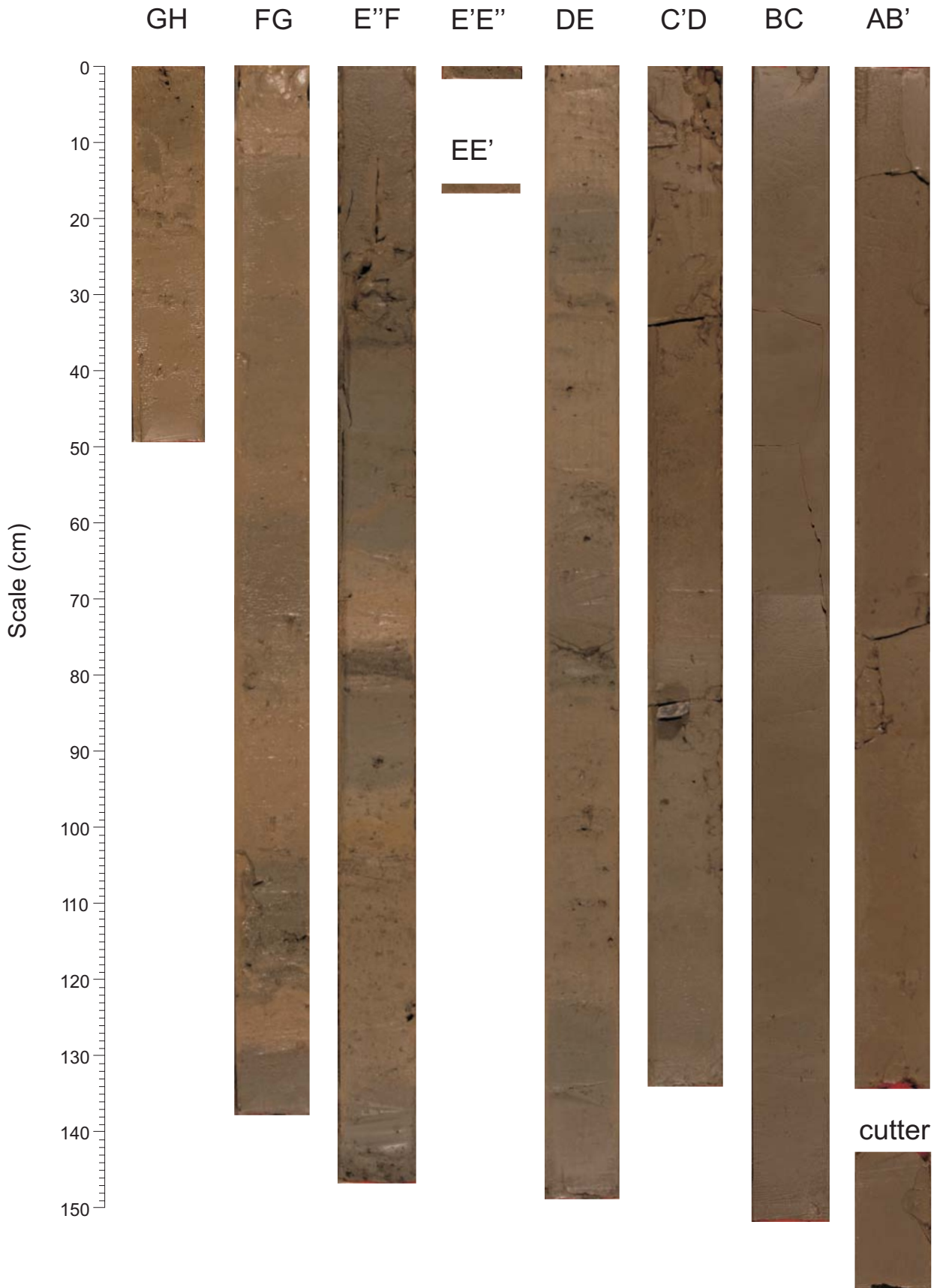
SE



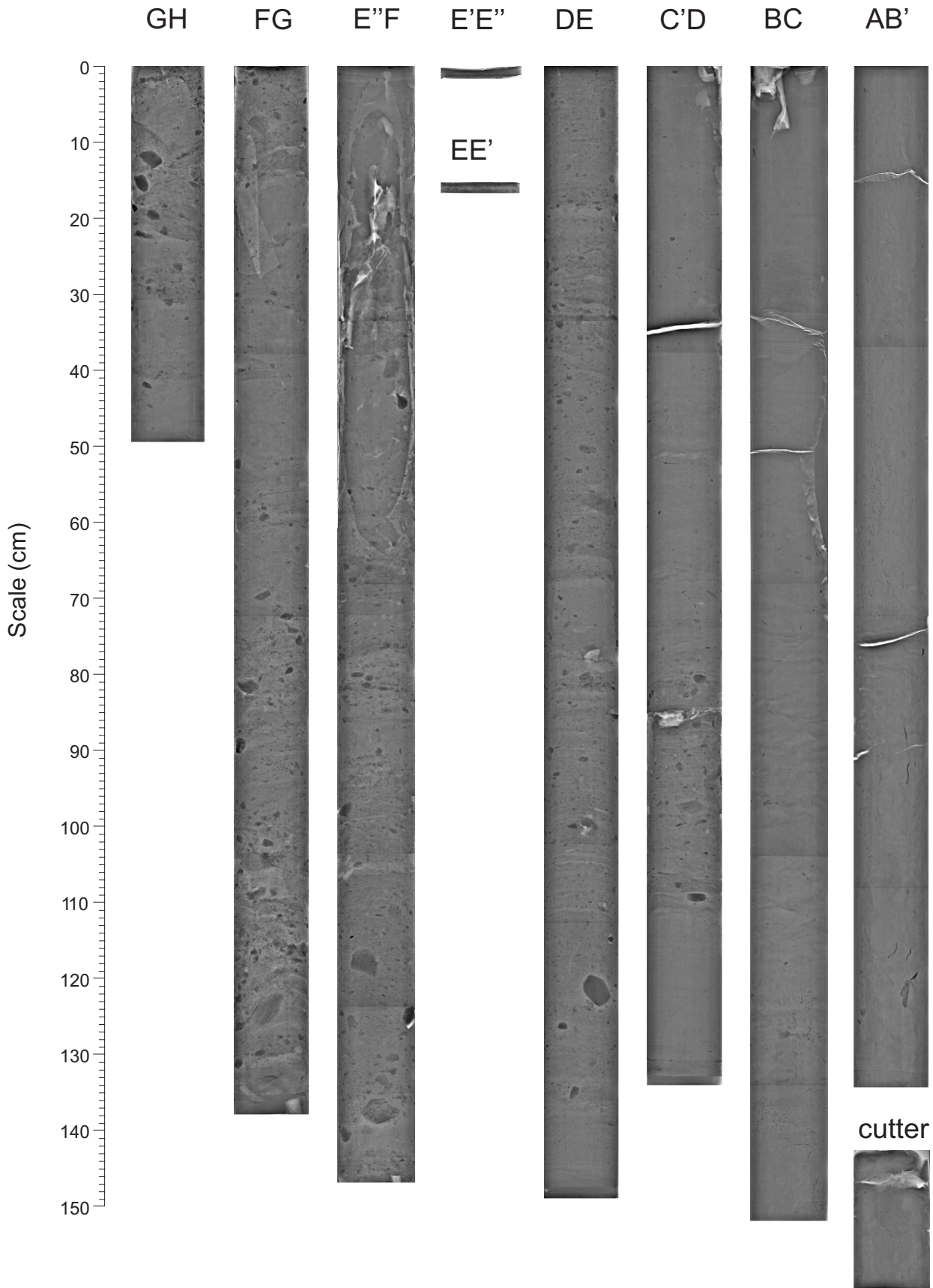
225/1956

225/2101

2006040 0005 Piston Core

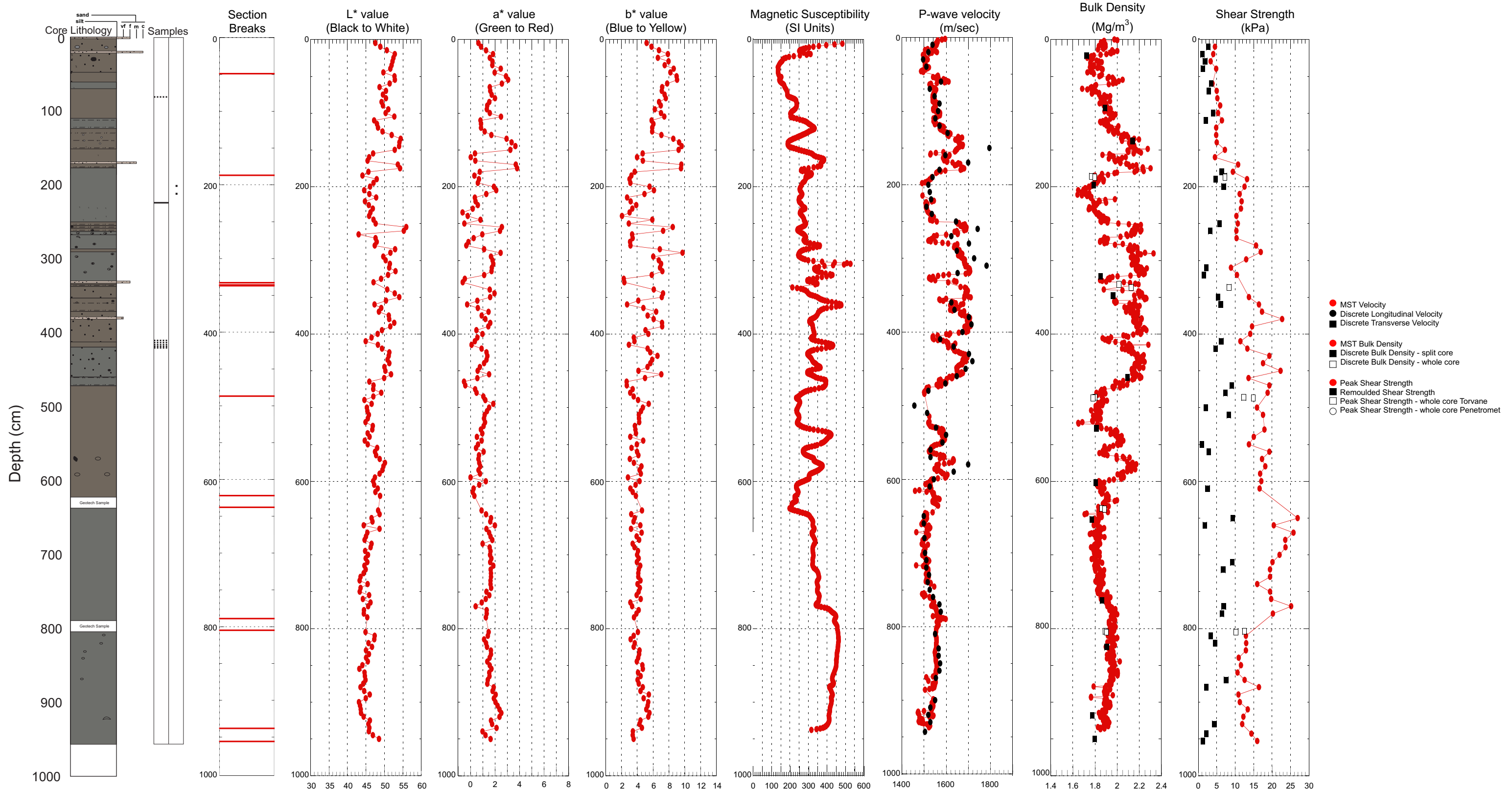


2006040 0005 Piston Core



Hudson 2006040 Piston Core 0005

TD 956 cm 54°42.8512 N 52°54.7916 W Water depth 1148 m

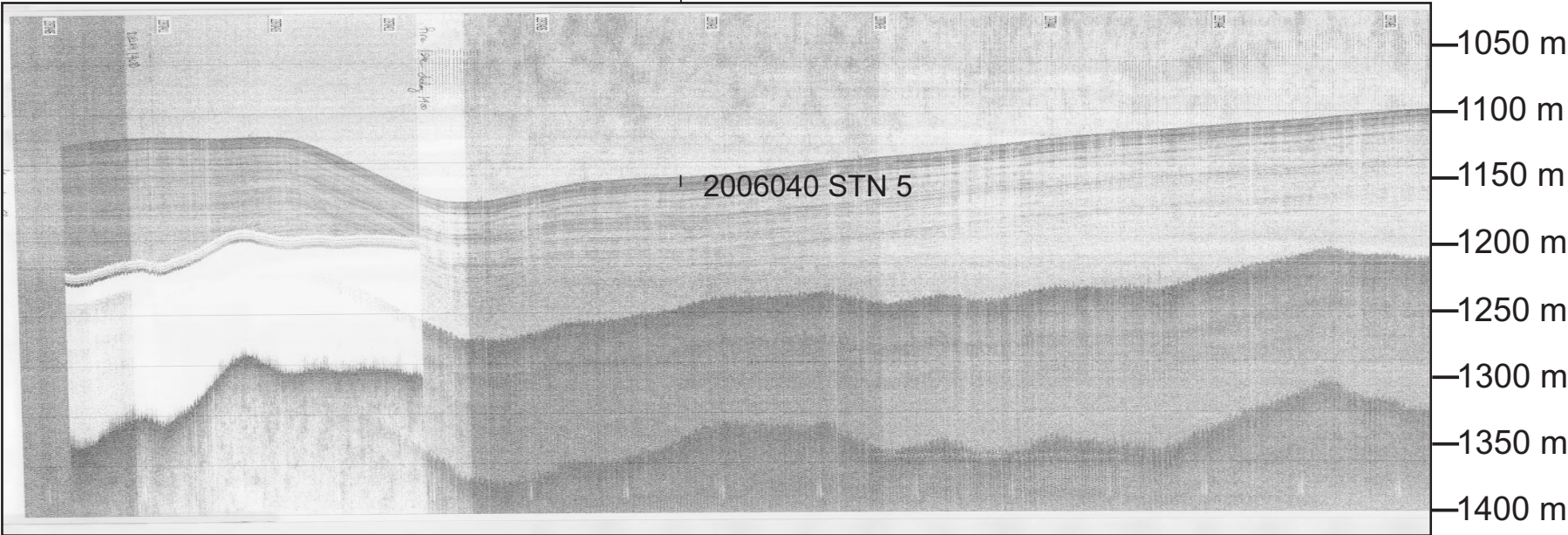


2006040-0005 PC Hunttec Figure

228/0430

NE

SW



228/0405

228/0451

2006040 0006 Piston Core

FG

E'F

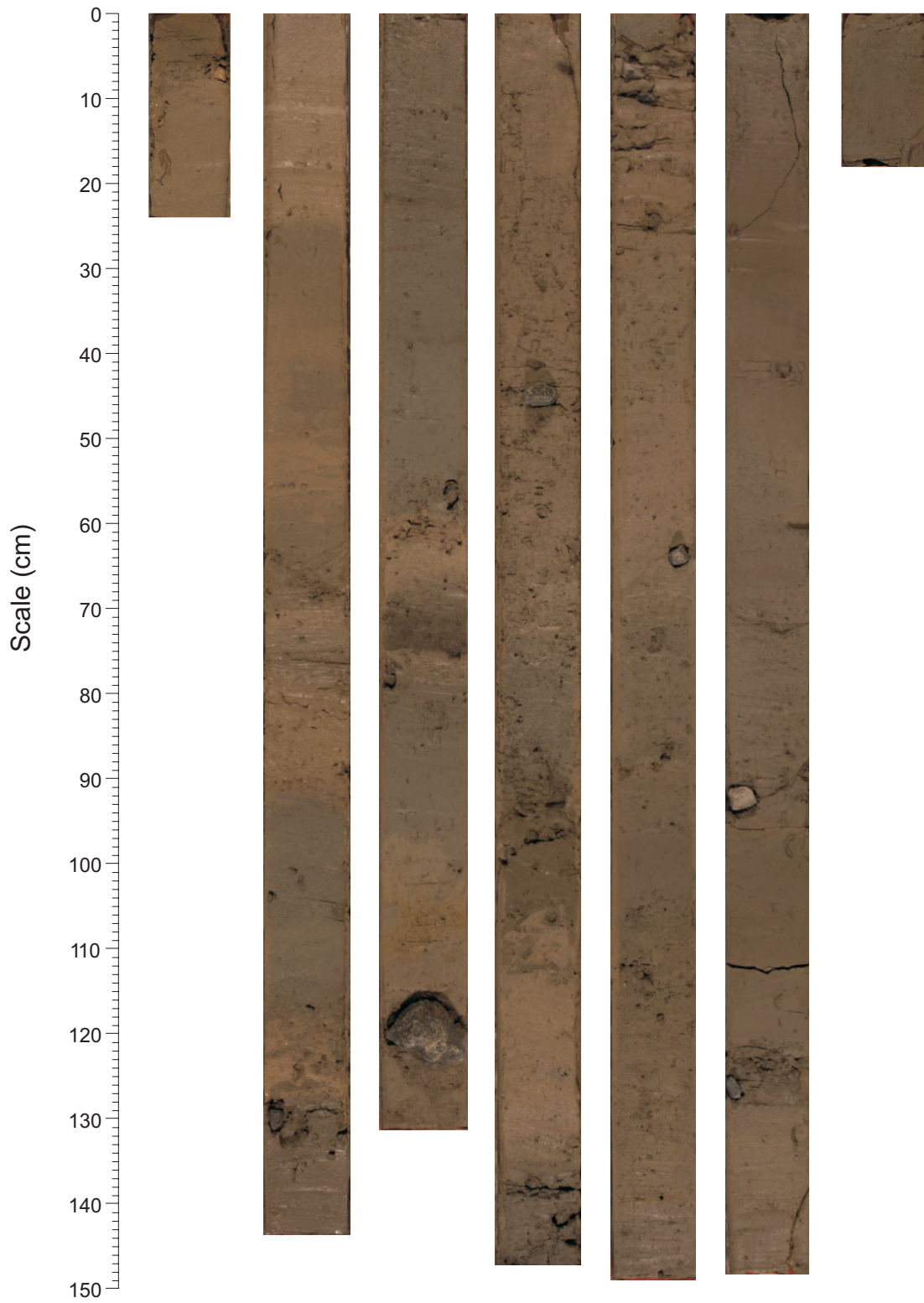
DE

CD

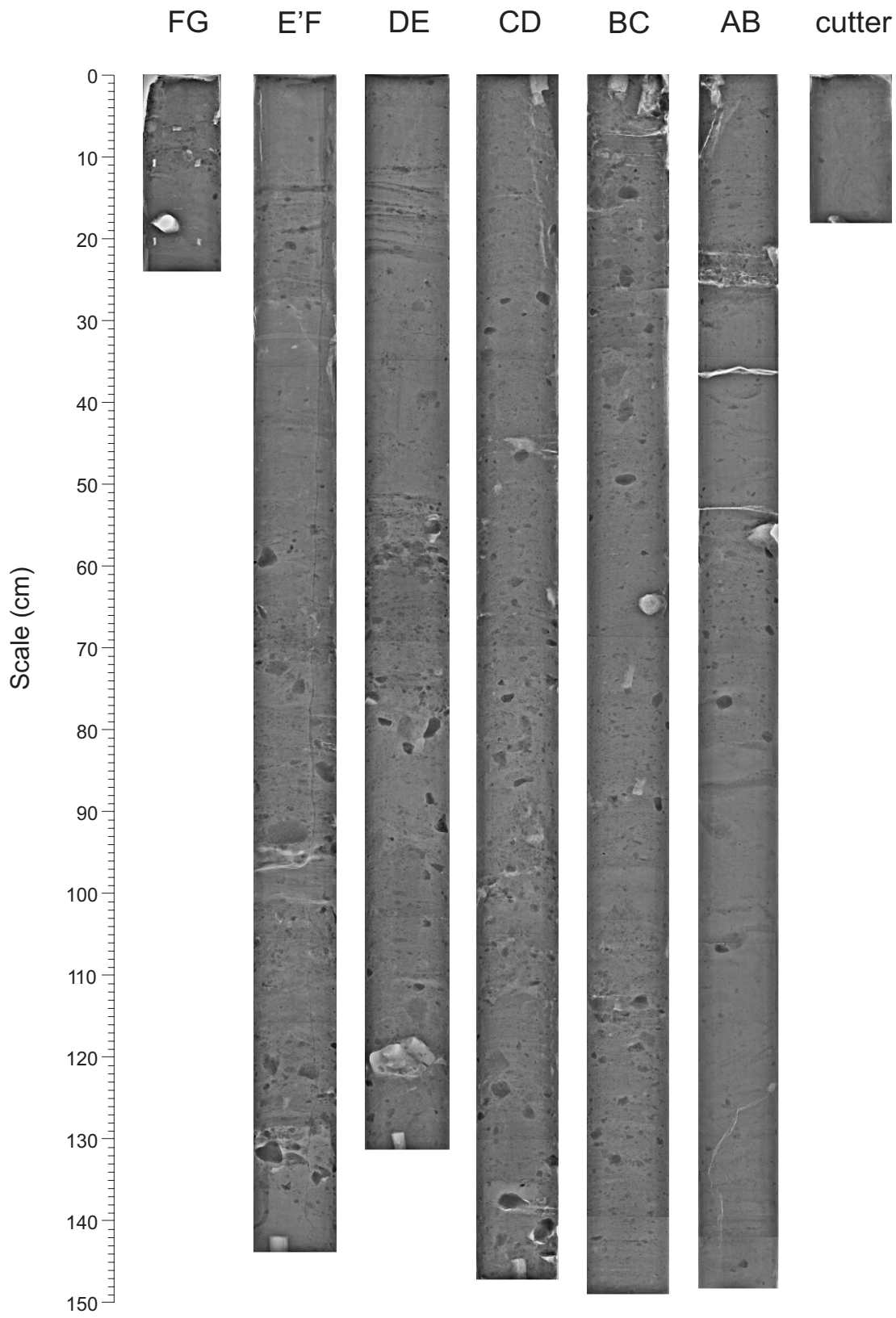
BC

AB

cutter

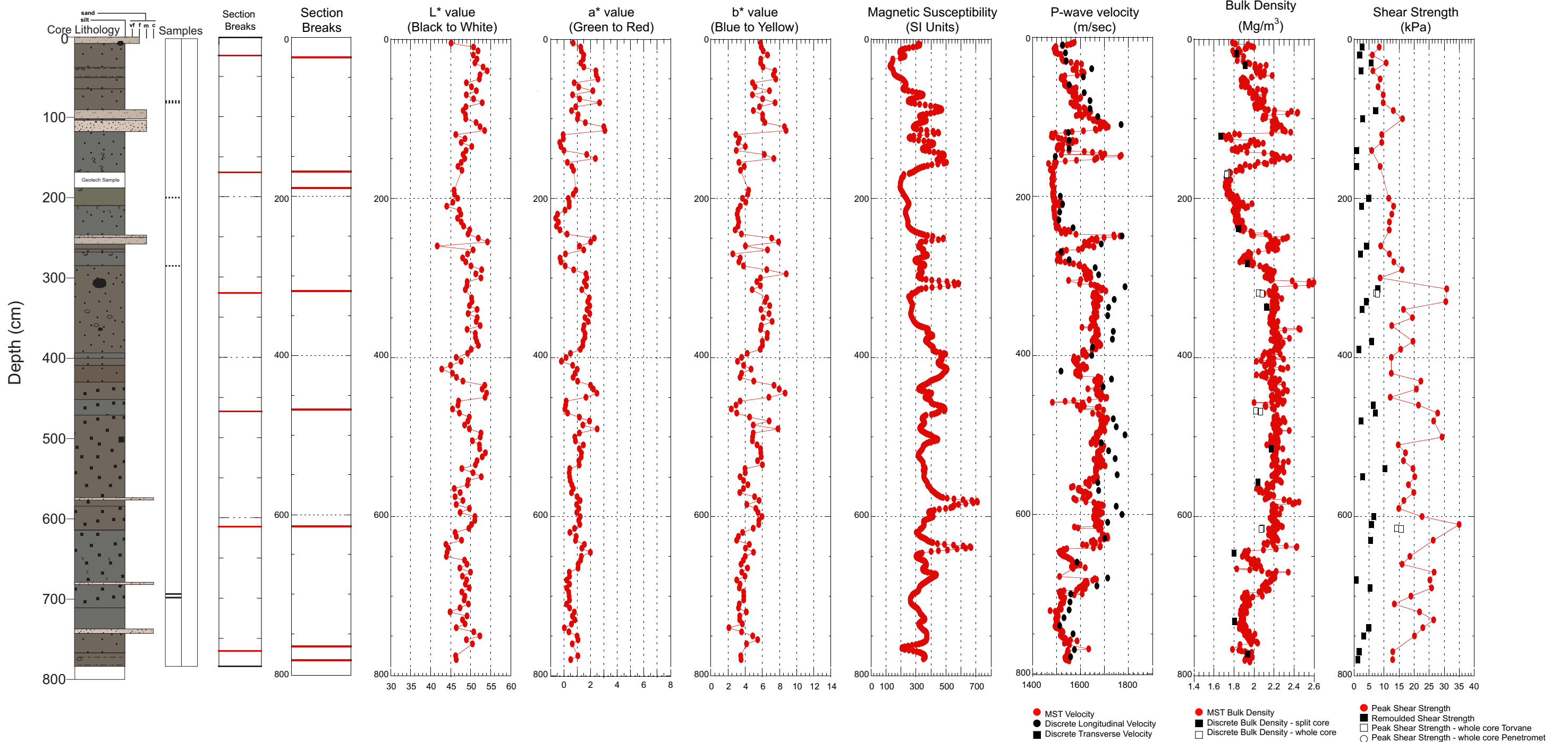


2006040 0006 Piston Core

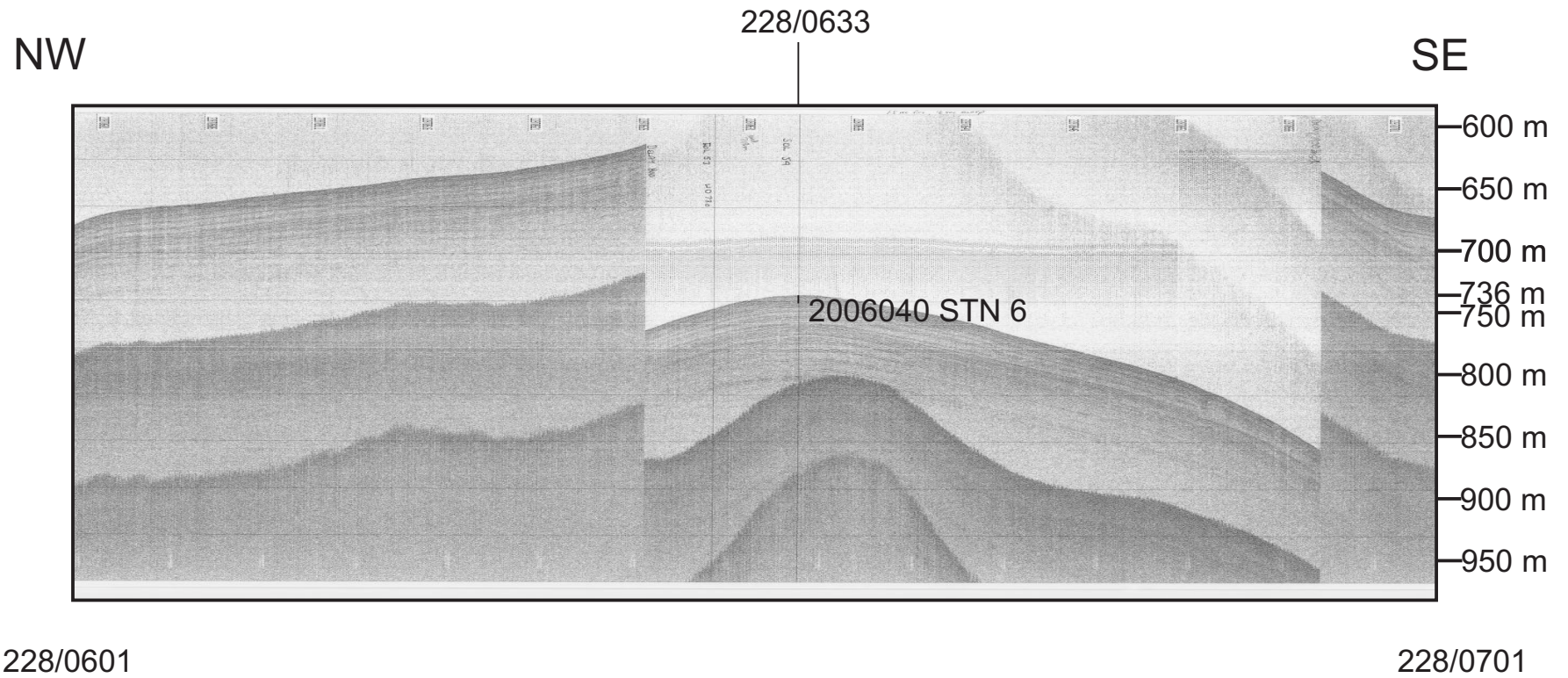


Hudson 2006040 Piston Core 0006

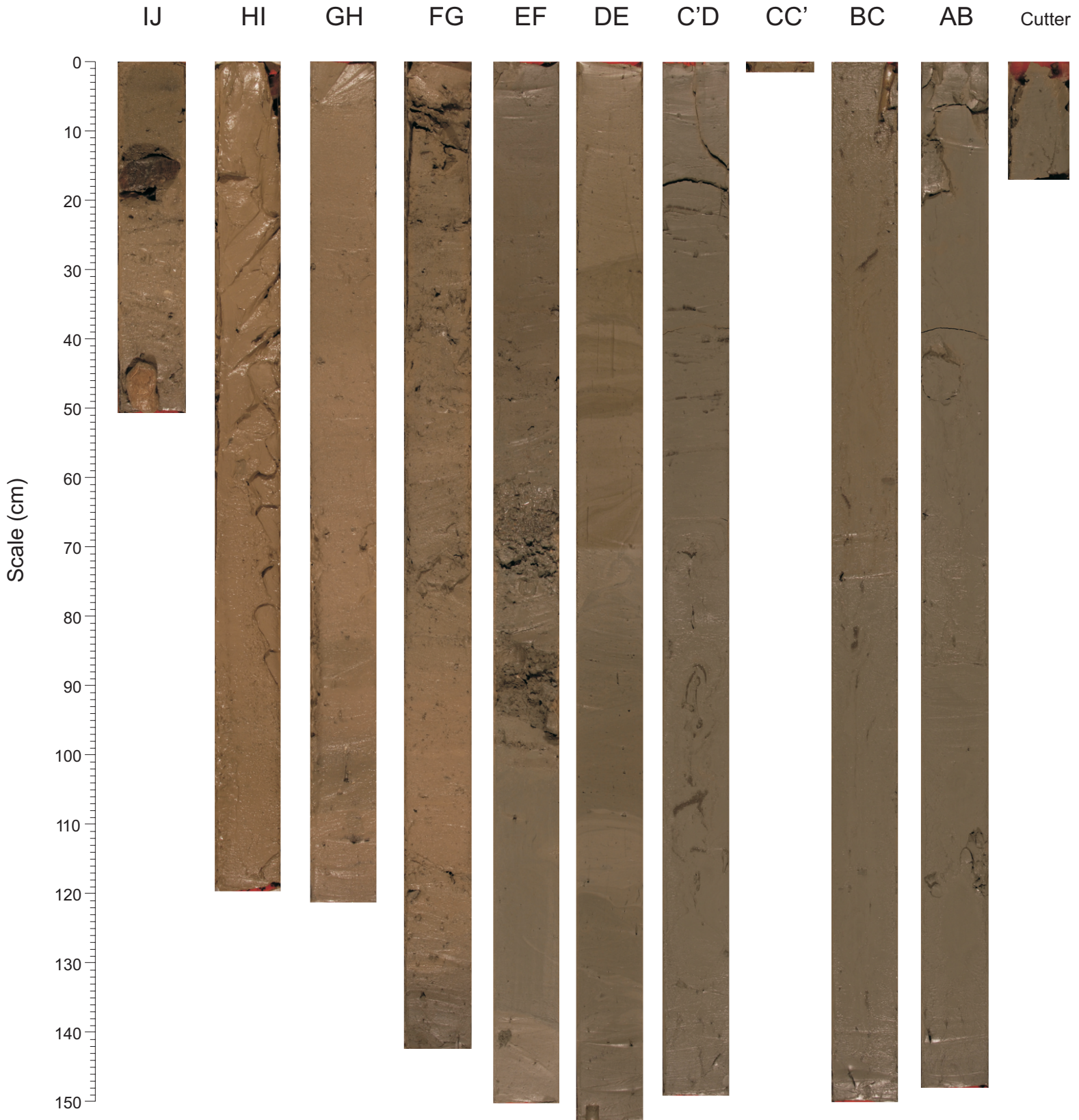
TD 784 cm 54°40.6617 N 53°9.4374 W Water depth 736 m



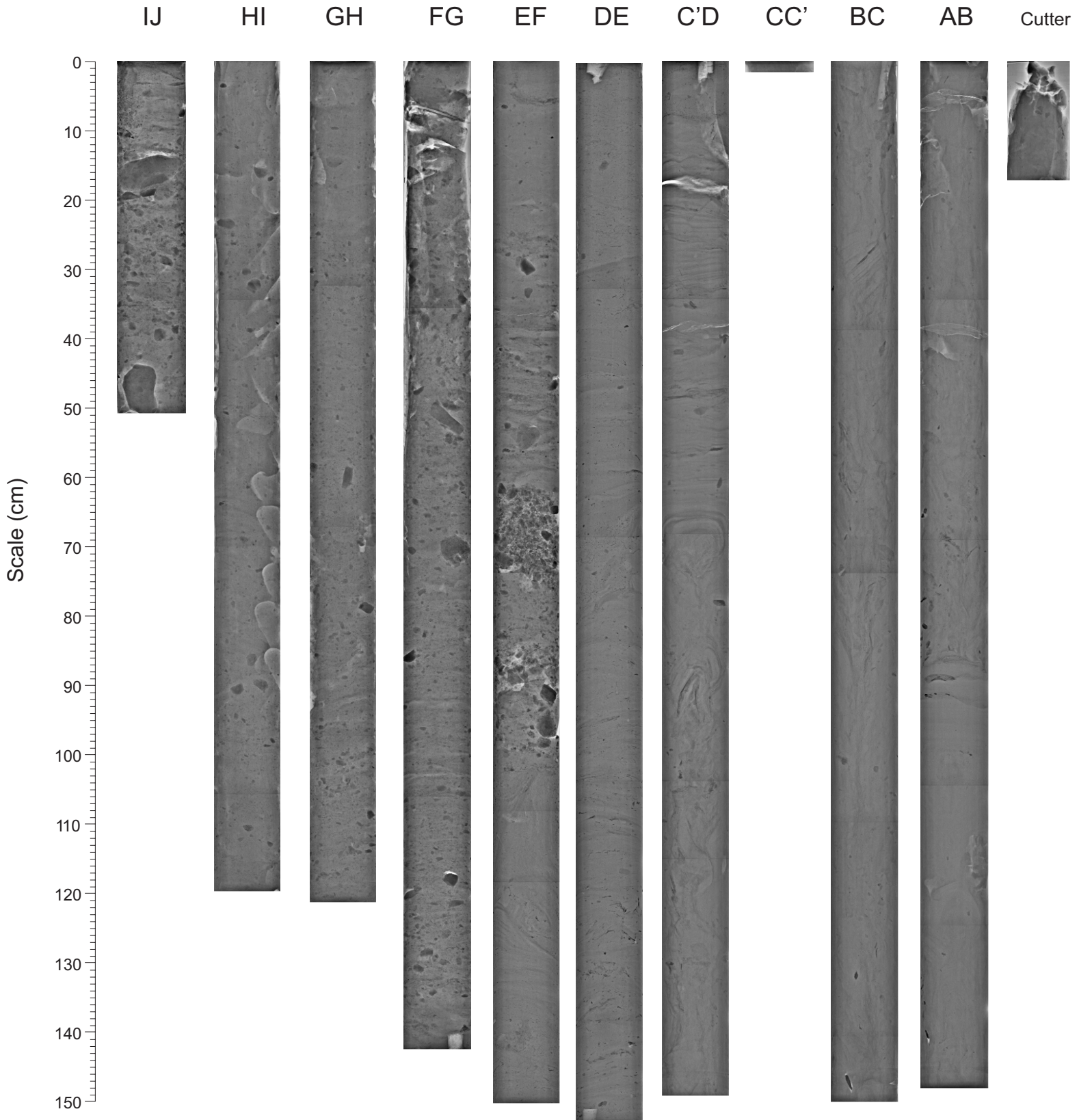
2006040-0006 PC Hunttec Figure



2006040 0037 Piston Core

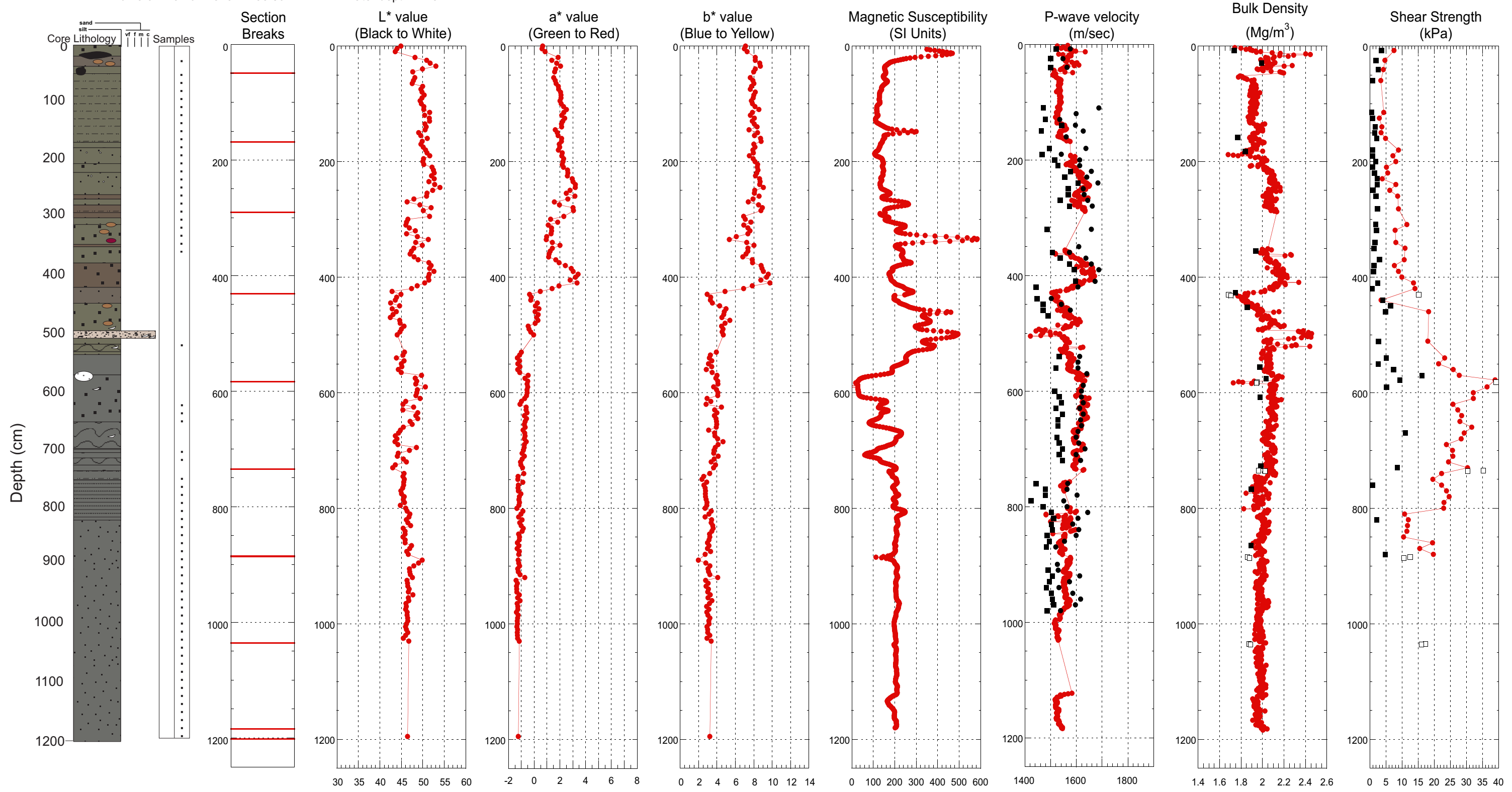


2006040 0037 Piston Core



Hudson 2006040 Piston Core 0037

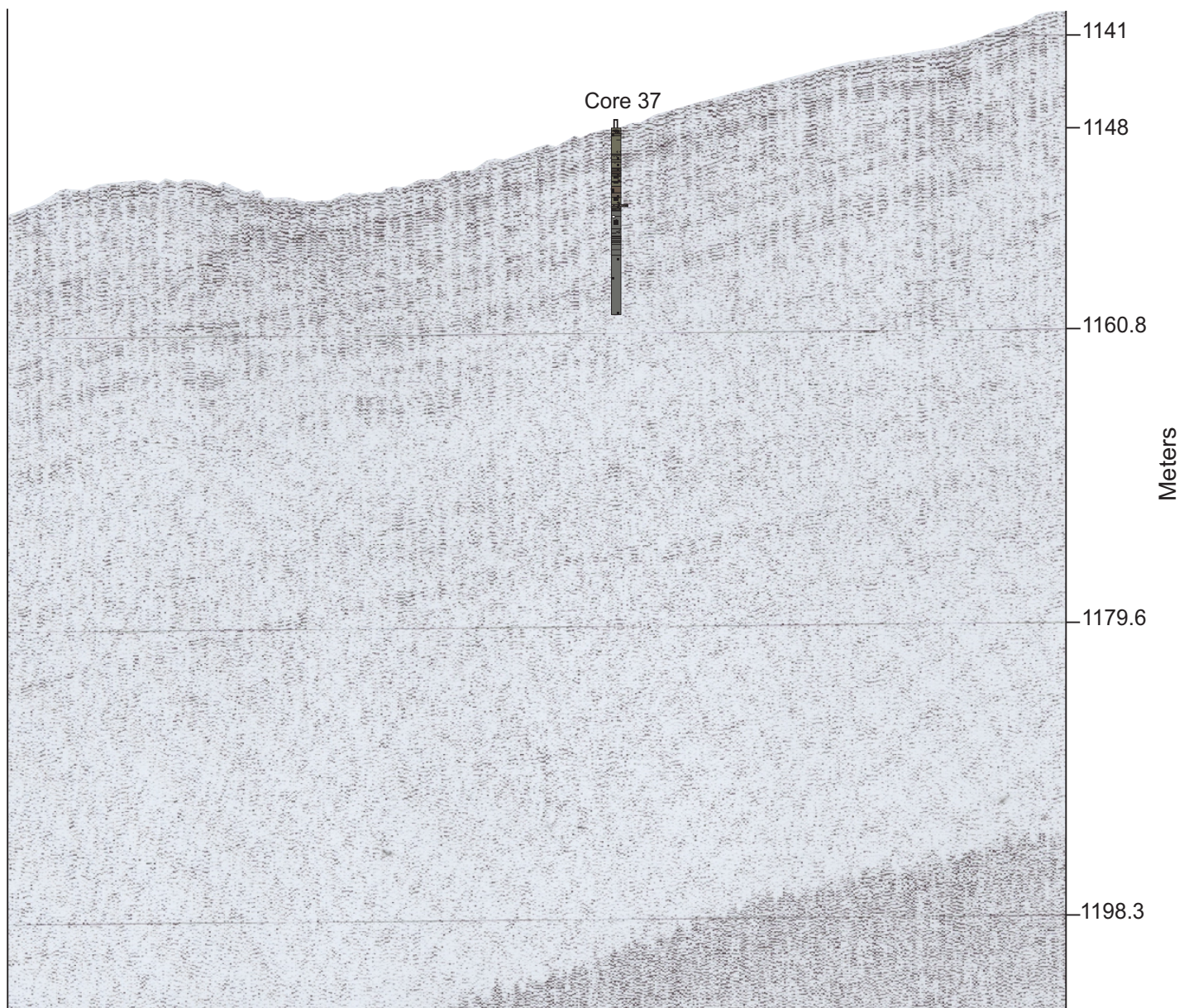
TD 1201.5 cm 57°02.2525 N 58°39.7722 W Water depth 1148 m



- MST Velocity
- Discrete Longitudinal Velocity
- Discrete Transverse Velocity
- MST Bulk Density
- Discrete Bulk Density - split core
- Discrete Bulk Density - whole core
- Peak Shear Strength
- Remoulded Shear Strength
- Peak Shear Strength - whole core Torvane
- Peak Shear Strength - whole core Penetromet

NE

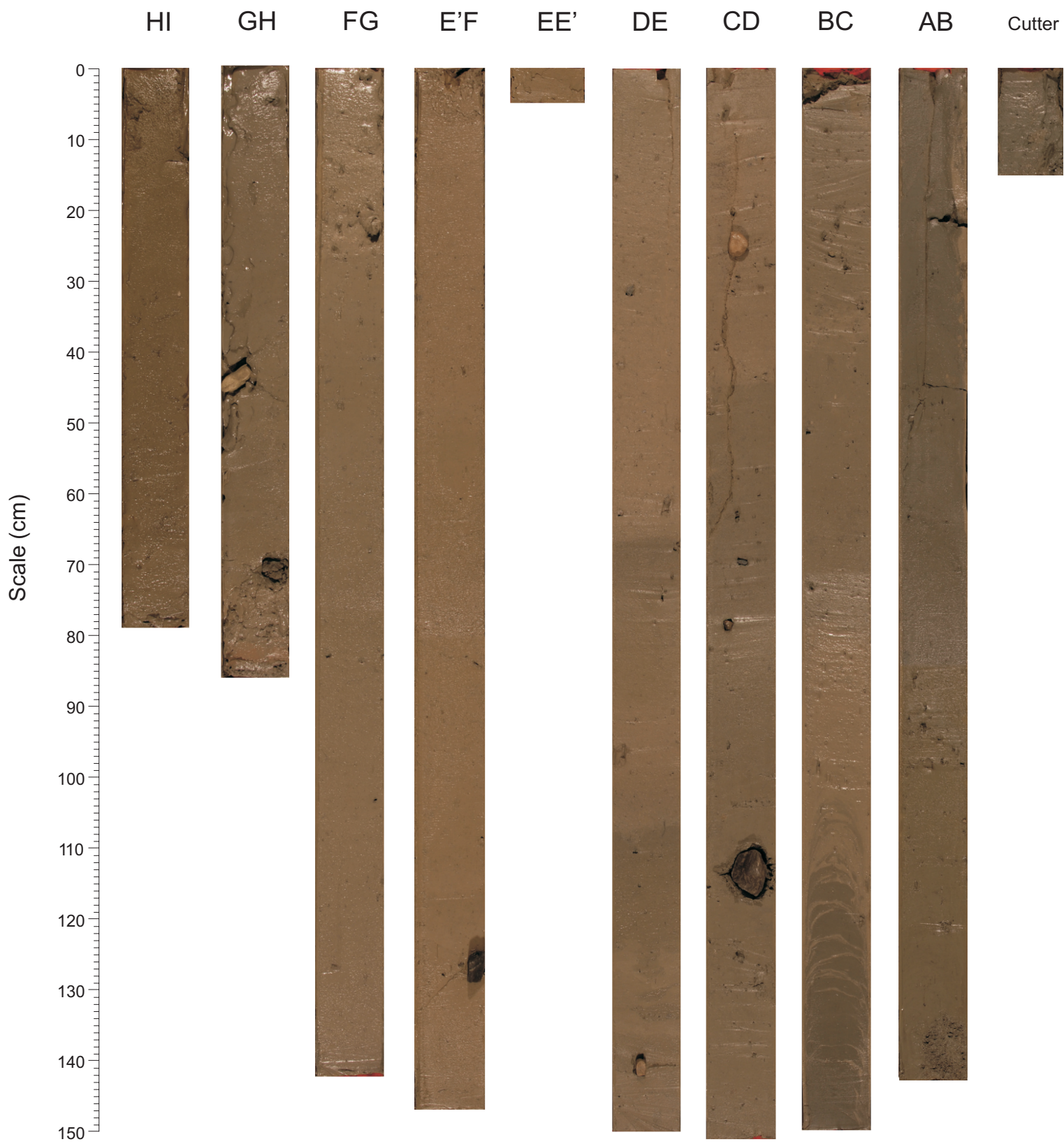
SW



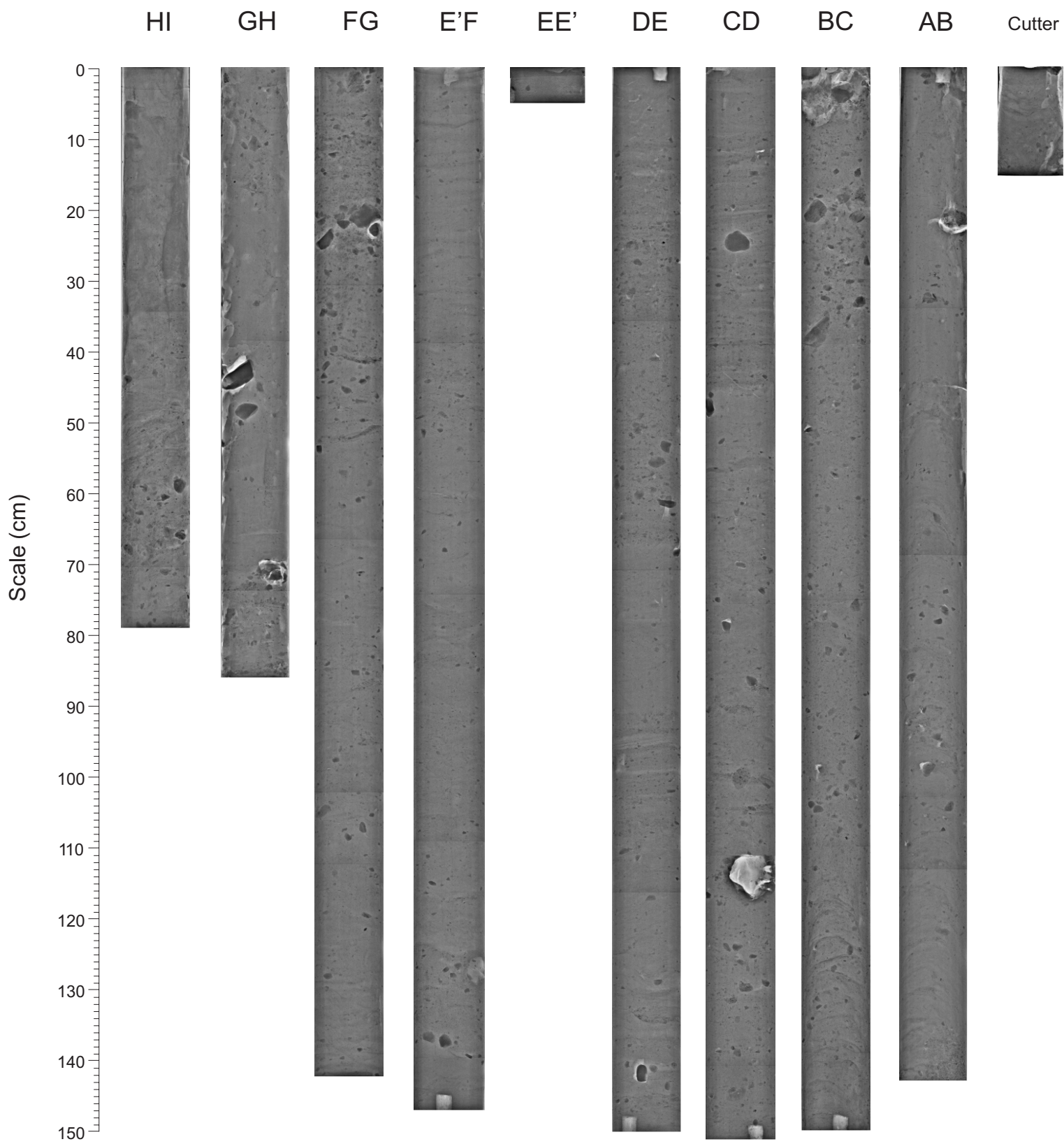
226/0751

226/0800

2006040 0038 Piston Core

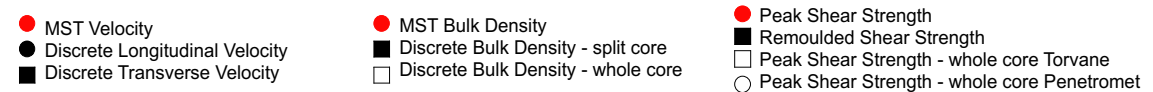
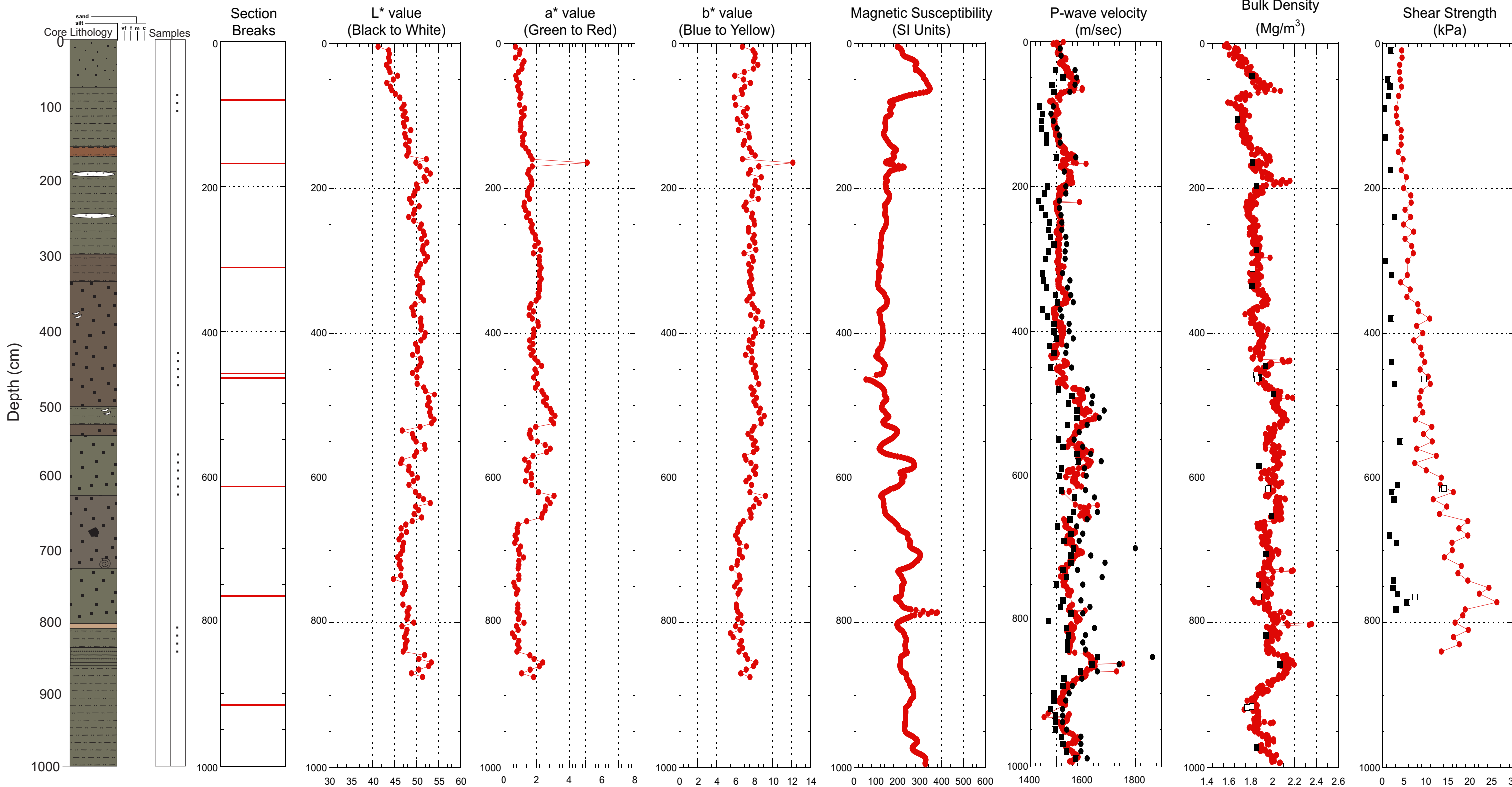


2006040 0038 Piston Core



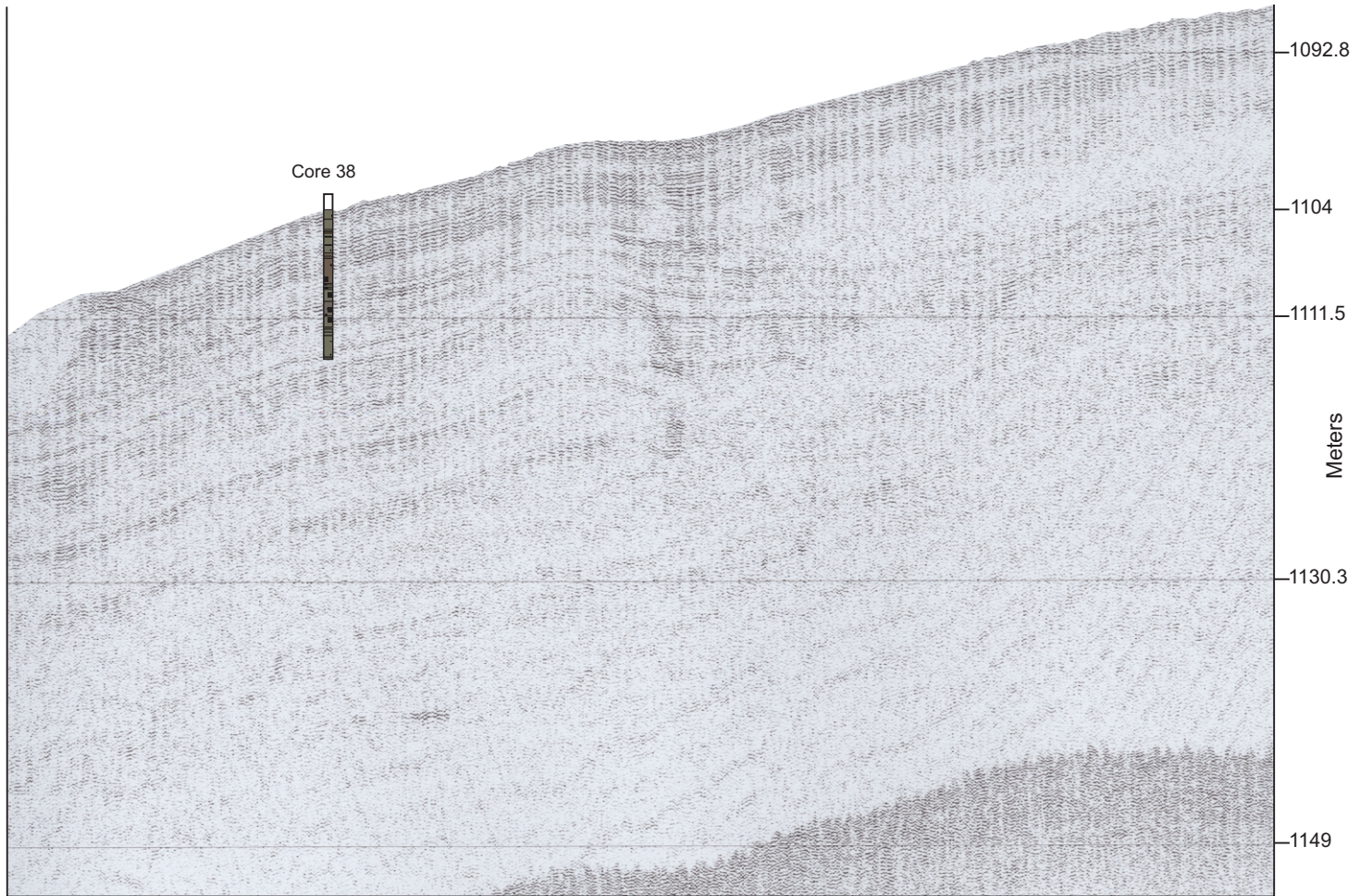
Hudson 2006040 Piston Core 0038

TD 1076 cm 57°01.2482 N 58°42.1321 W Water depth 1104 m



NE

SW



226/0812

226/0825

2006040 0039 Piston Core

HI

GH

FG

EF

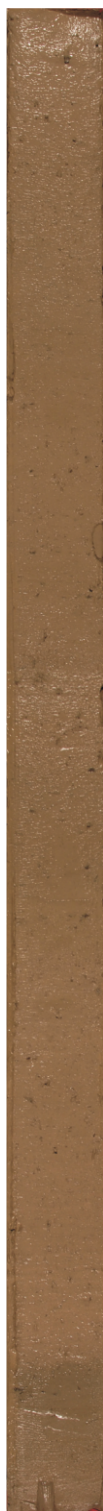
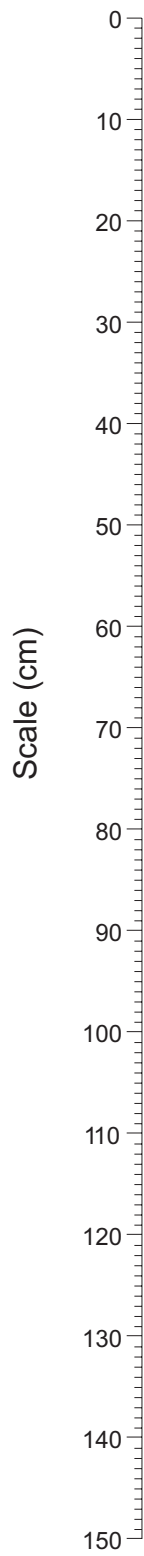
DE

CD

BC

AB

Cutter



2006040 0039 Piston Core

HI

GH

FG

EF

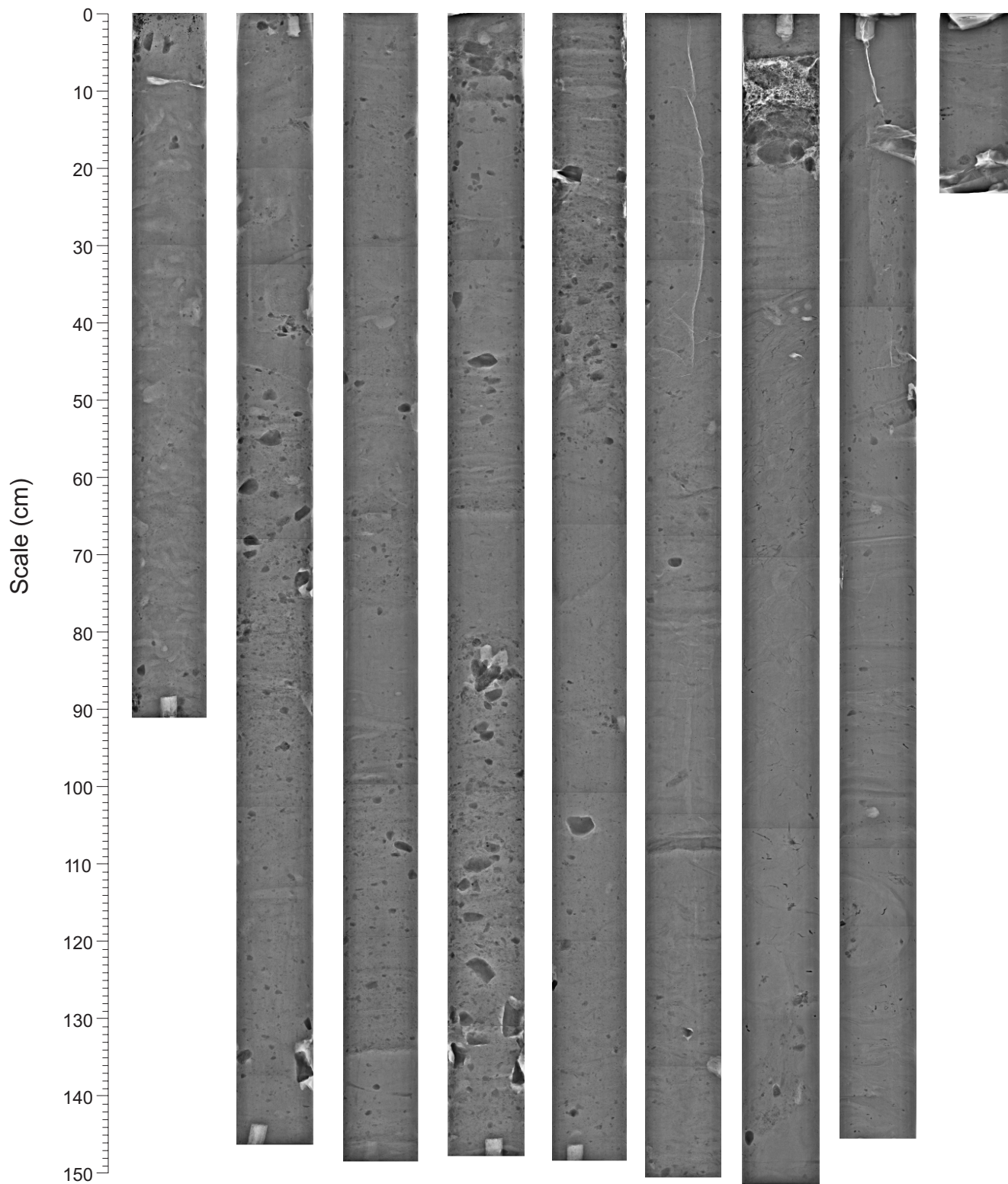
DE

CD

BC

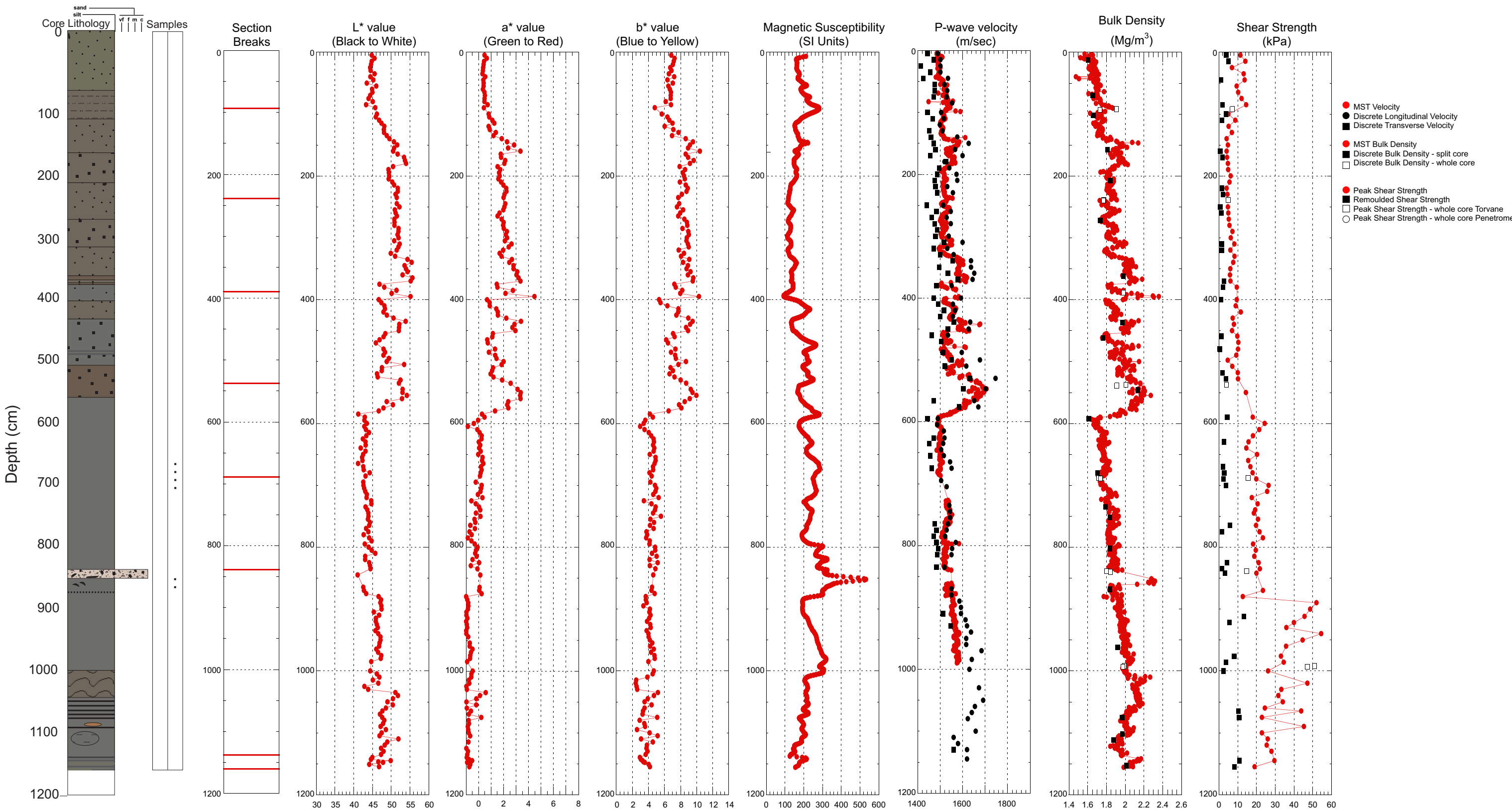
AB

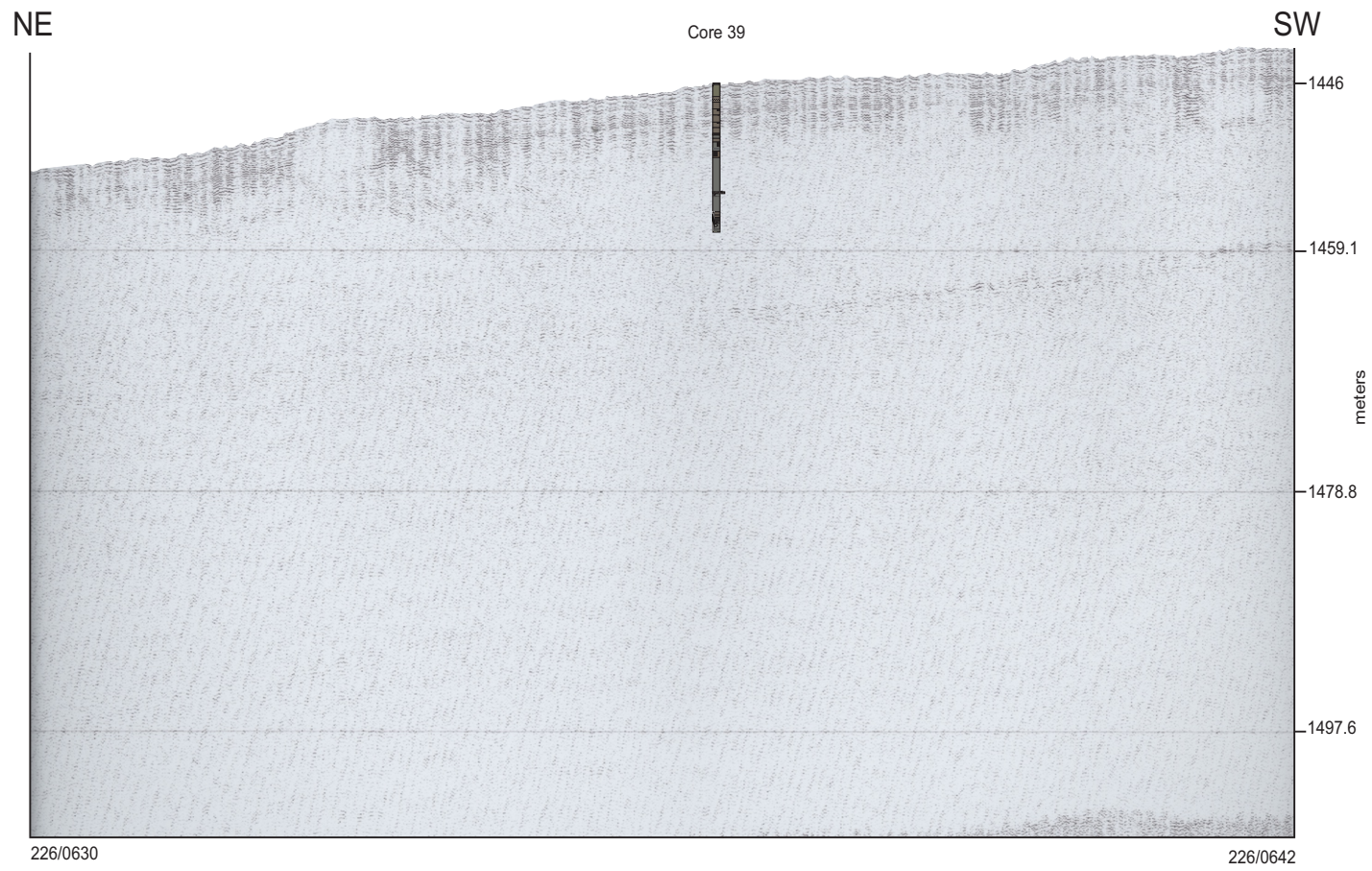
Cutter



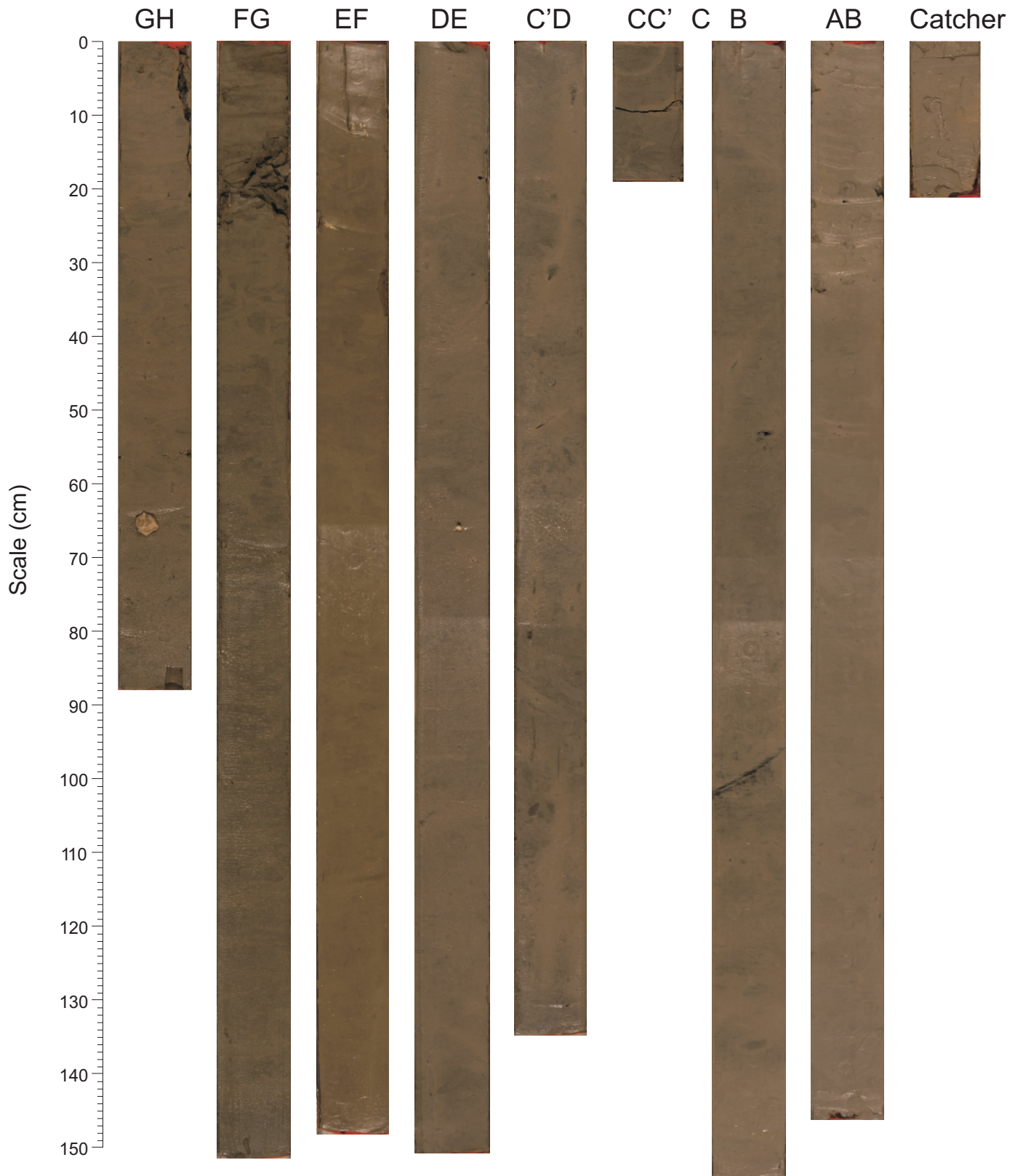
Hudson 2006040 Piston Core 0039

TD 1161 cm 57°06.0781 N 58°30.8505 W Water depth 1446 m

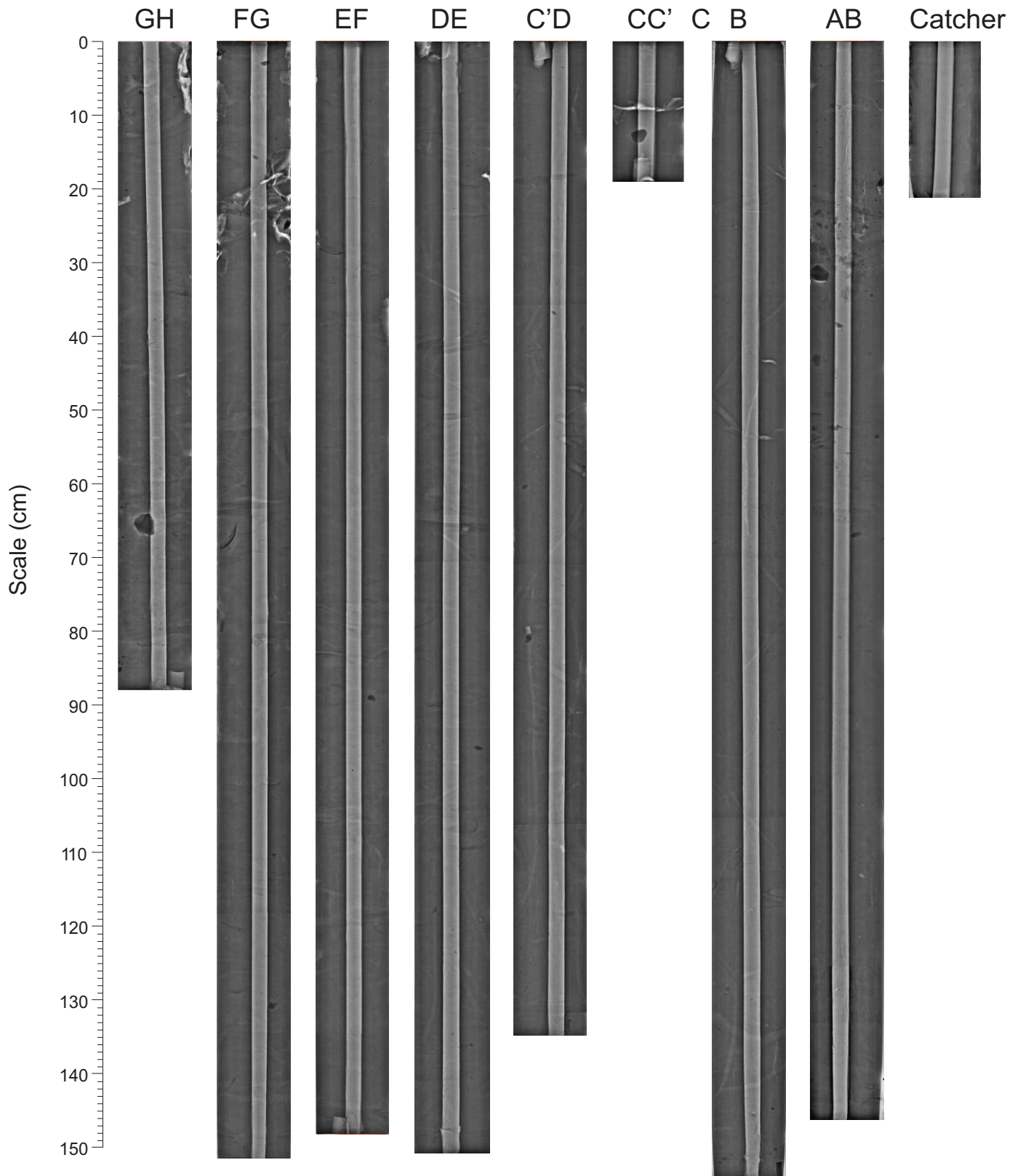




2006040 0040 Piston Core

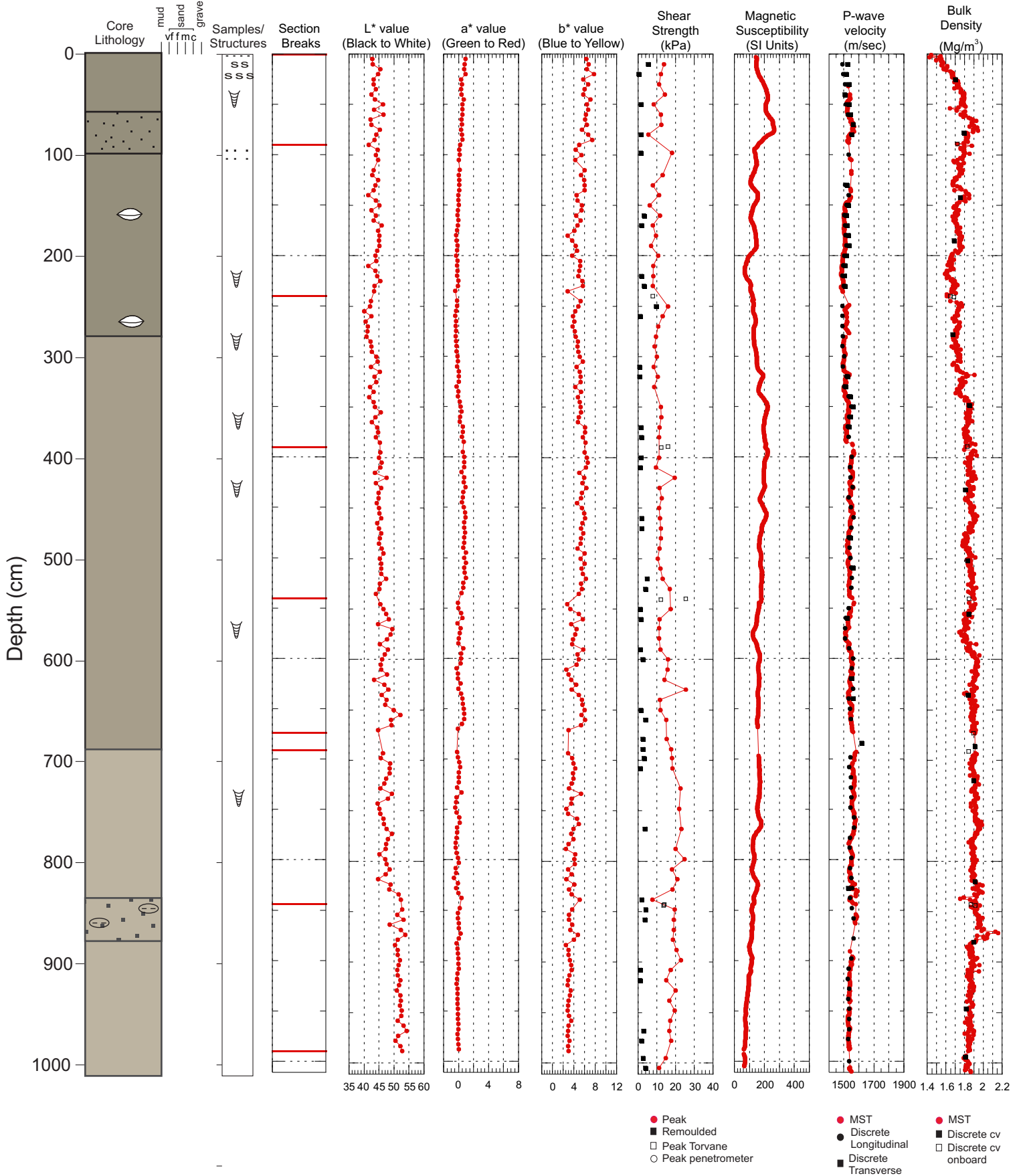


2006040 0040 Piston Core

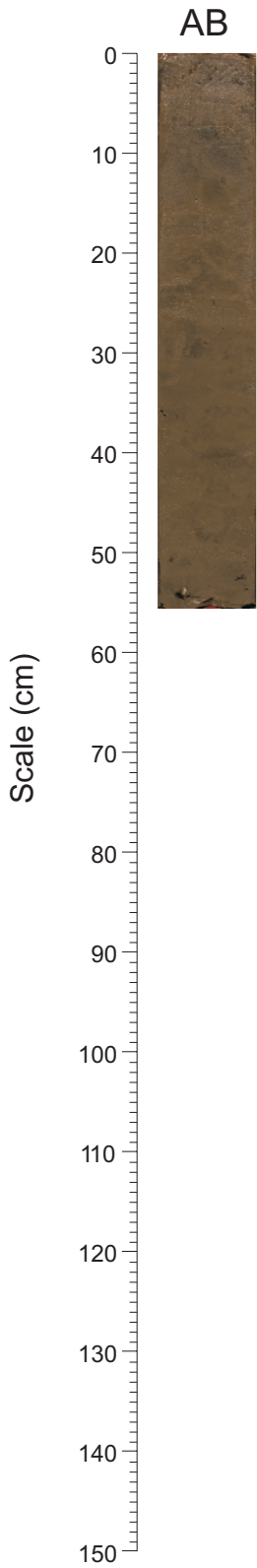


Hudson 2006040 Piston Core 0040

TD 1011cm 58.758385° N -61.868660° W Water depth 203 m

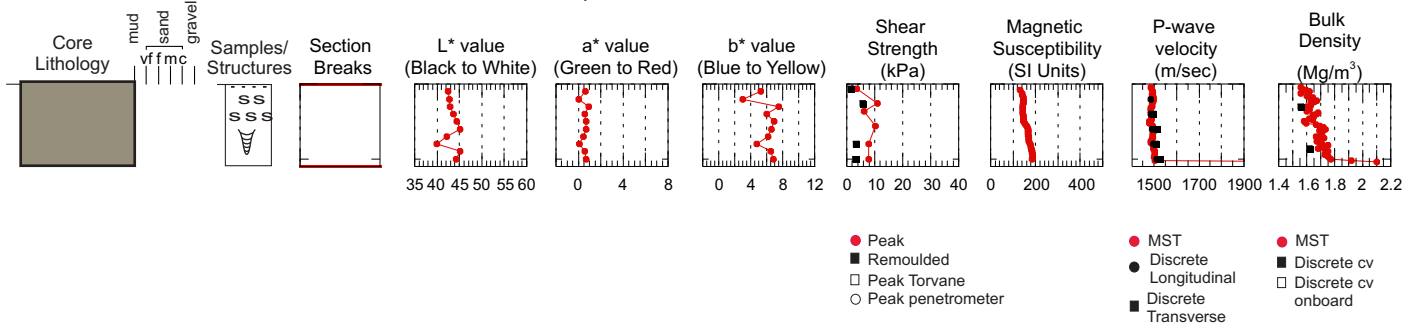


2006040 0040 Trigger Weight Core



Hudson 2006040 Trigger Weight Core 0040

TD 55cm 58.758385° N -61.868660° W Water depth 203 m



2006040 0041 Piston Core

DE

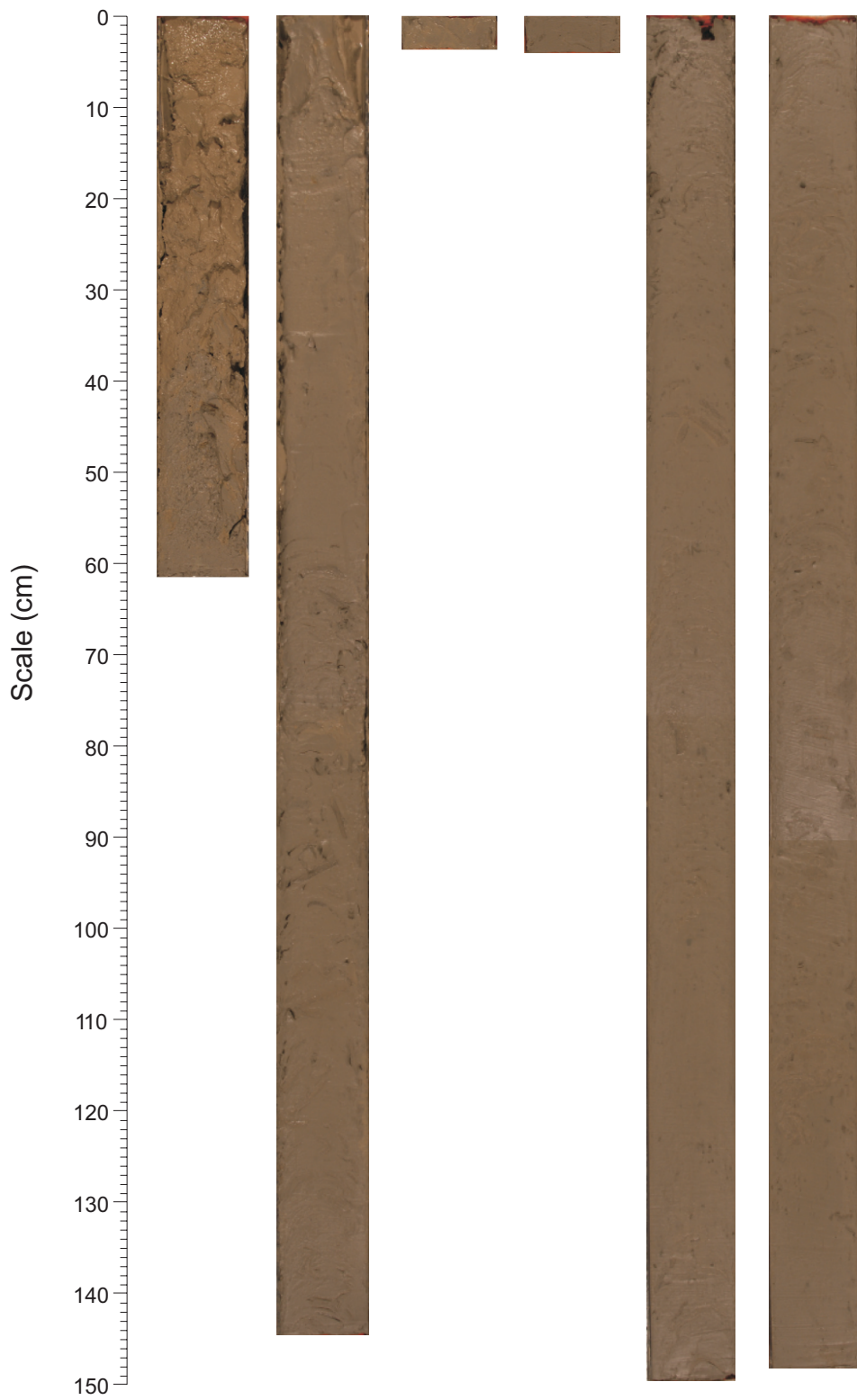
C'D

C'C''

CC'

BC

AB



2006040 0041 Piston Core

DE

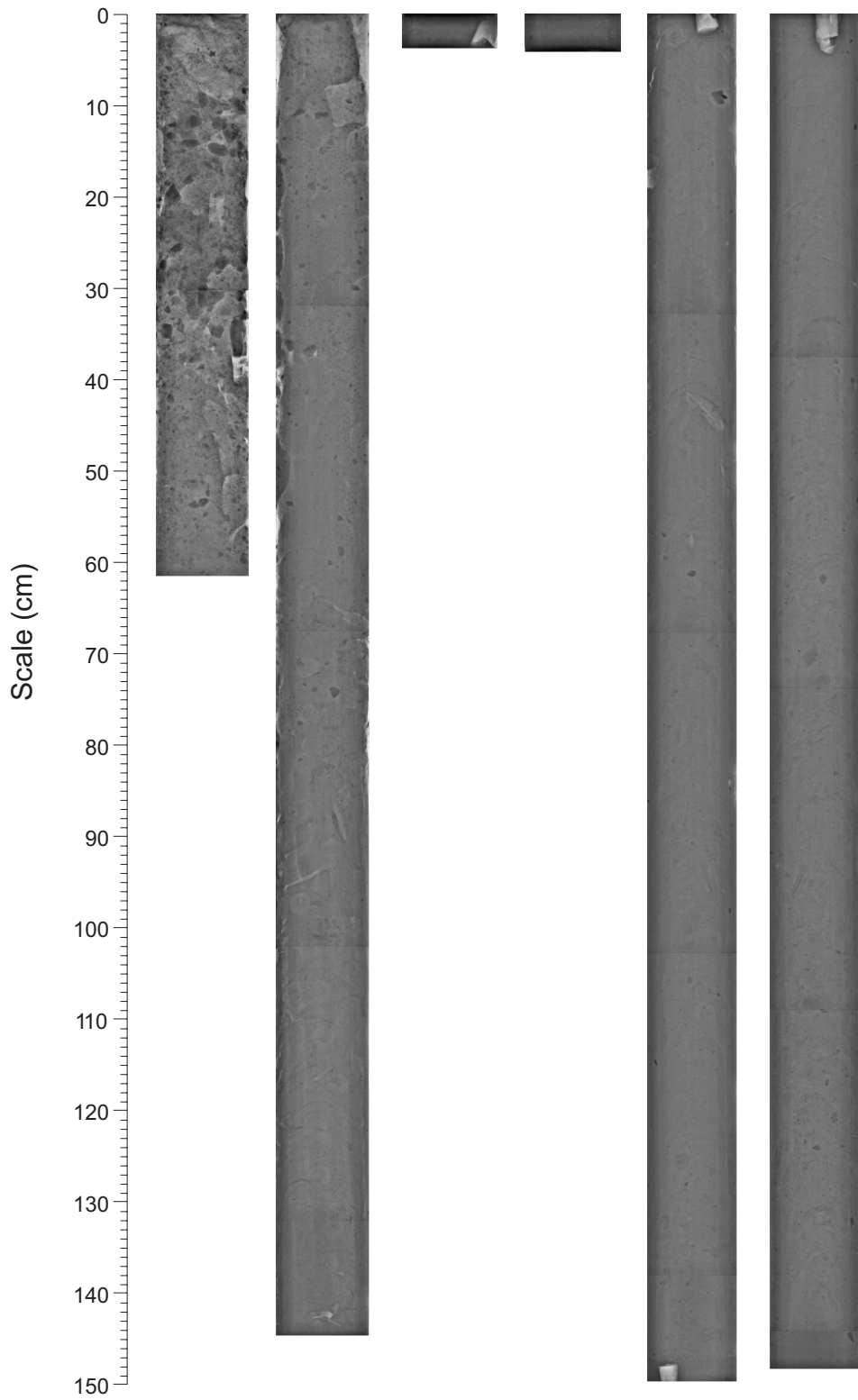
C'D

C'C''

CC'

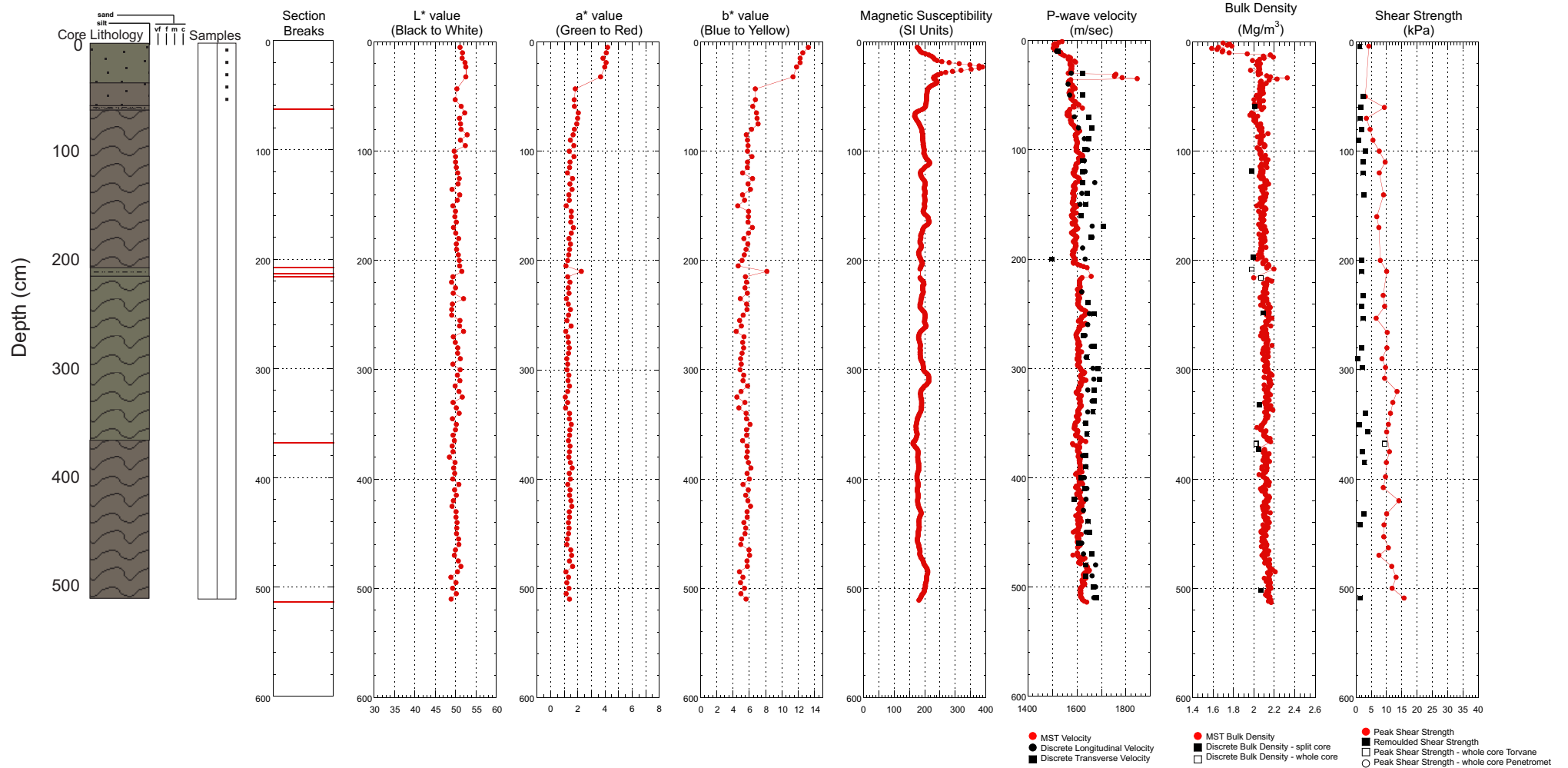
BC

AB



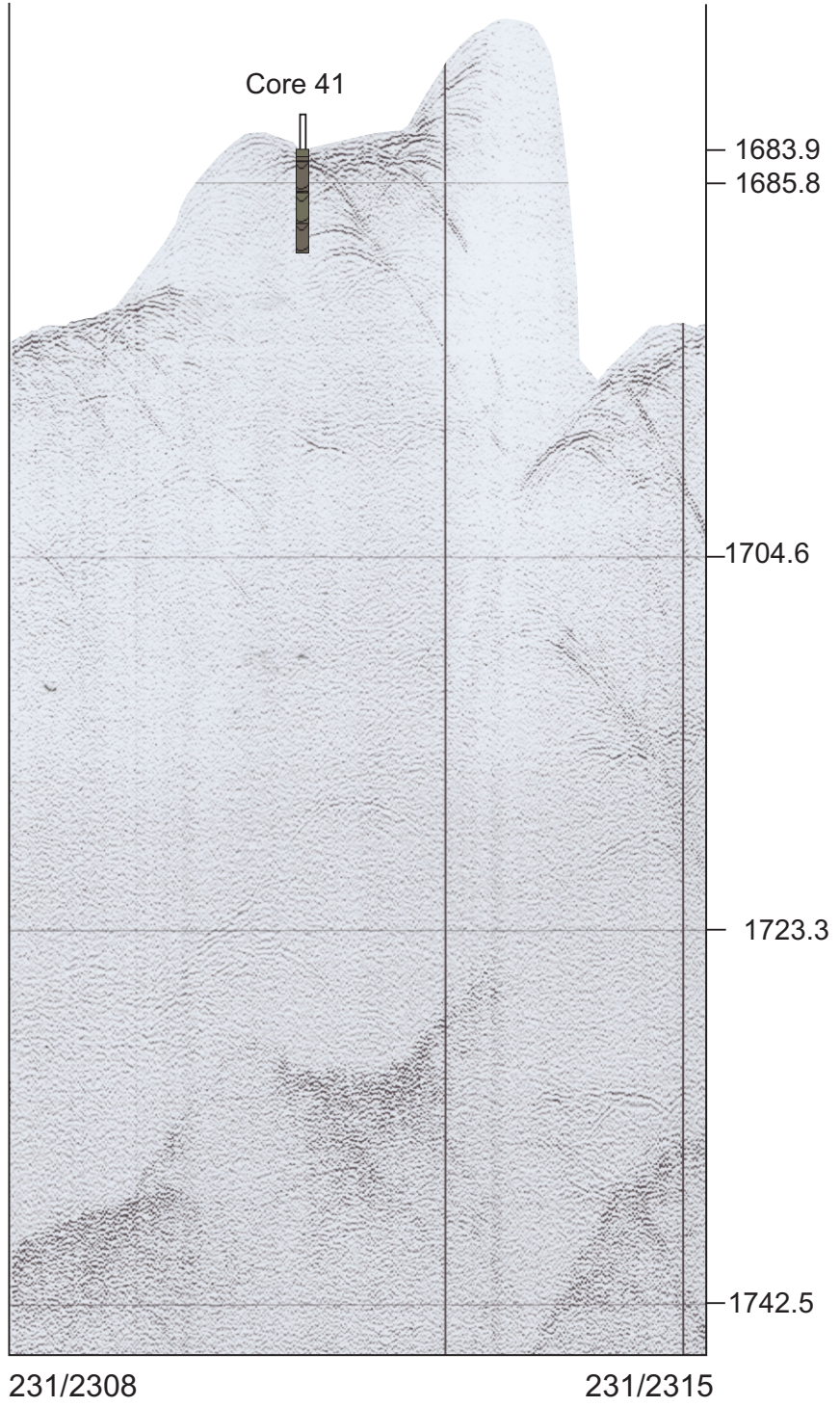
Hudson 2006040 Piston Core 0041

TD 515 cm 61°18.6134 N 60°19.8703 W Water depth 1683.9 m



SW

NE

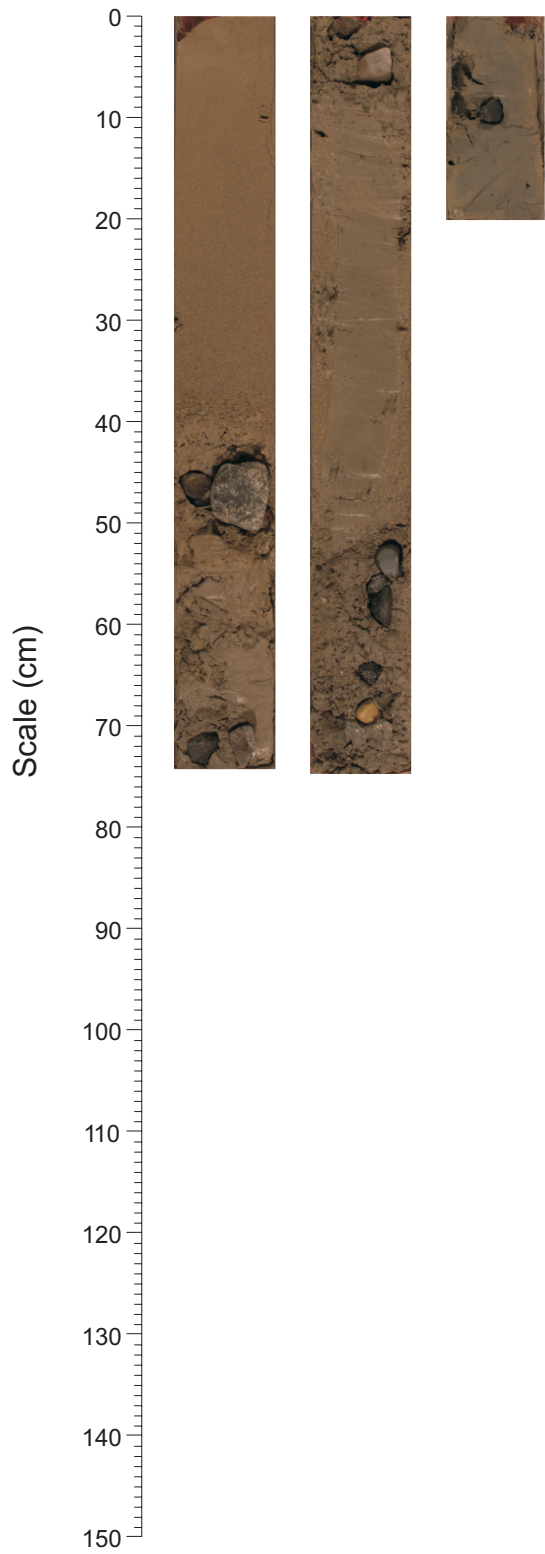


2006040 0042 Piston Core

BC

AB

Catcher

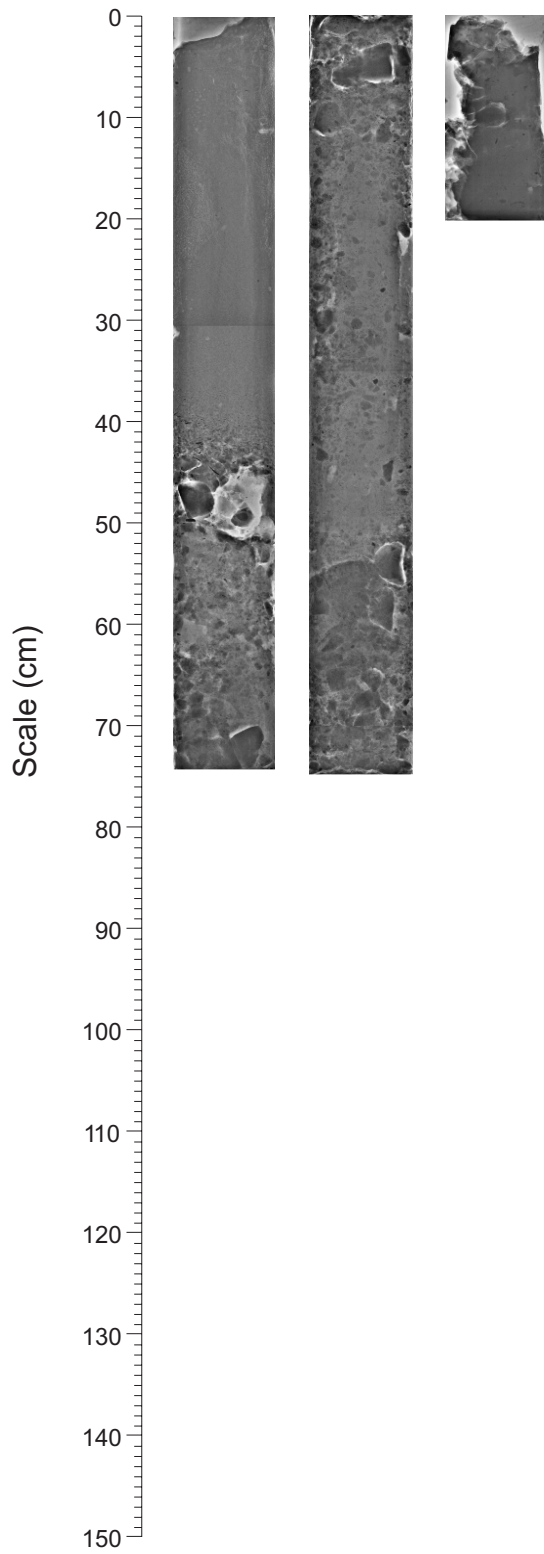


2006040 0042 Piston Core

BC

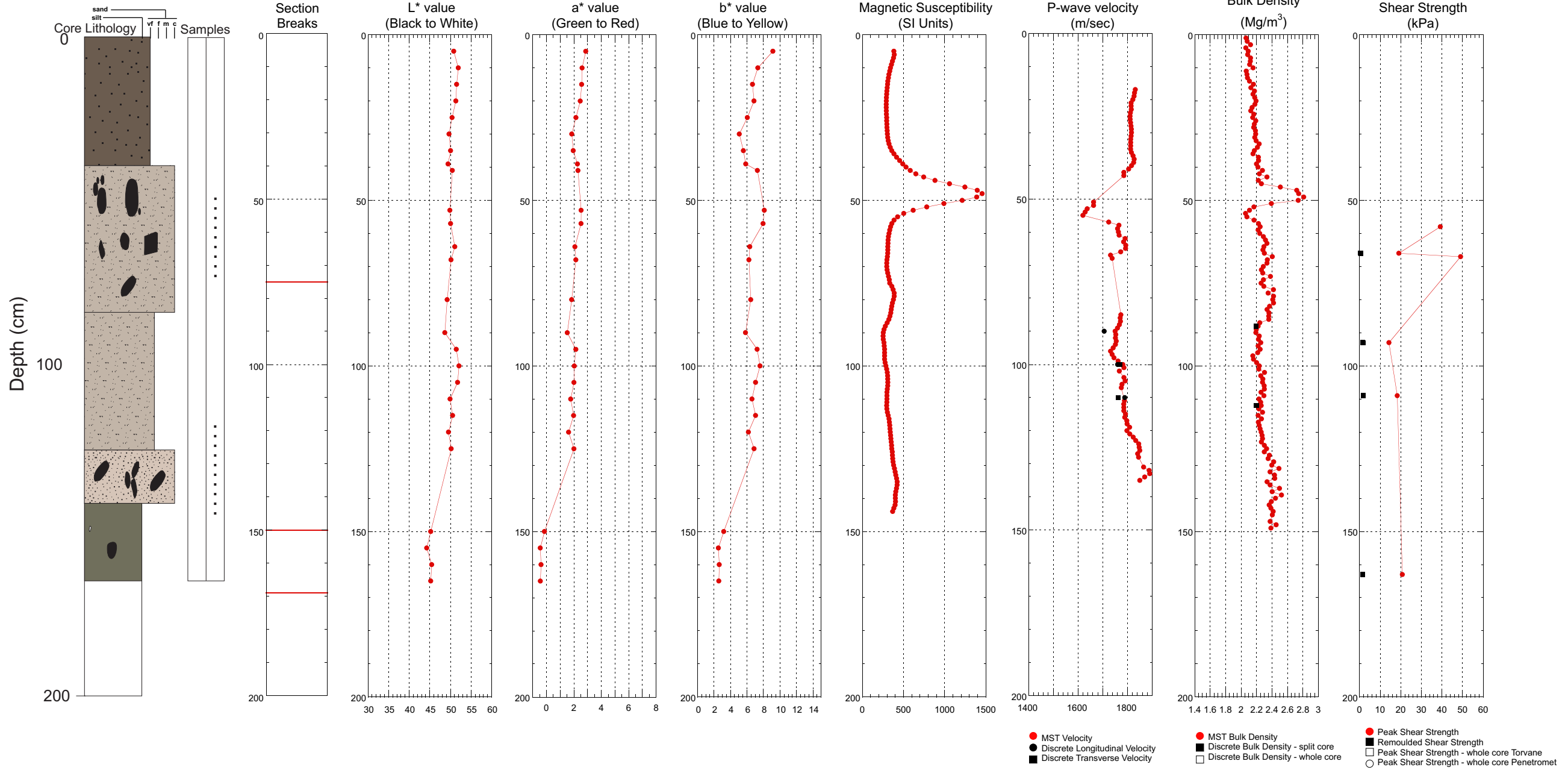
AB

Catcher



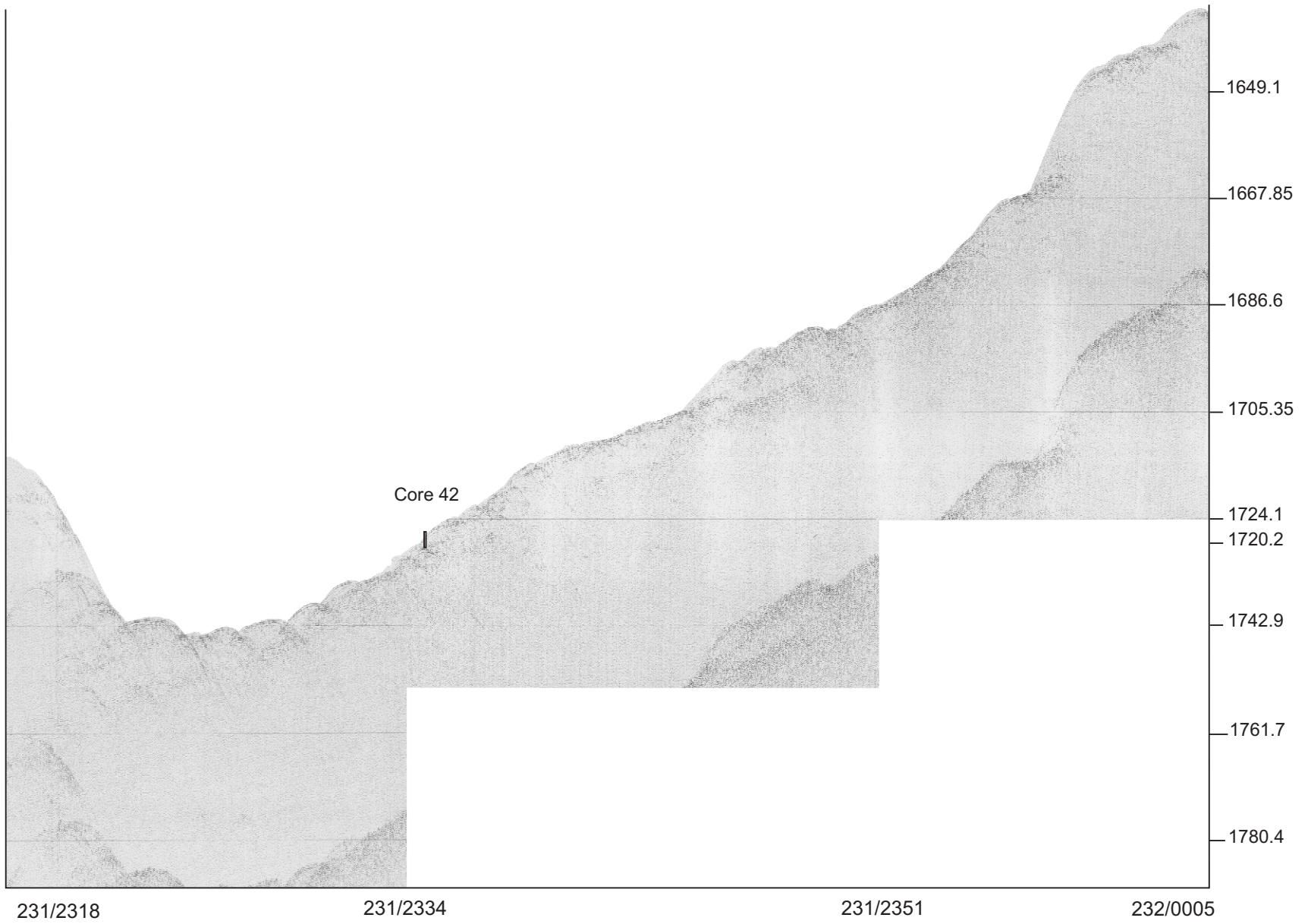
Hudson 2006040 Piston Core 0042

TD 169 cm 61°20.8756 N 60°20.4314 W Water depth 1720.2 m



SE

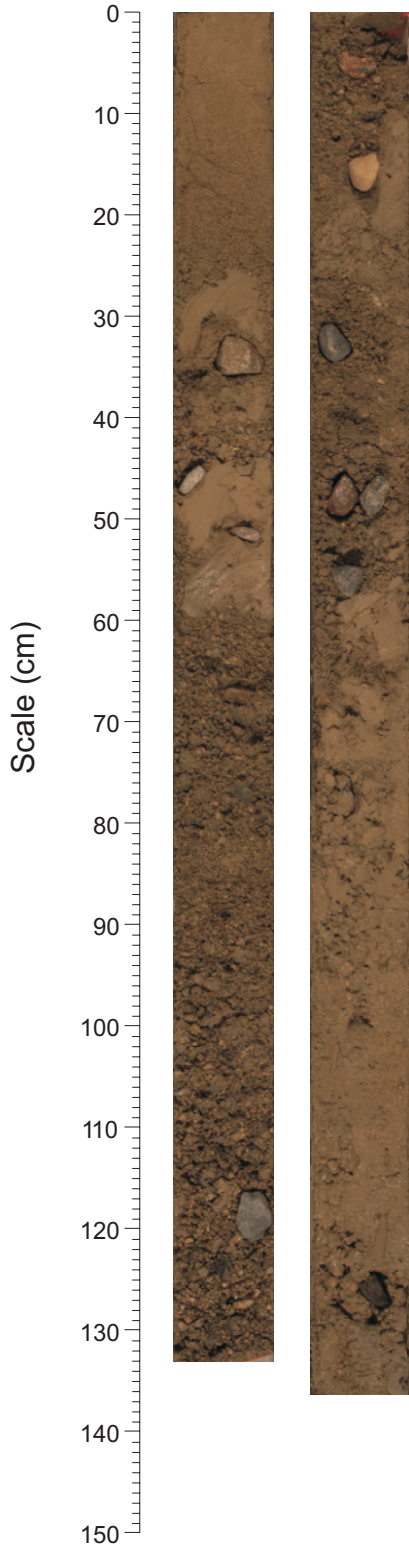
NW



2006040 0043 Piston Core

BC

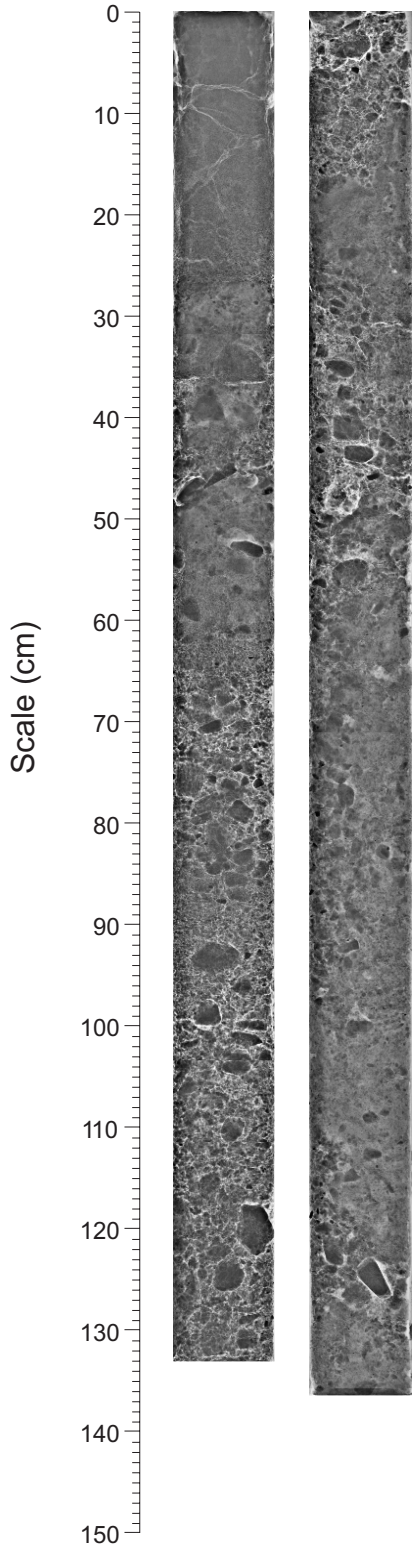
AB



2006040 0043 Piston Core

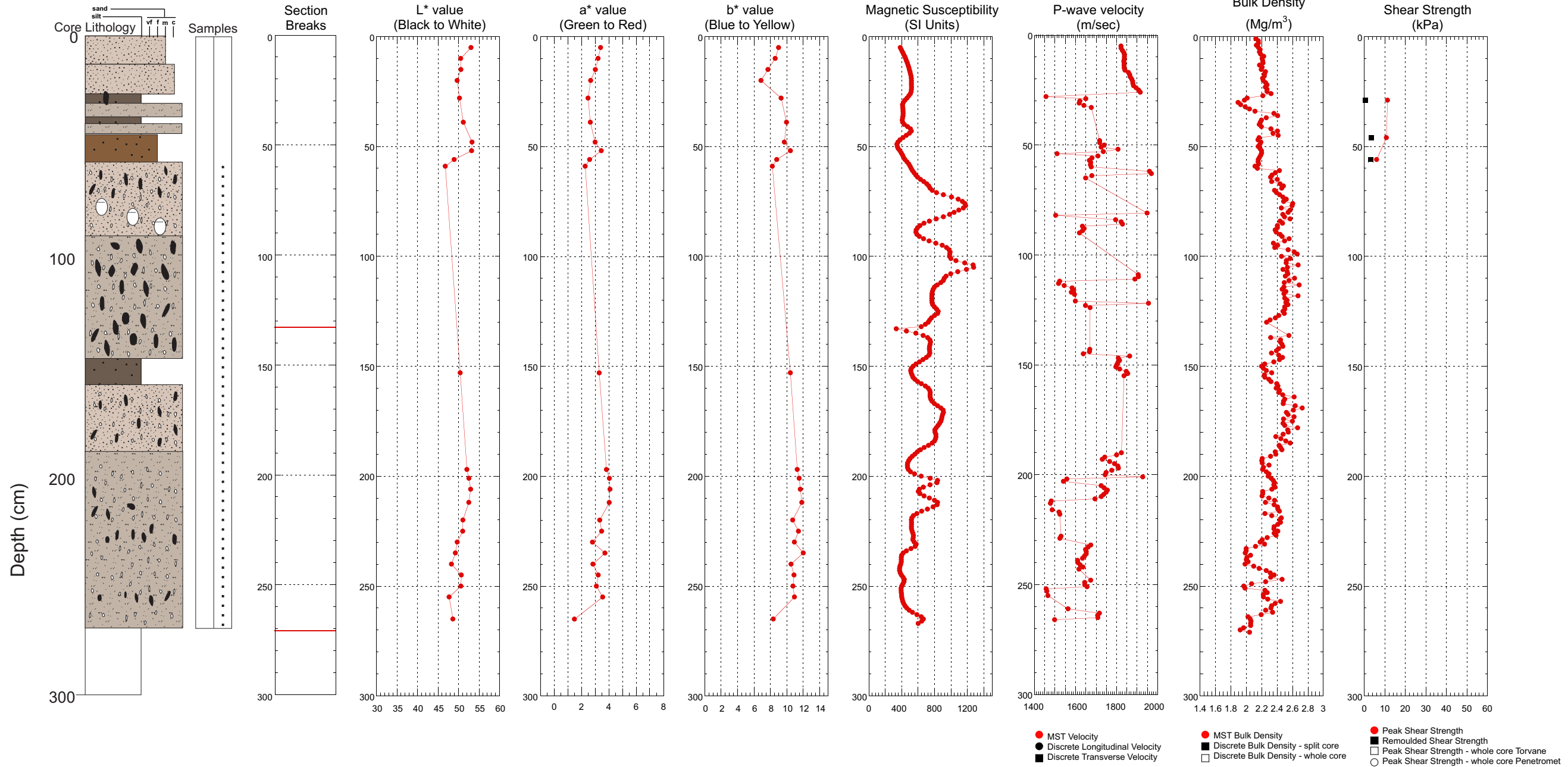
BC

AB



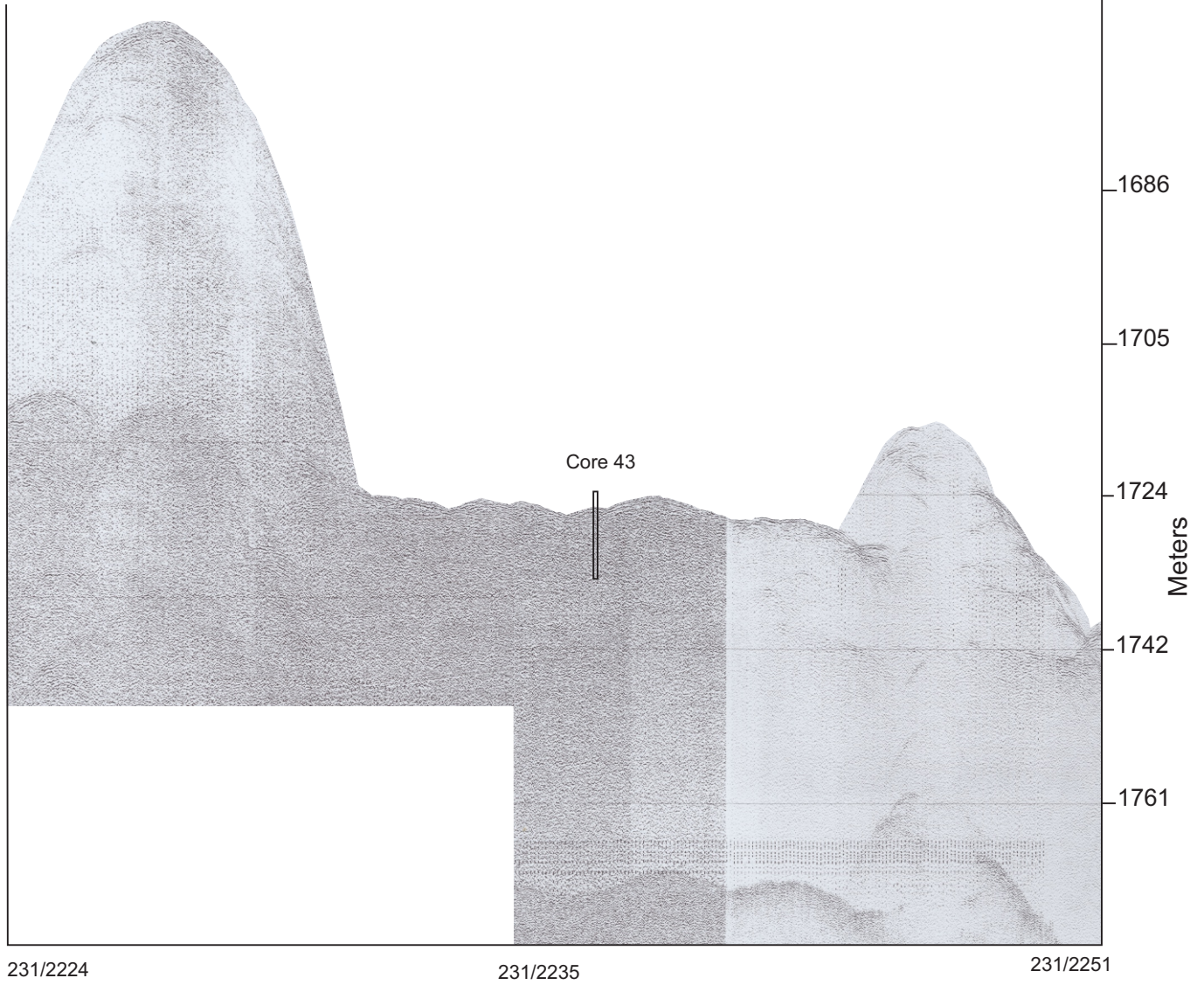
Hudson 2006040 Piston Core 0043

TD 271 cm 61°16.3459 N 60°24.6793 W Water depth 1725.1 m



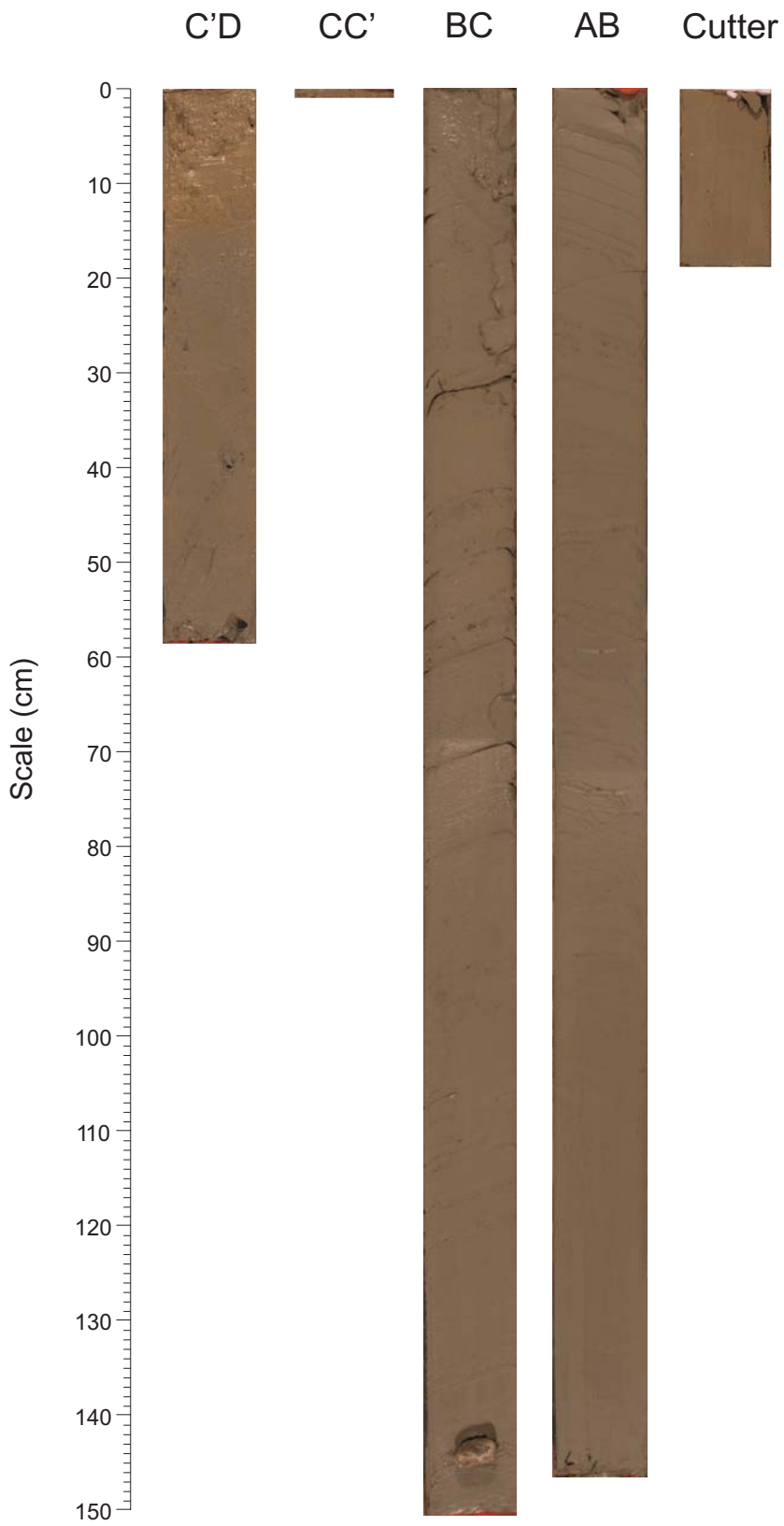
SW

NE

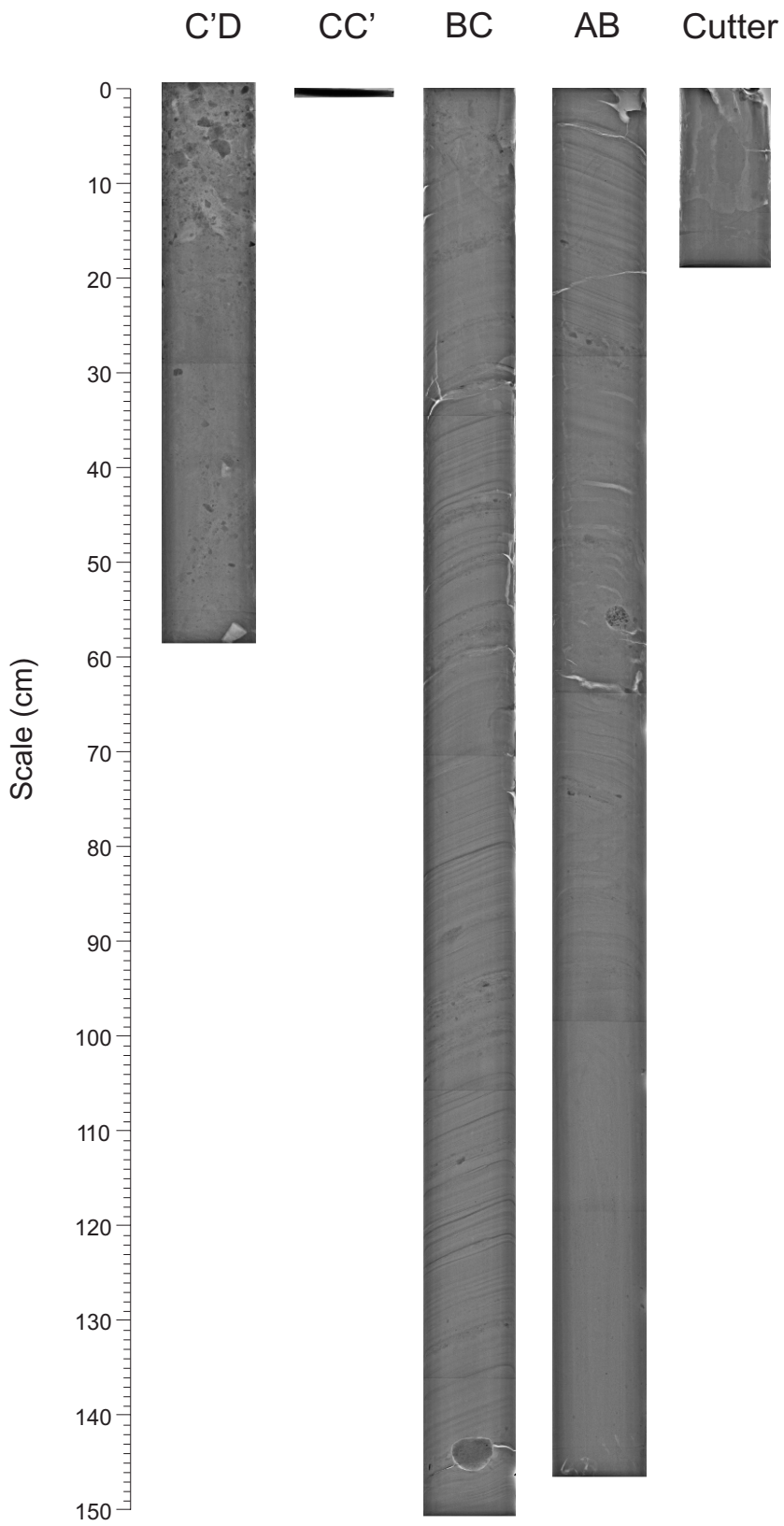


Gully floor

2006040 0044 Piston Core

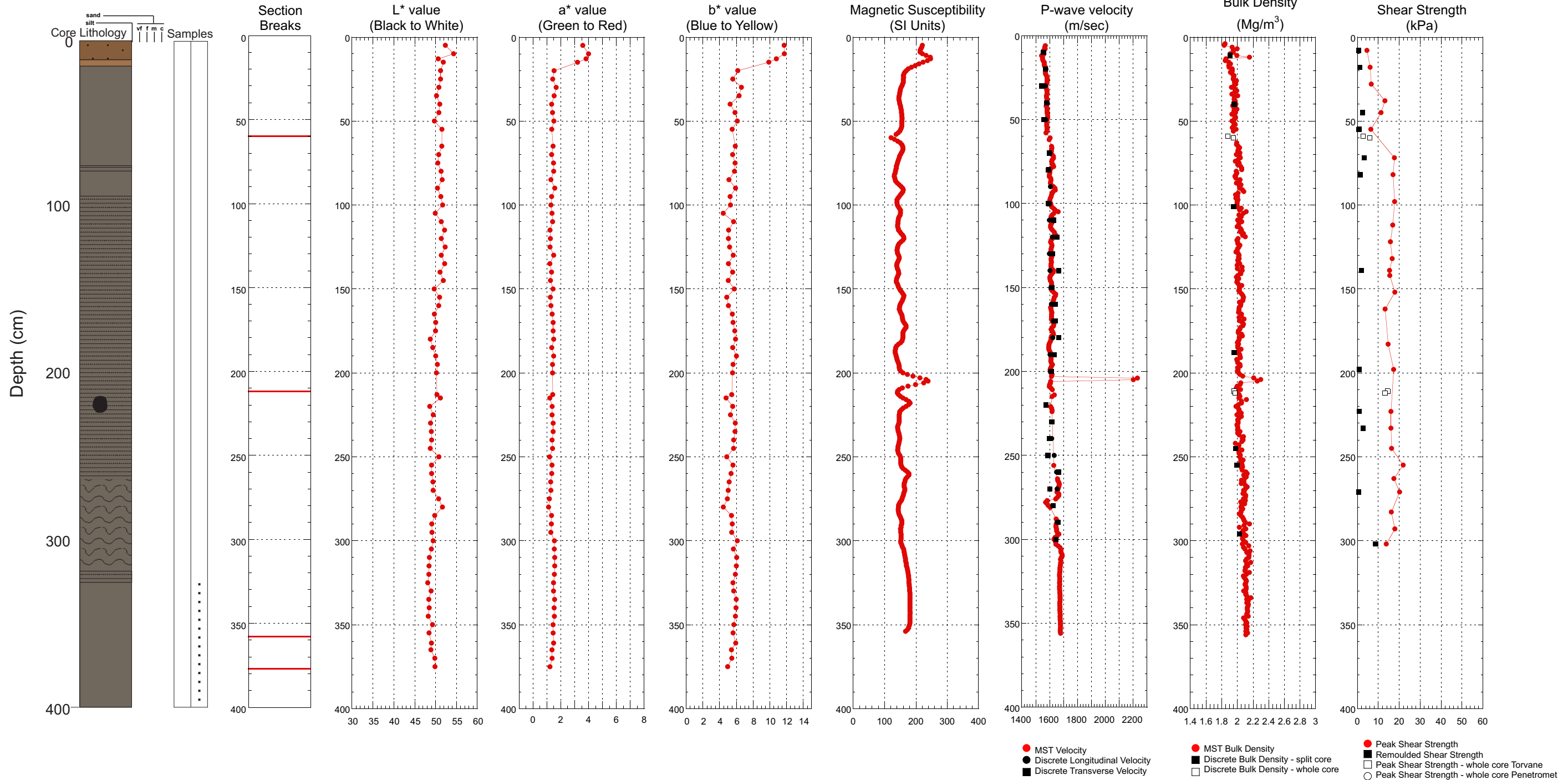


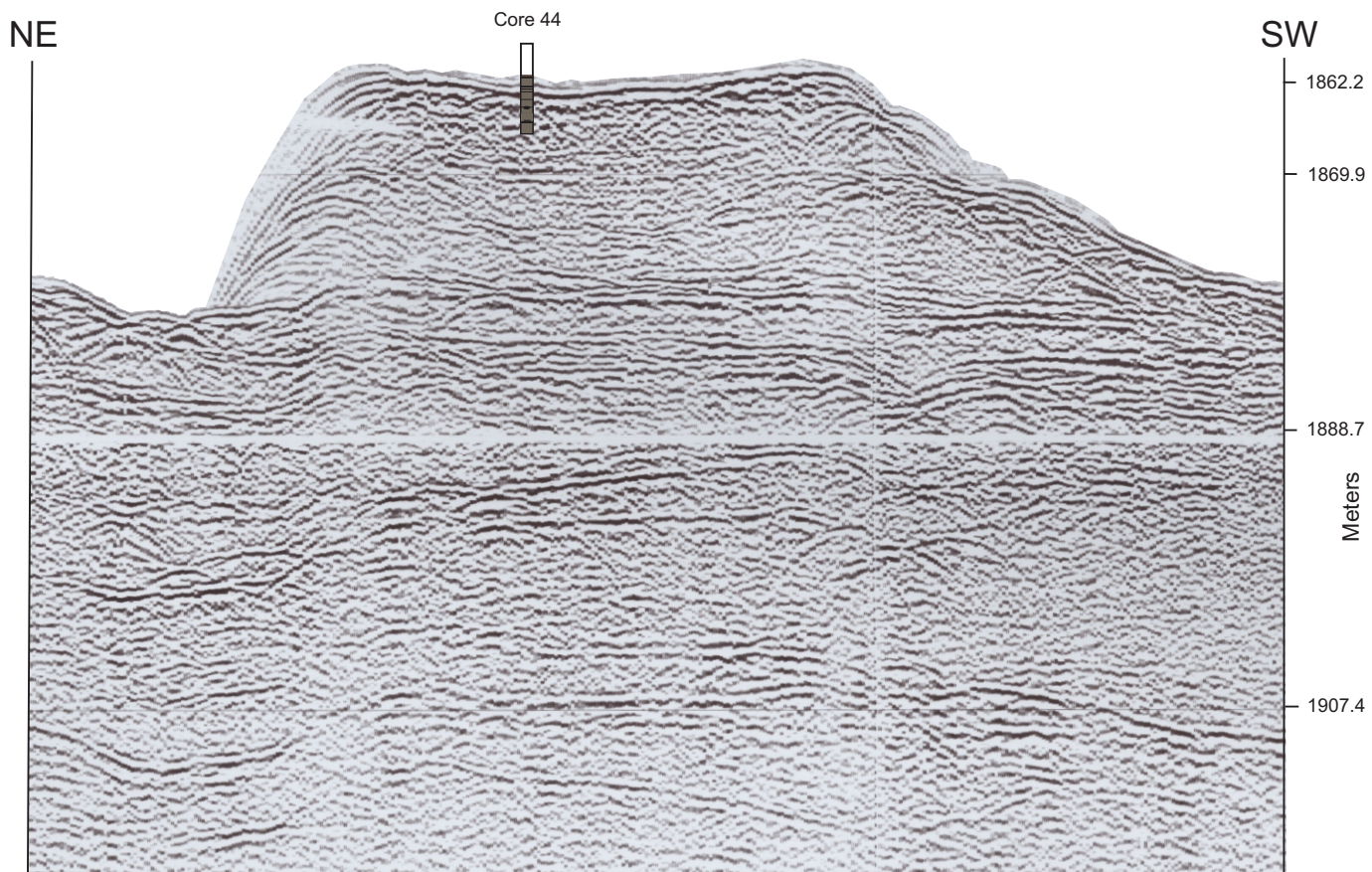
2006040 0044 Piston Core



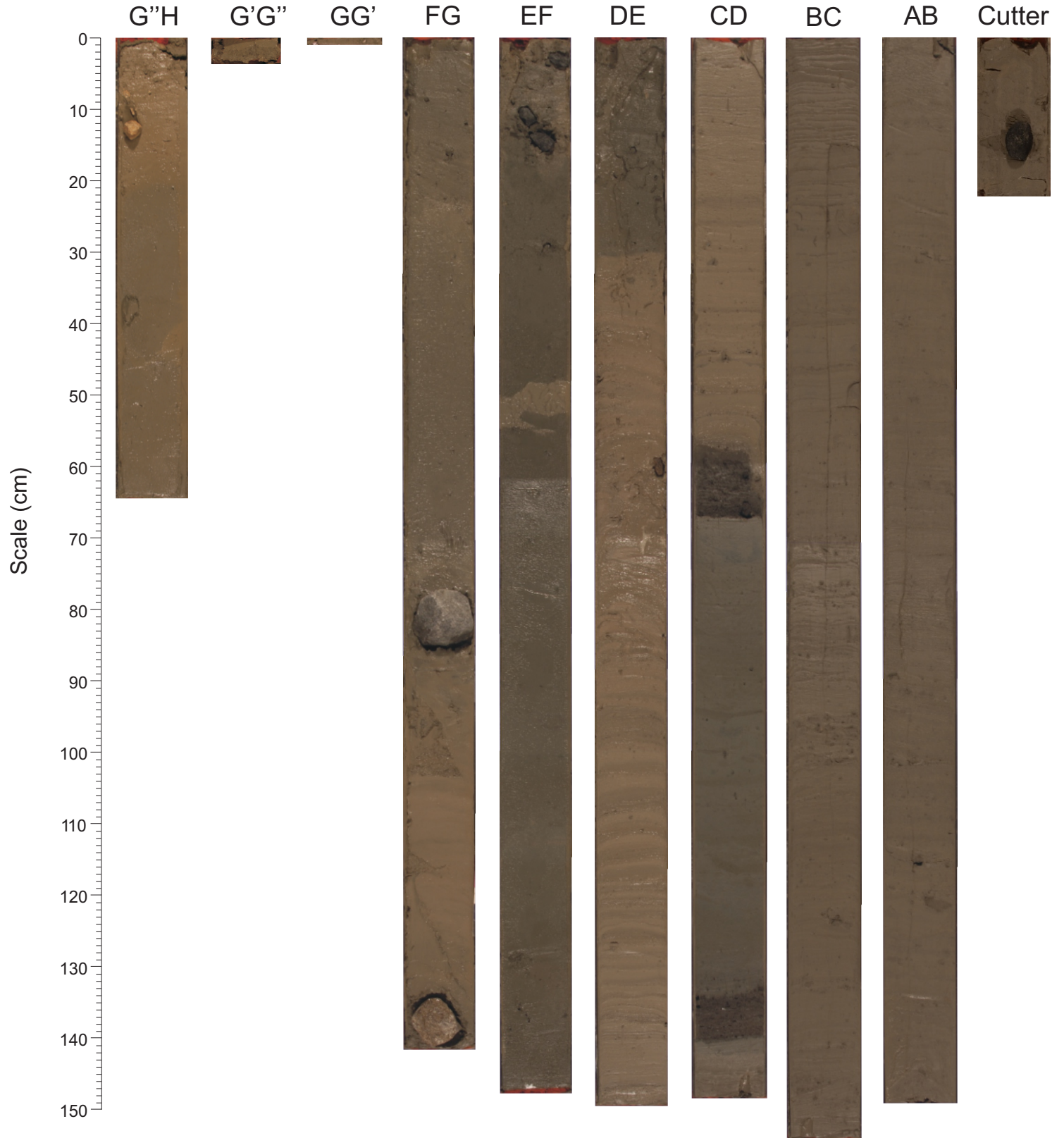
Hudson 2006040 Piston Core 0044

TD 377cm 61°16.9793 N 60°11.3129 W Water depth 1862.2 m

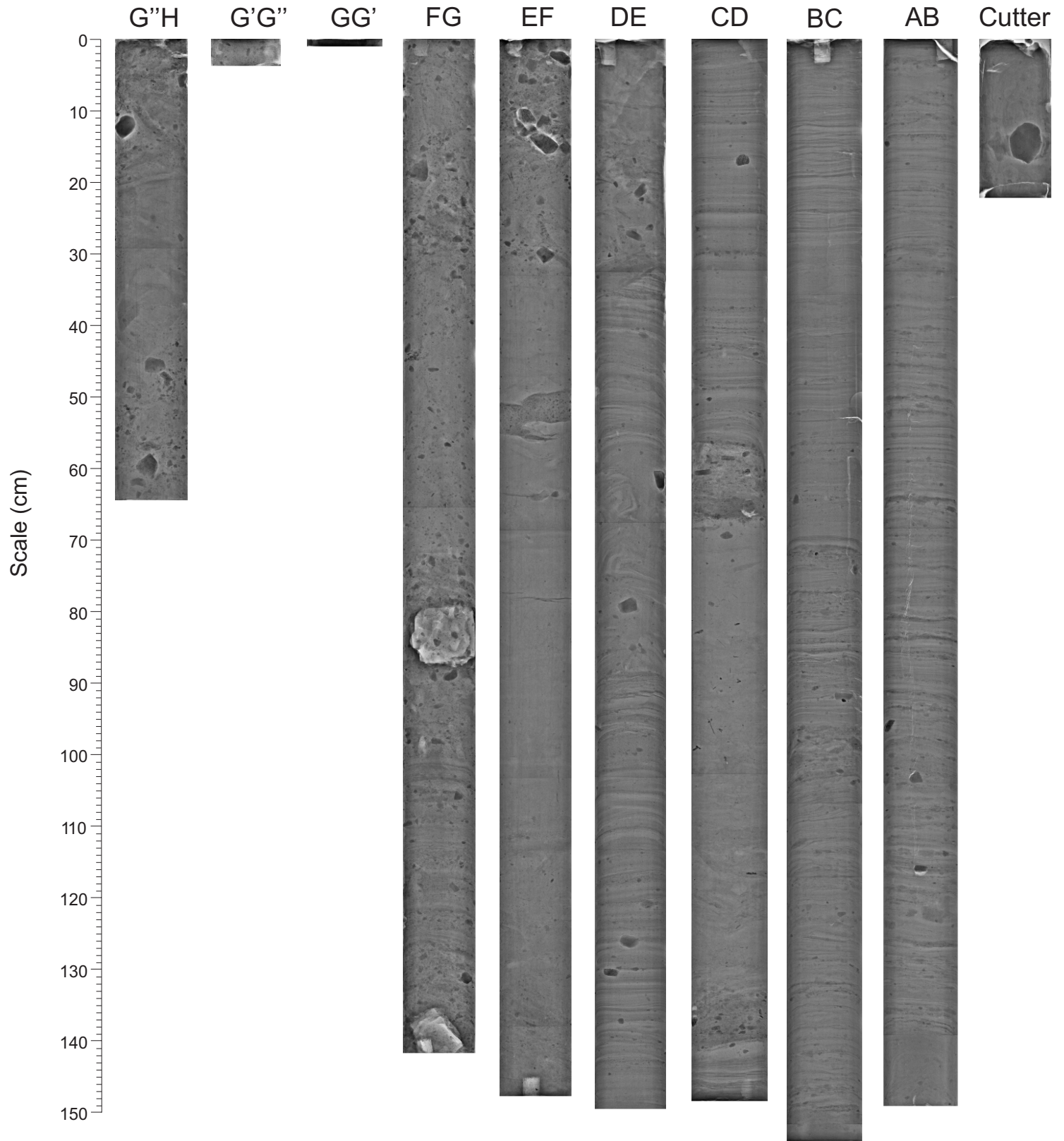




2006040 0045 Piston Core

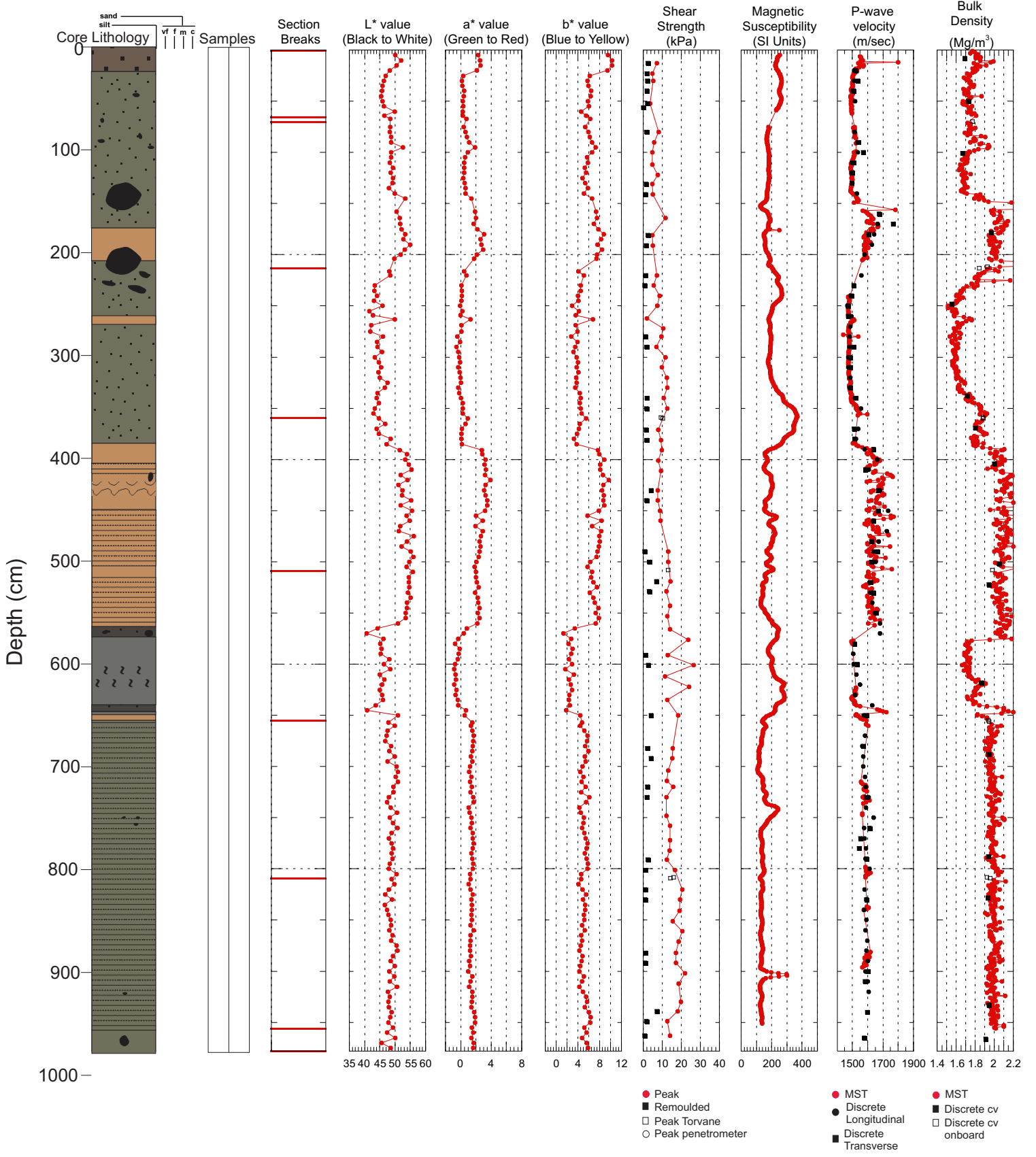


2006040 0045 Piston Core

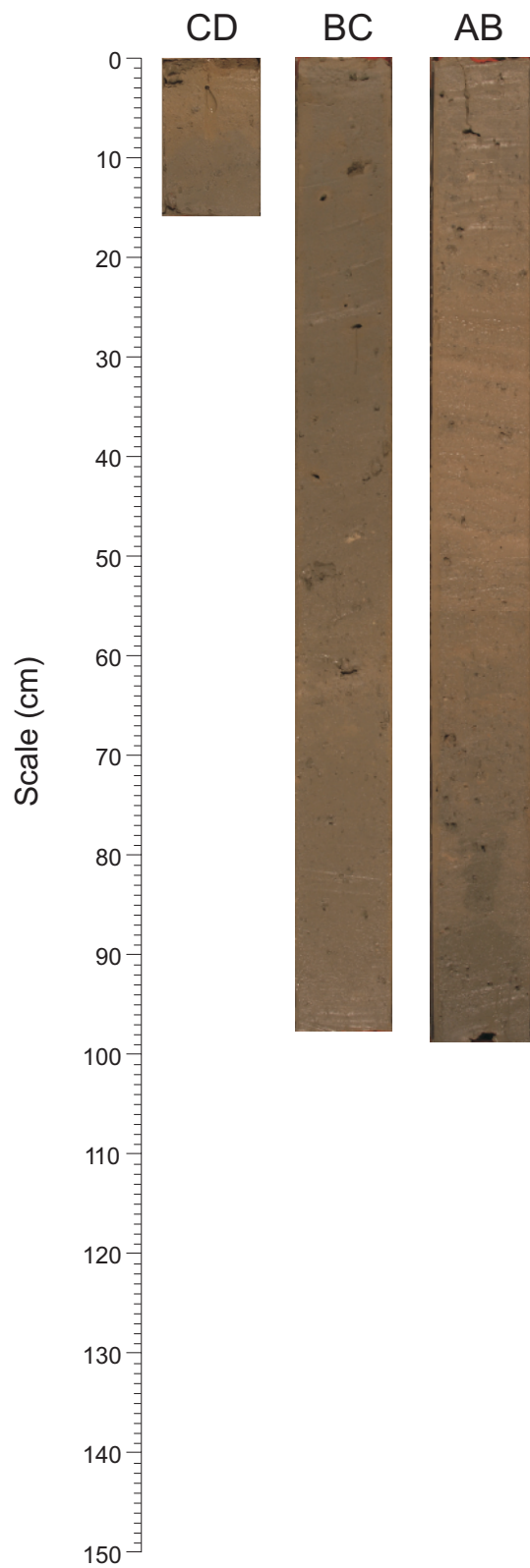


Hudson 2006040 Piston Core 0045

TD 978 cm 60°43.5520 N 60°33.1028 W Water depth 1589.1 m

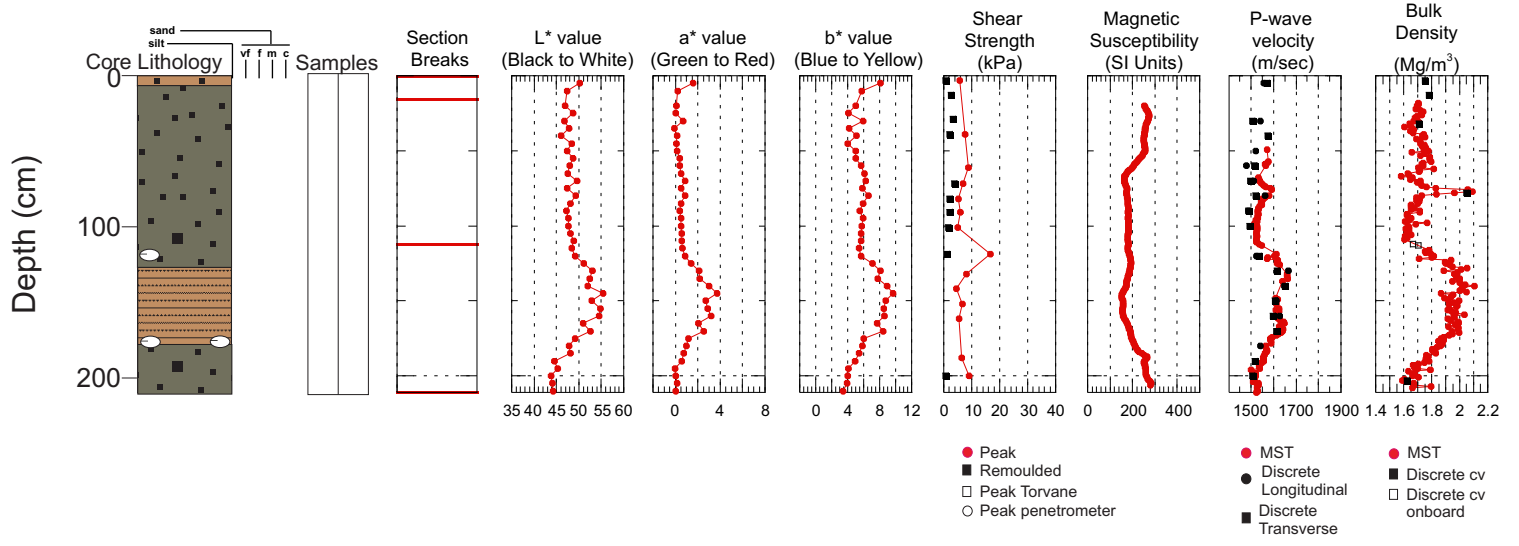


2006040 0045 Trigger Weight Core

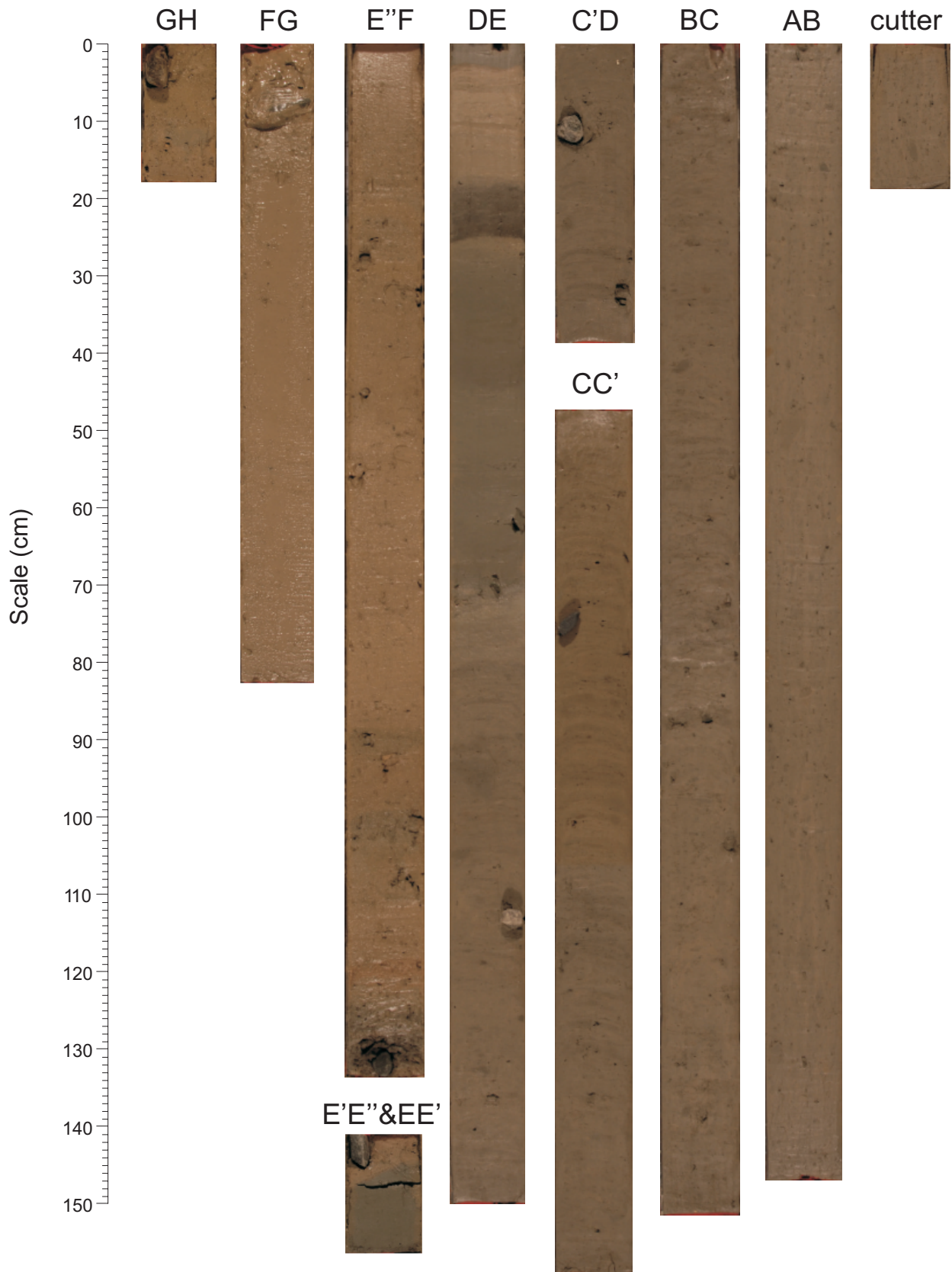


Hudson 2006040 Trigger Weight Core 0045

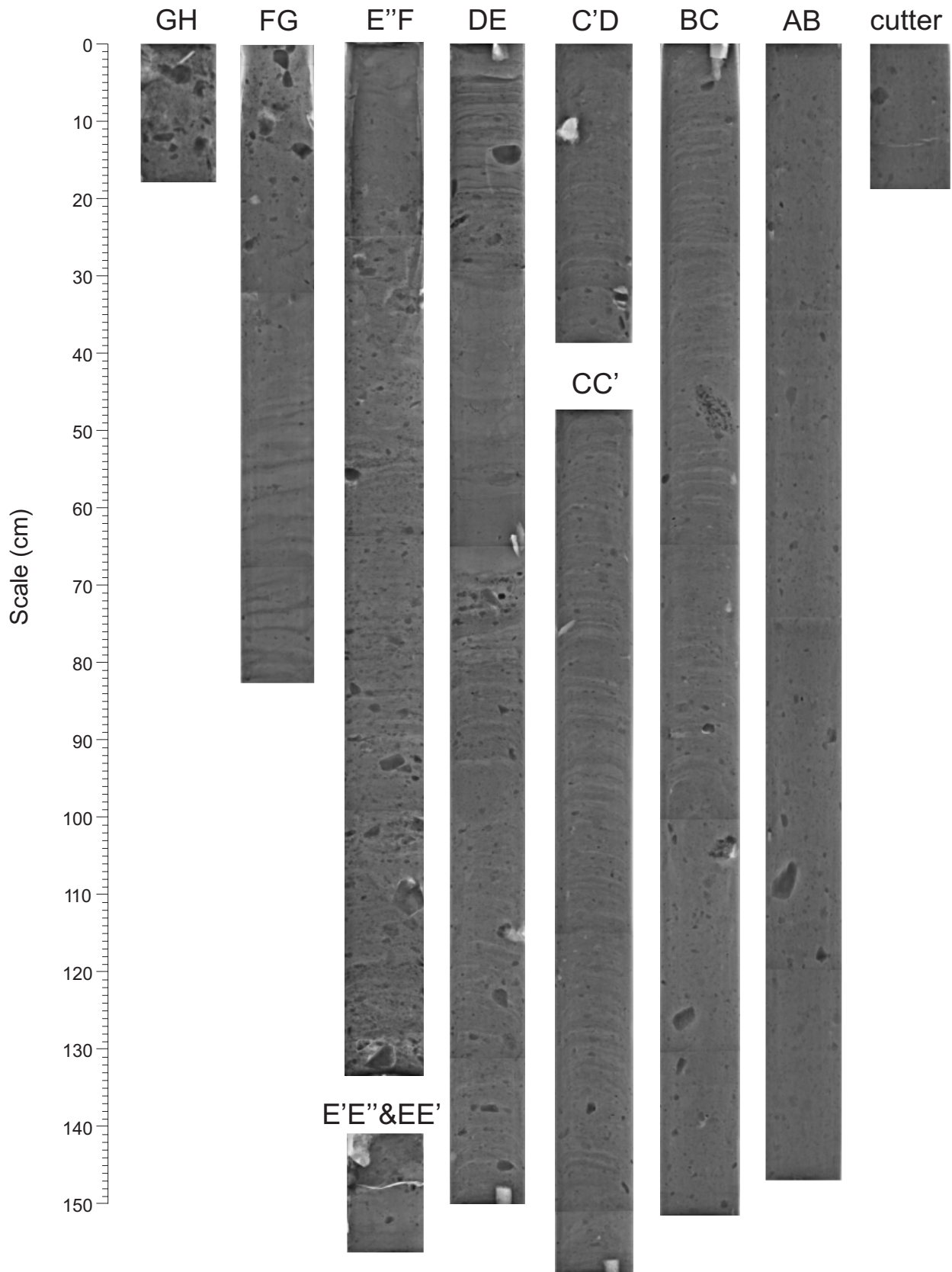
TD 211 cm 60°43.5520 N 60°33.1028 W Water depth 1589.1 m



2006040 0046 Piston Core

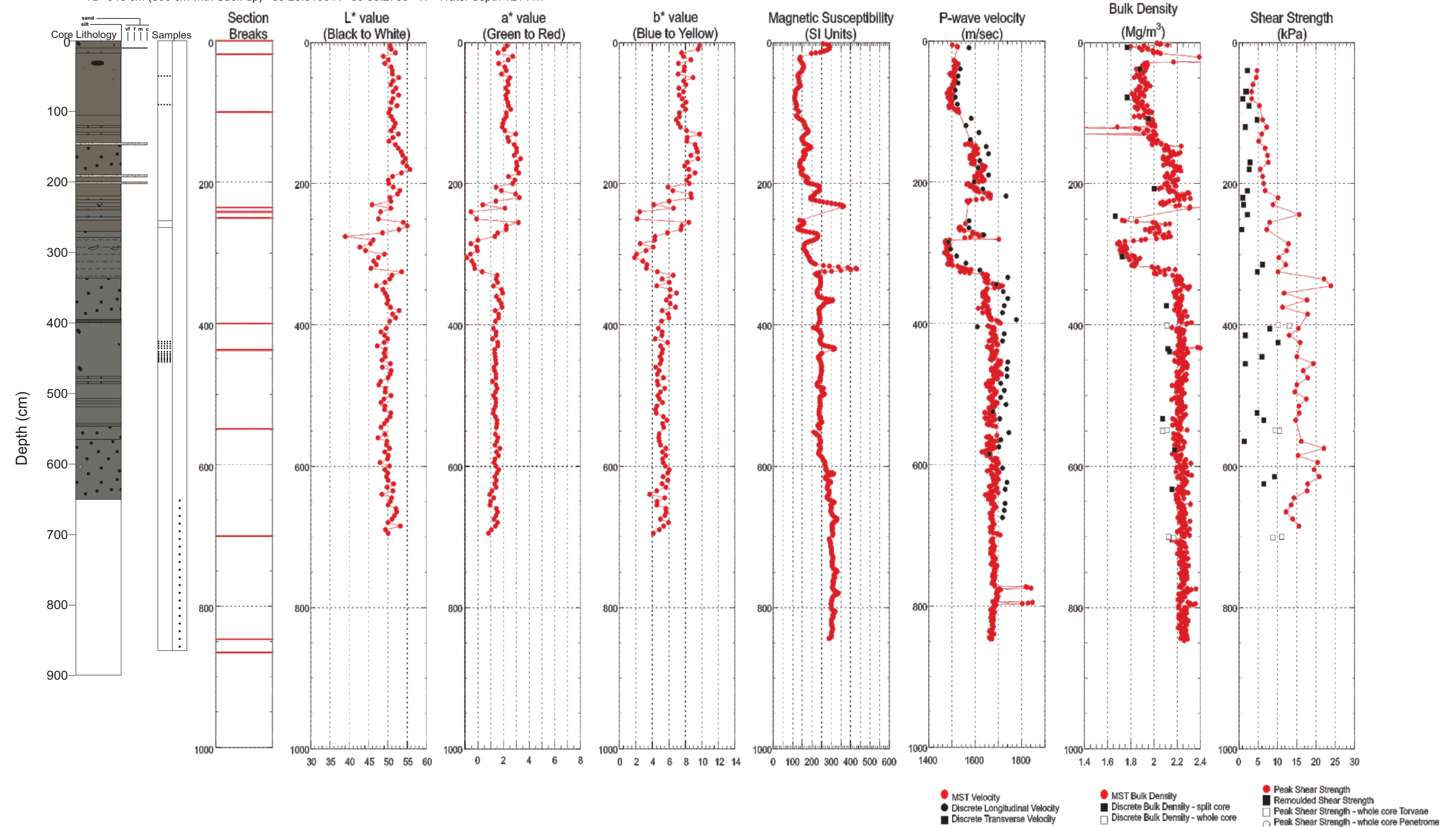


2006040 0046 Piston Core

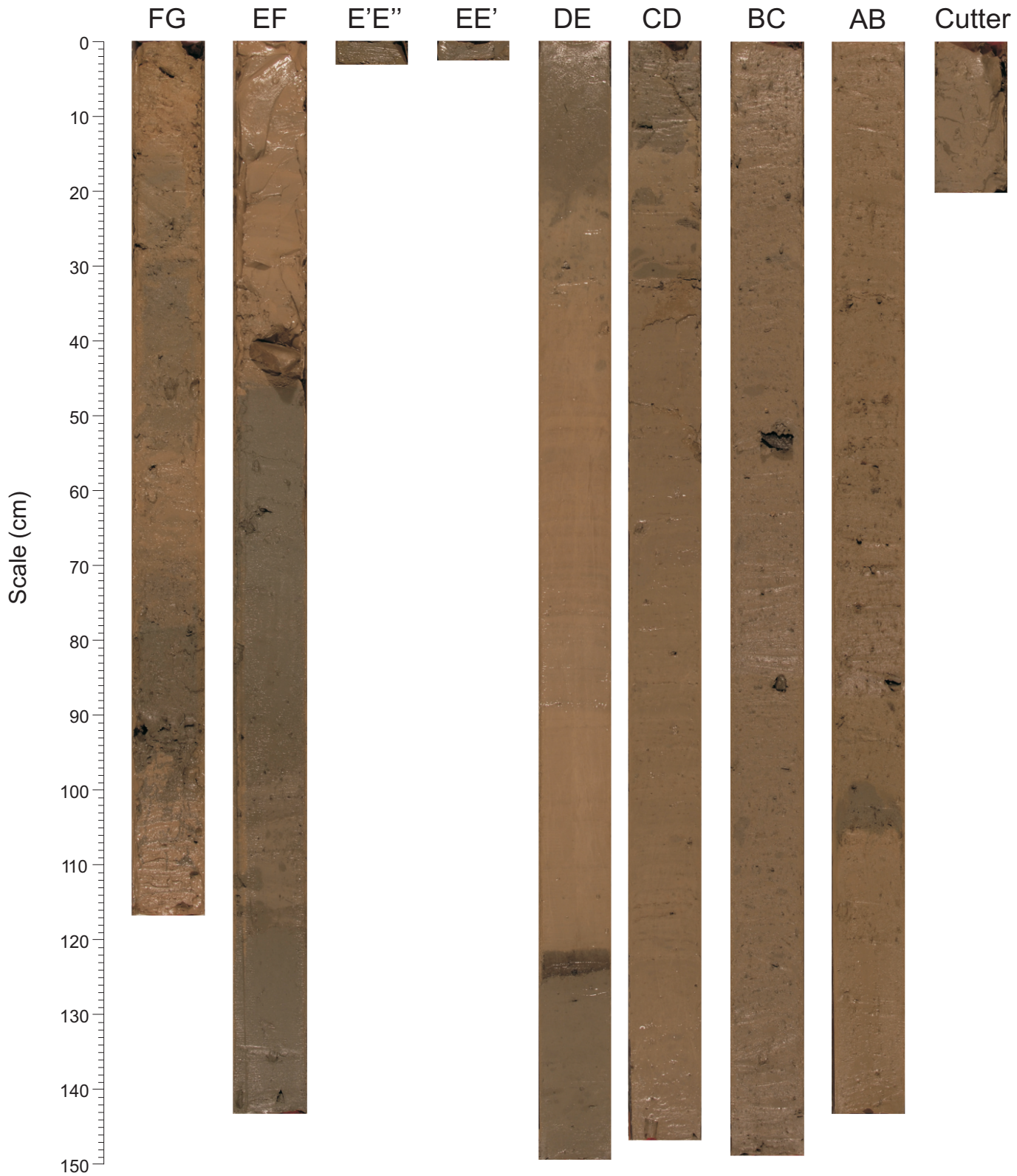


Hudson 2006040 Piston Core 0046

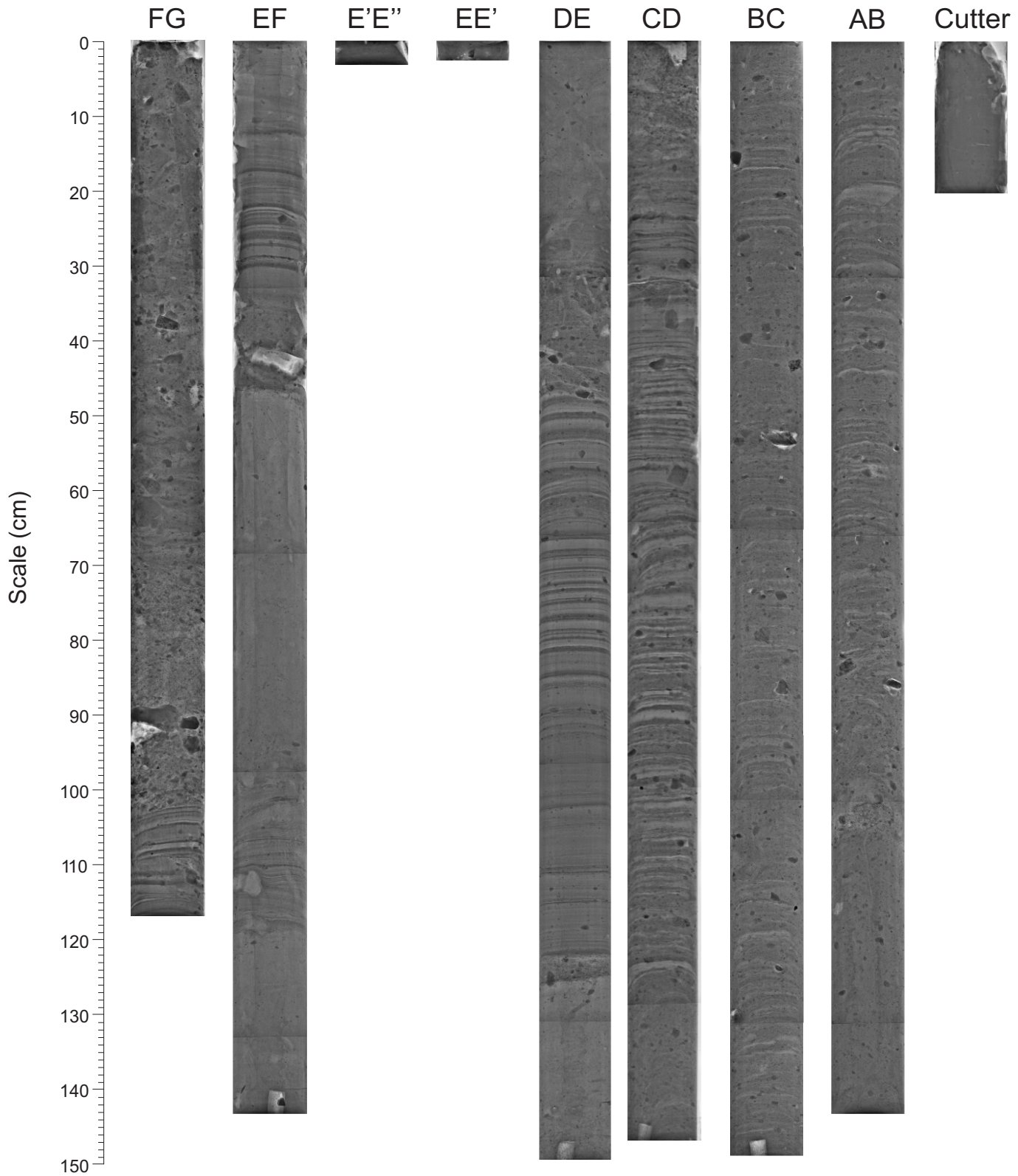
TD 646 cm (866 cm with Suck-up) 59°25.6486 N 59°53.2786 W Water depth 1214 m



2006040 0047 PistonCore

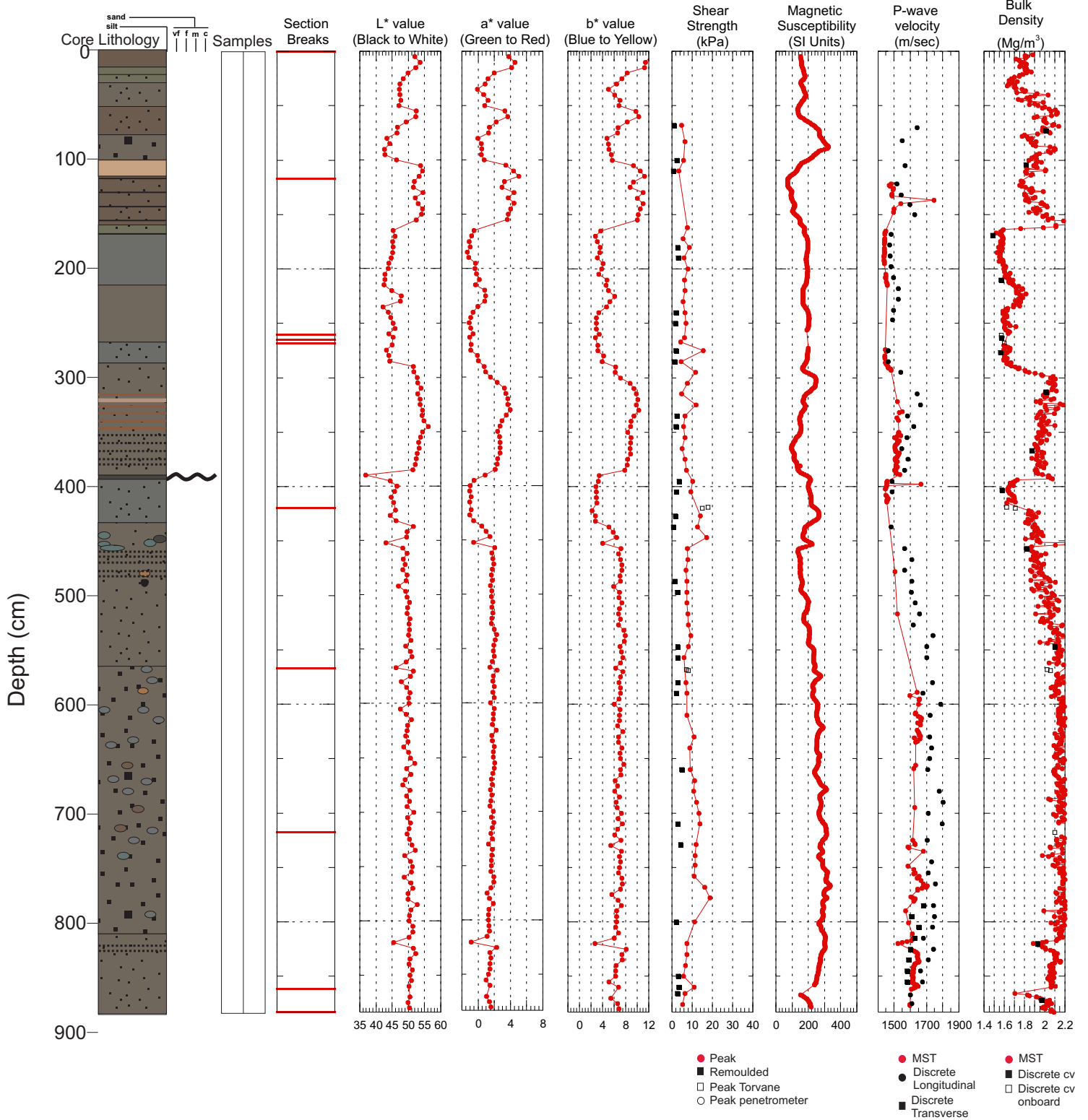


2006040 0047 PistonCore



Hudson 2006040 Piston Core 0047

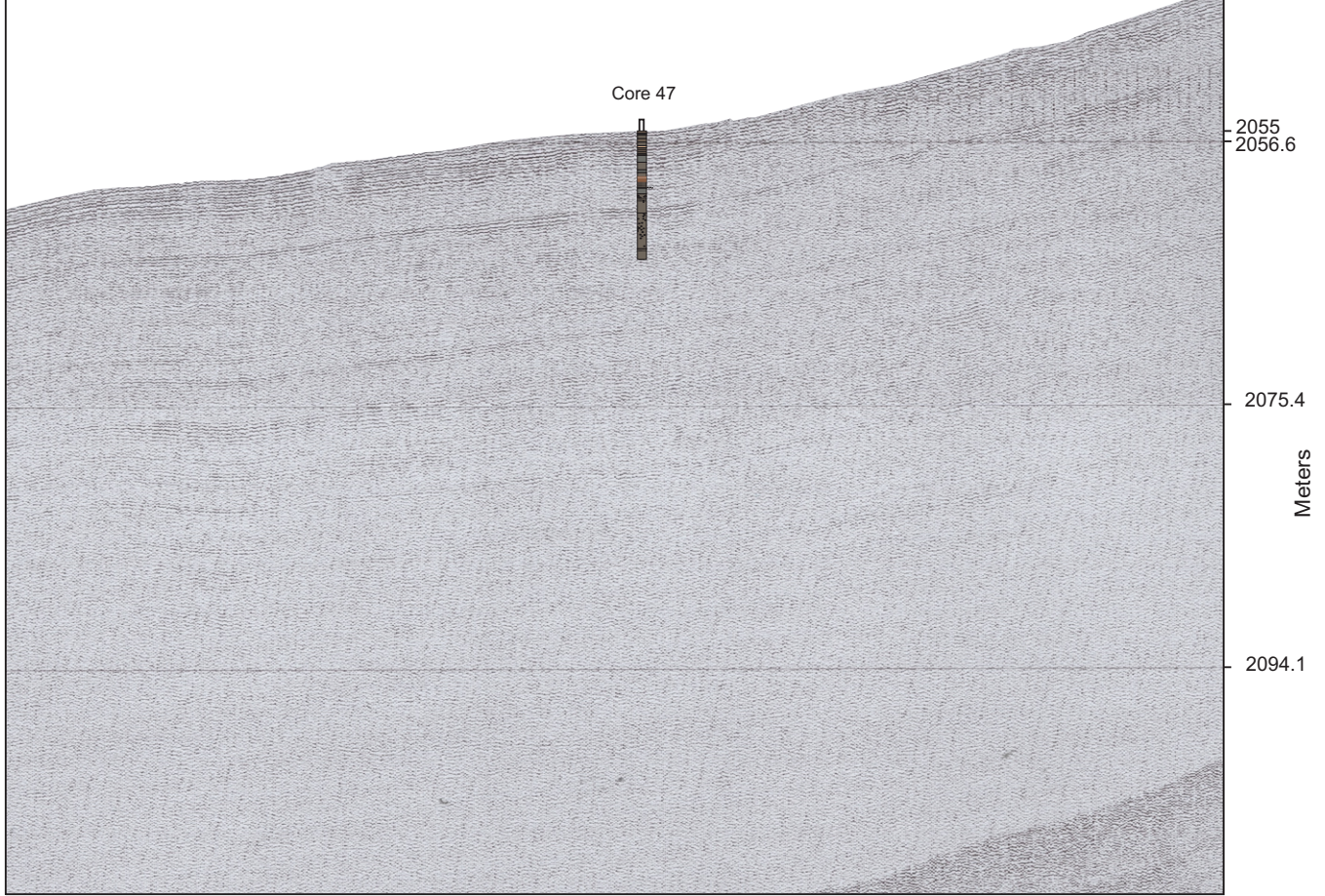
TD 883 cm 59°27.0365 N 59°22.2293 W Water depth 2049 m



SW

NE

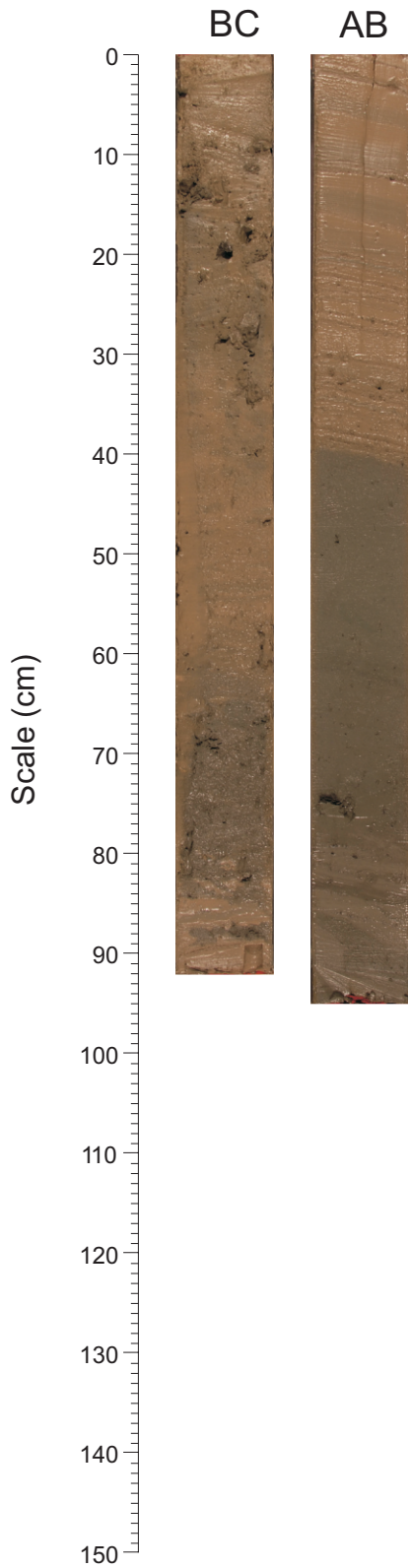
Core 47



234/0405

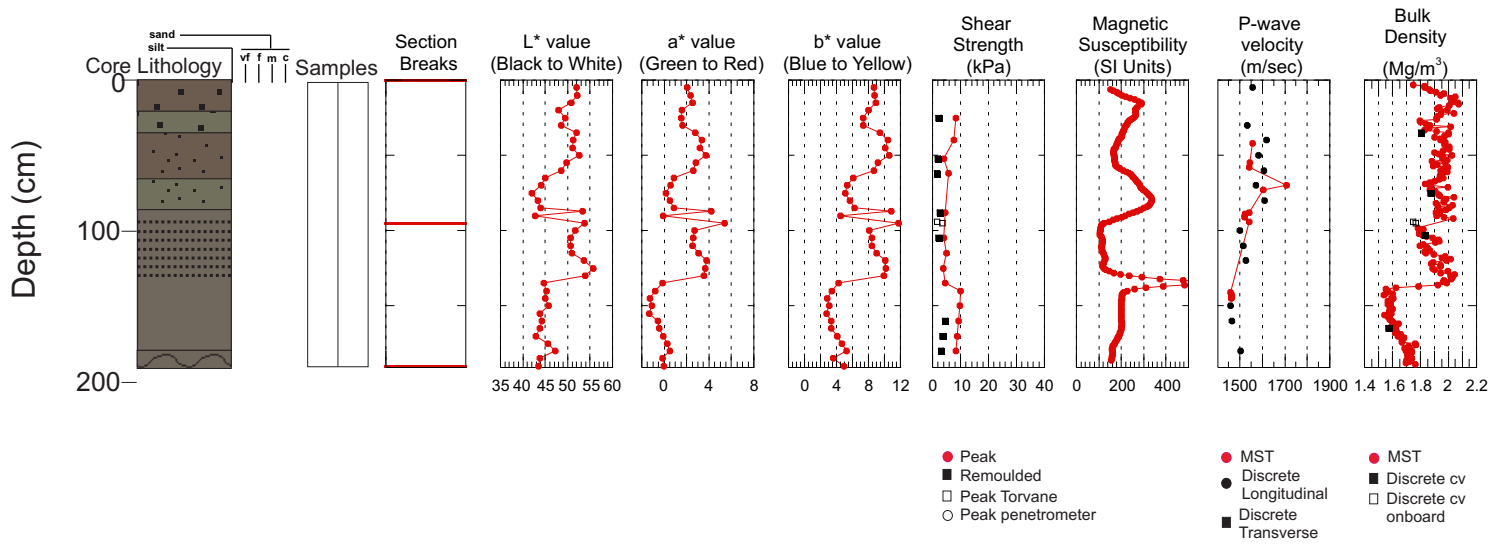
234/0417

2006040 0047 Trigger Weight Core

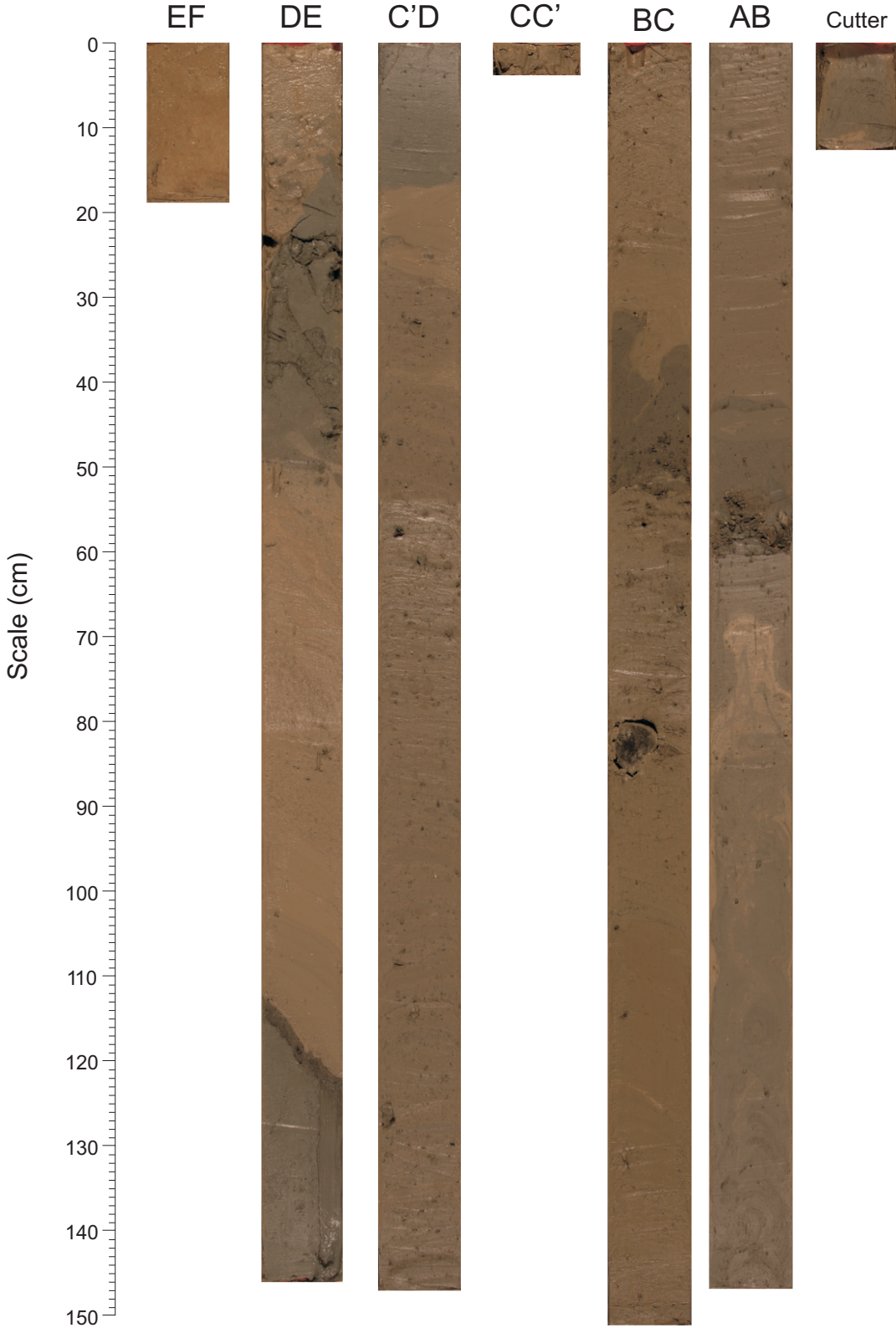


Hudson 2006040 Trigger Weight Core 0047

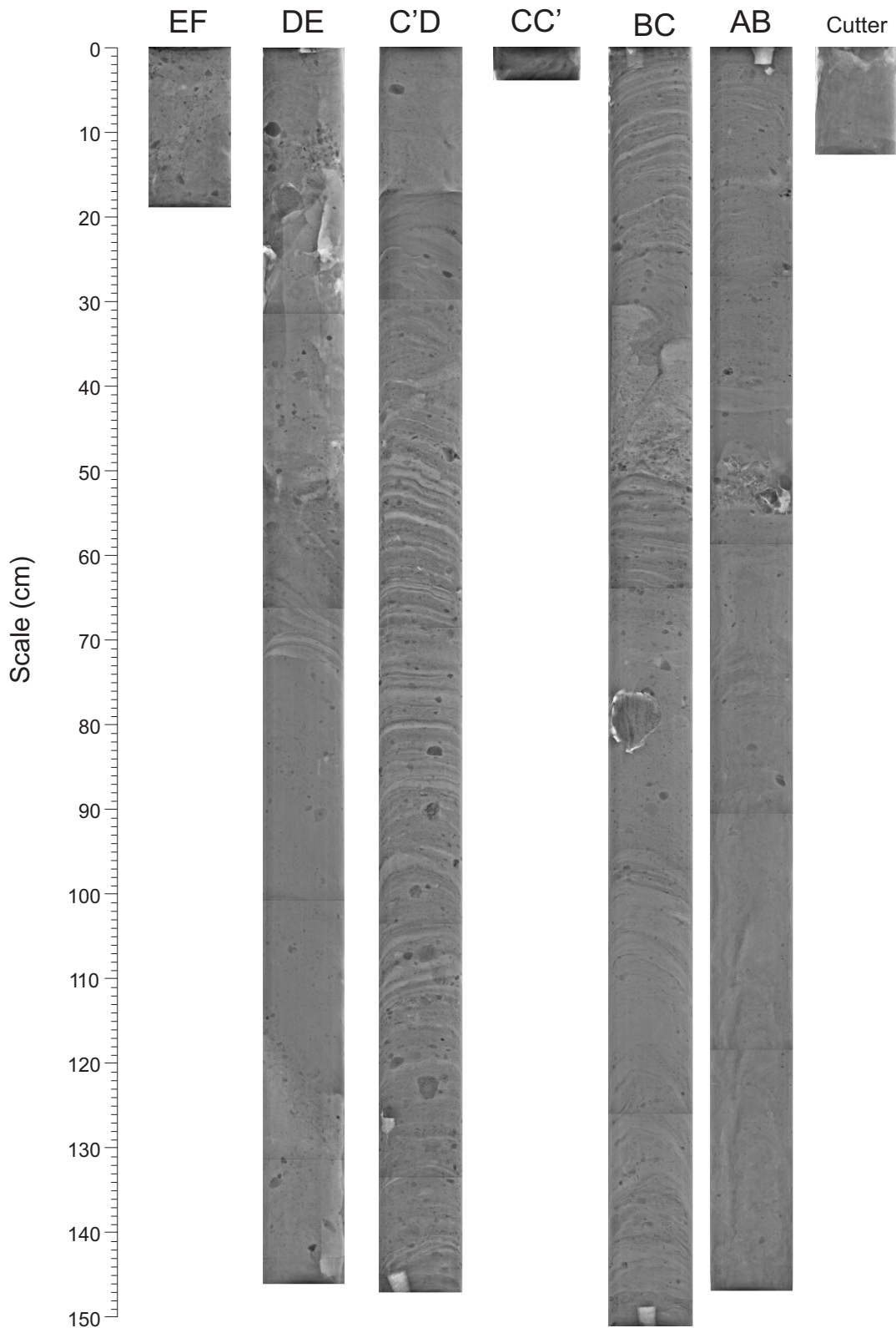
TD 191 cm 59°27.0365 N 59°22.2293 W Water depth 2049 m



2006040 0048 Piston Core

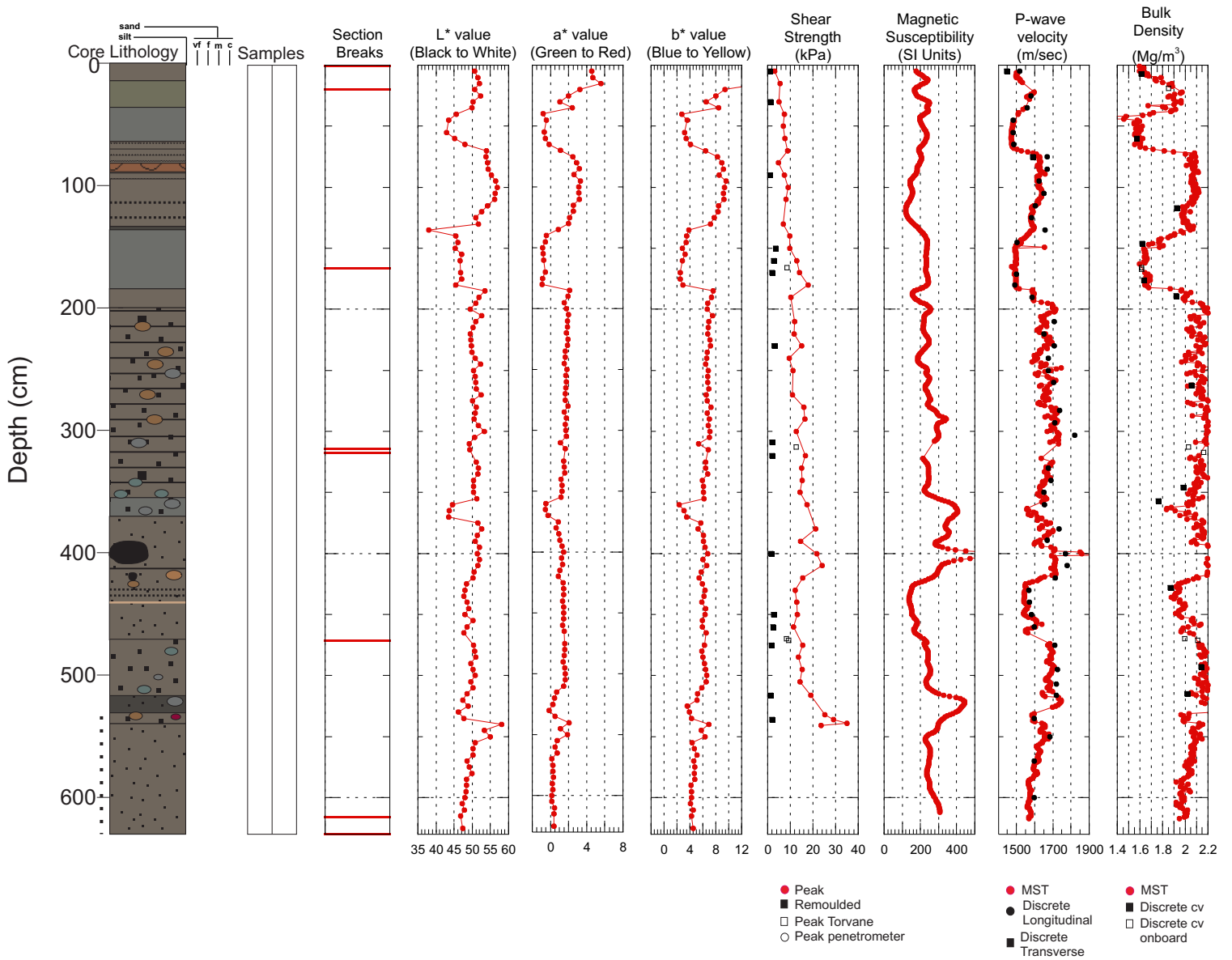


2006040 0048 Piston Core



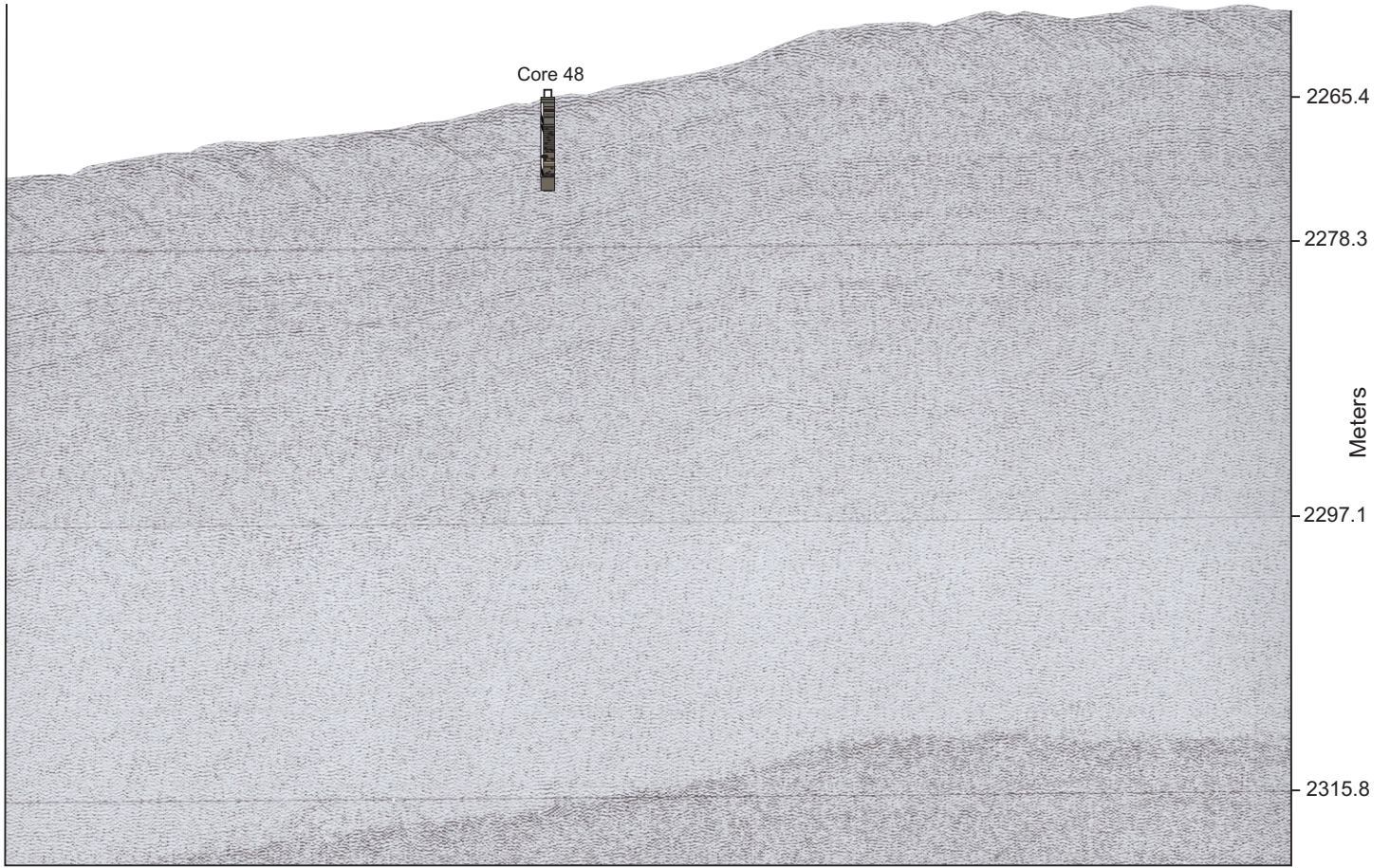
Hudson 2006040 Piston Core 0048

TD 630 cm 59°27.6379 N 59°07.7014 W Water depth 2275 m



SW

NE



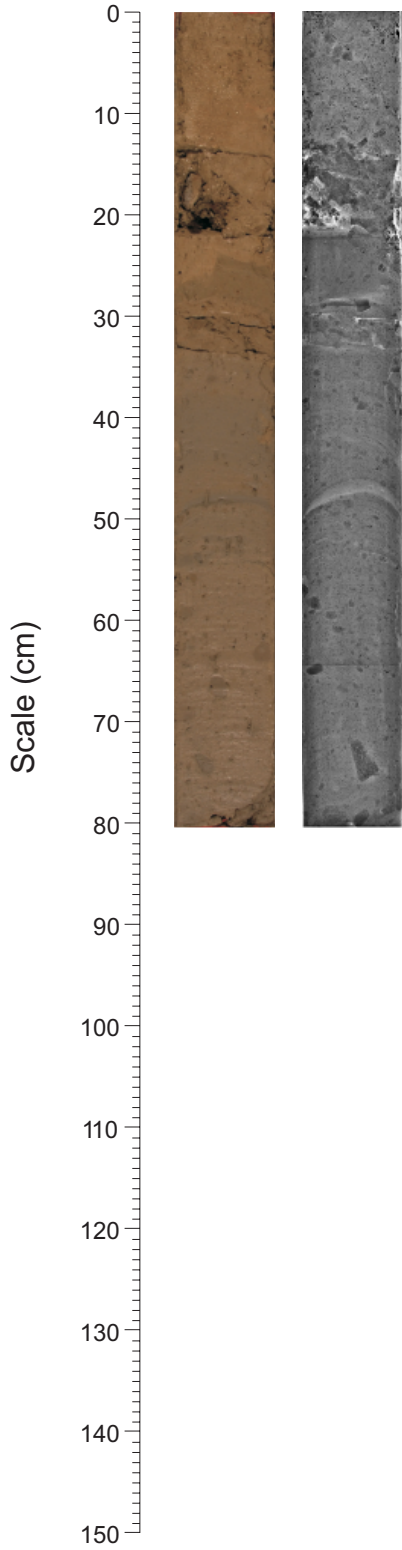
234/0245

234/0300

2006040 0049 Piston Core

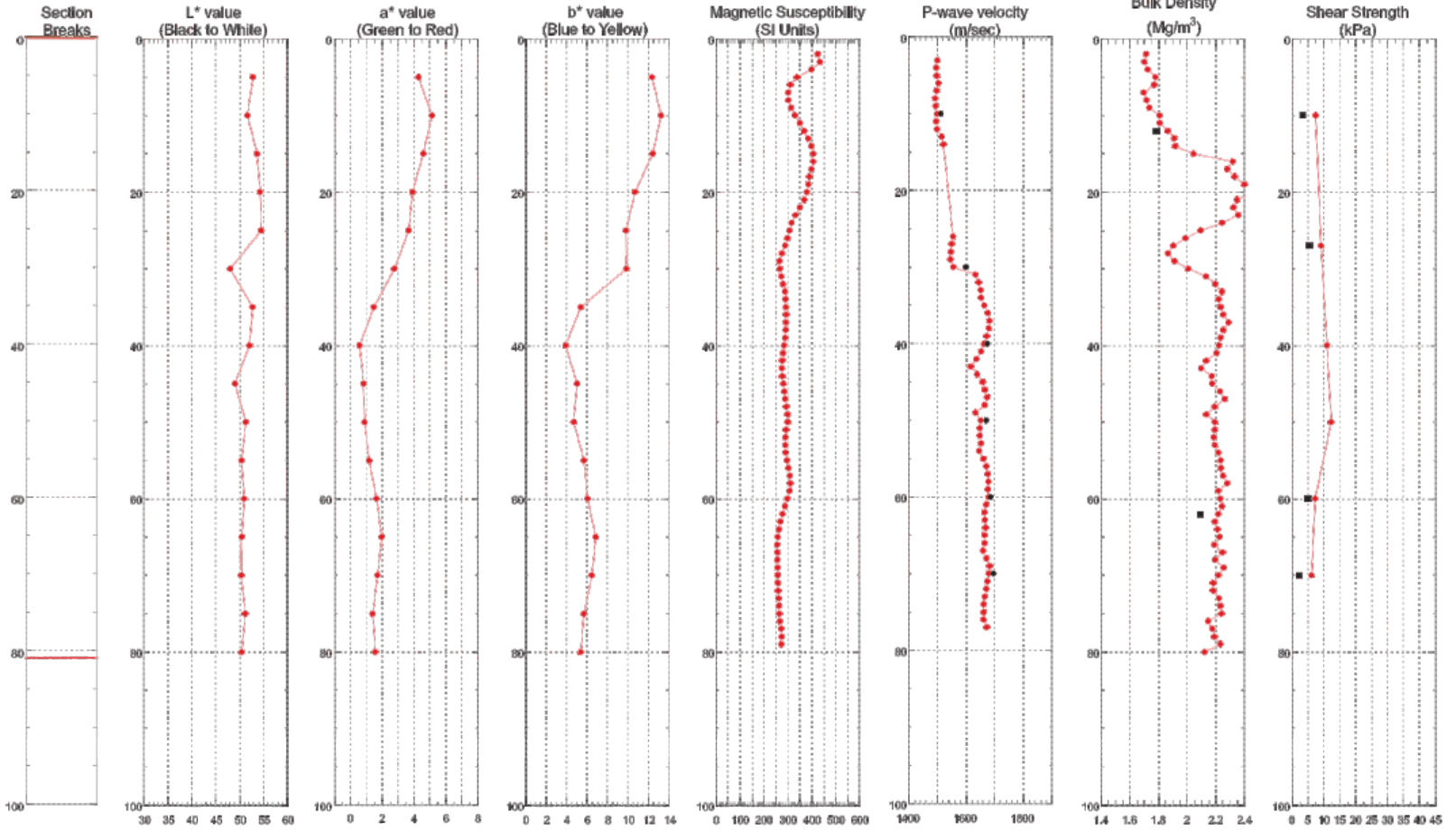
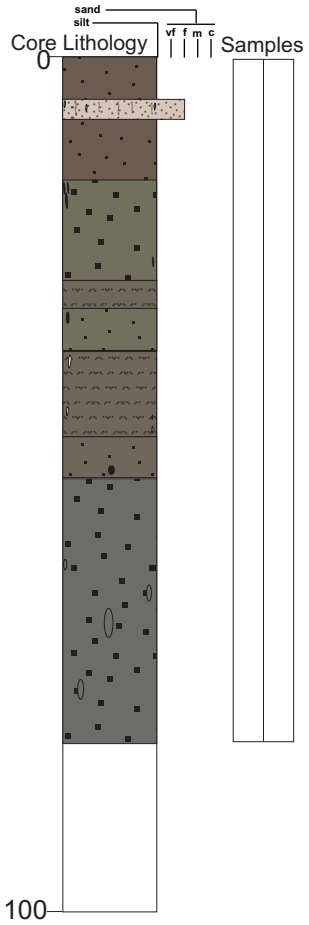
AB

AB



Hudson 2006040 Piston Core 0049

TD 81 cm 58°26.6298 N 58°24.6799 W Water depth 2360 m



- MST Velocity
- Discrete Longitudinal Velocity
- Discrete Transverse Velocity
- MST Bulk Density
- Discrete Bulk Density - split core
- Discrete Bulk Density - whole core
- Peak Shear Strength
- Remoulded Shear Strength
- Peak Shear Strength - whole core Torvane
- Peak Shear Strength - whole core Piezometer

NE

SW

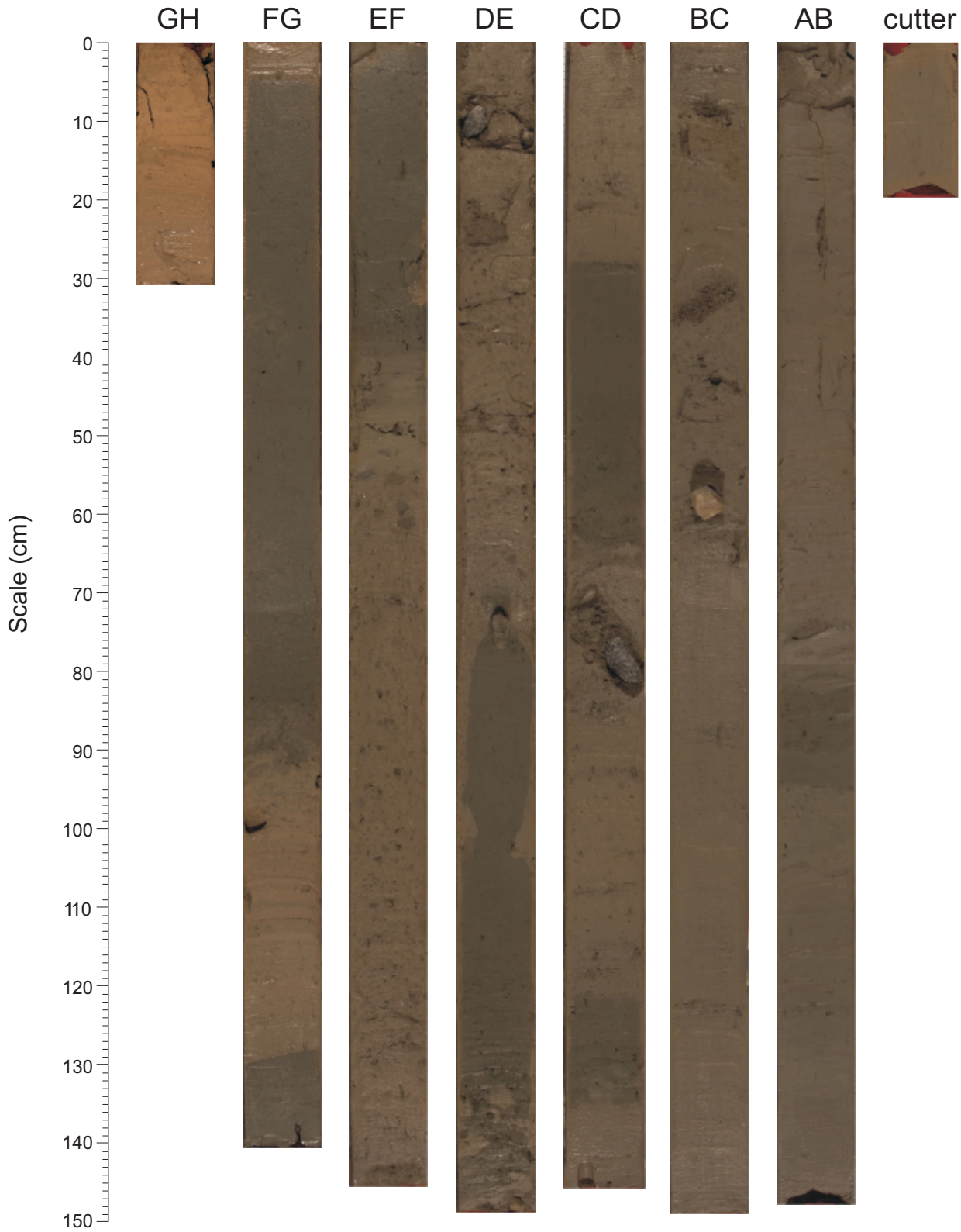
236/0801, 2360 mbsl, core length 0.85 m



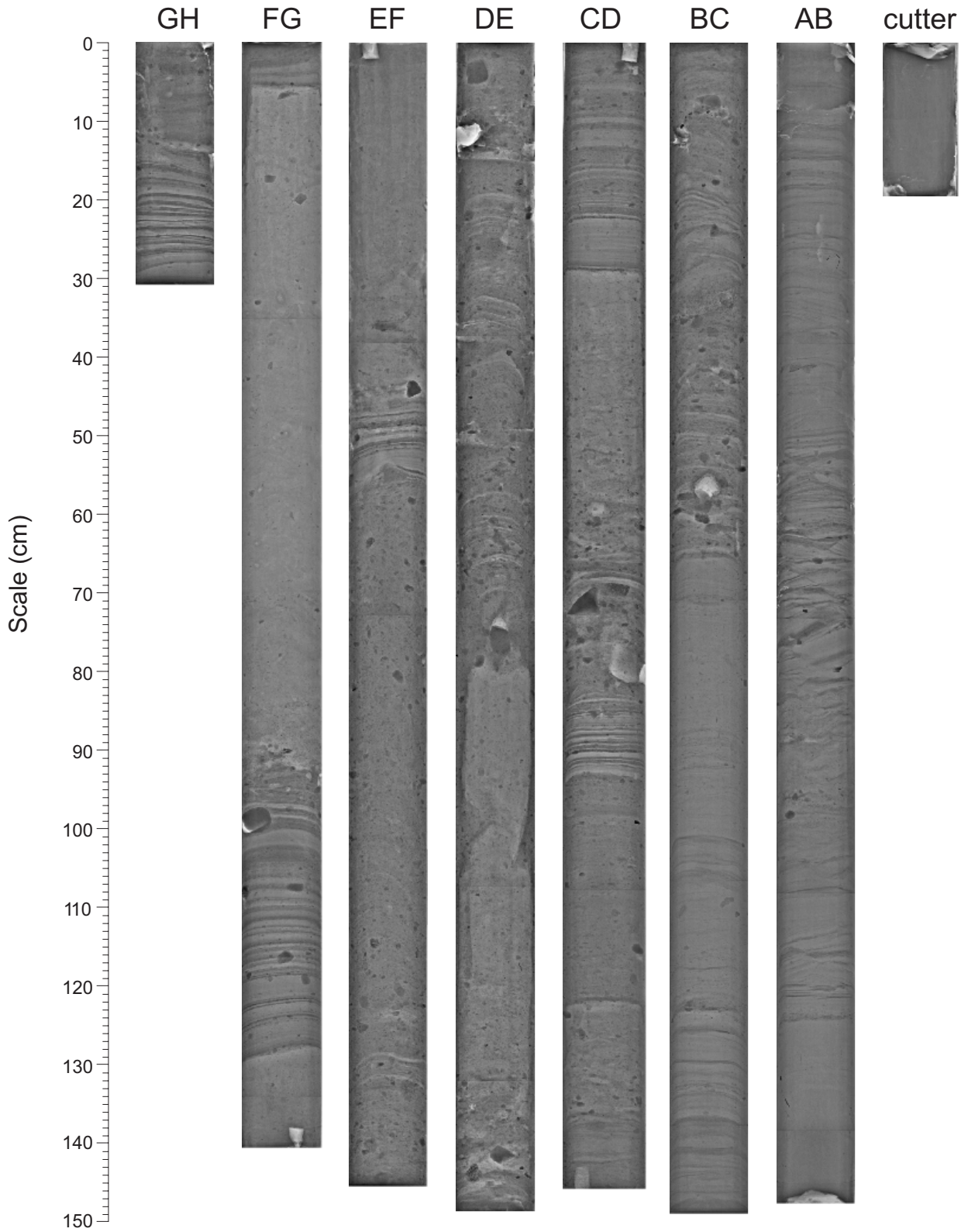
236/0806

Huntec
236/0811

2006040 0050 Piston Core

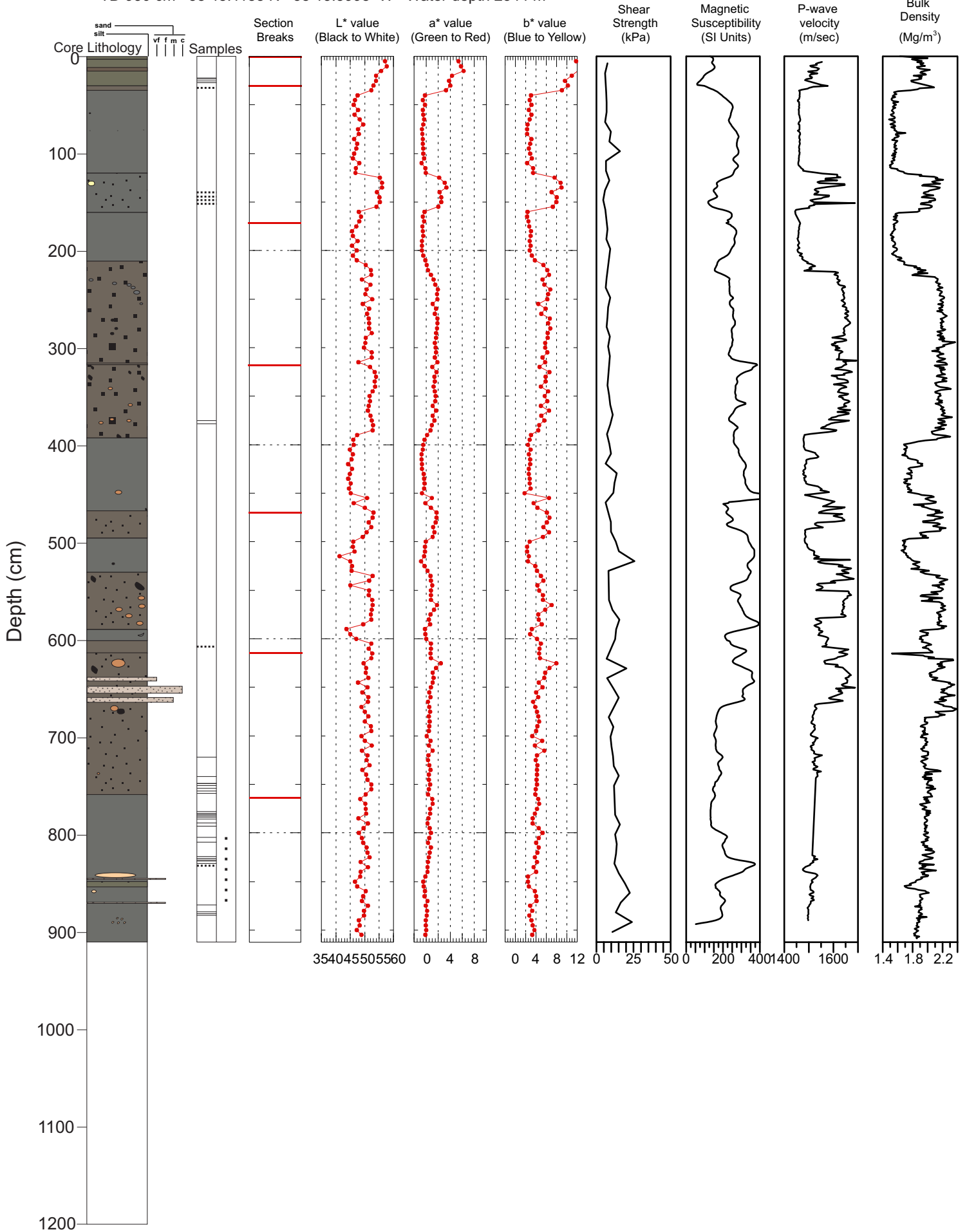


2006040 0050 Piston Core



Hudson 2006040 Piston Core 0050

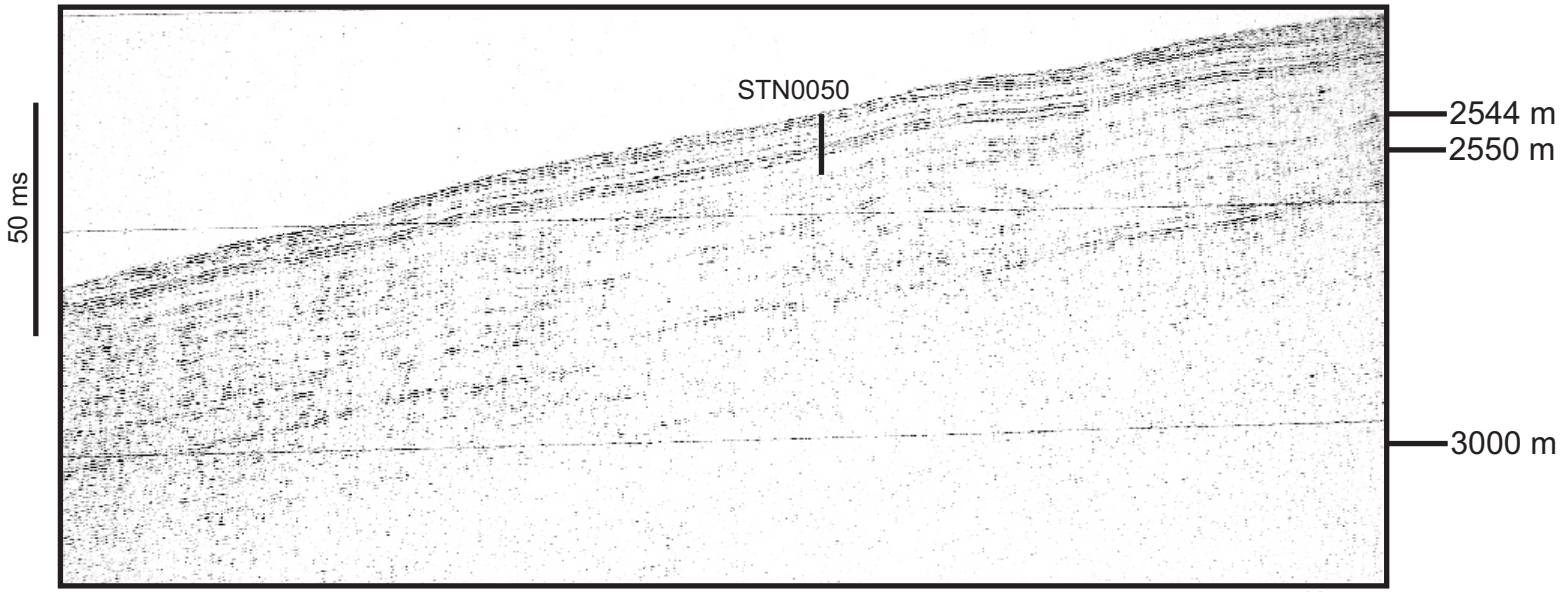
TD 930 cm 58°48.1188 N 58°13.5998 W Water depth 2544 m



NE

SW

236/0621, 2544mbsl, core length 9.69 m

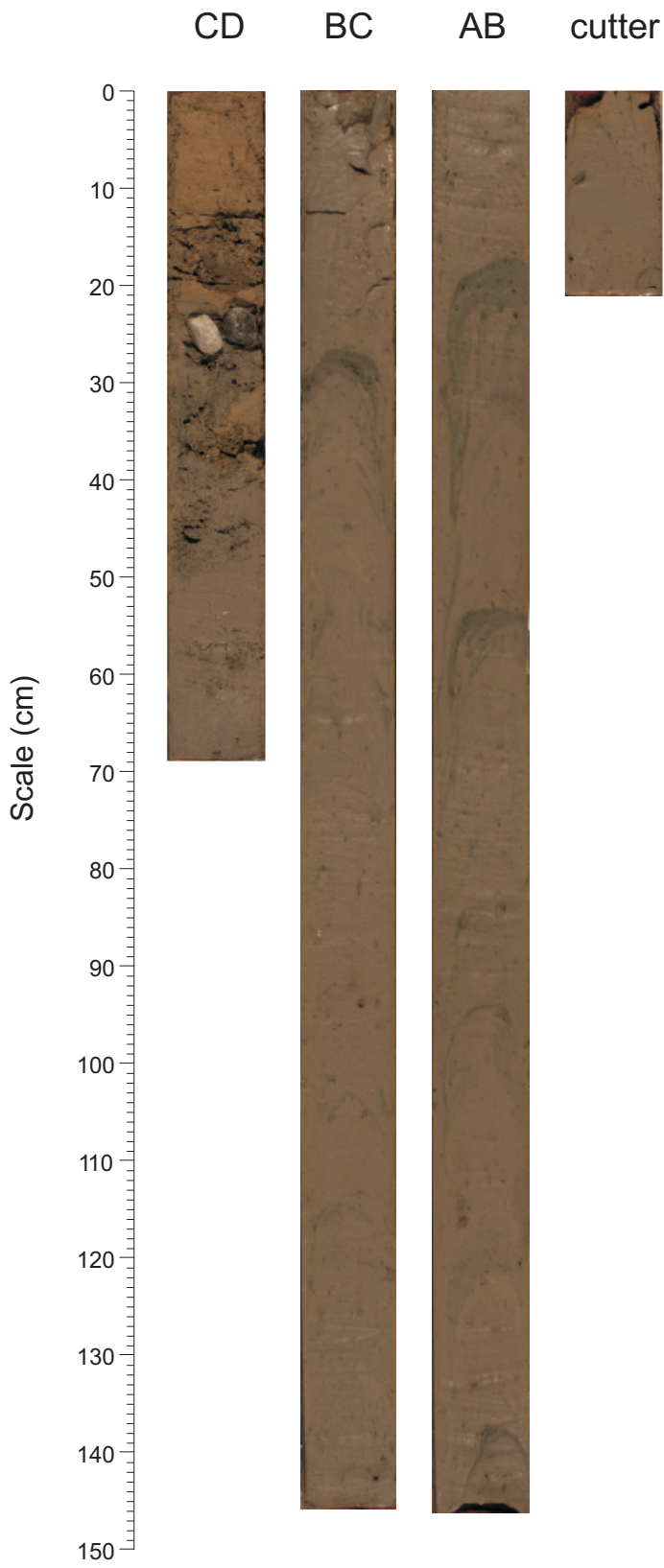


Huntec

236/0616

236/0626

2006040 0051 Piston Core



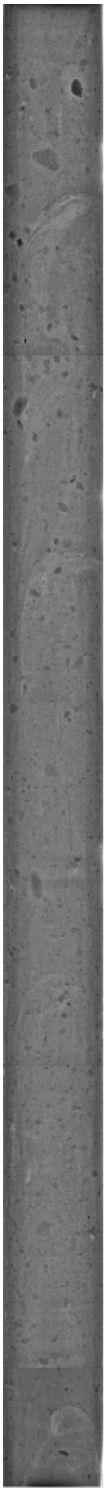
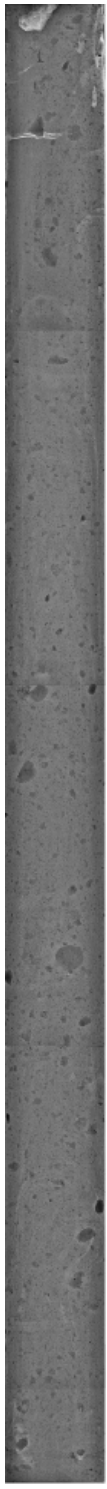
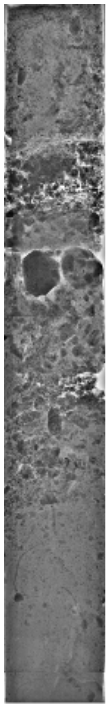
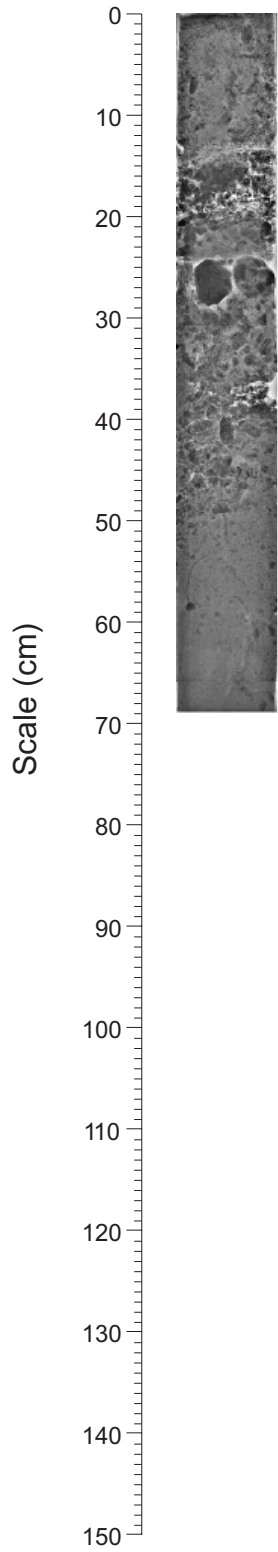
2006040 0051 Piston Core

CD

BC

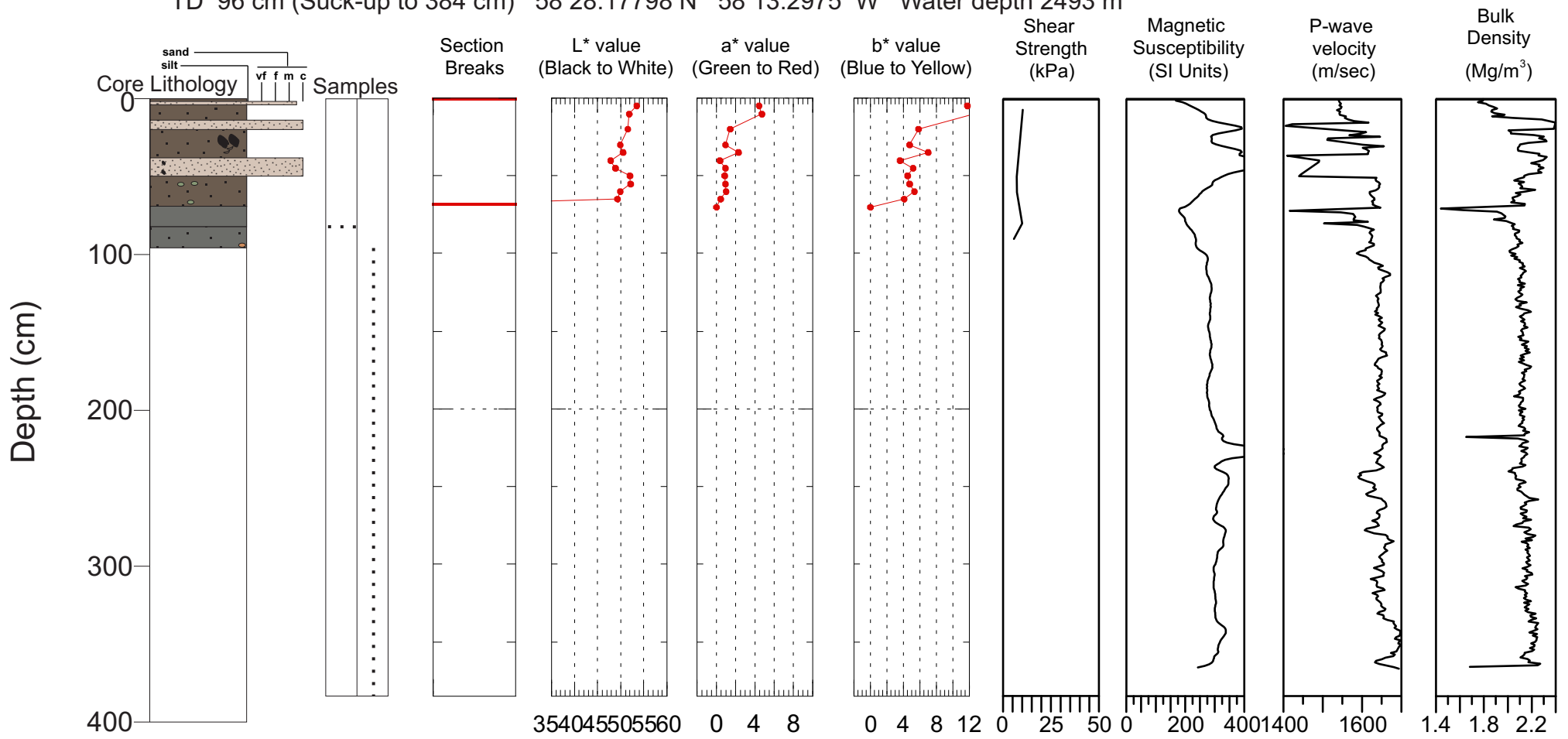
AB

cutter



Hudson 2006040 Piston Core 0051

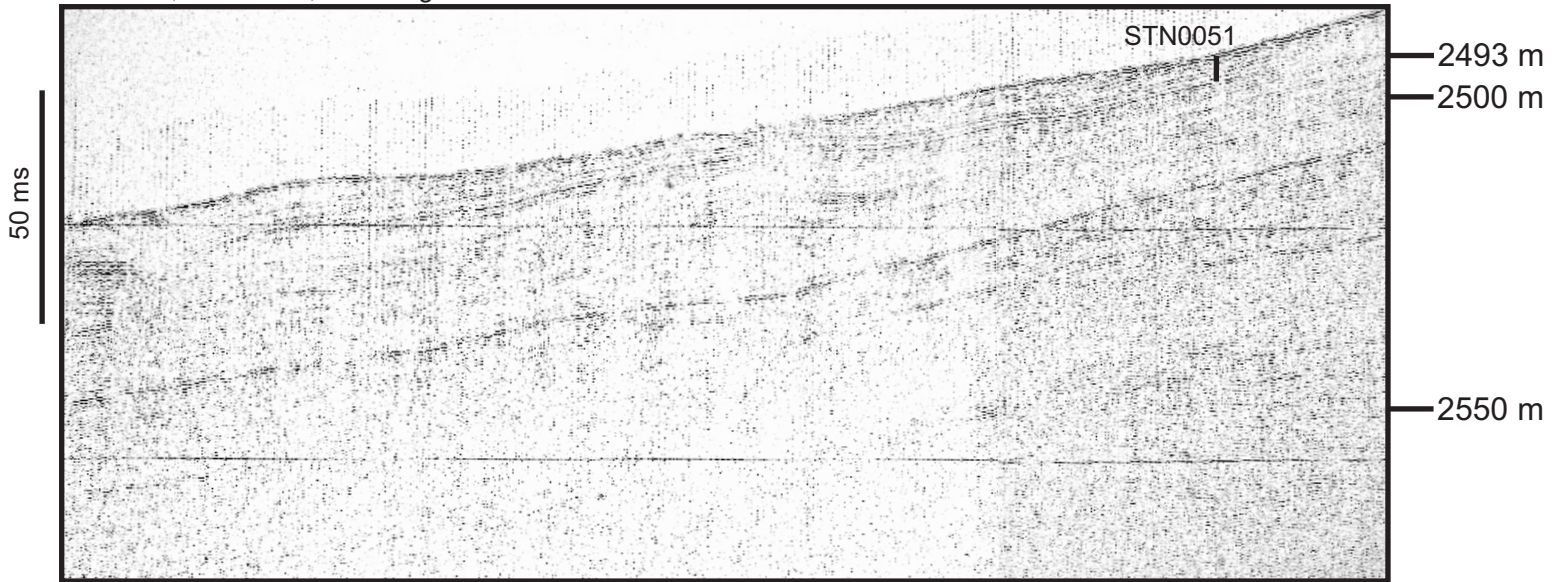
TD 96 cm (Suck-up to 384 cm) 58°28.17798 N 58°13.2975 W Water depth 2493 m



NE

SW

236/0652, 2493 mbsl, core length 3.99 m



236/0648

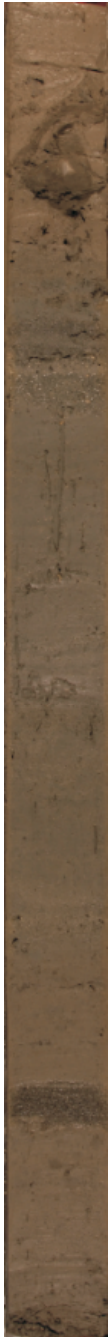
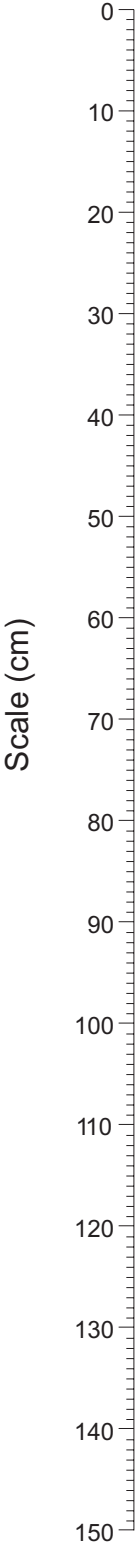
Huntec

236/0656

2006040 0052 Piston Core

BC

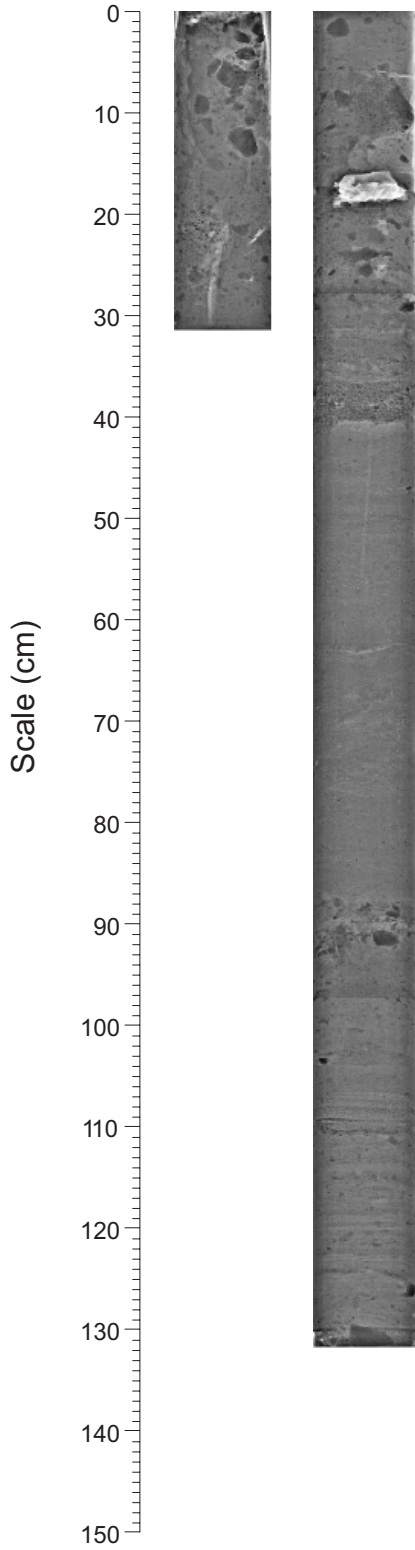
AB



2006040 0052 Piston Core

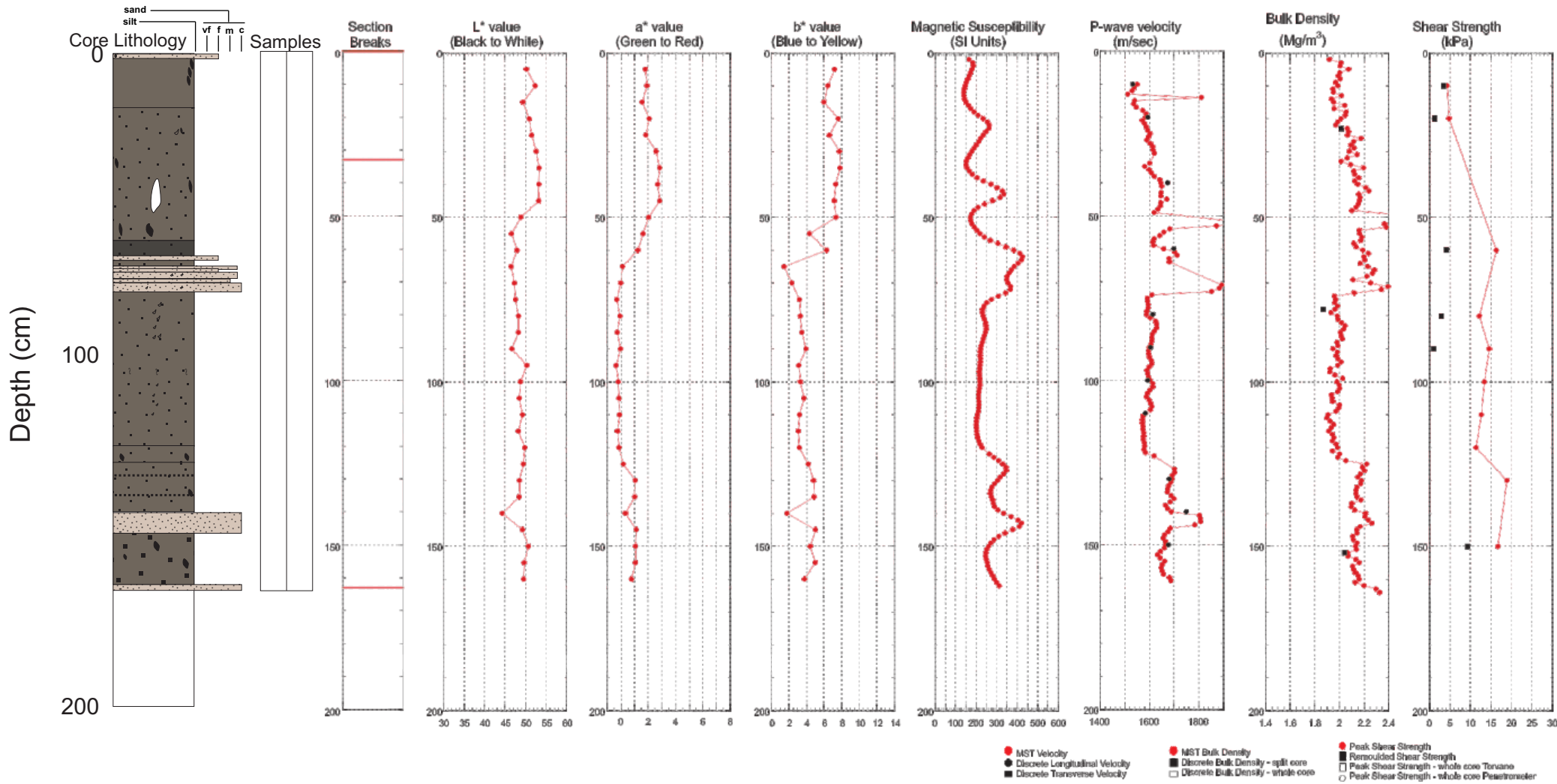
BC

AB



Hudson 2006040 Piston Core 0052

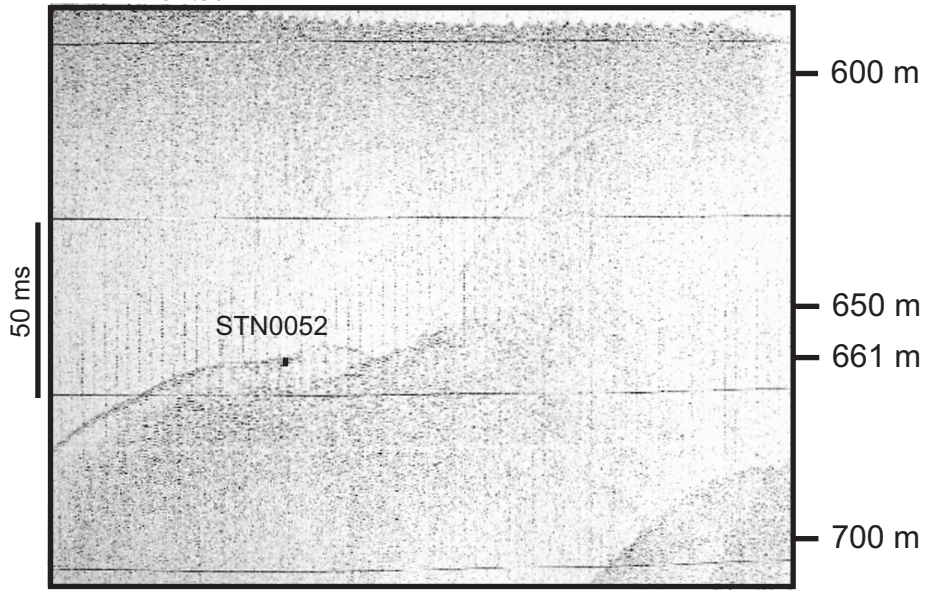
TD 164 cm 58°15.60066 N 59°43.3782 W Water depth 661 m



NE

237/0331, 661 mbsl, core length 1.78 m
Huntec

SW



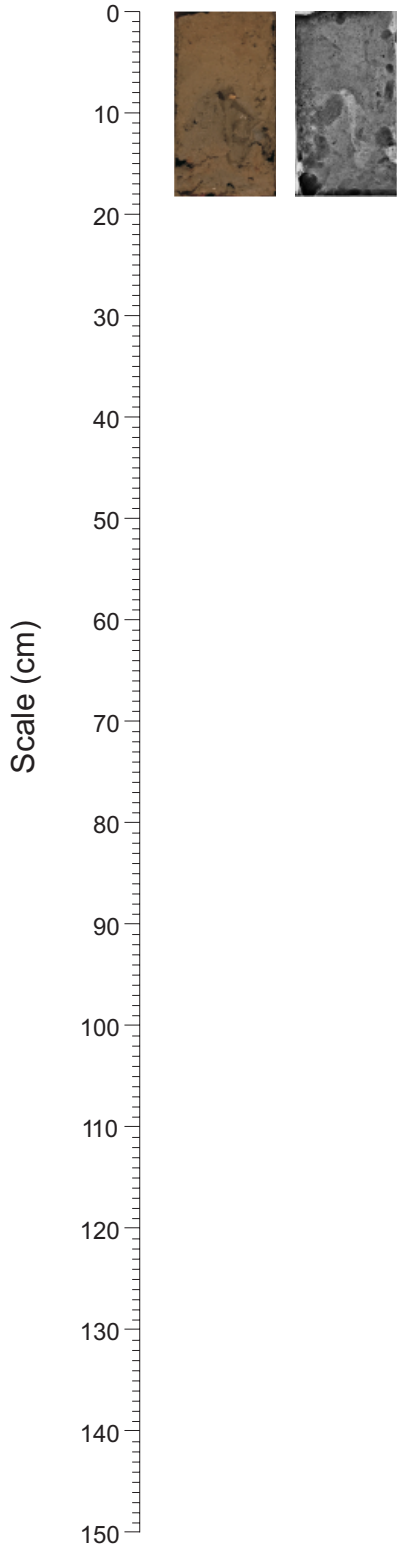
237/0329

237/0333

2006040 0053 Piston Core

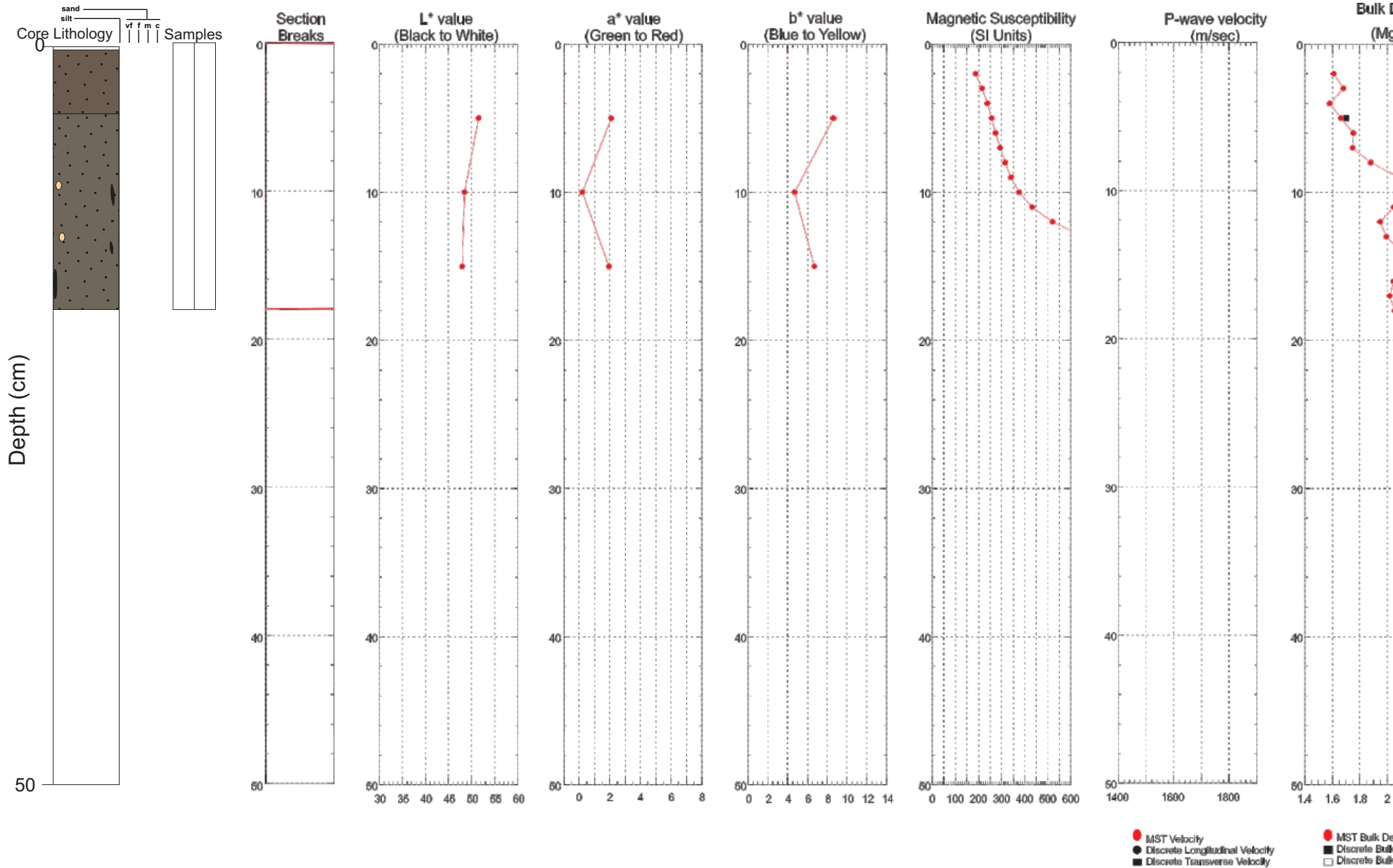
AB

AB



Hudson 2006040 Piston Core 0053

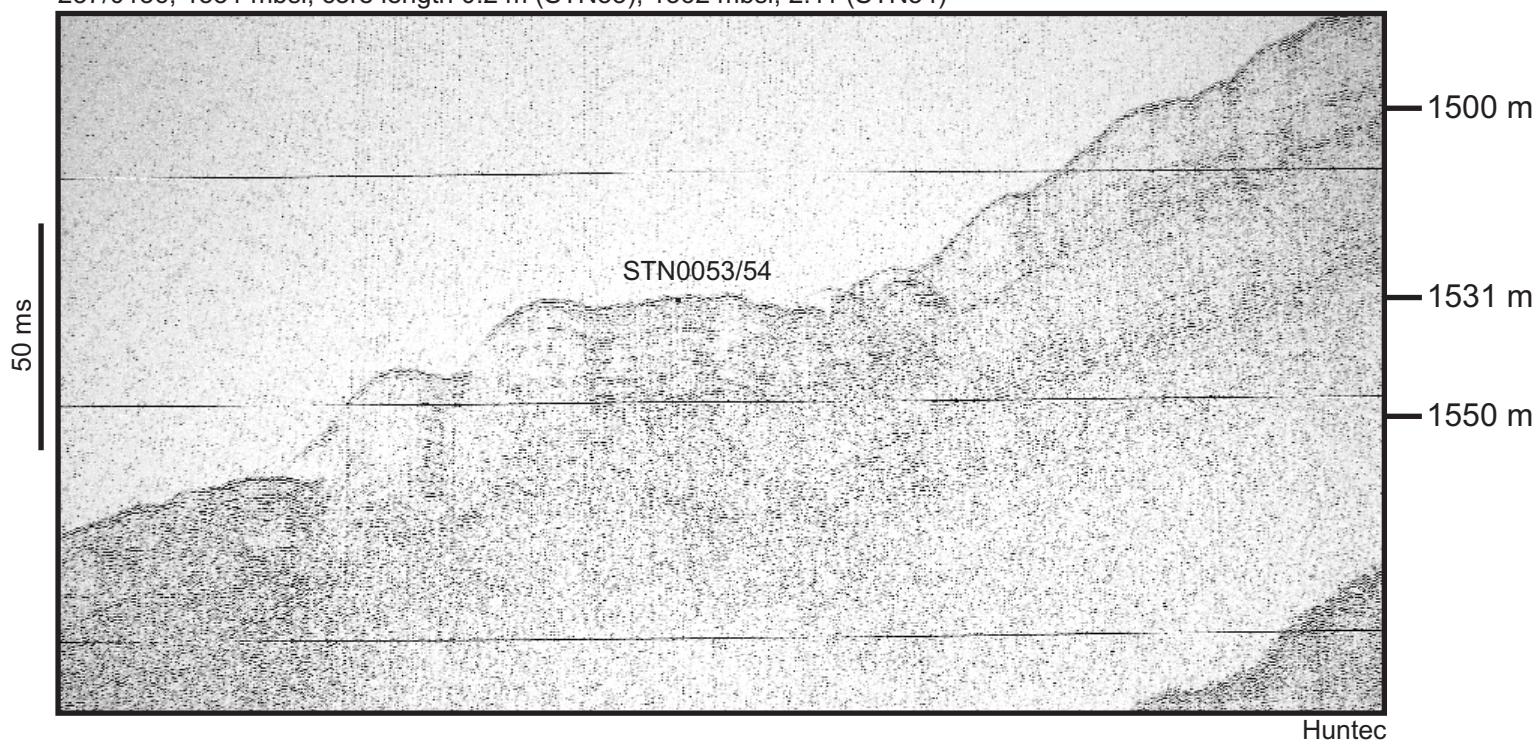
TD 18 cm 58°18.47256 N 59°23.30358 W Water depth 1531 m



NE

SW

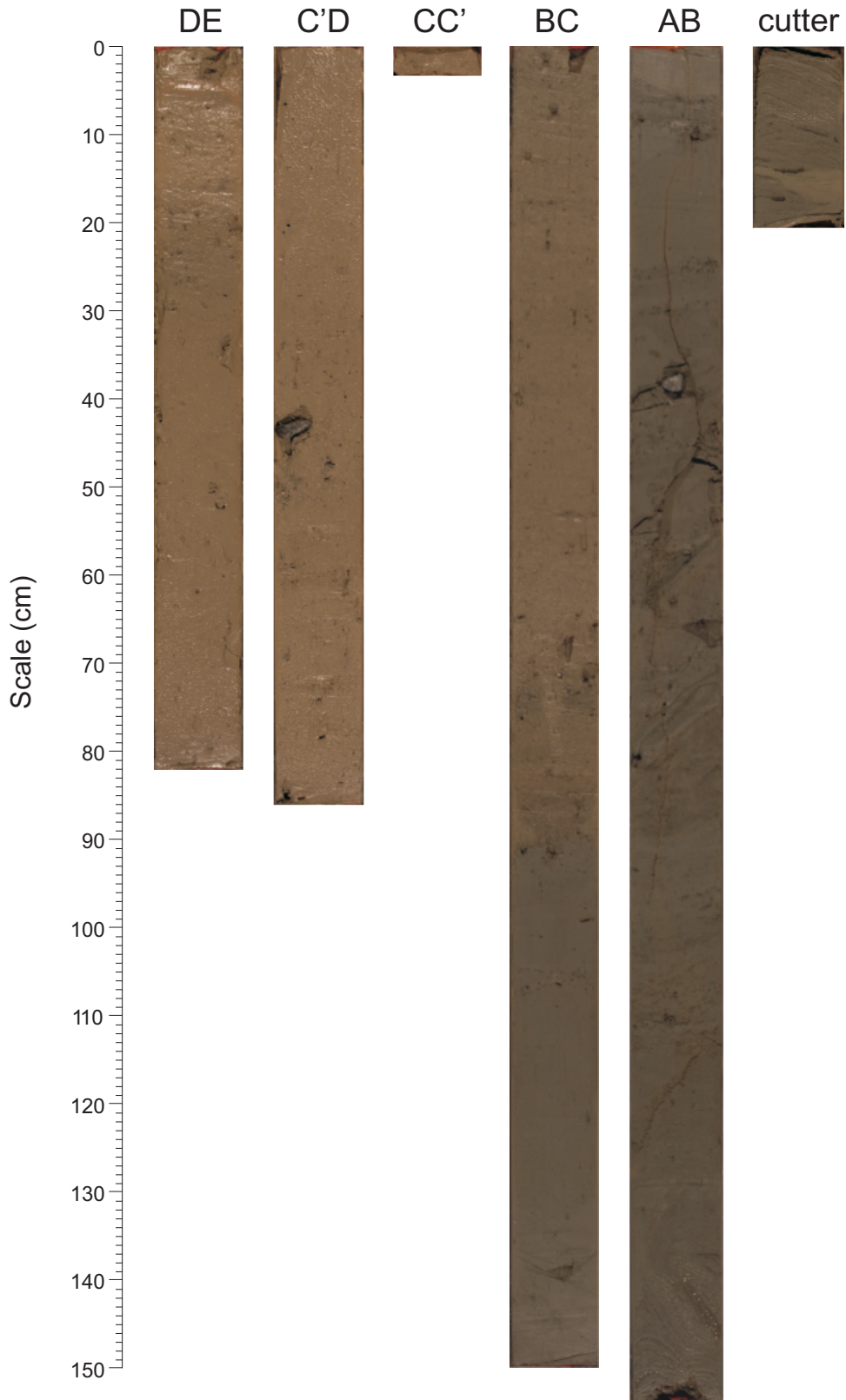
237/0136, 1531 mbsl, core length 0.2 m (STN53); 1562 mbsl, 2.11 (STN54)



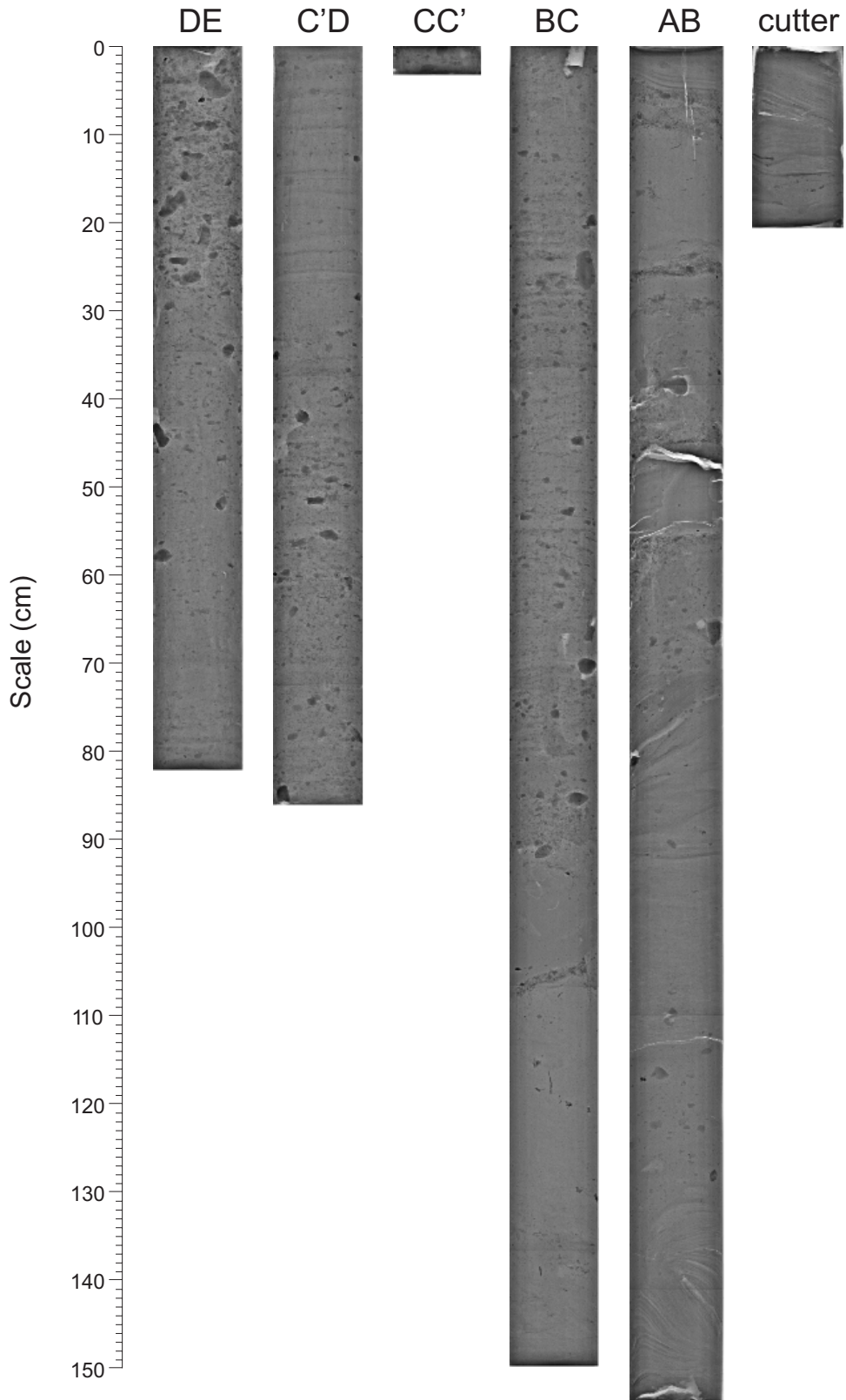
237/0126

237/0146

2006040 0055 Piston Core

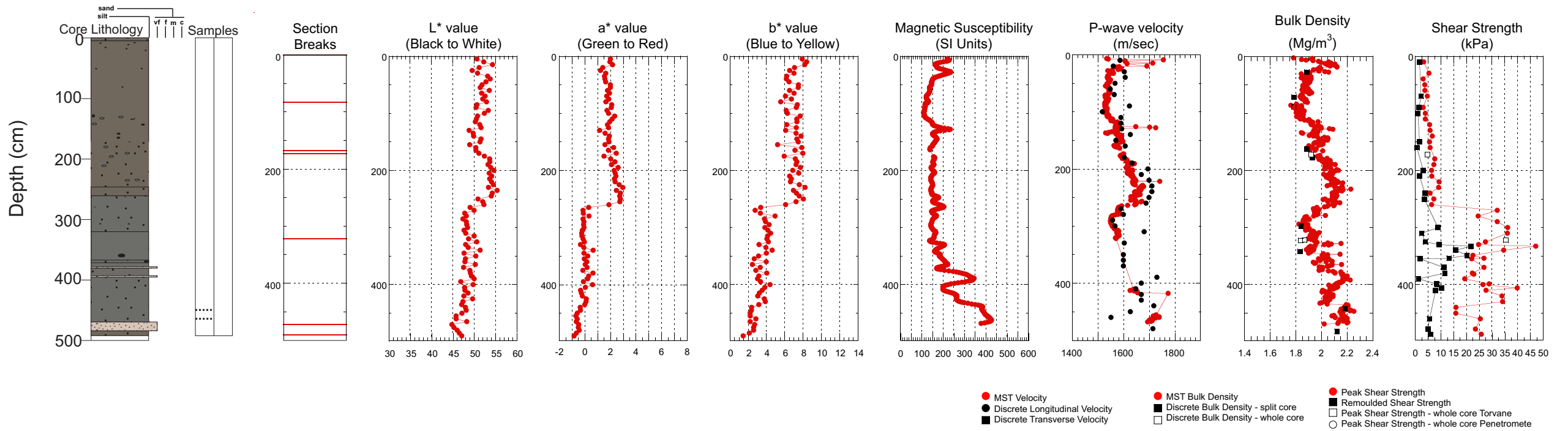


2006040 0055 Piston Core



Hudson 2006040 Piston Core 0055

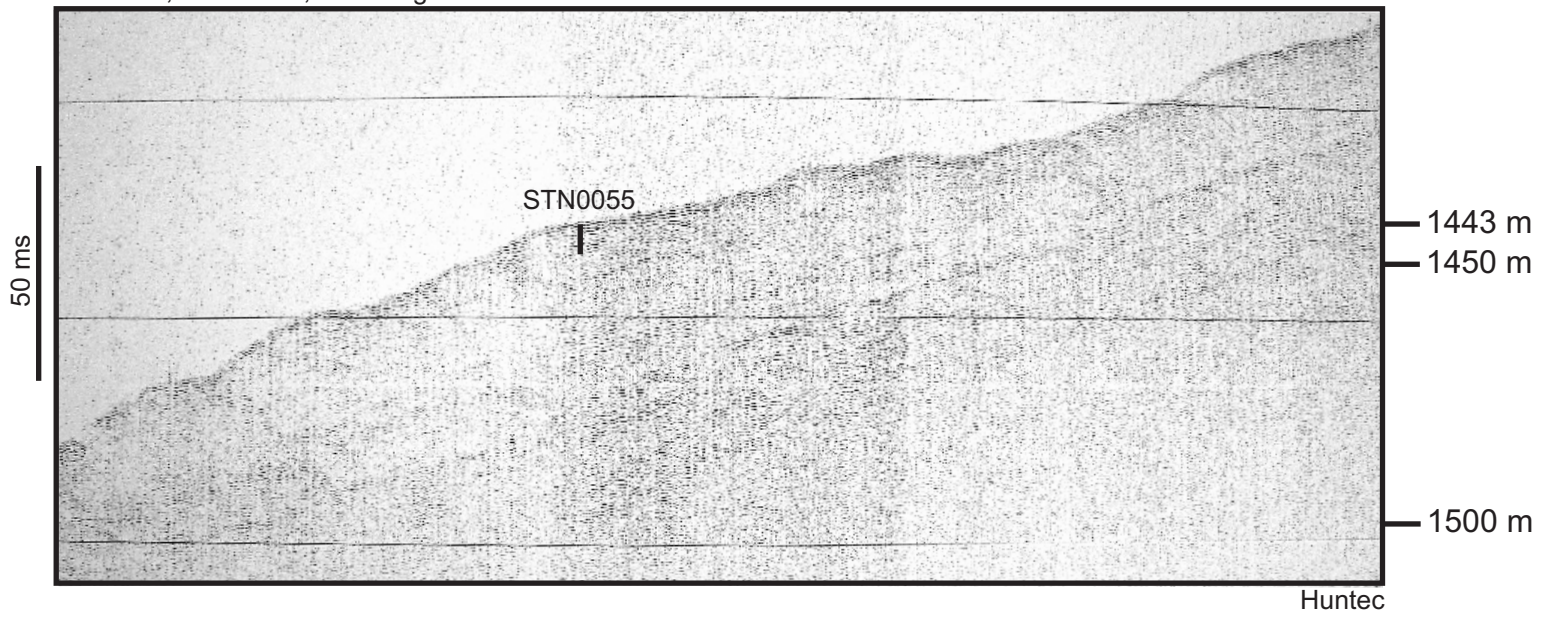
TD 492 cm 59°17.7948 N 59°27.71538 W Water depth 1443 m



NE

SW

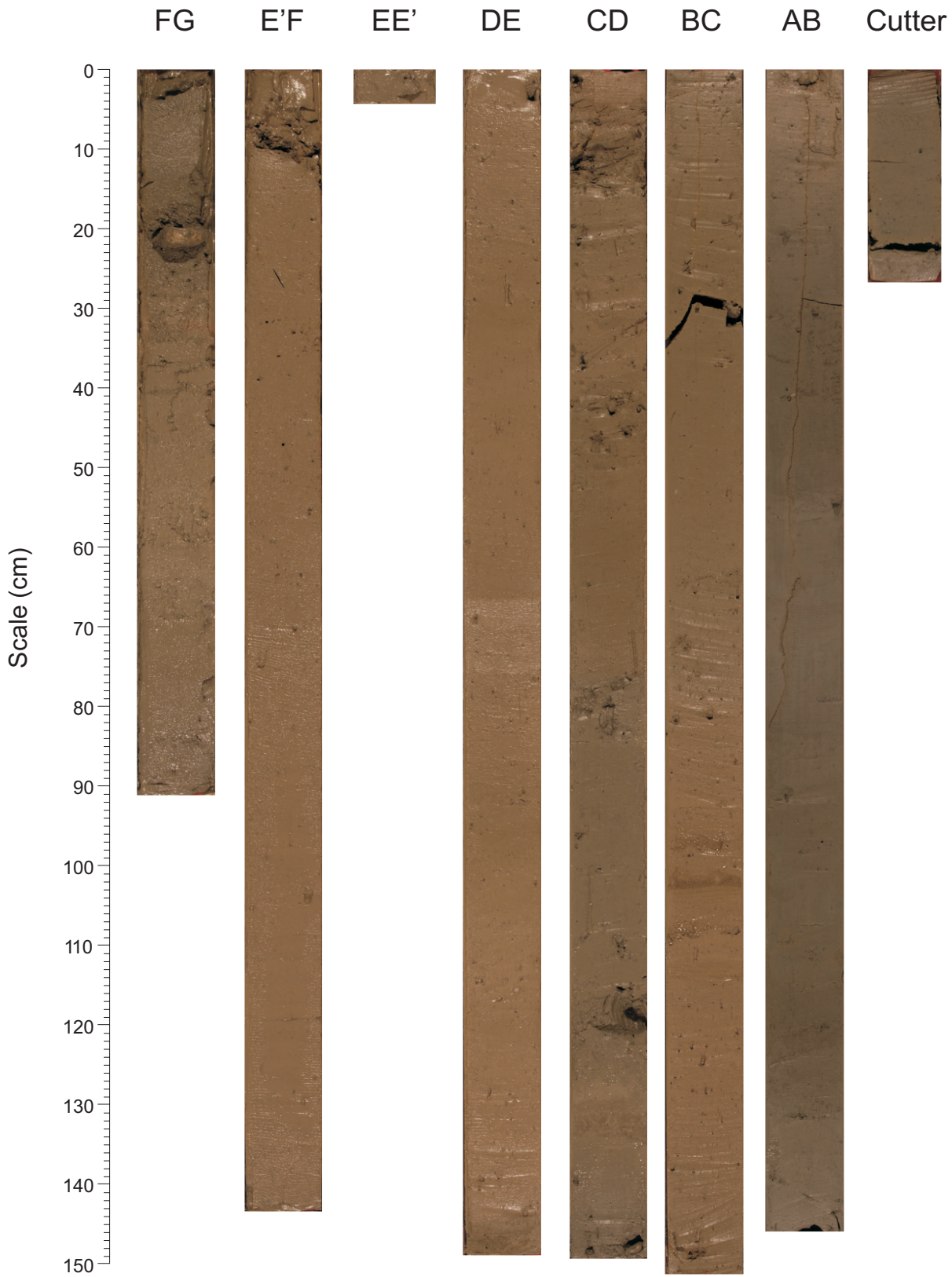
237/0201, 1443 mbsl, core length 5.11 m



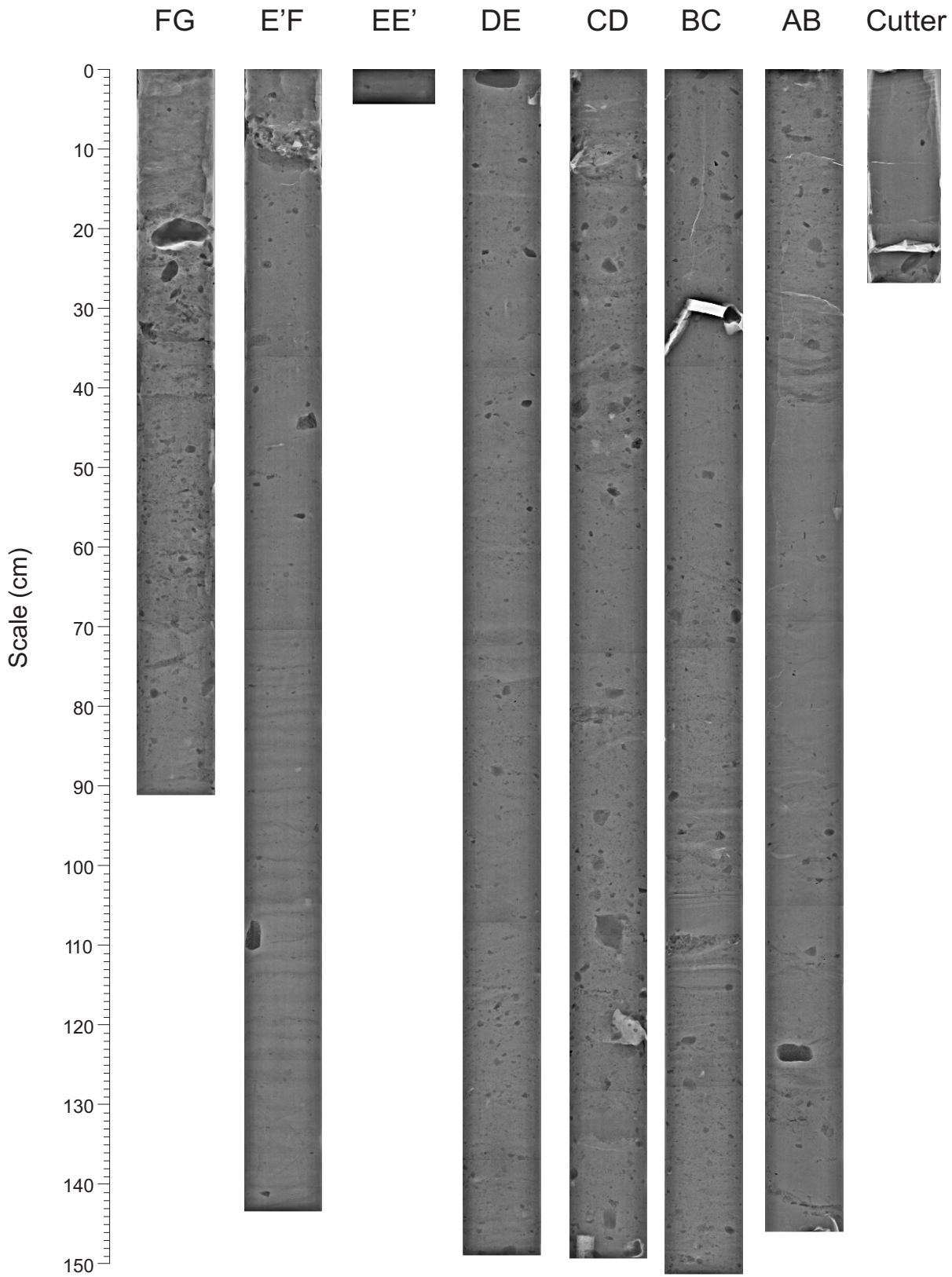
237/0151

237/0211

2006040 0056 Piston Core

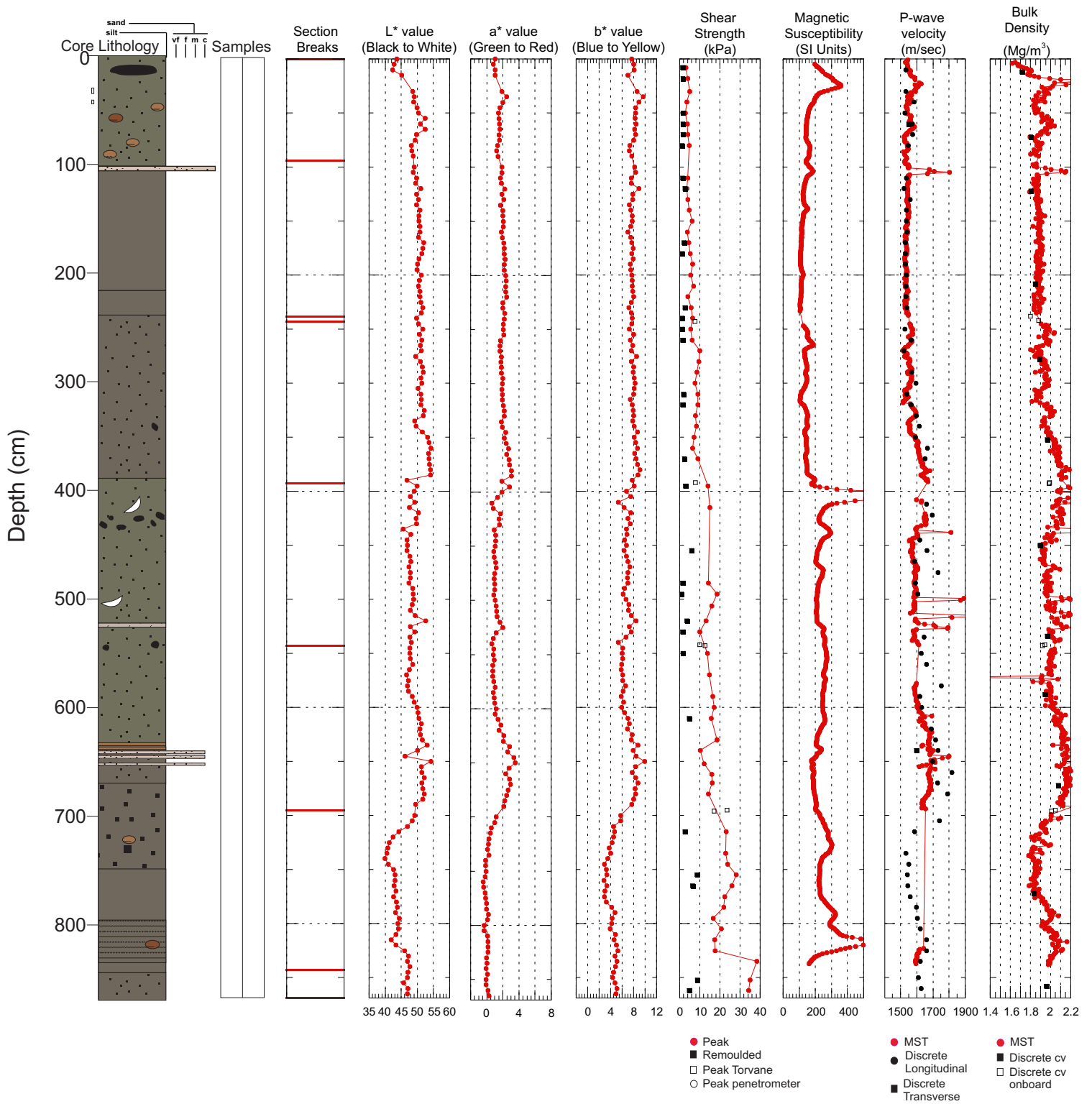


2006040 0056 Piston Core



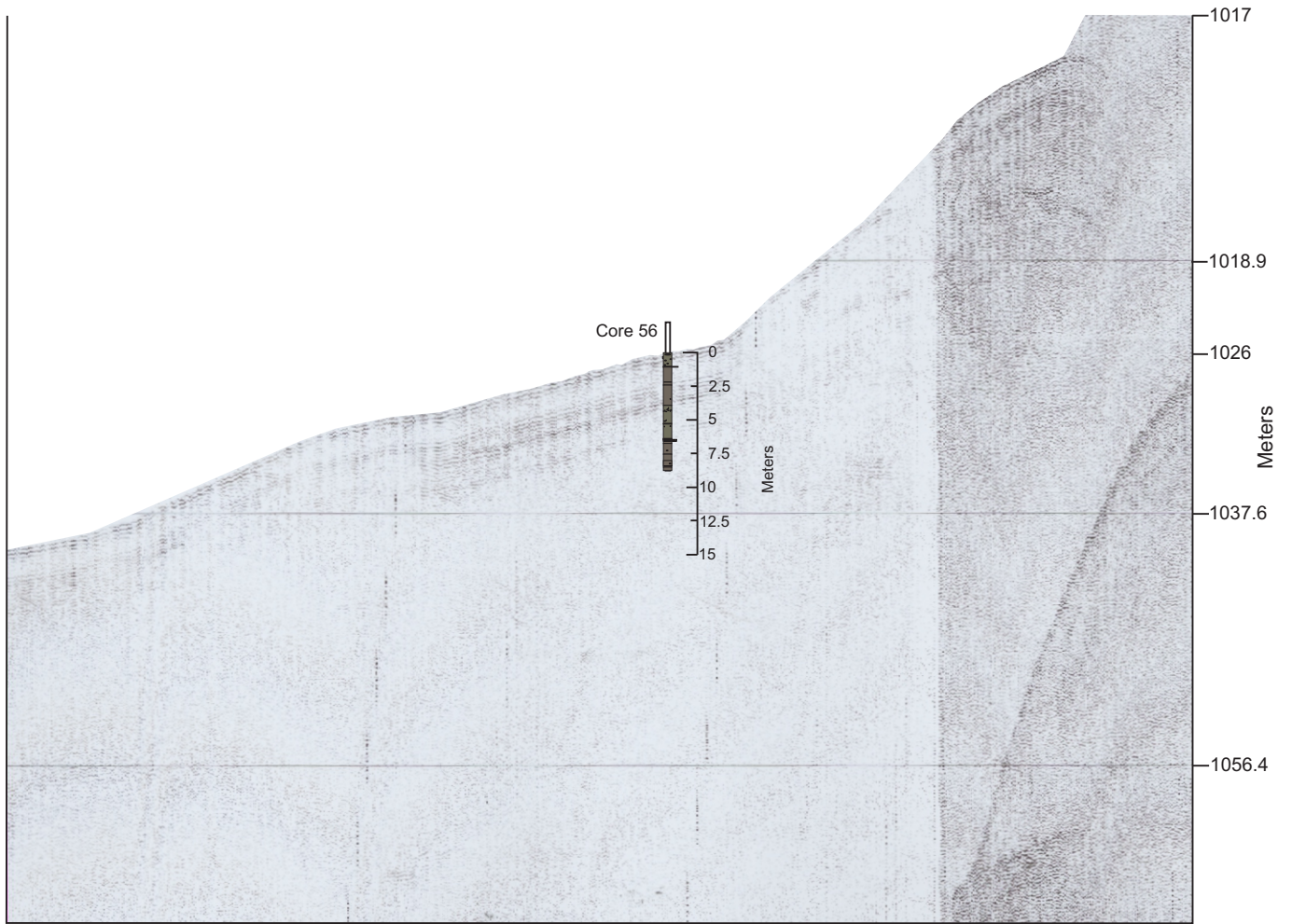
Hudson 2006040 Piston Core 0056

TD 869 cm 57°32.0449 N 59°11.6065 W Water depth 1020 m



NE

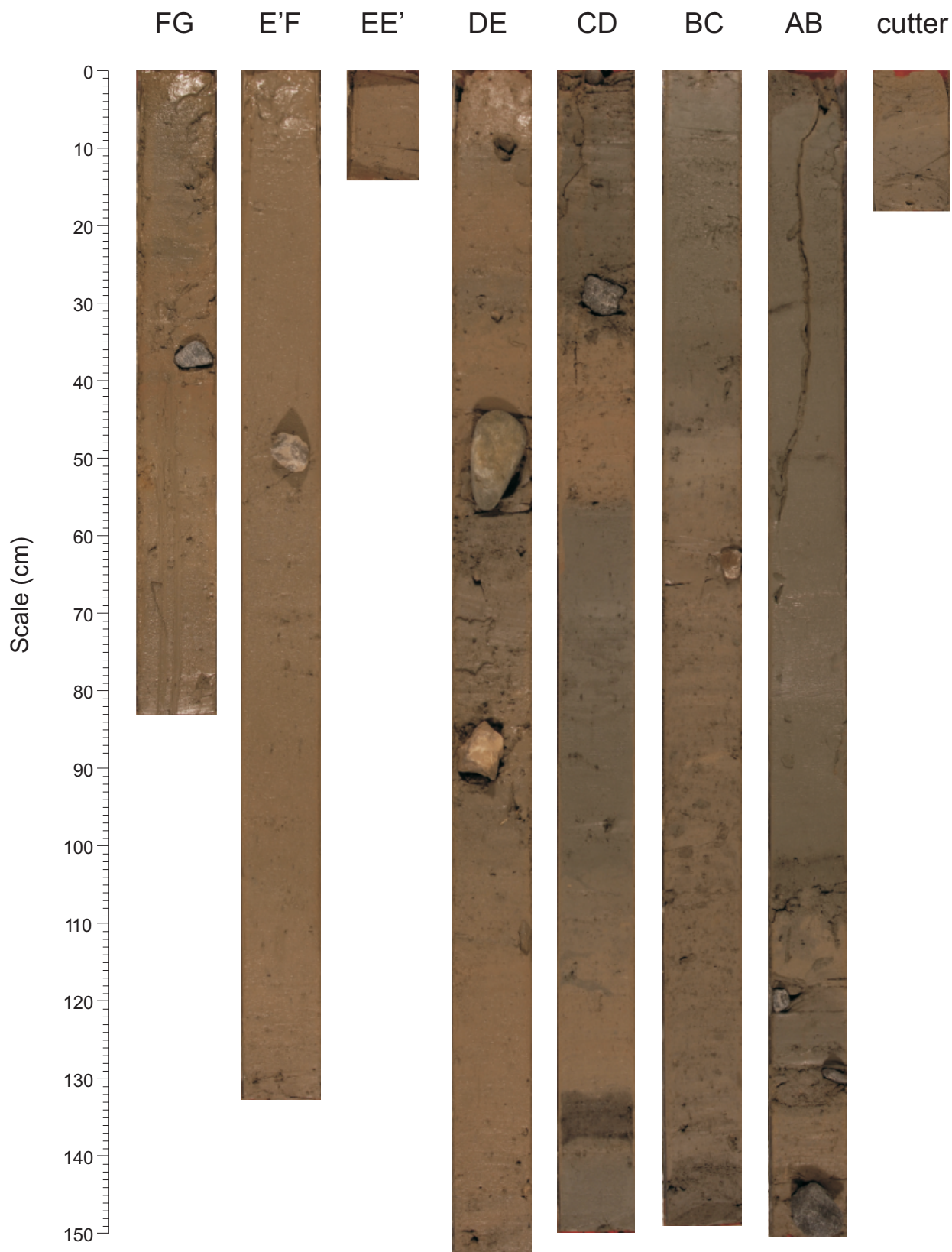
SW



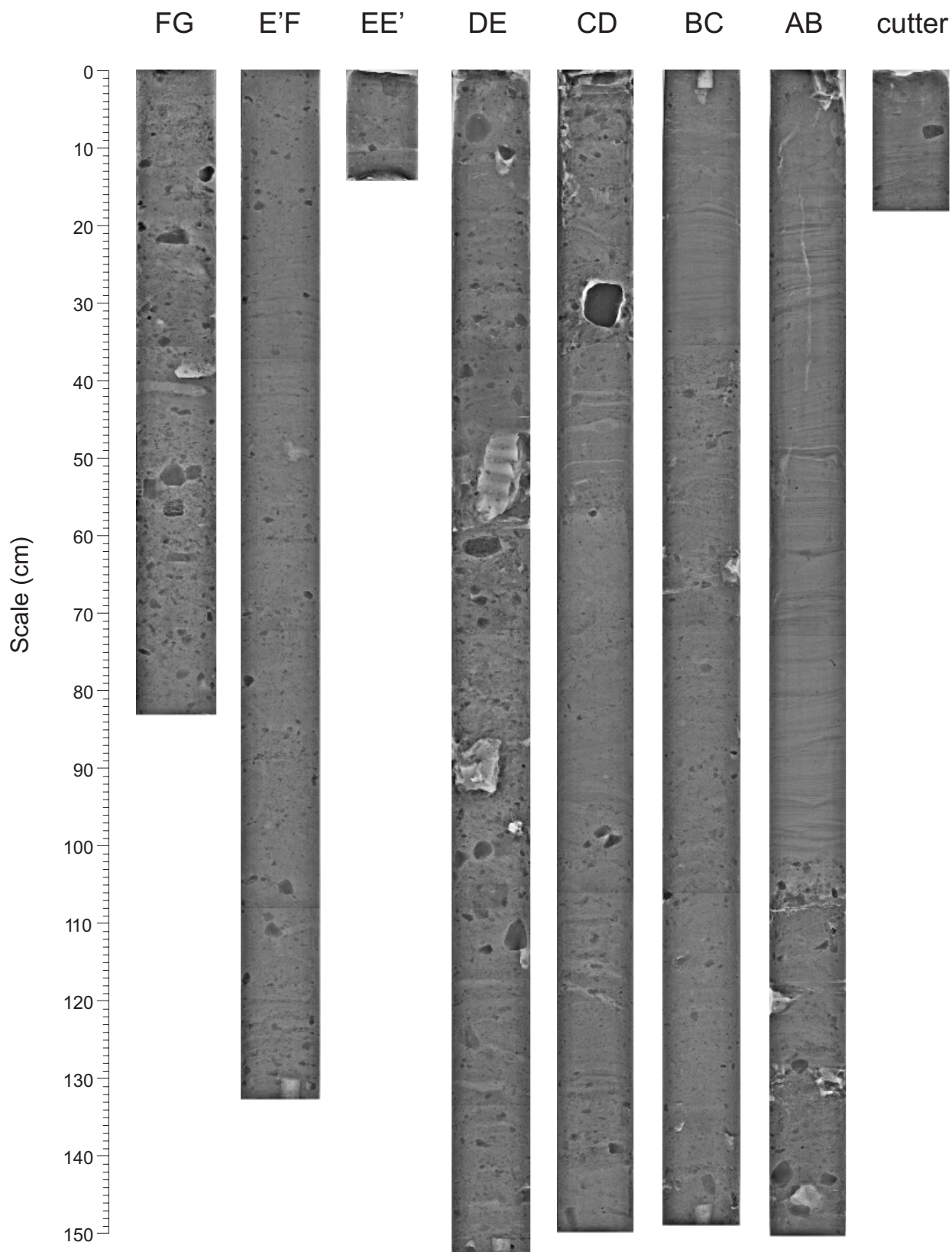
238/0859

238/0912

2006040 0057 Piston Core

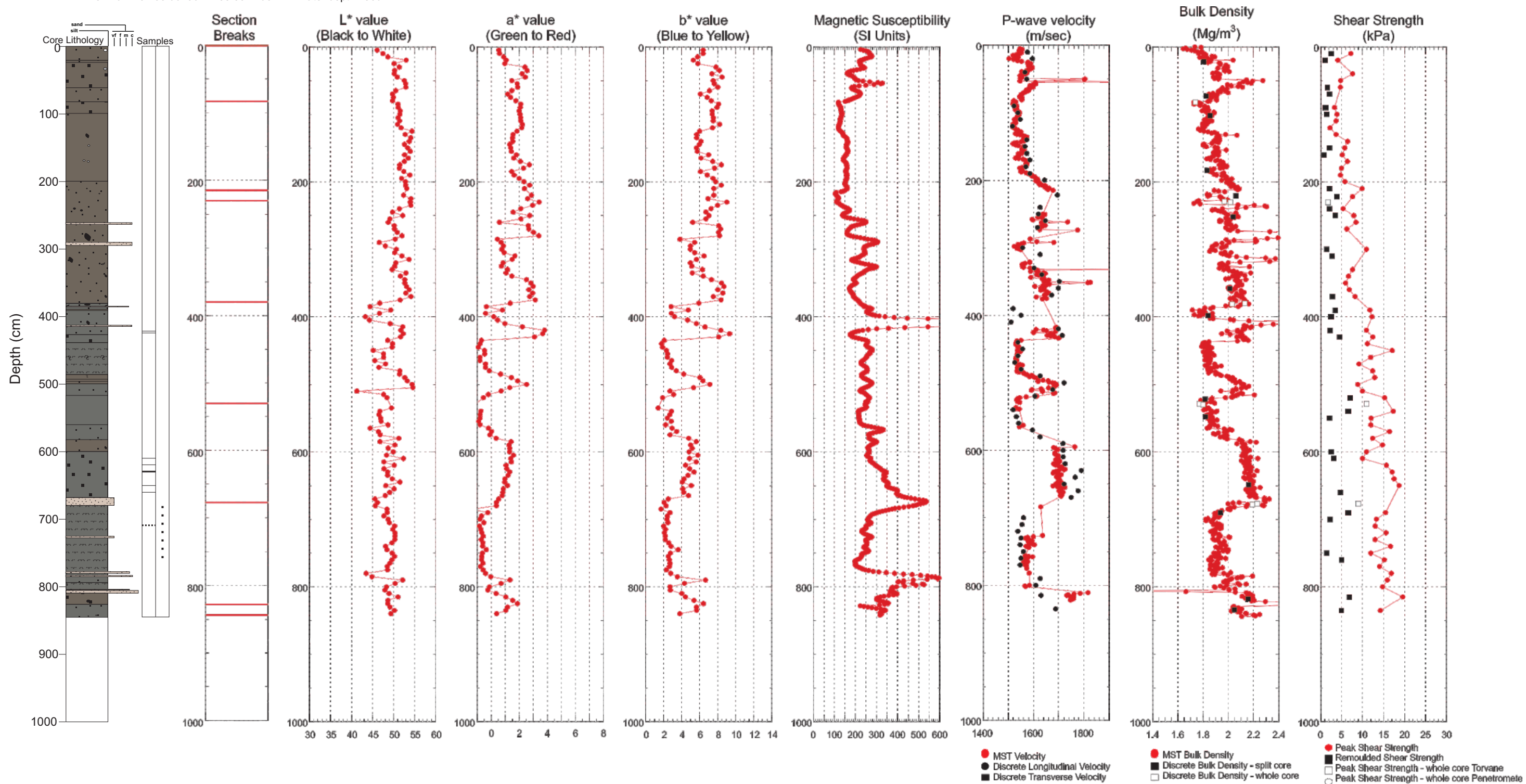


2006040 0057 Piston Core



Hudson 2006040 Piston Core 0057

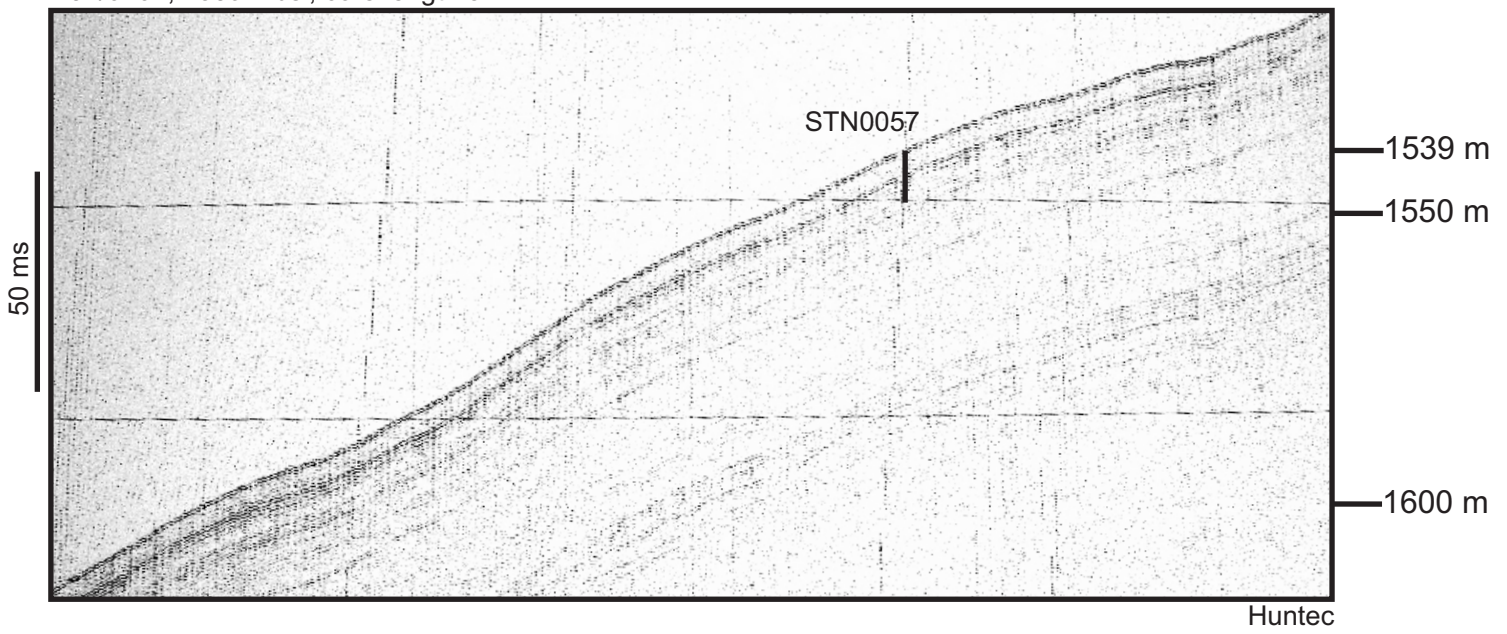
TD 847 cm 57°35.06136 N 58°55.4295 W Water depth 1539 m



NE

SW

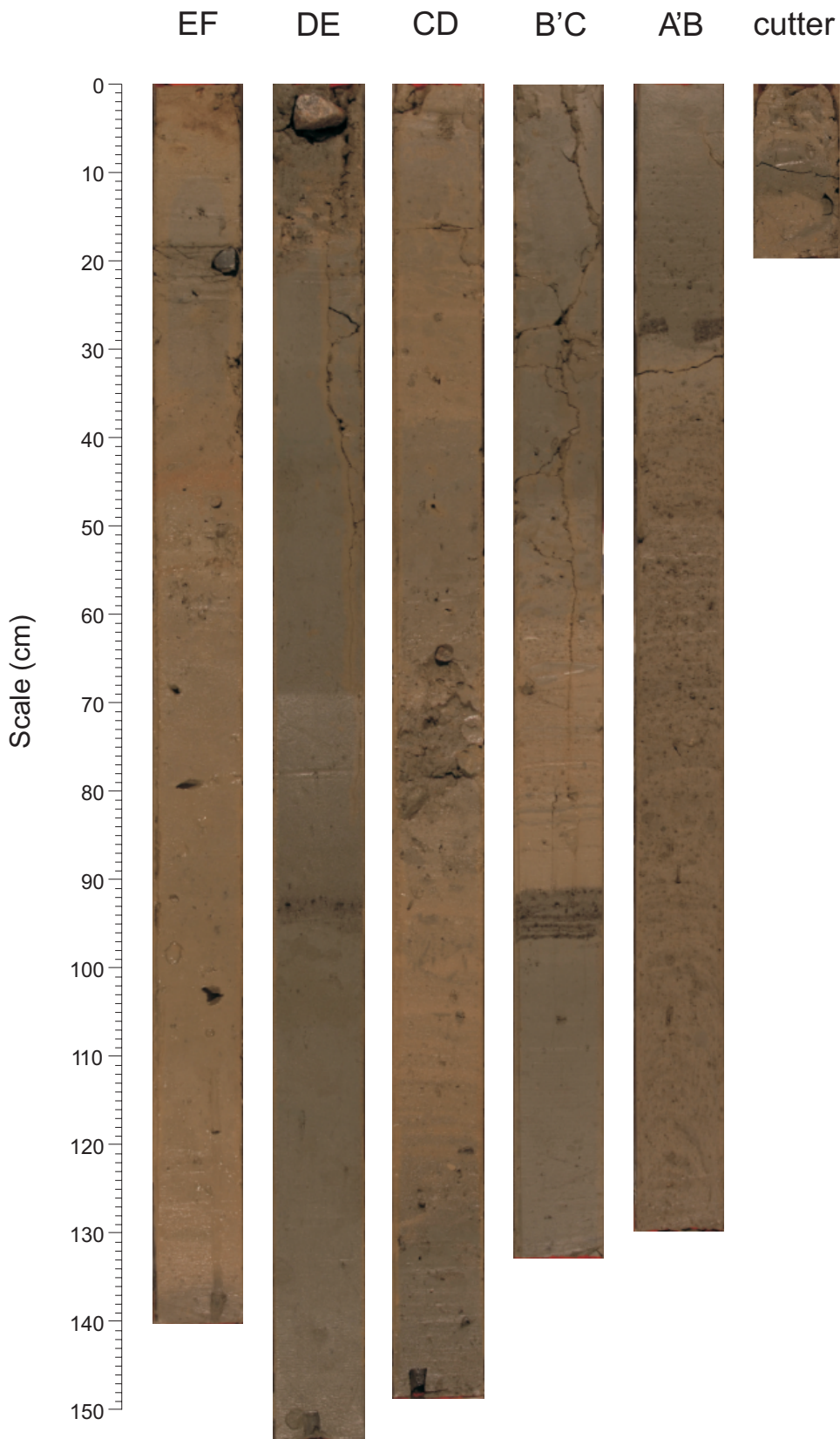
237/0707, 1539 mbsl, core length 8.71 m



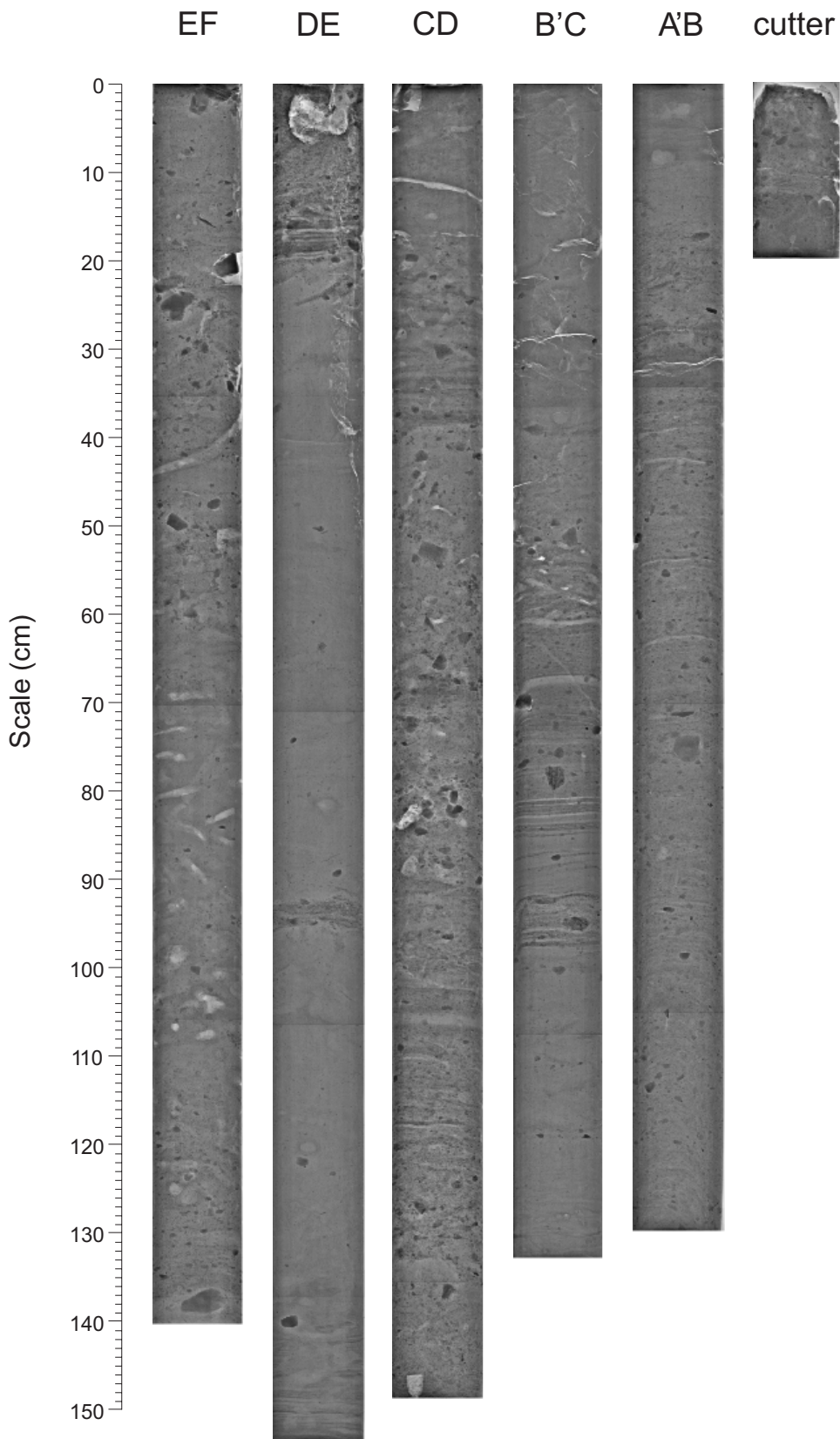
238/0654

238/0714

2006040 0058 Piston Core

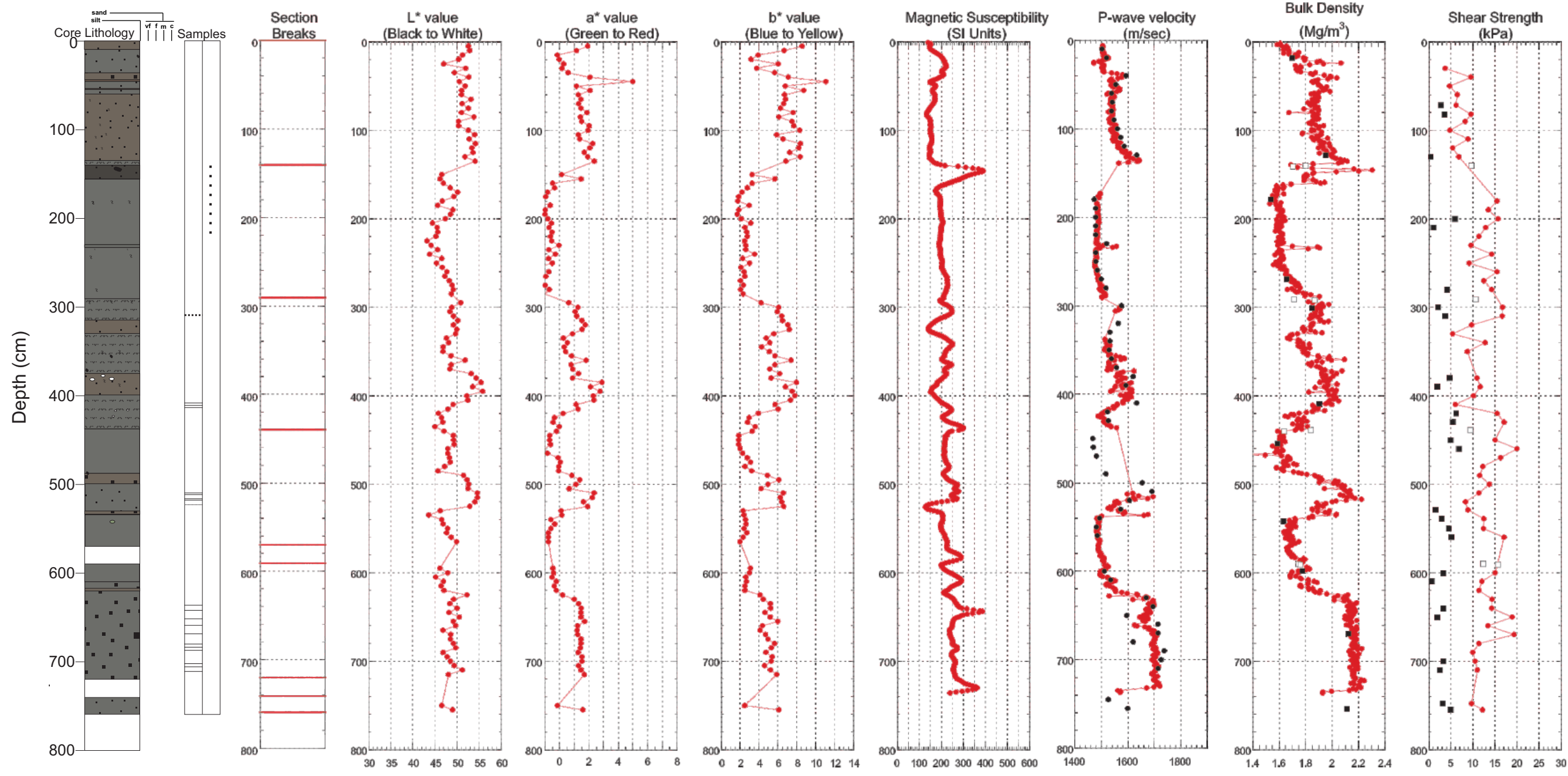


2006040 0058 Piston Core



Hudson 2006040 Piston Core 0058

TD 760 cm 57°40.5680 N 58°19.39143 W Water depth 1999 m

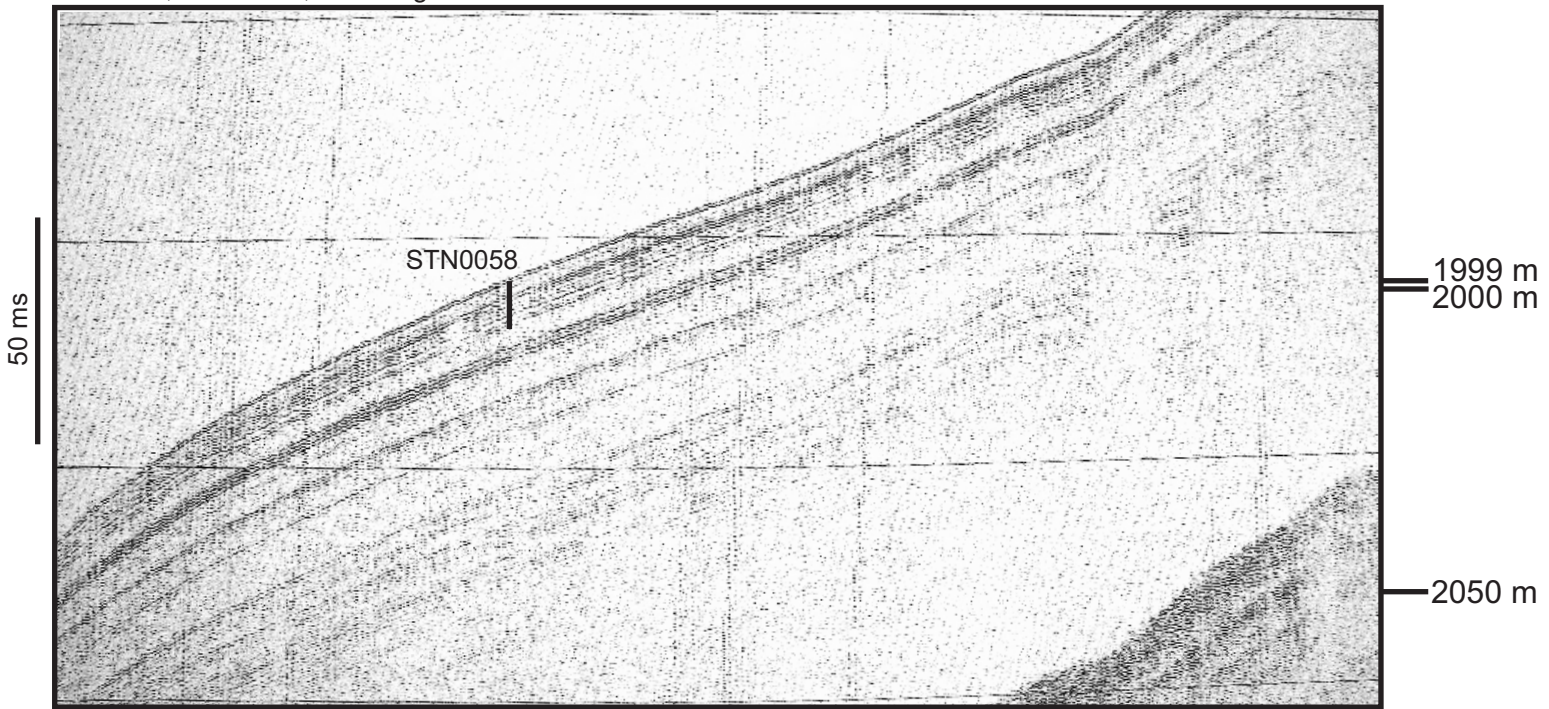


● MST Velocity
● Discrete Longitudinal Velocity
■ Discrete Transverse Velocity
● MST Bulk Density
■ Discrete Bulk Density - split core
 Discrete Bulk Density - whole core
● Peak Shear Strength
■ Remoulded Shear Strength
 Peak Shear Strength - whole core Torvane
 Peak Shear Strength - whole core Penetrom

NE

SW

238/0505, 1999 mbsl, core length 7.78 m

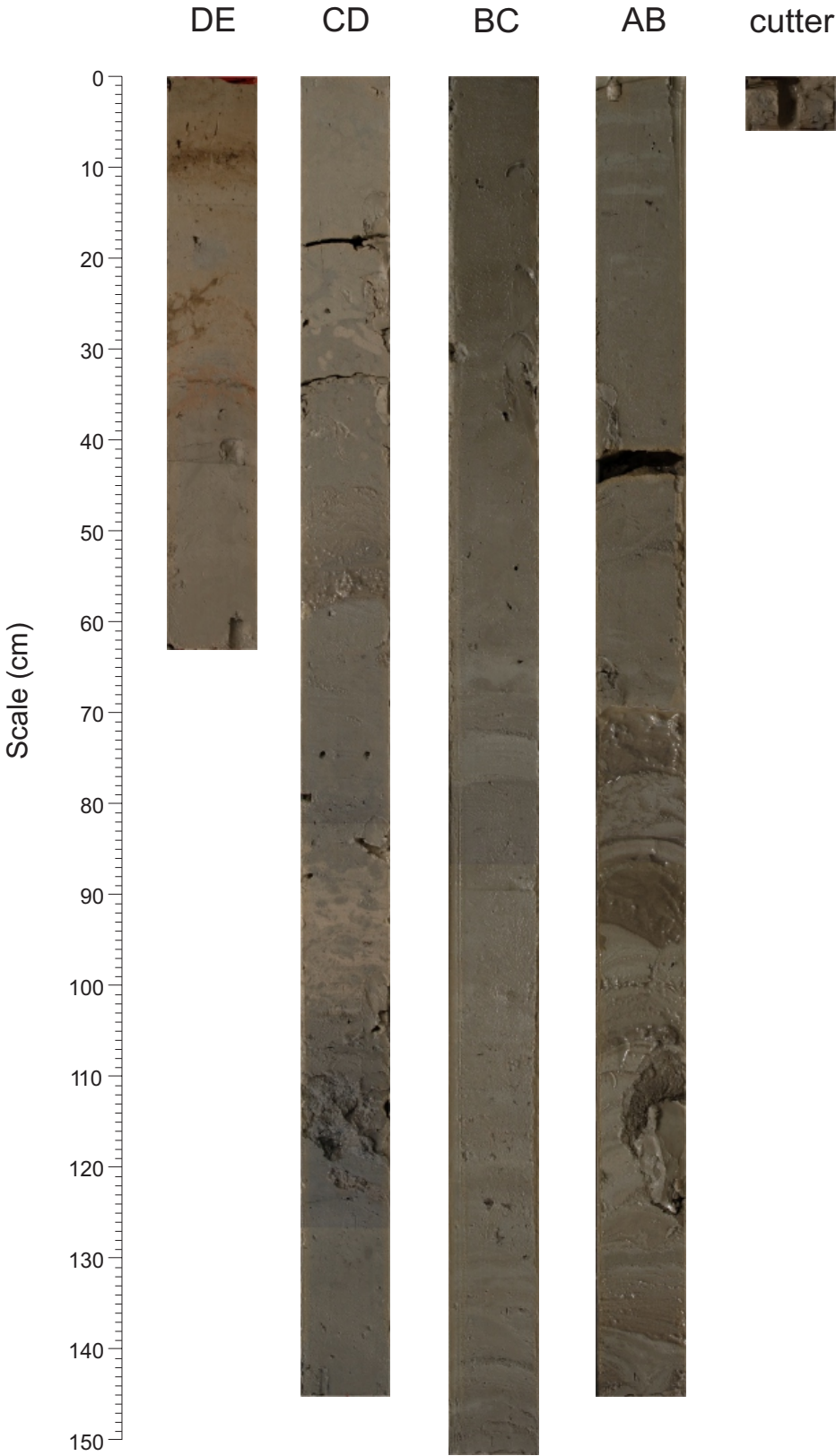


Huntec

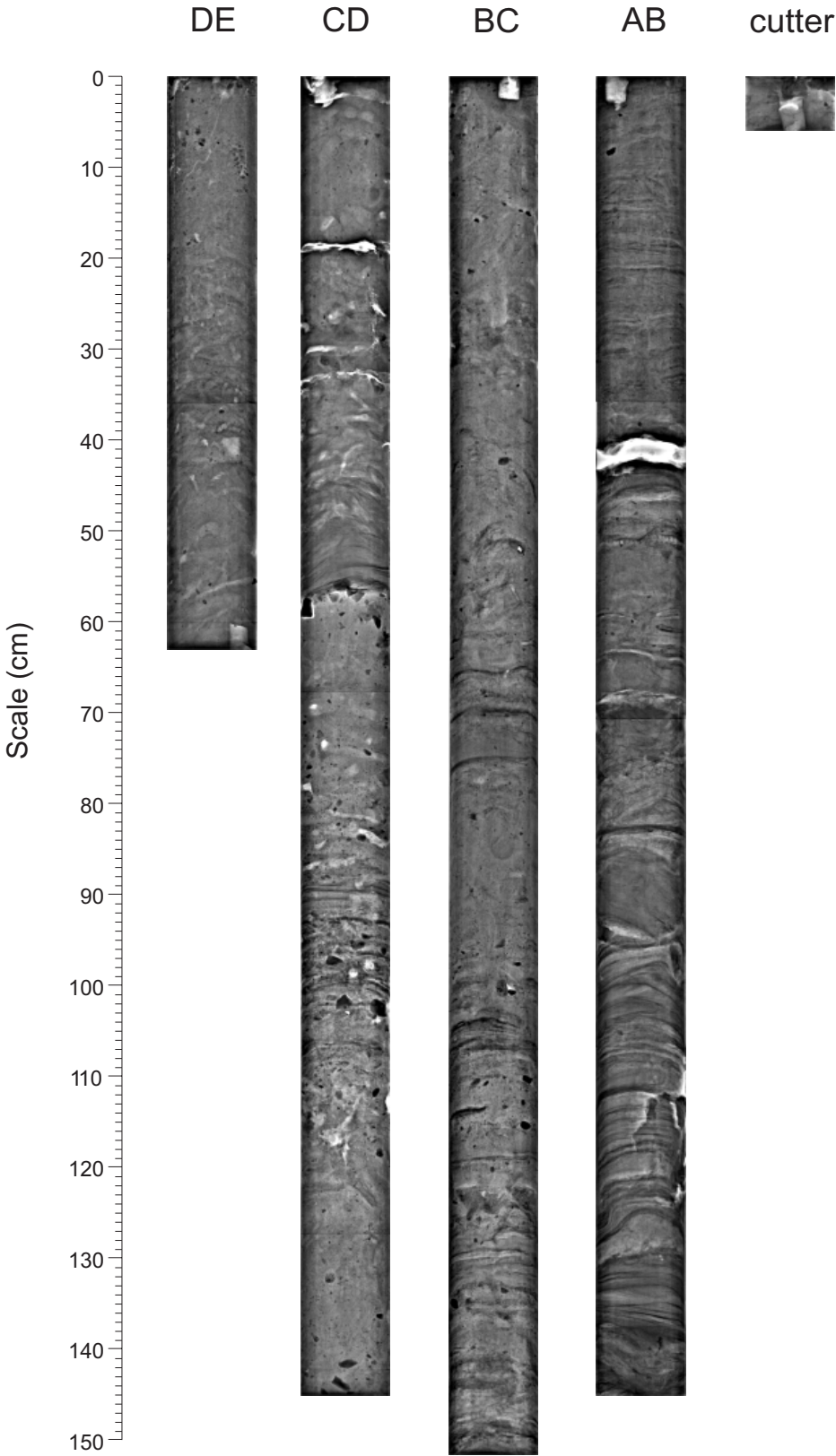
238/0459

238/0514

2006040 0059 PistonCore

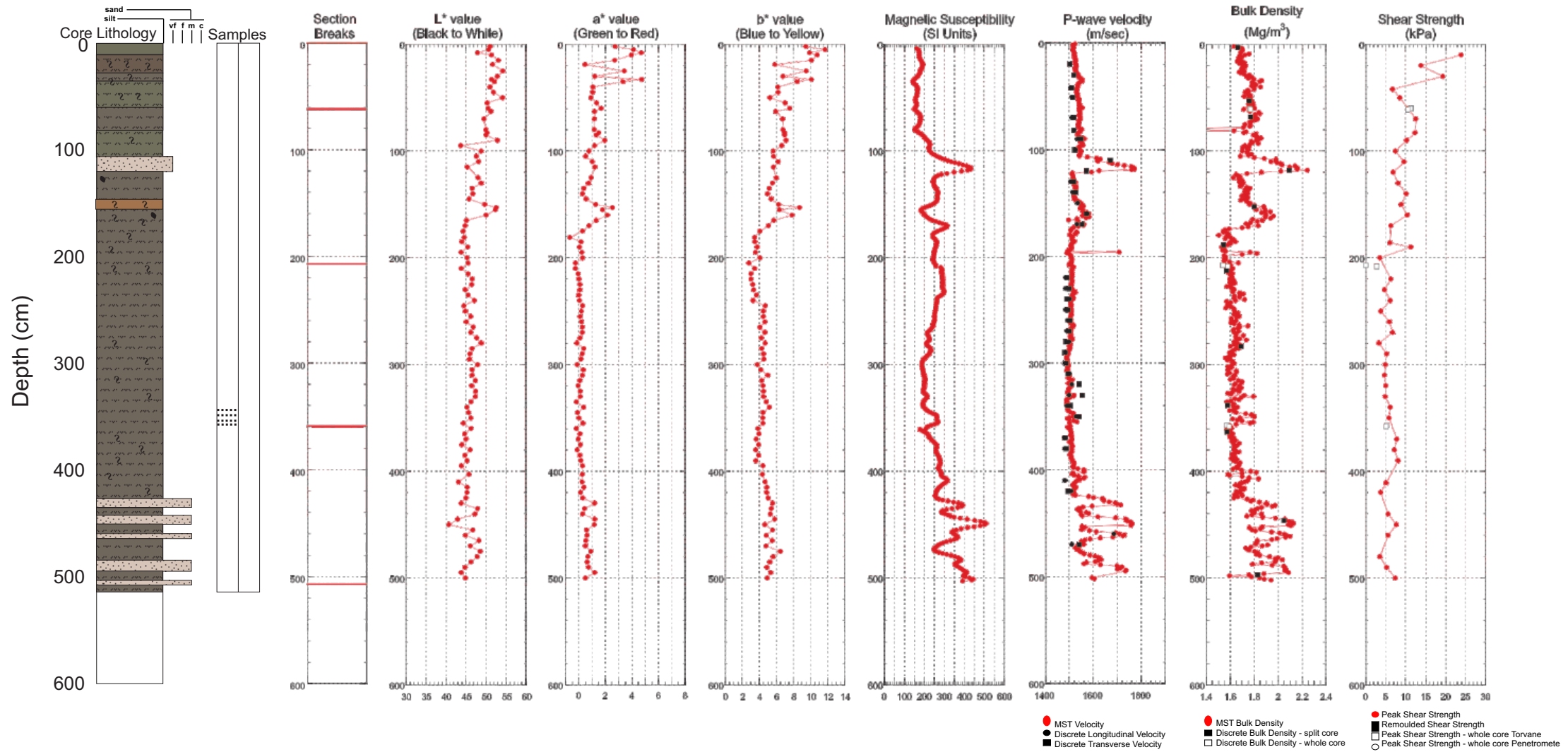


2006040 0059 PistonCore



Hudson 2006040 Piston Core 0059

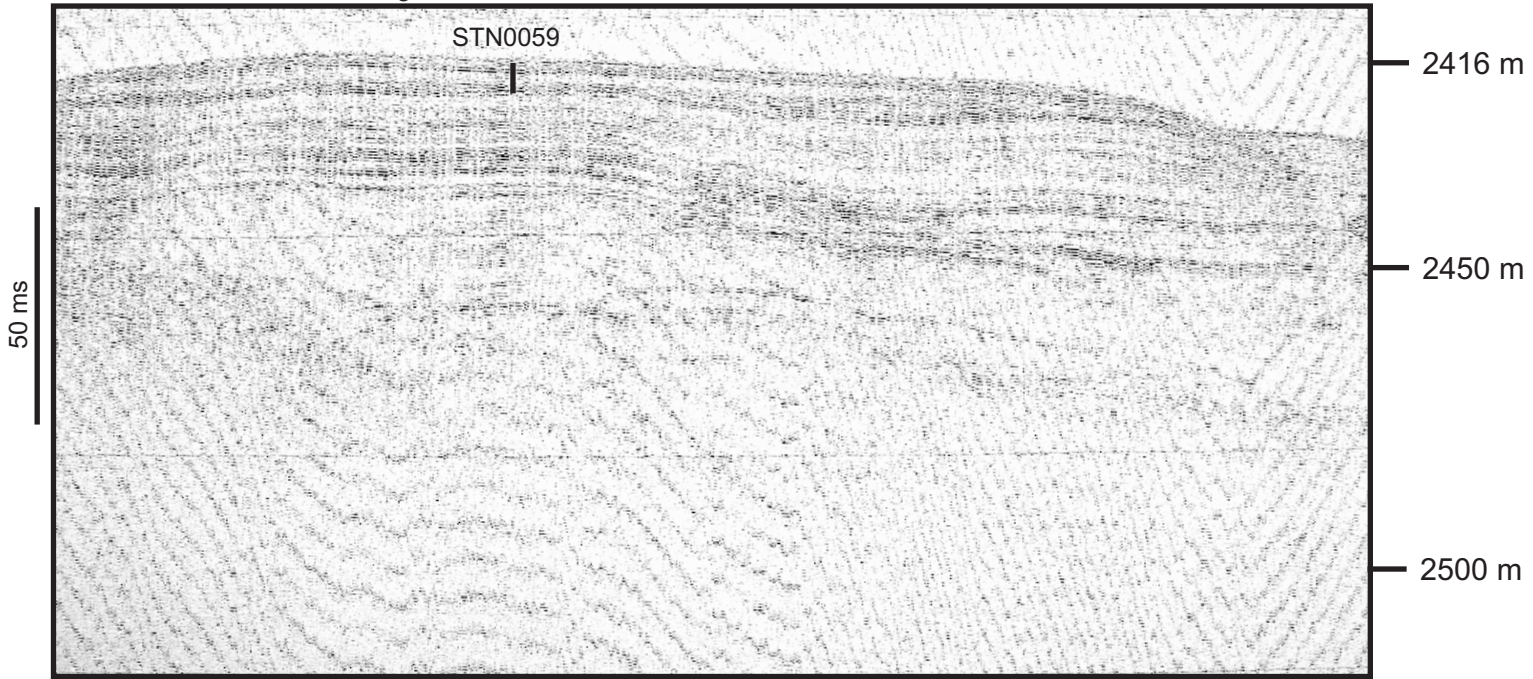
TD 514 cm 57°05.7722 N 57°08.6122 W Water depth 2416 m



SE

NW

225/1908, 2422 mbsl, core length 5.24 m

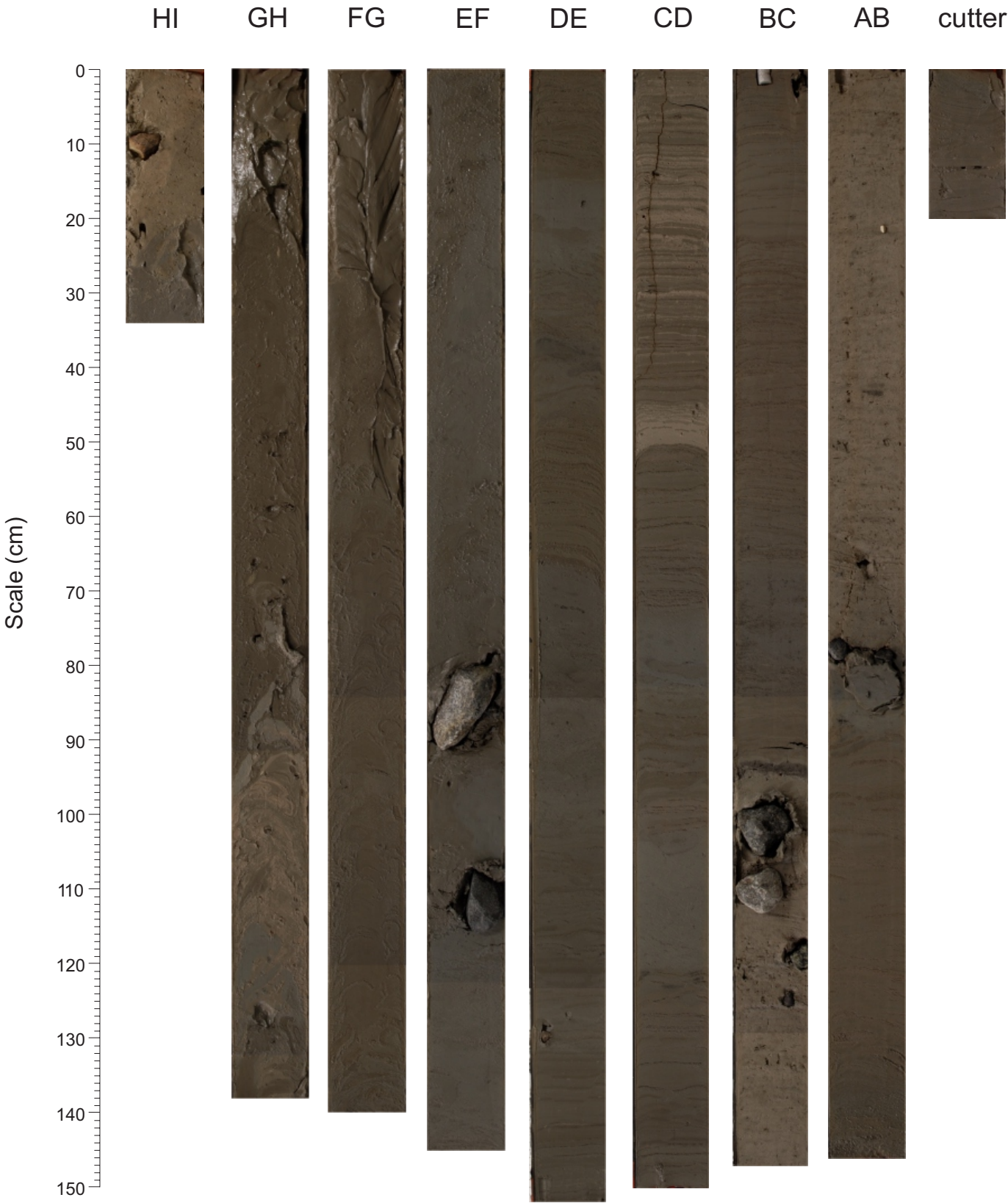


Huntec

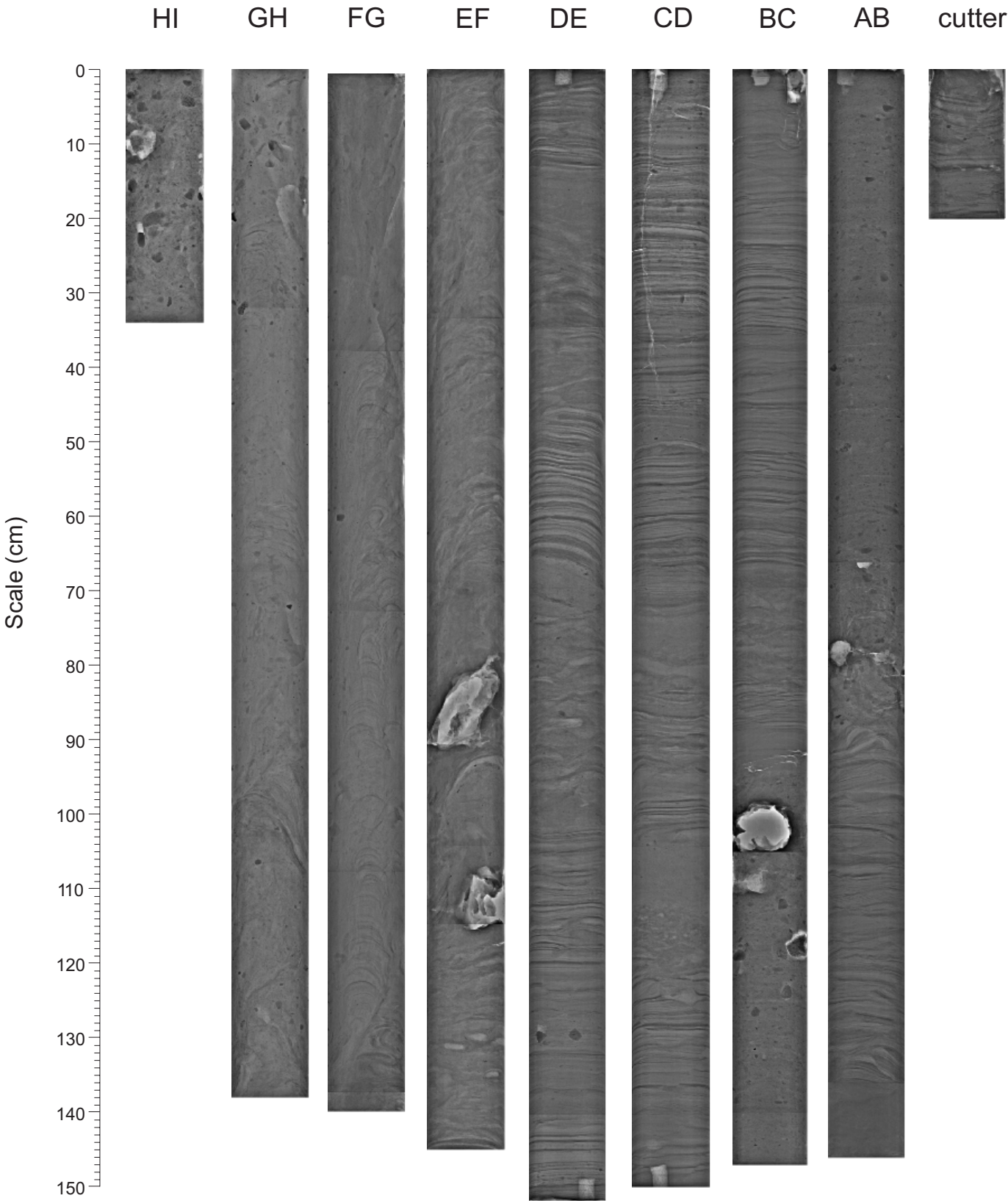
225/1905

225/1920

2006040 0060 Piston Core

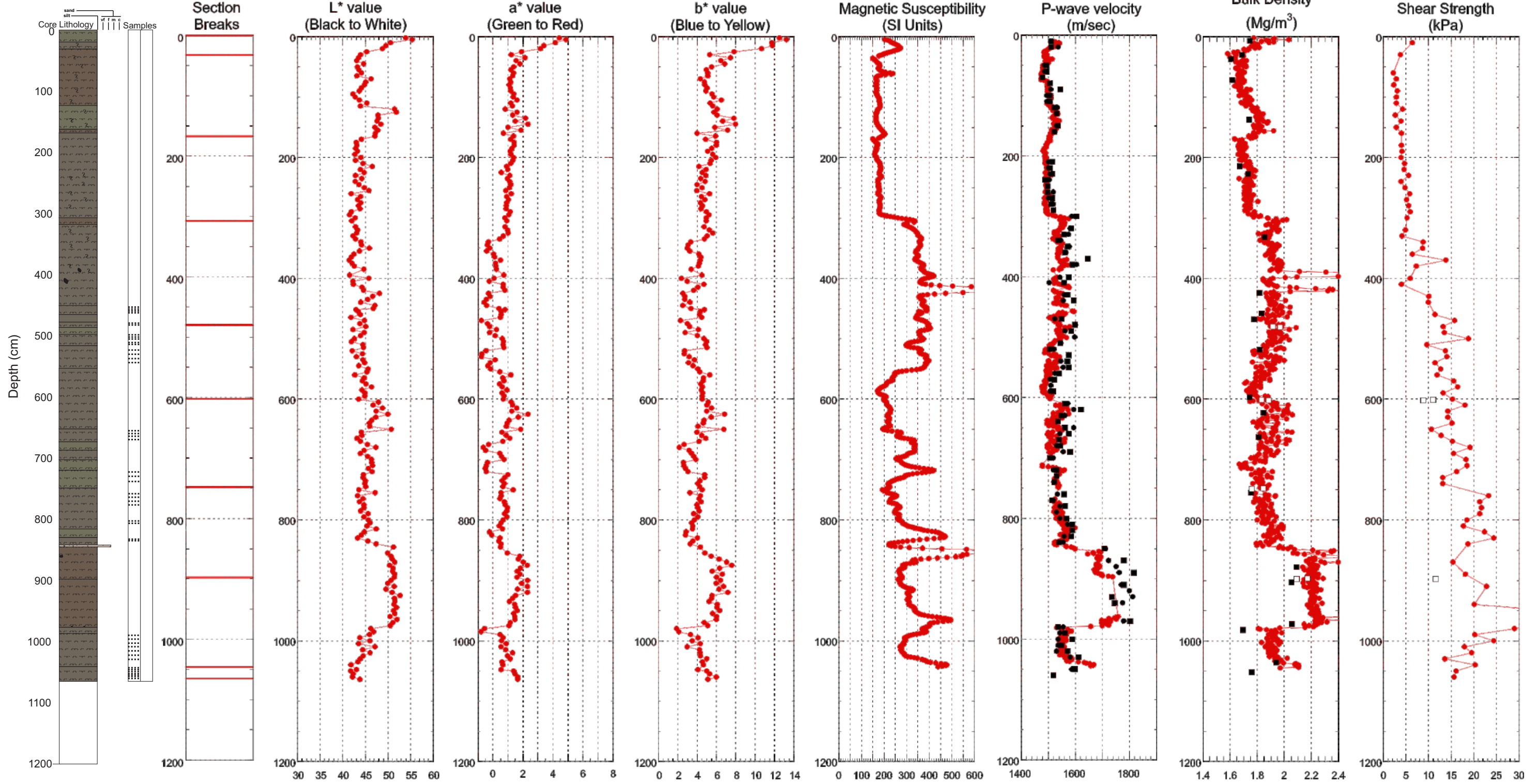


2006040 0060 Piston Core



Hudson 2006040 Piston Core 0060

TD 1065 cm 57°01.9698 N 57°02.7486 W Water depth 2278 m

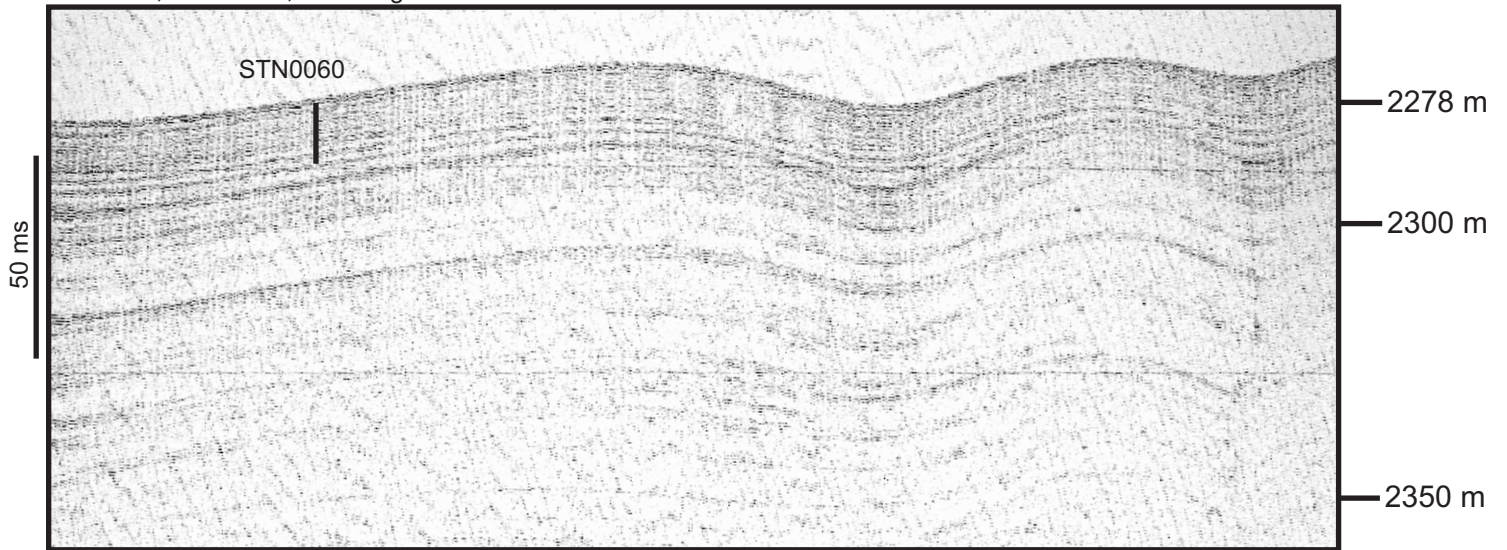


- MST Velocity
- Discrete Longitudinal Velocity
- Discrete Transverse Velocity
- MST Bulk Density
- Discrete Bulk Density - split core
- Discrete Bulk Density - whole core
- Peak Shear Strength
- Remoulded Shear Strength
- Peak Shear Strength - whole core Torvane
- Peak Shear Strength - whole core Penetromete

SE

NW

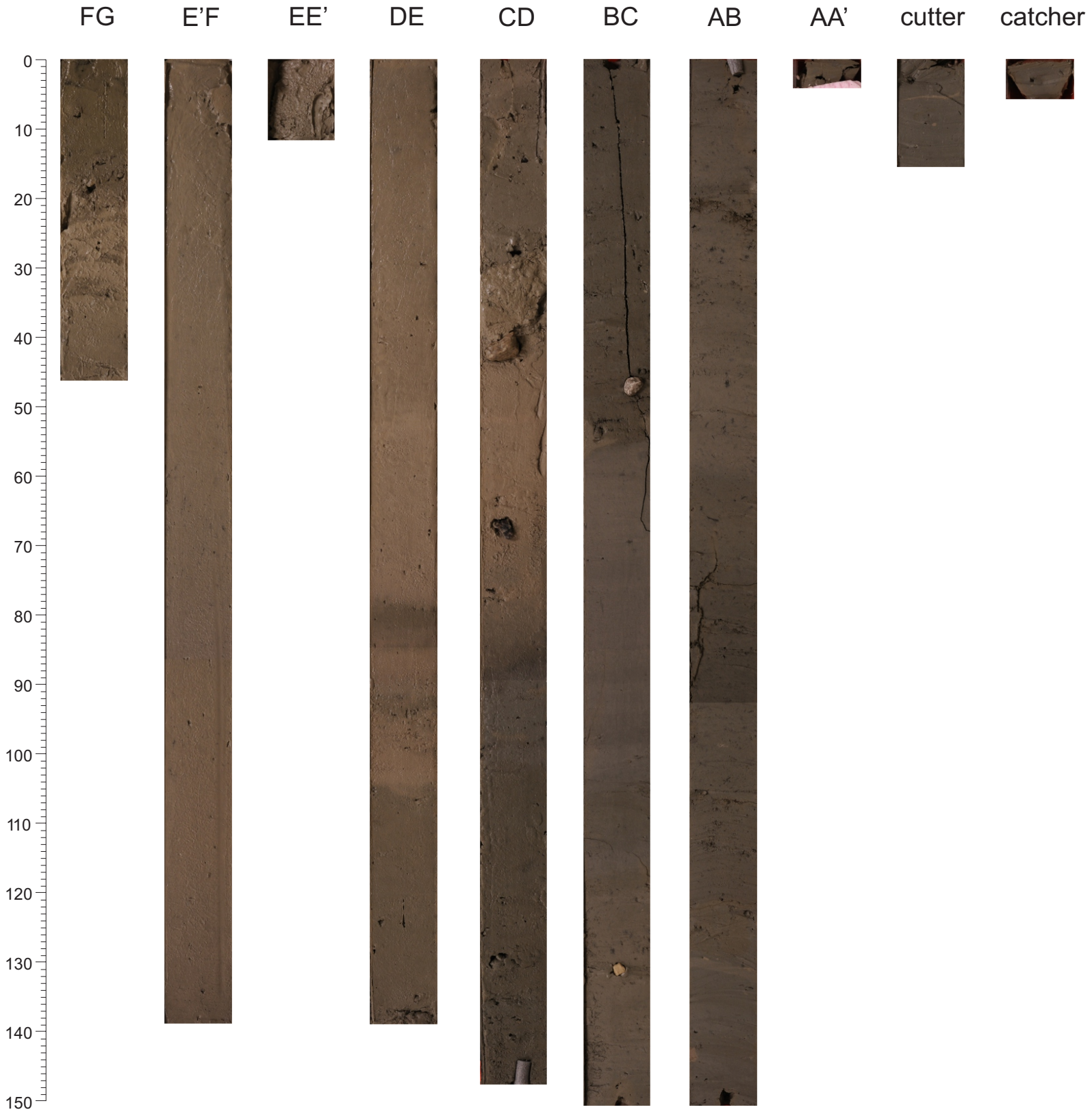
225/1810, 2284 mbsl, core length 11.19 m



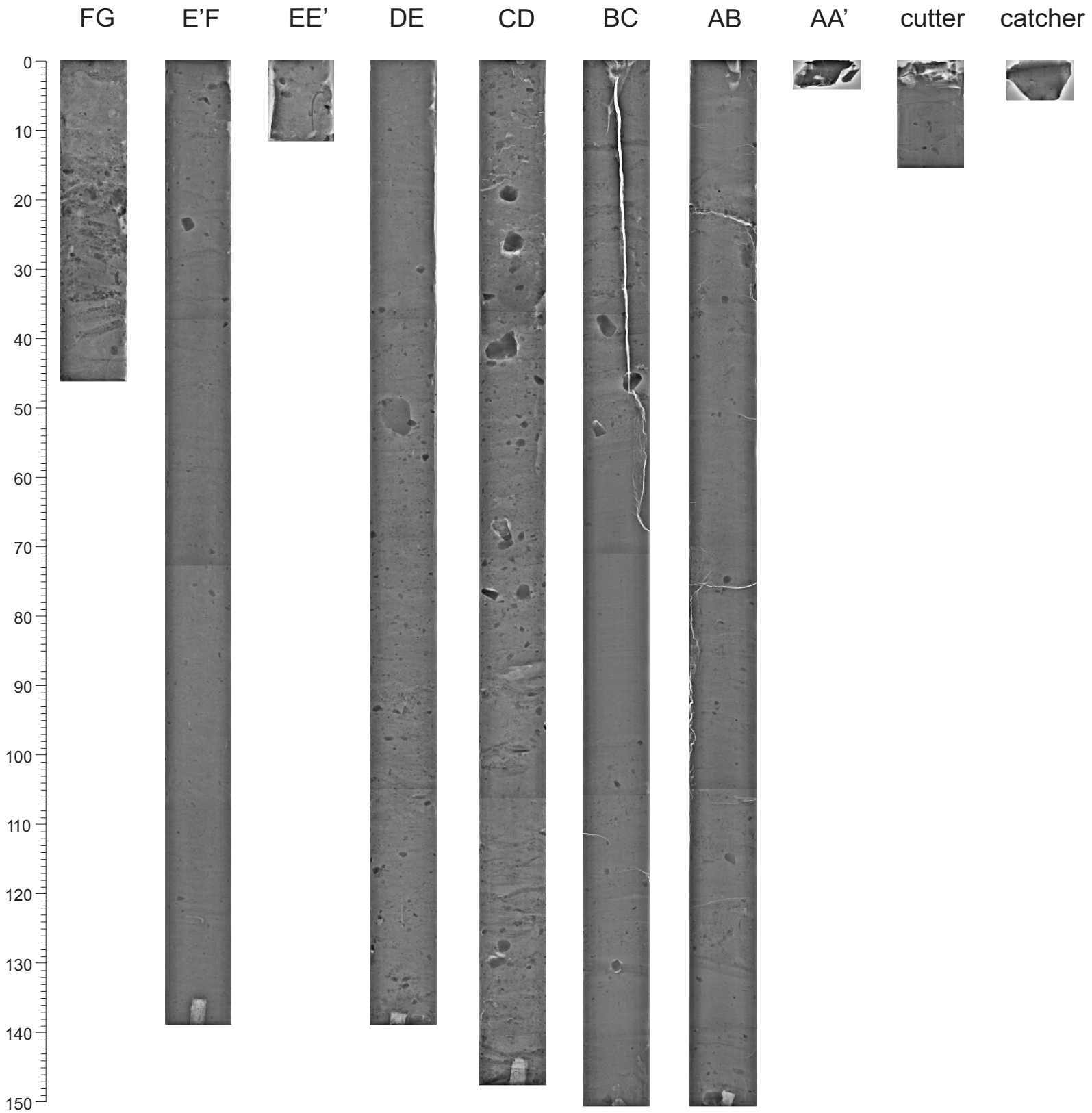
225/1805

Huntec
225/1825

2008027 0003 PistonCore

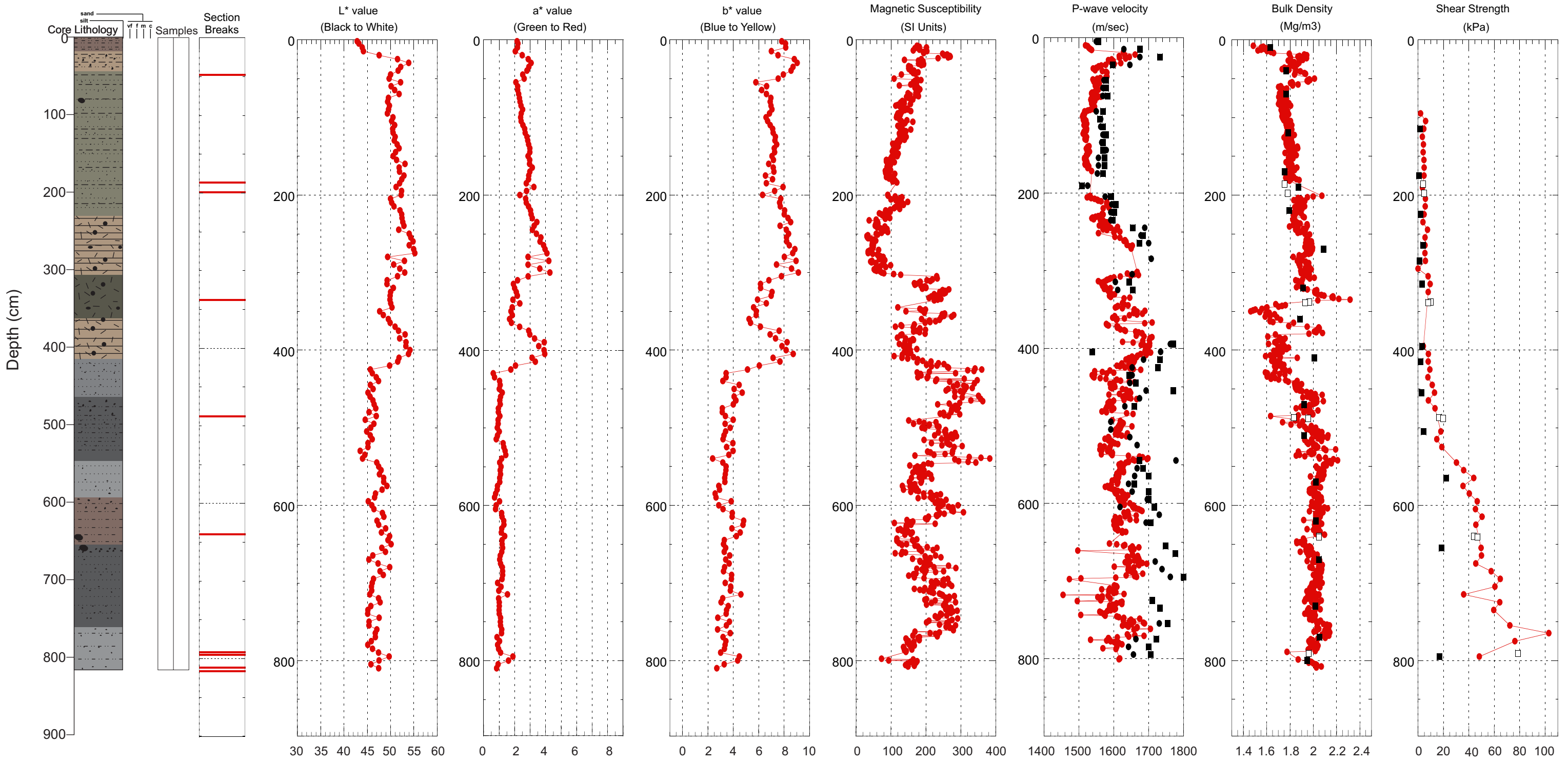


2008027 0003 PistonCore



Hudson 2008027 Piston Core 0003

TD 817cm 55.684492° N -56.854861° W Water depth 962 m



- MST Velocity
- Discrete Longitudinal Velocity
- Discrete Transverse Velocity
- MST Bulk Density
- Discrete Bulk Density - split core
- Discrete Bulk Density - whole core
- Peak Shear Strength
- Remoulded Shear Strength
- Peak Shear Strength - whole core Torvane
- Peak Shear Strength - whole core Penetromete

2008027 0003 Trigger Weight Core

BC

AB

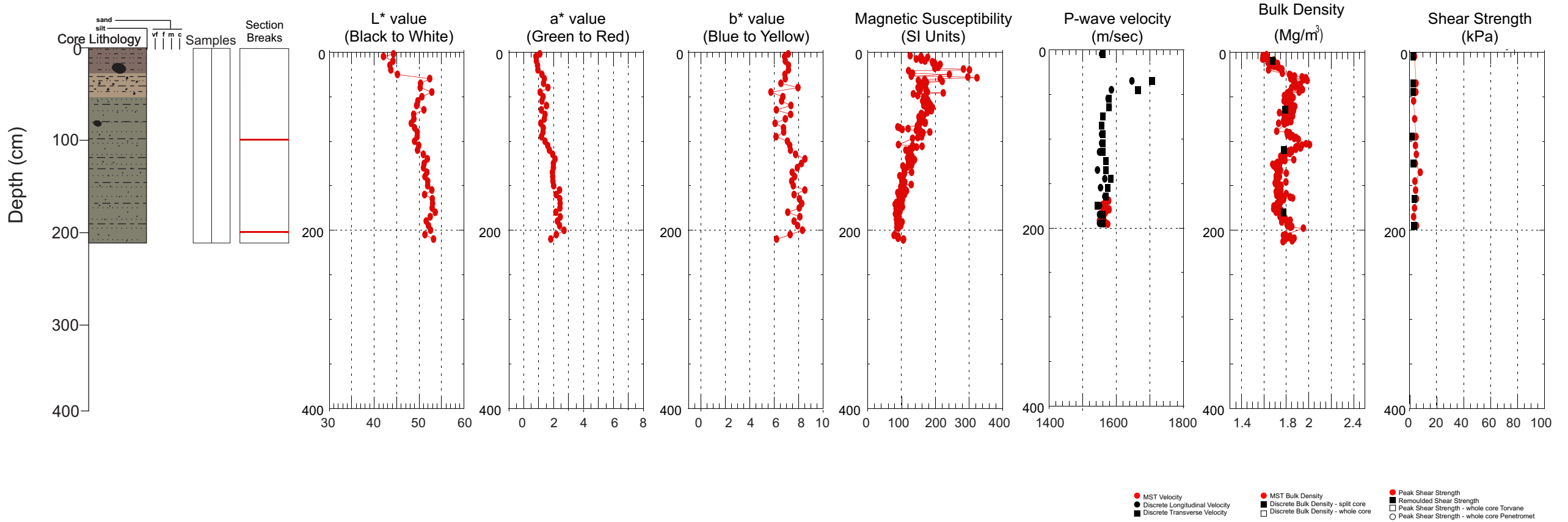
Cutter

0
10
20
30
40
50
60
70
80
90
100
110
120
130
140
150

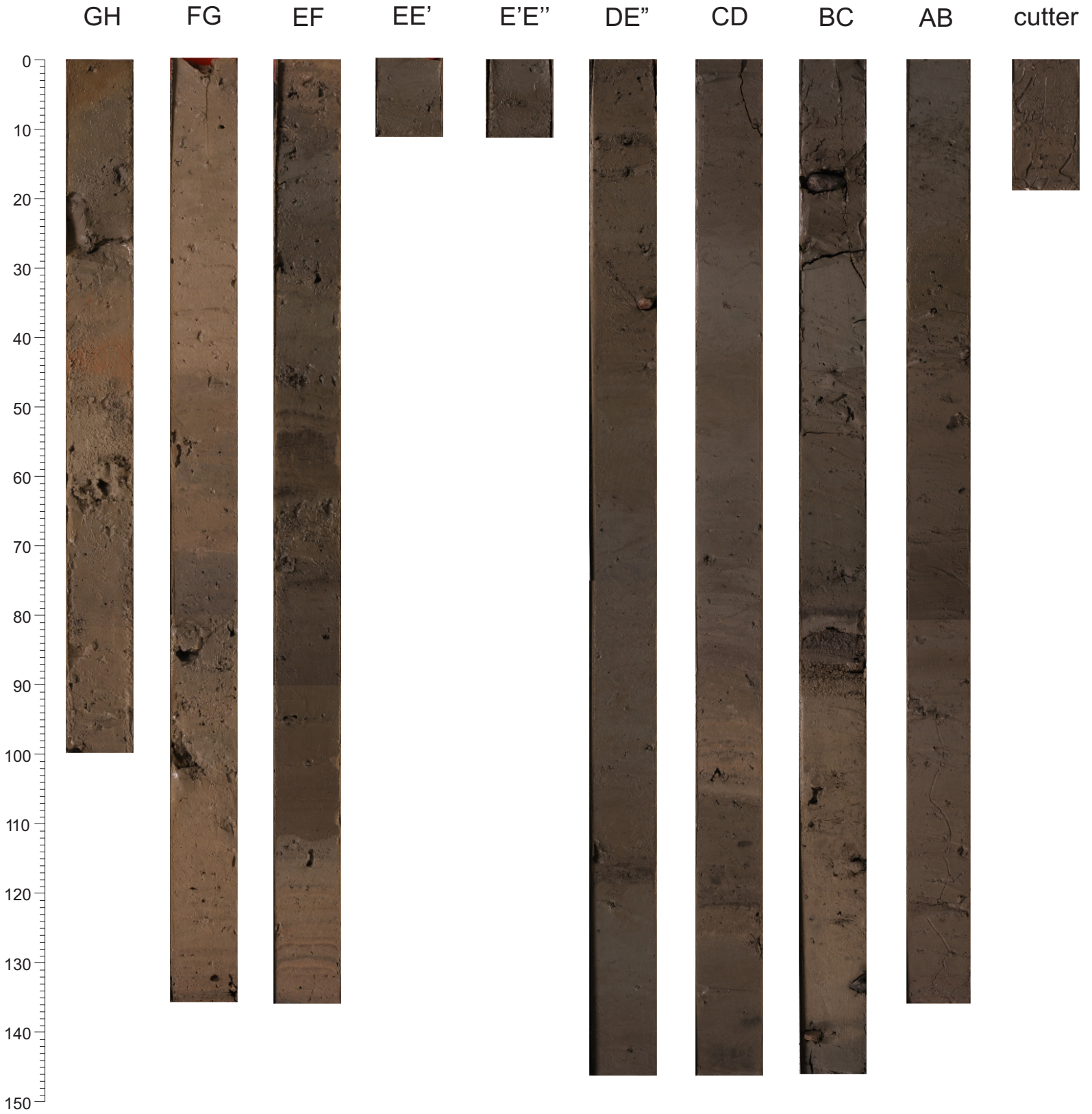


Hudson 2008027 Trigger Weight Core 0003

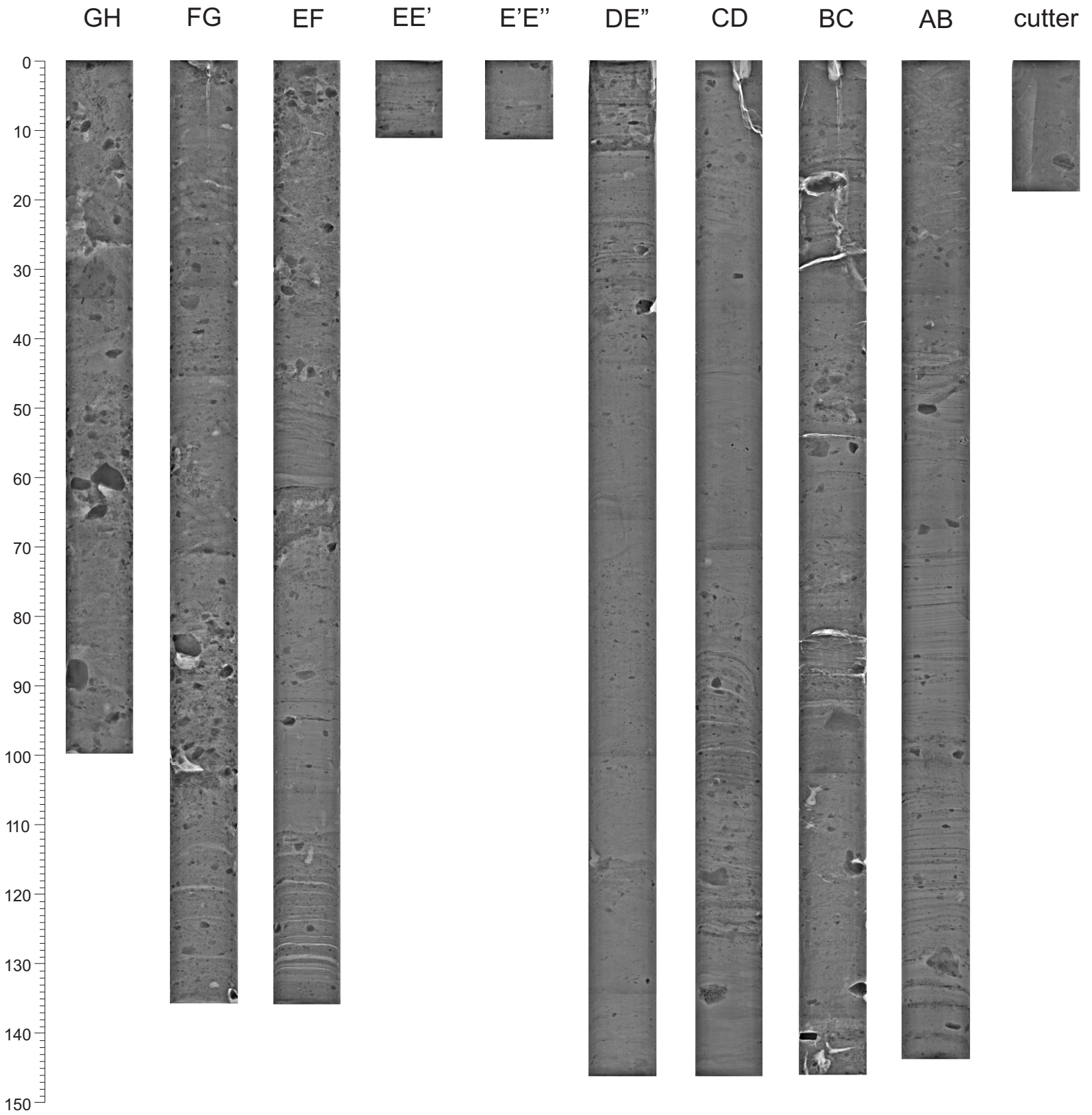
TD 215cm 55.684492° N -56.854861° W Water depth 962 m



2008027 0004 PistonCore

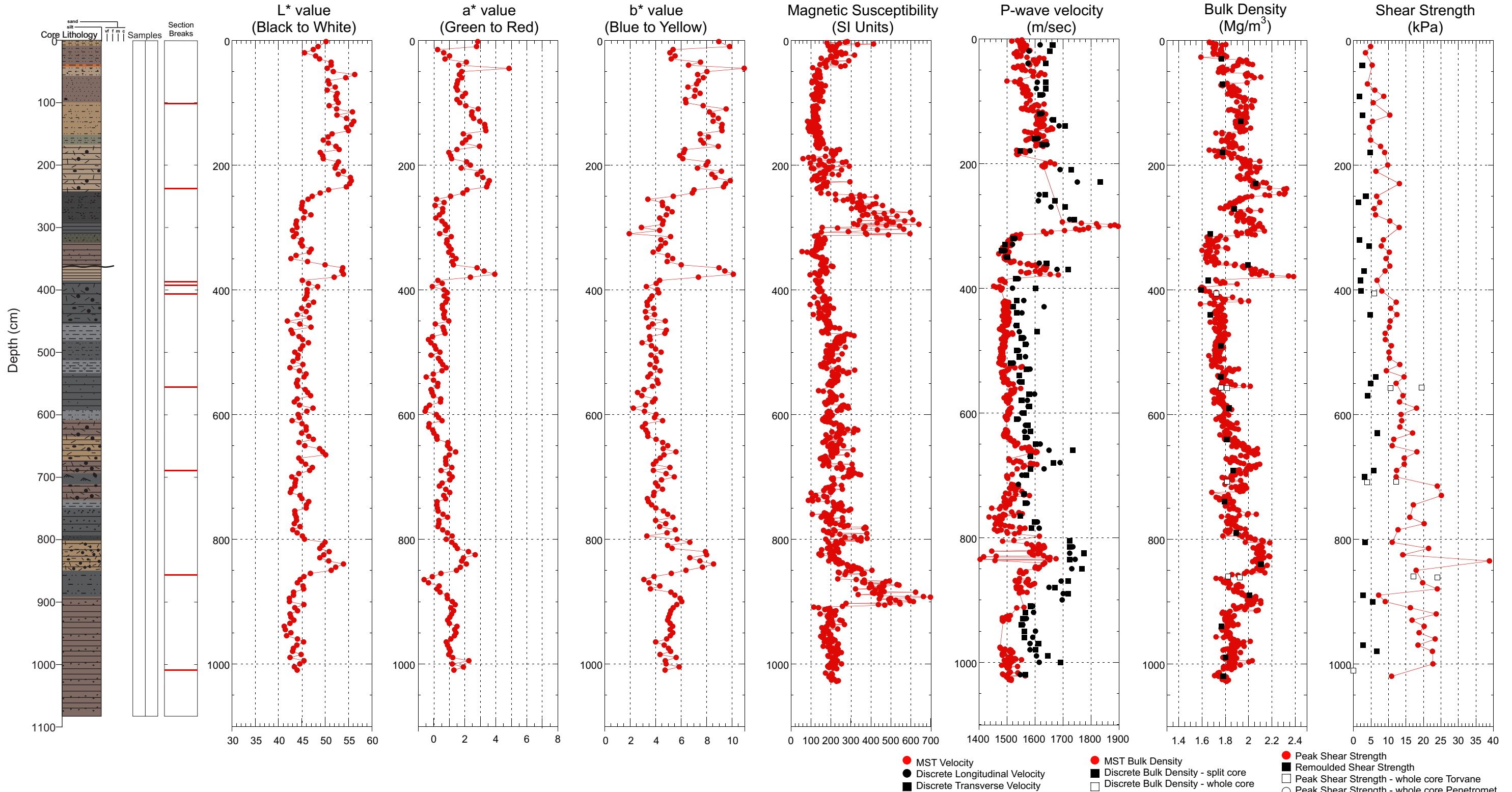


2008027 0004 PistonCore



Hudson 2008027 Piston Core 0004

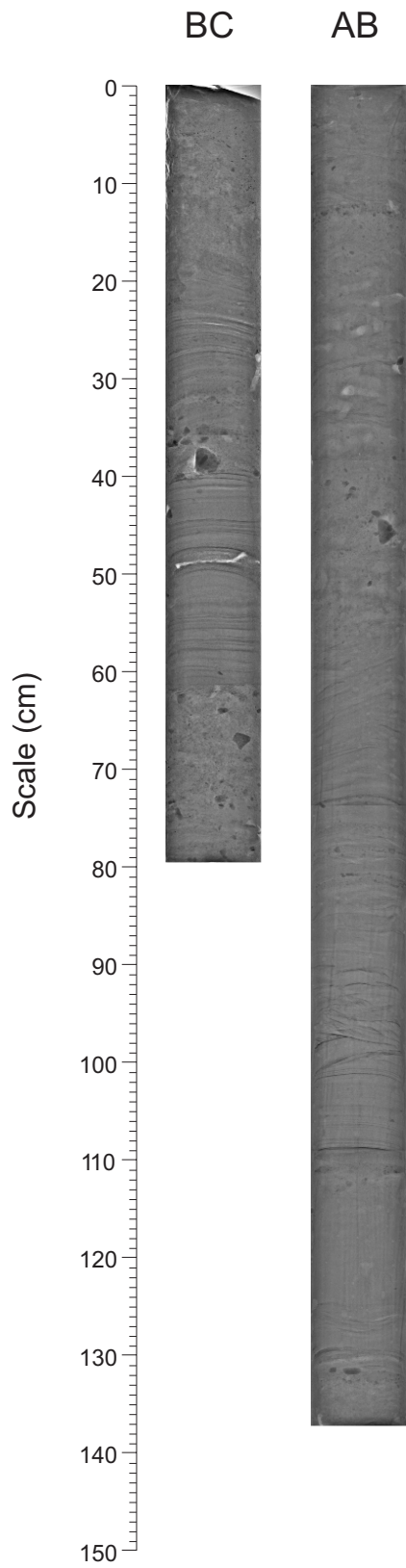
TD 1080cm 55.863813° N -56.766839° W Water depth 1981 m



2008027 0008 PistonCore

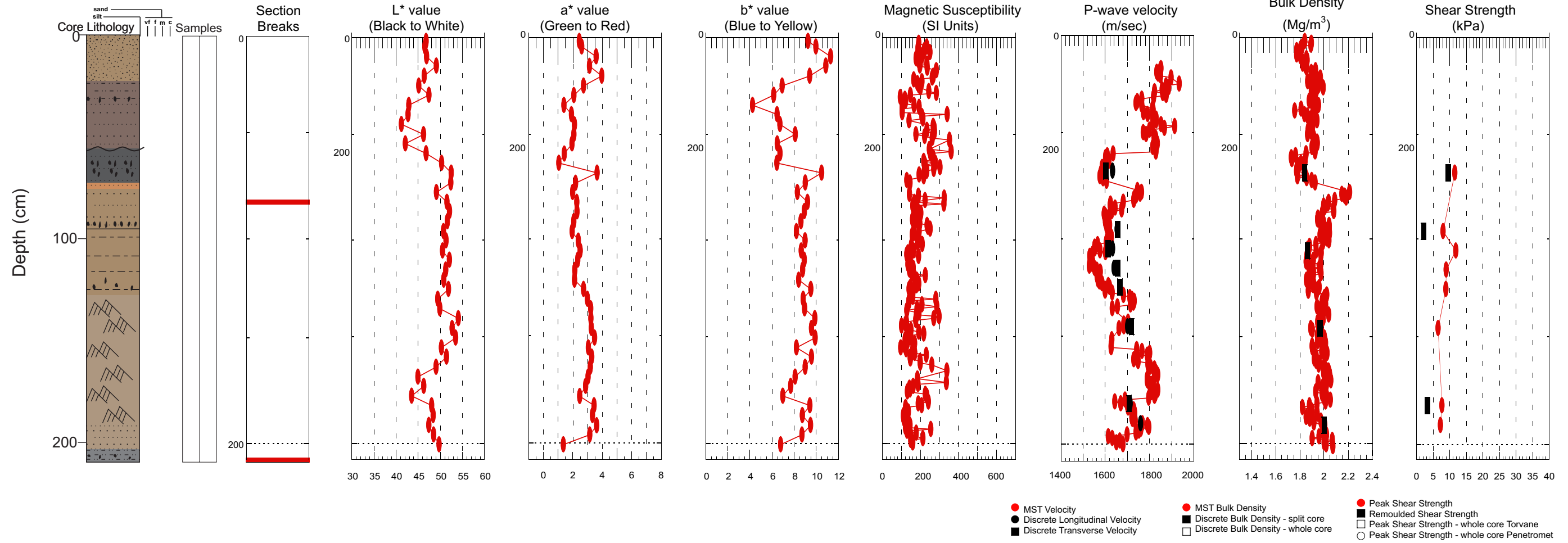


2008027 0008 PistonCore



Hudson 2008027 Piston Core 0008

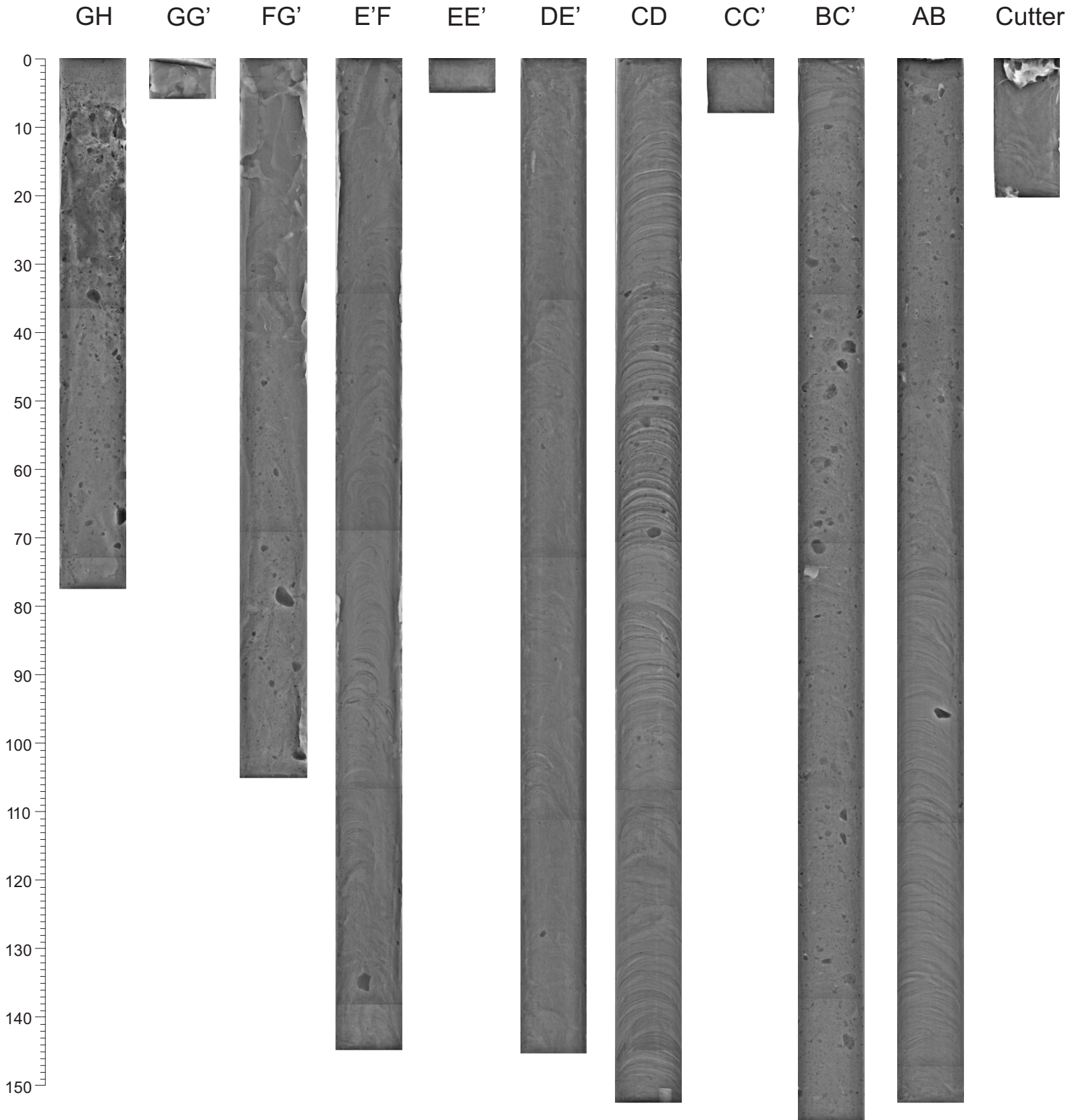
TD 213cm 55.856830° N -57.577238° W Water depth 2256 m



2008027 0009 PistonCore

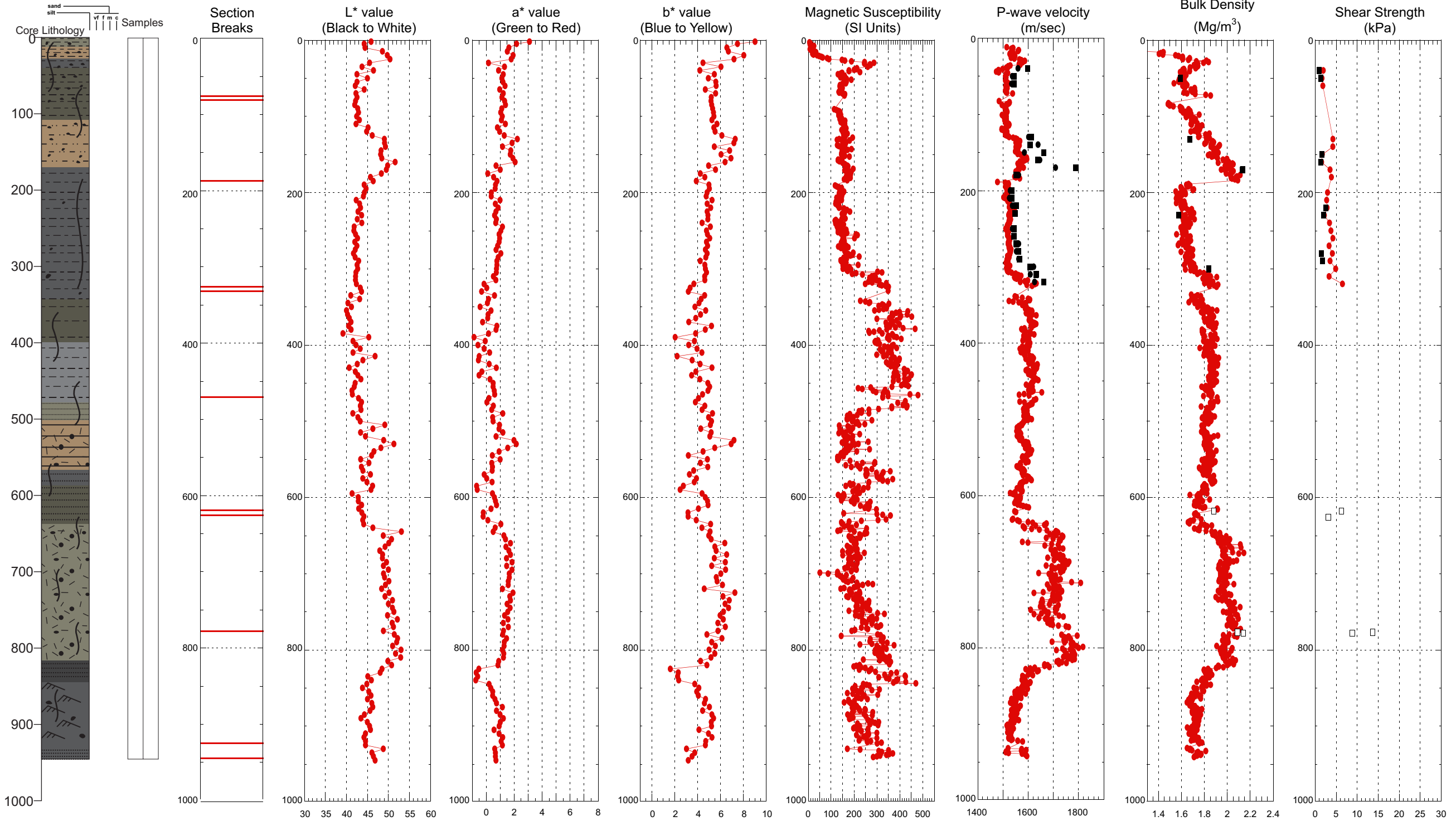


2008027 0009 PistonCore



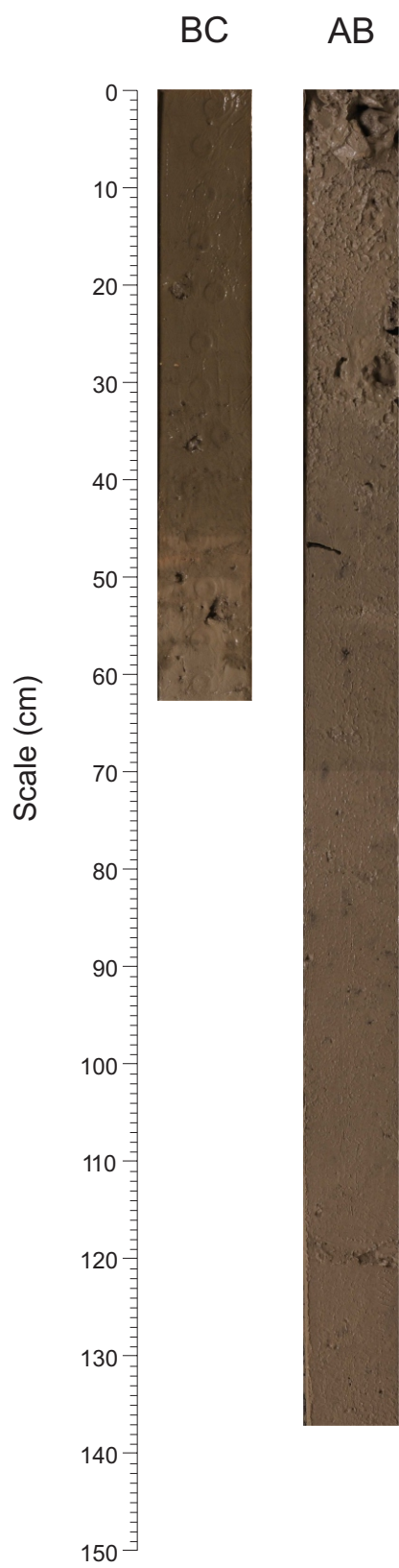
Hudson 2008027 Piston Core 0009

TD 945cm 56.844670° N -57.522352° W Water depth 2015 m

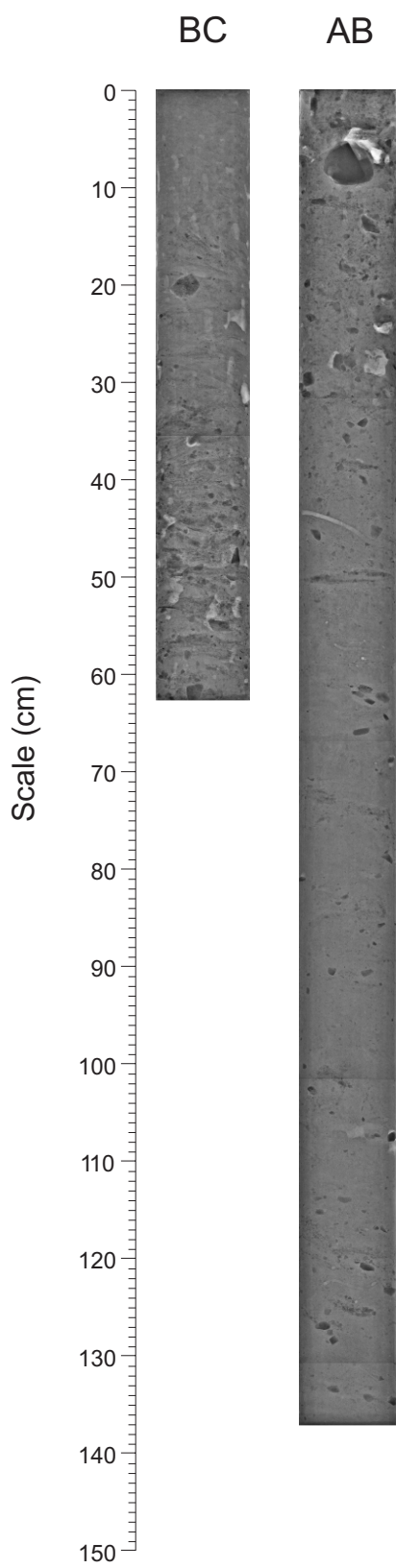


- MST Velocity
- Discrete Longitudinal Velocity
- Discrete Transverse Velocity
- MST Bulk Density
- Discrete Bulk Density - split core
- Discrete Bulk Density - whole core
- Peak Shear Strength
- Remoulded Shear Strength
- Peak Shear Strength - whole core Torvane
- Peak Shear Strength - whole core Penetromet

2008027 0011 PistonCore

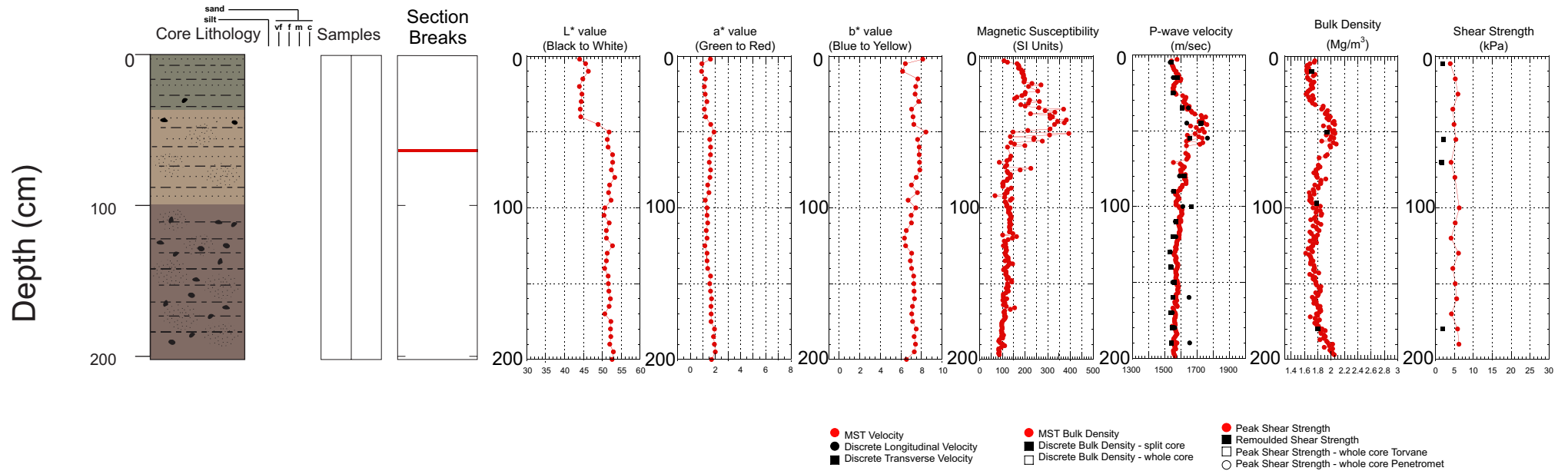


2008027 0011 PistonCore

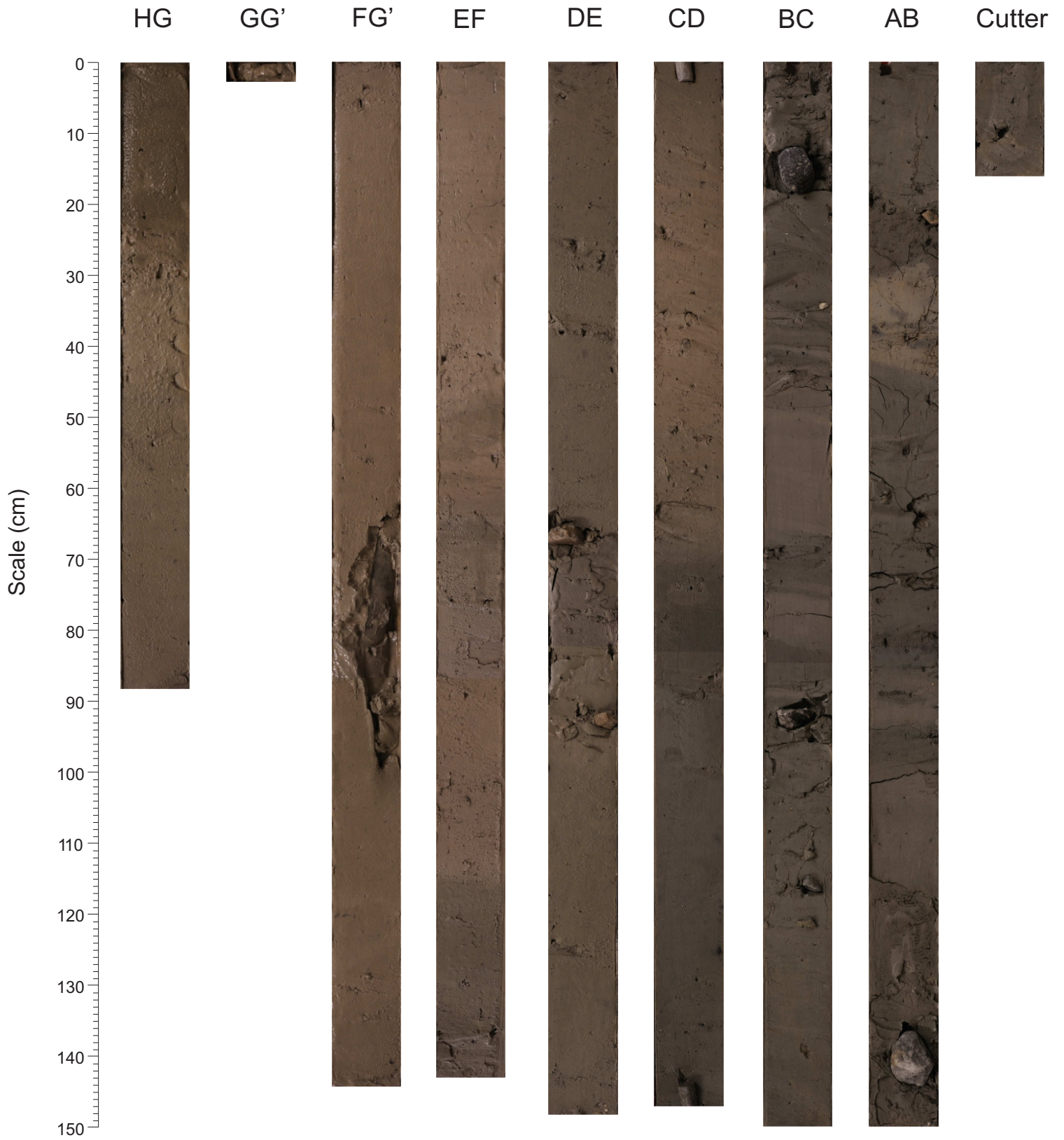


Hudson 2008027 Piston Core 0011

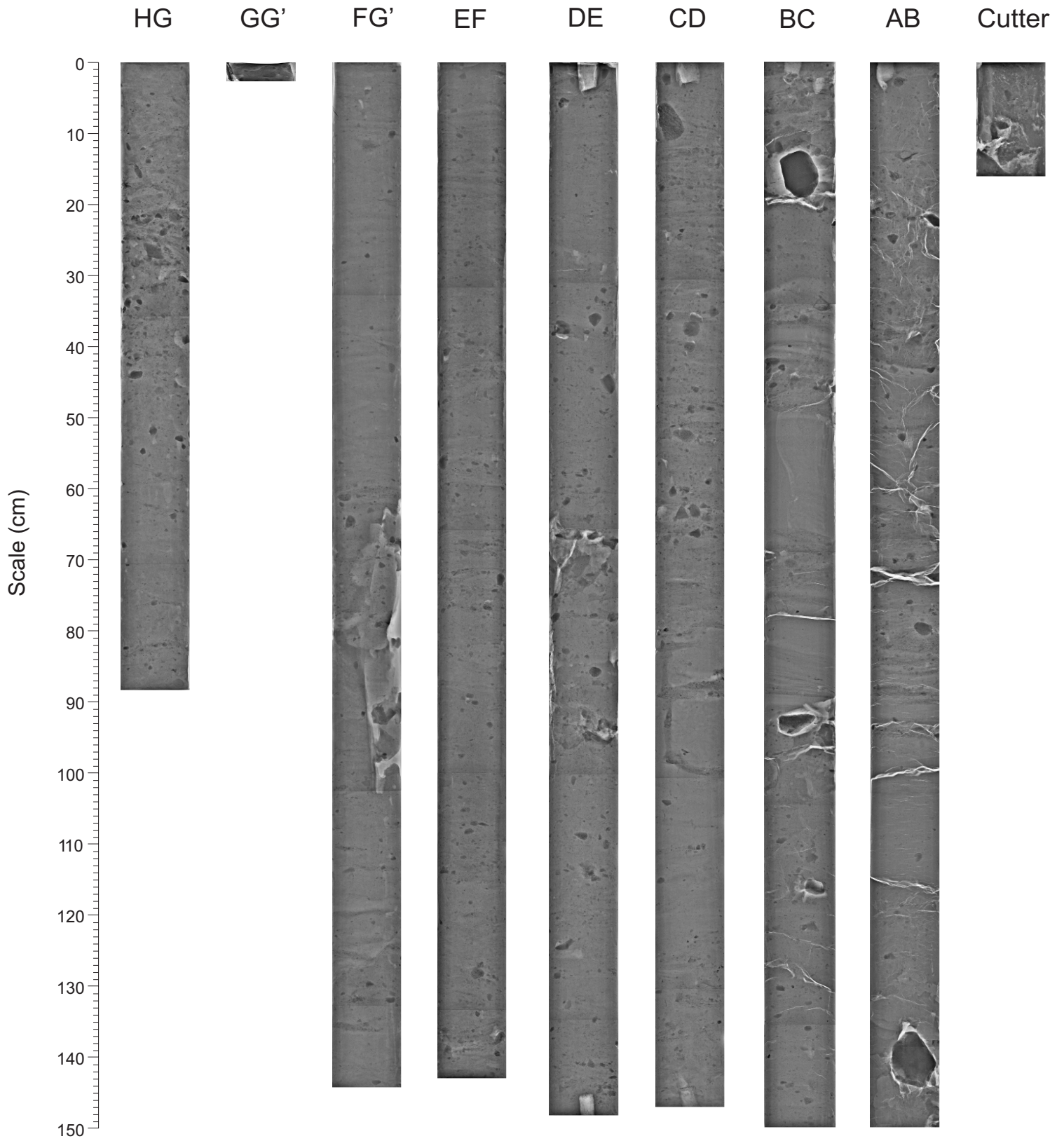
TD 202cm 56.984969° N -58.784199° W Water depth 723 m



2008027 0013 PistonCore

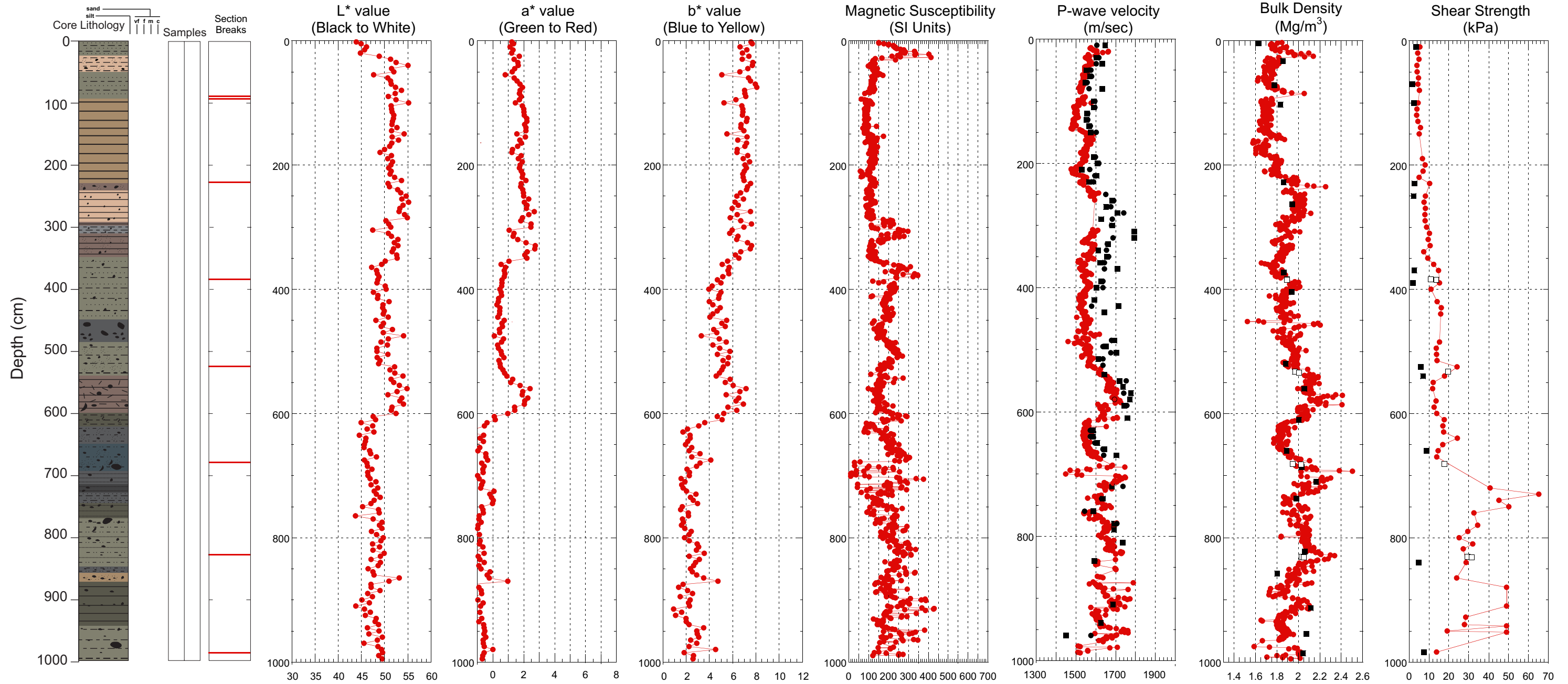


2008027 0013 PistonCore



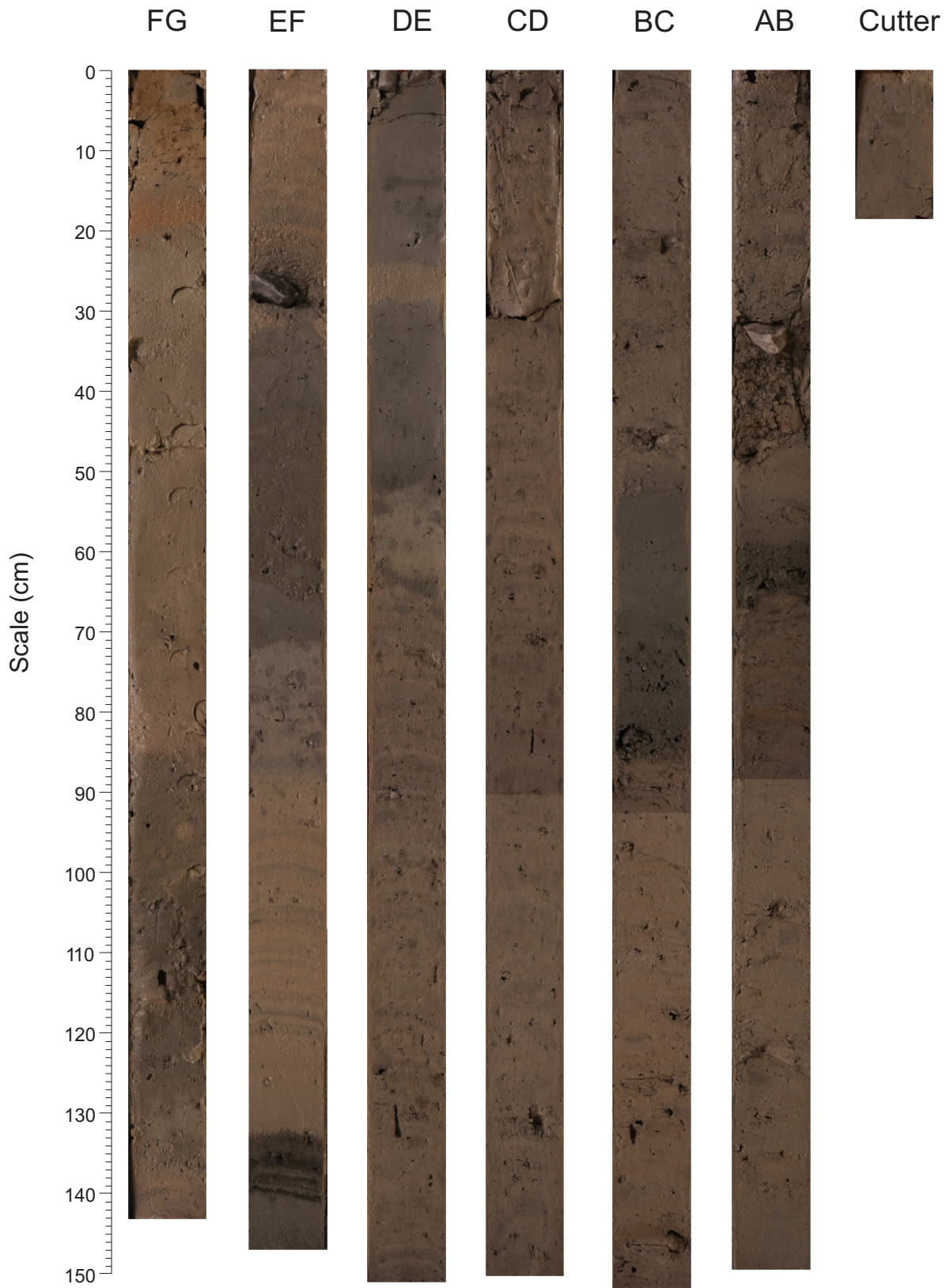
Hudson 2008027 Piston Core 0013

TD 998cm 56.985288° N -58.784021° W Water depth 715 m

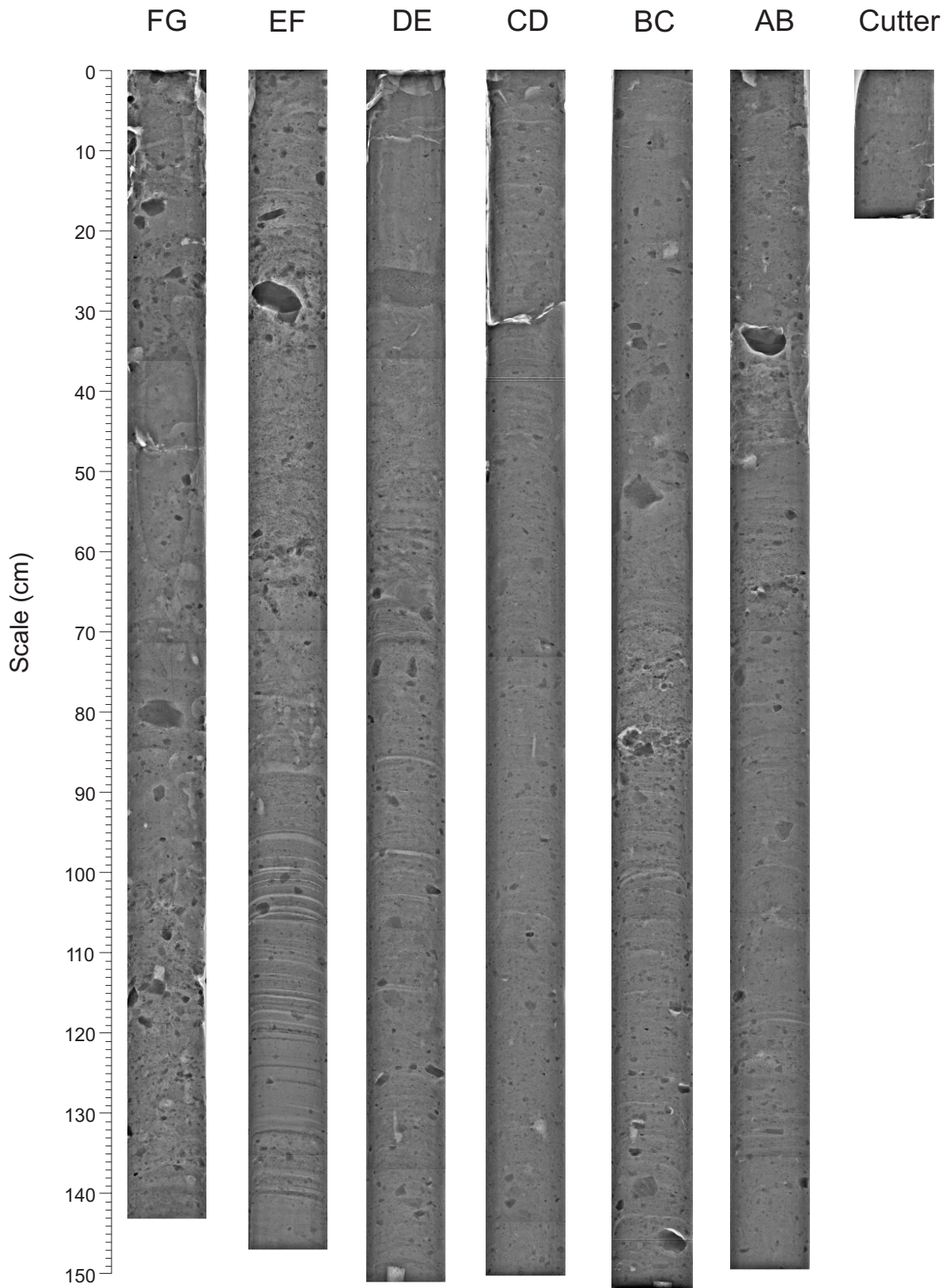


- MST Velocity
- Discrete Longitudinal Velocity
- Discrete Transverse Velocity
- MST Bulk Density
- Discrete Bulk Density - split core
- Discrete Bulk Density - whole core
- Peak Shear Strength
- Remoulded Shear Strength
- Peak Shear Strength - whole core Torvane
- Peak Shear Strength - whole core Penetromet

2008027 0014 PistonCore

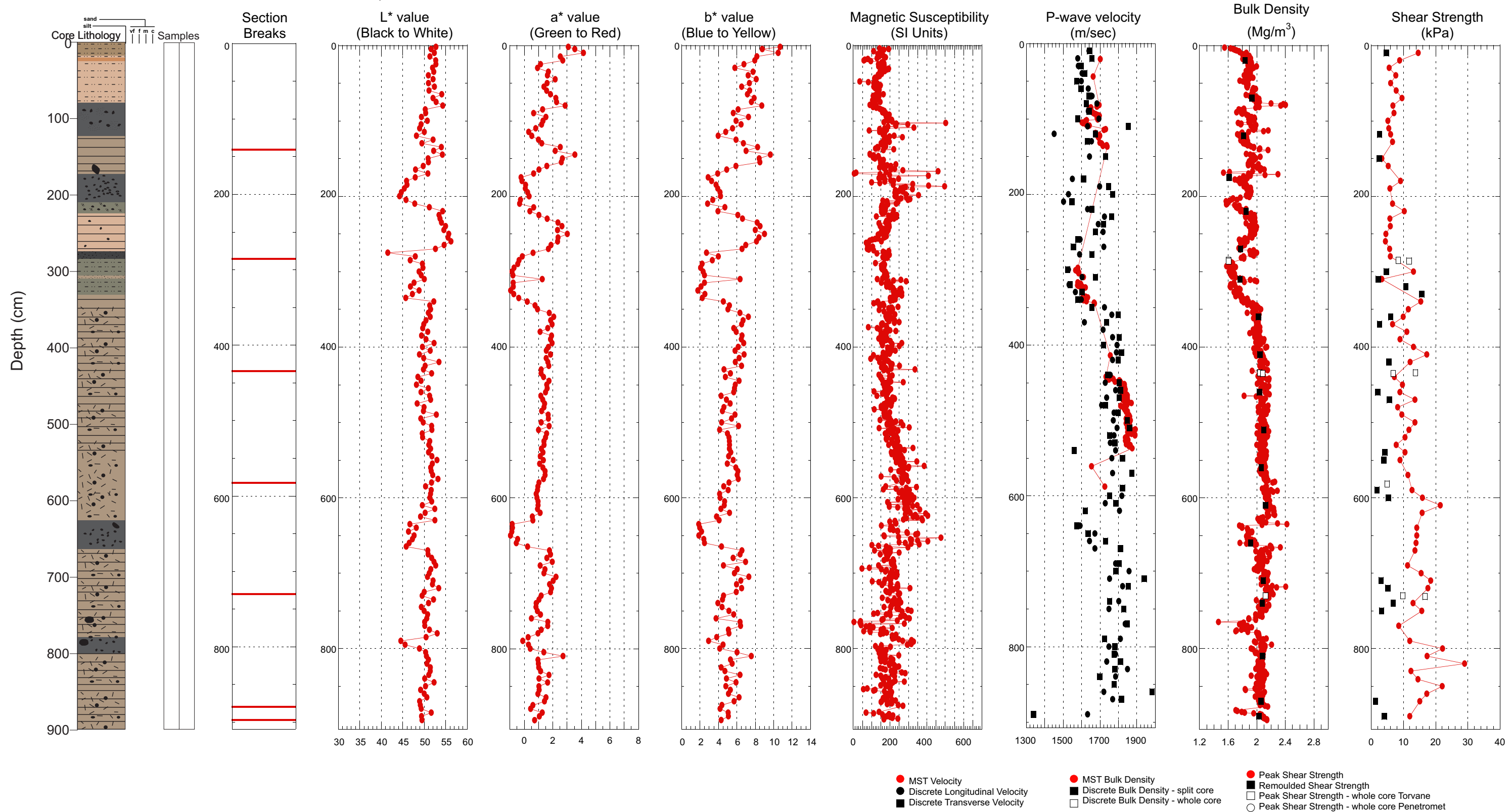


2008027 0014 PistonCore

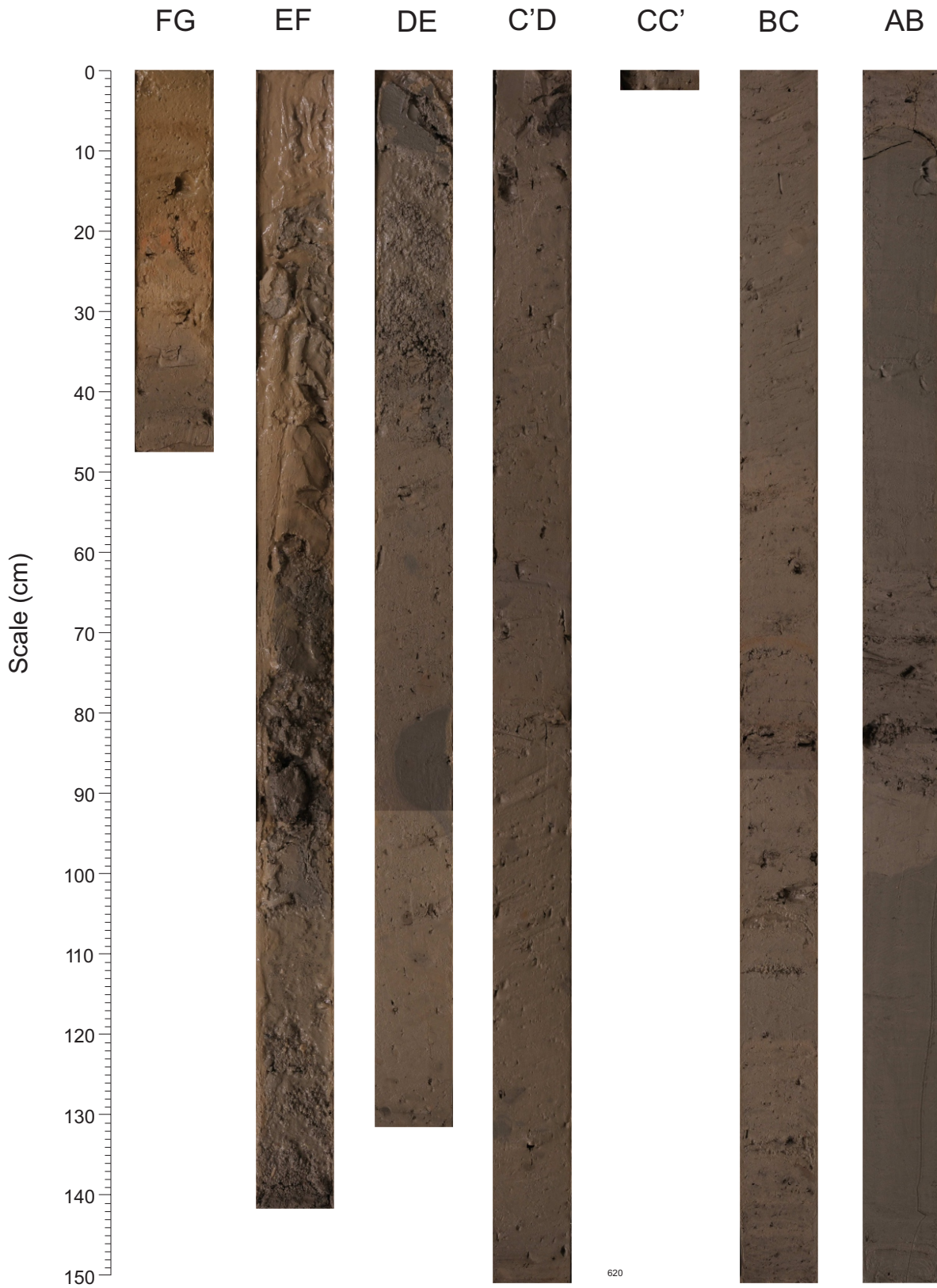


Hudson 2008027 Piston Core 0014

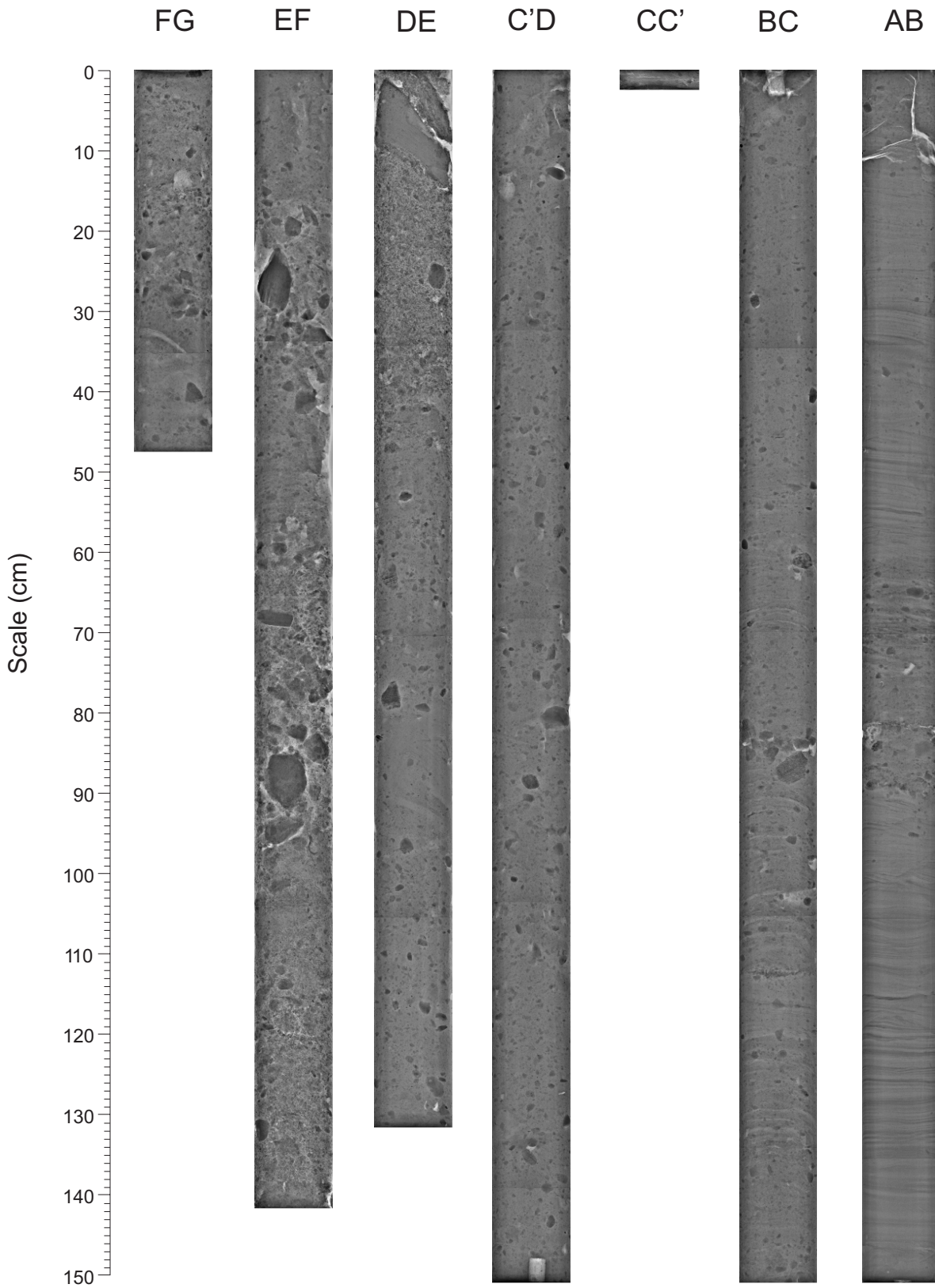
TD 898cm 57.693784° N -58.622293° W Water depth 2136 m



2008027 0015 PistonCore

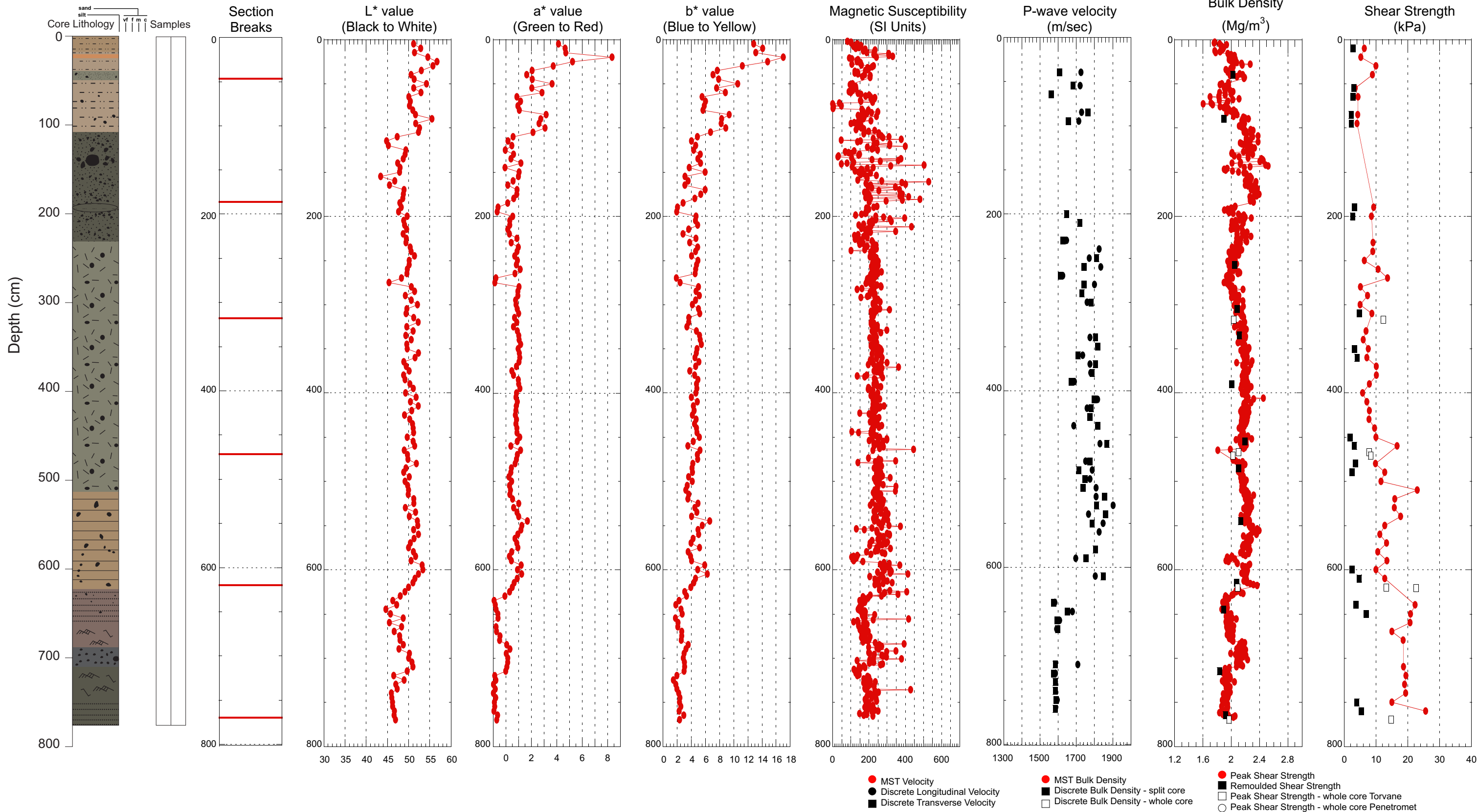


2008027 0015 PistonCore

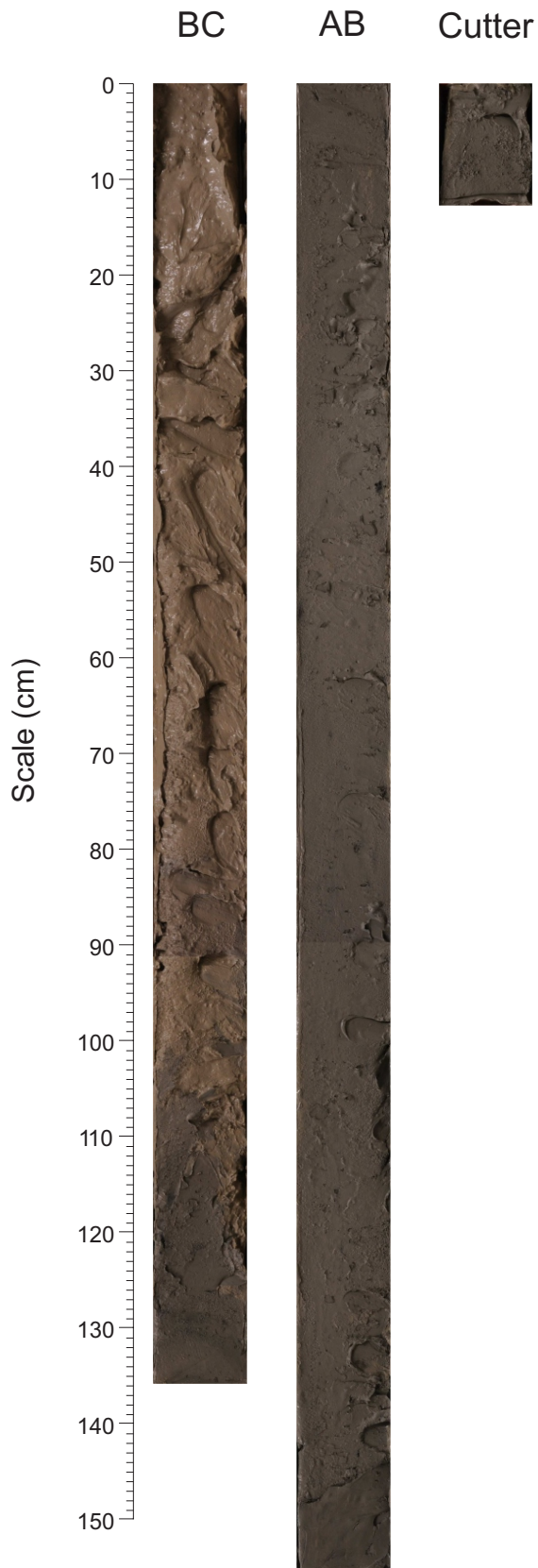


Hudson 2008027 Piston Core 0015

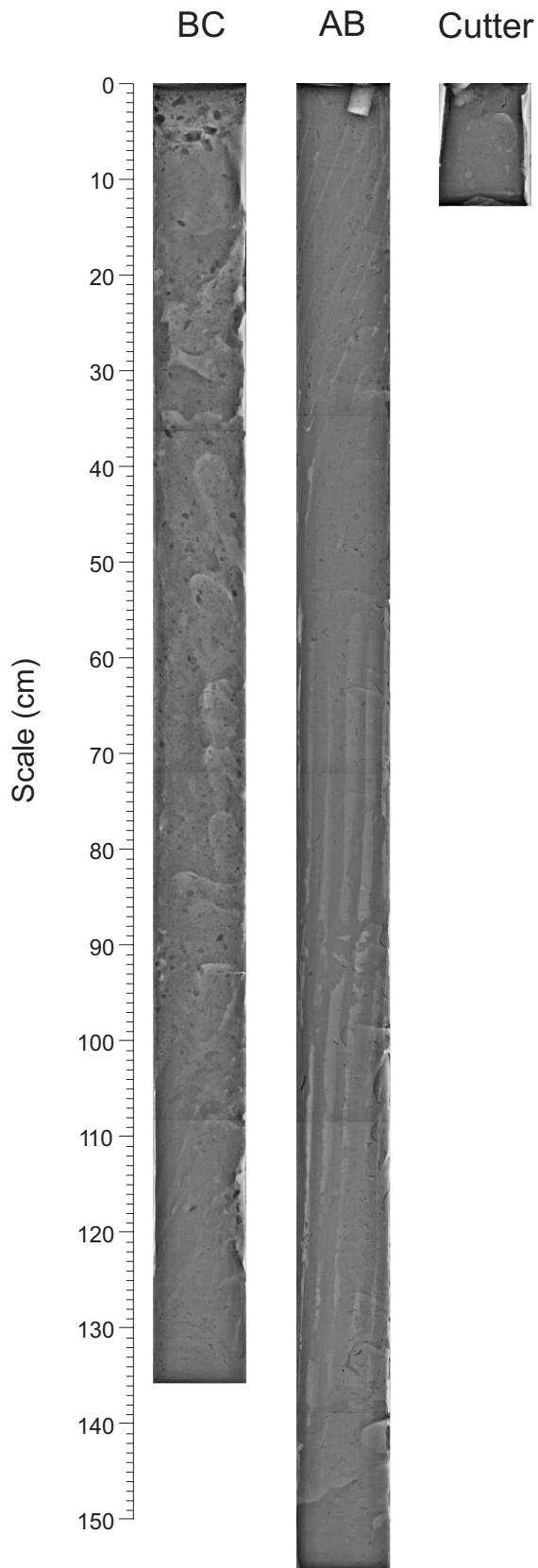
TD 770cm 57.3732212° N -58.655181° W Water depth 2114 m



2008027 0018 PistonCore

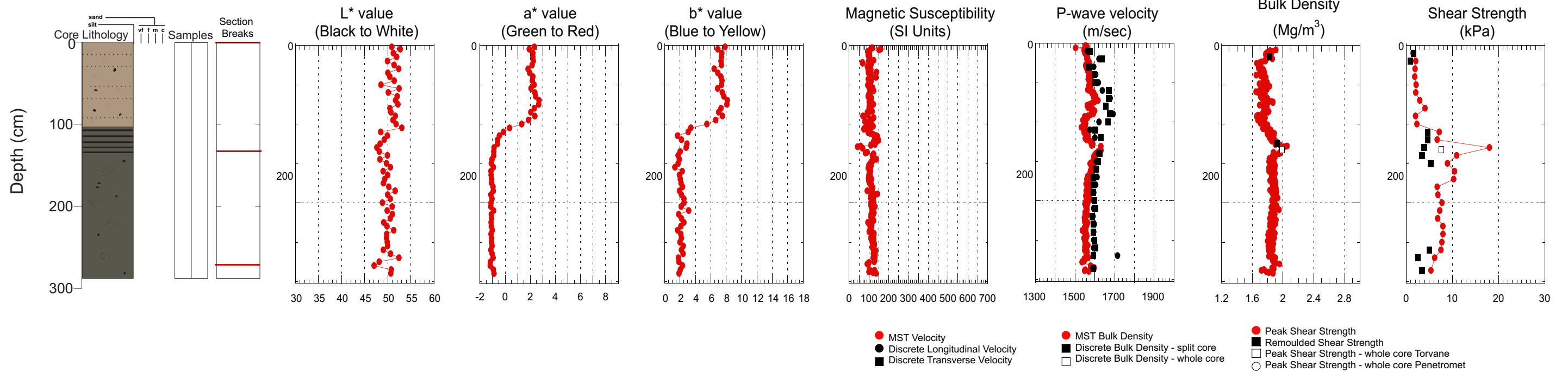


2008027 0018 PistonCore

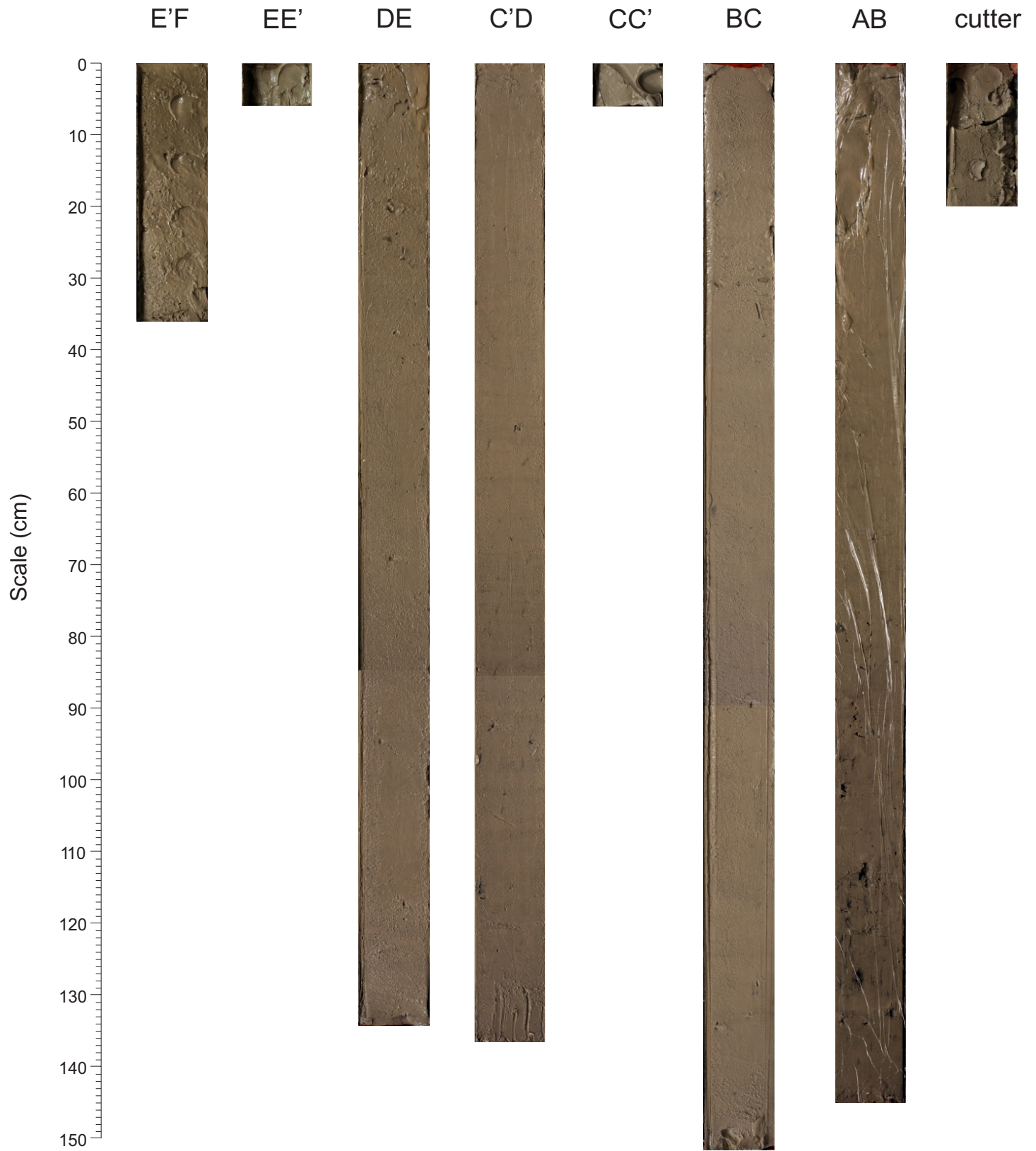


Hudson 2008027 Piston Core 0018

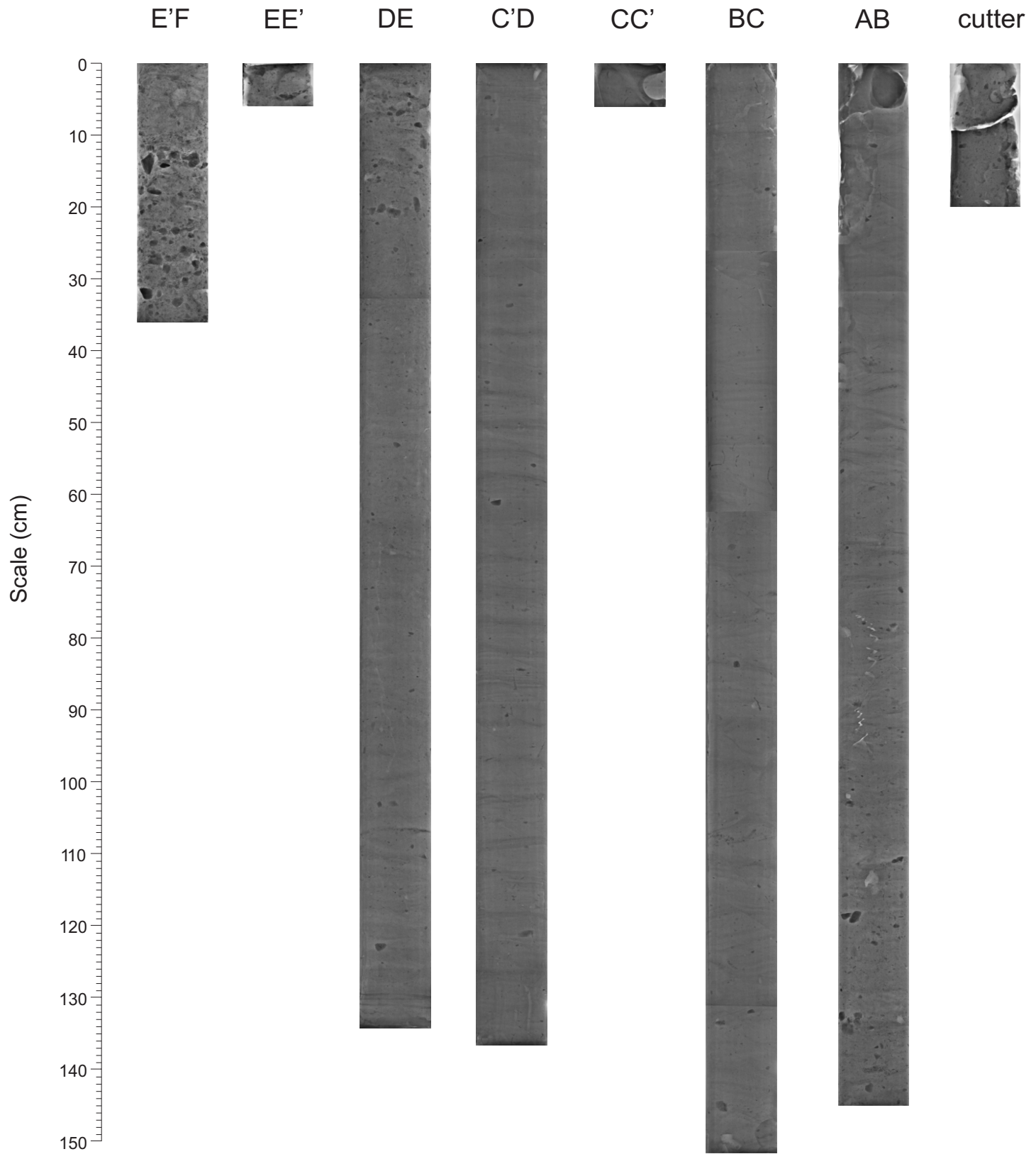
TD 293cm 58.22225° N -59.688785° W Water depth 940 m



2008027 0019 PistonCore

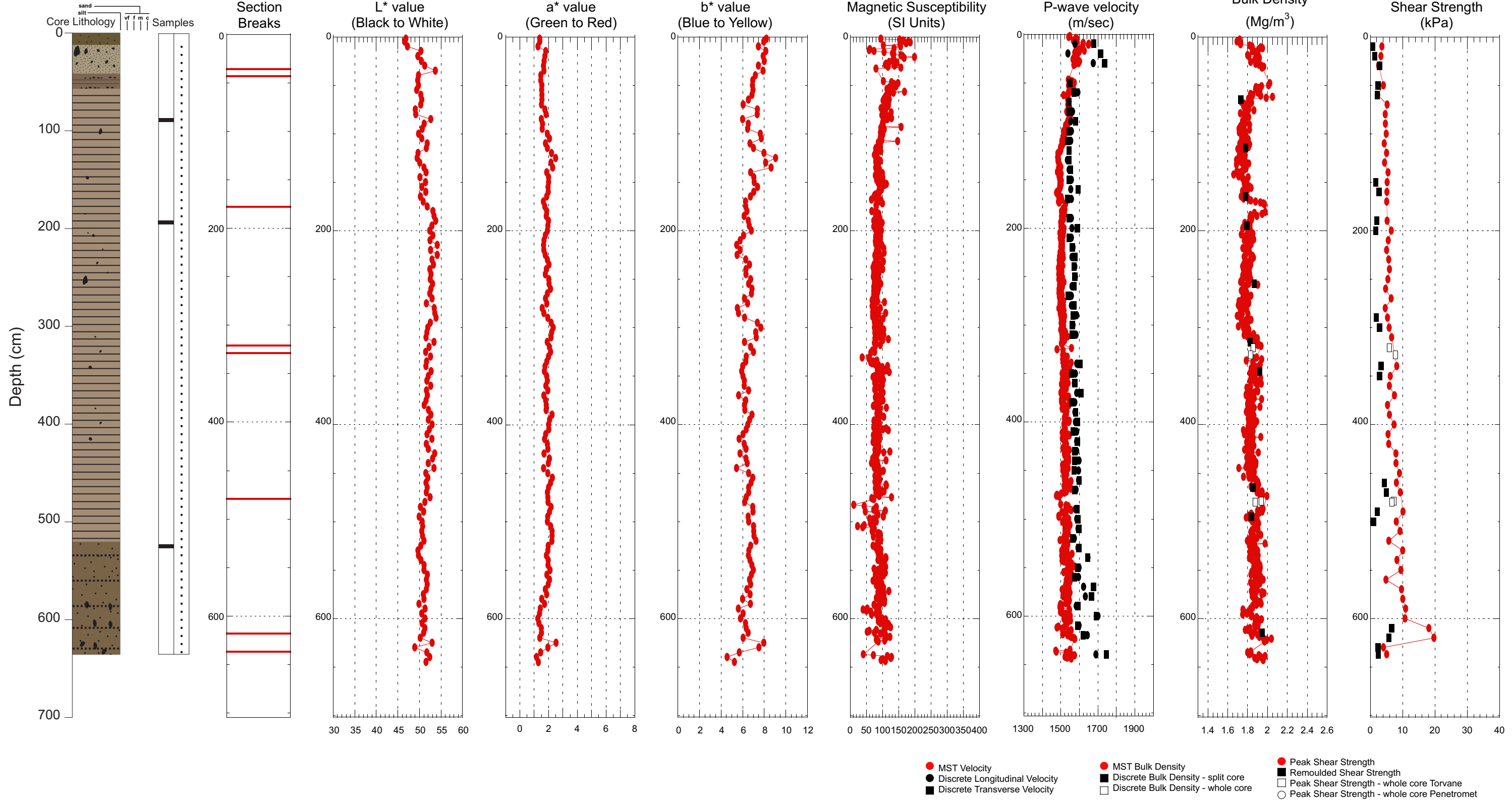


2008027 0019 PistonCore

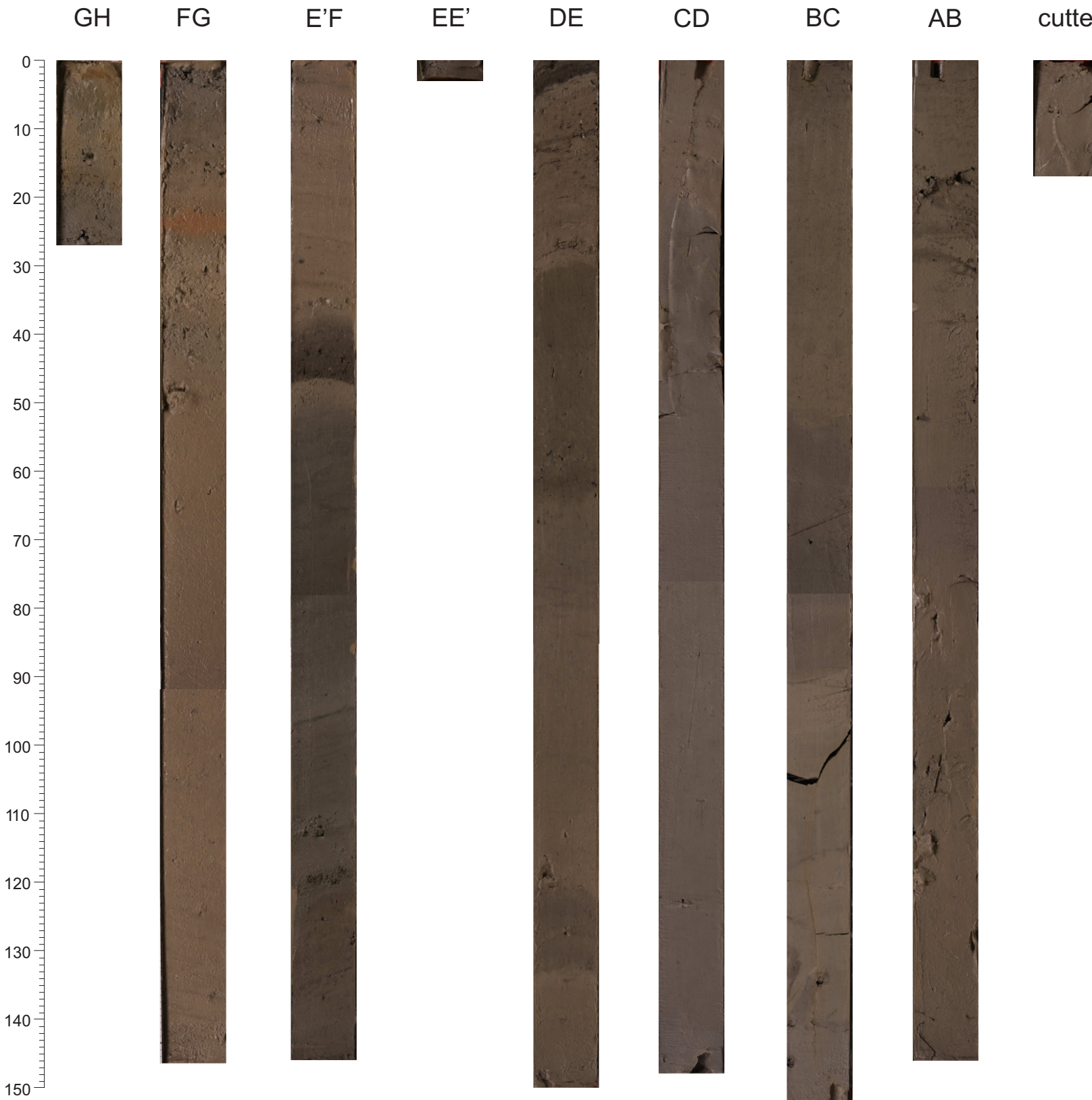


Hudson 2008027 Piston Core 0019

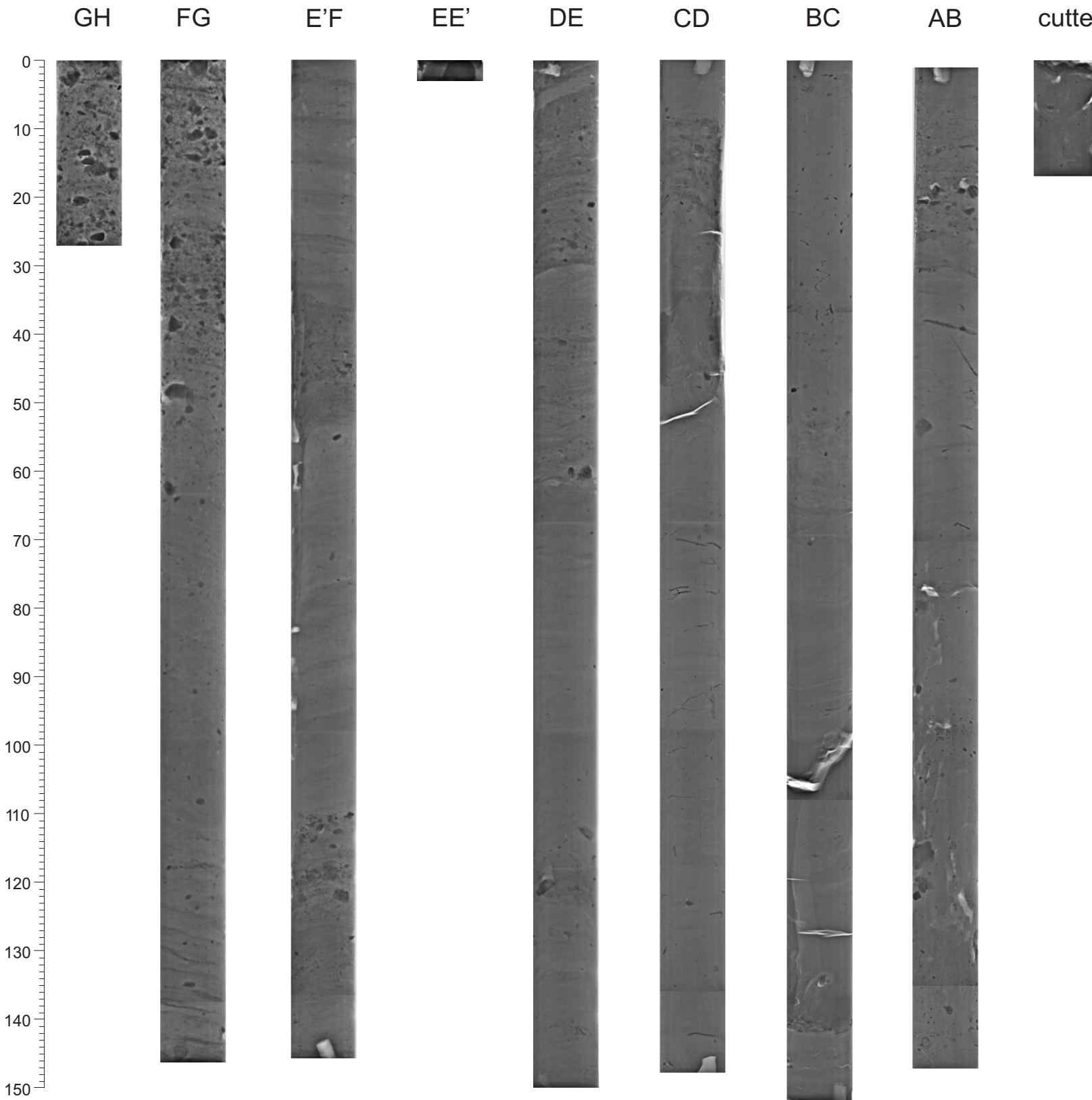
TD 647cm 59.509358° N -60.296444° W Water depth 806 m



2008027 0021 PistonCore



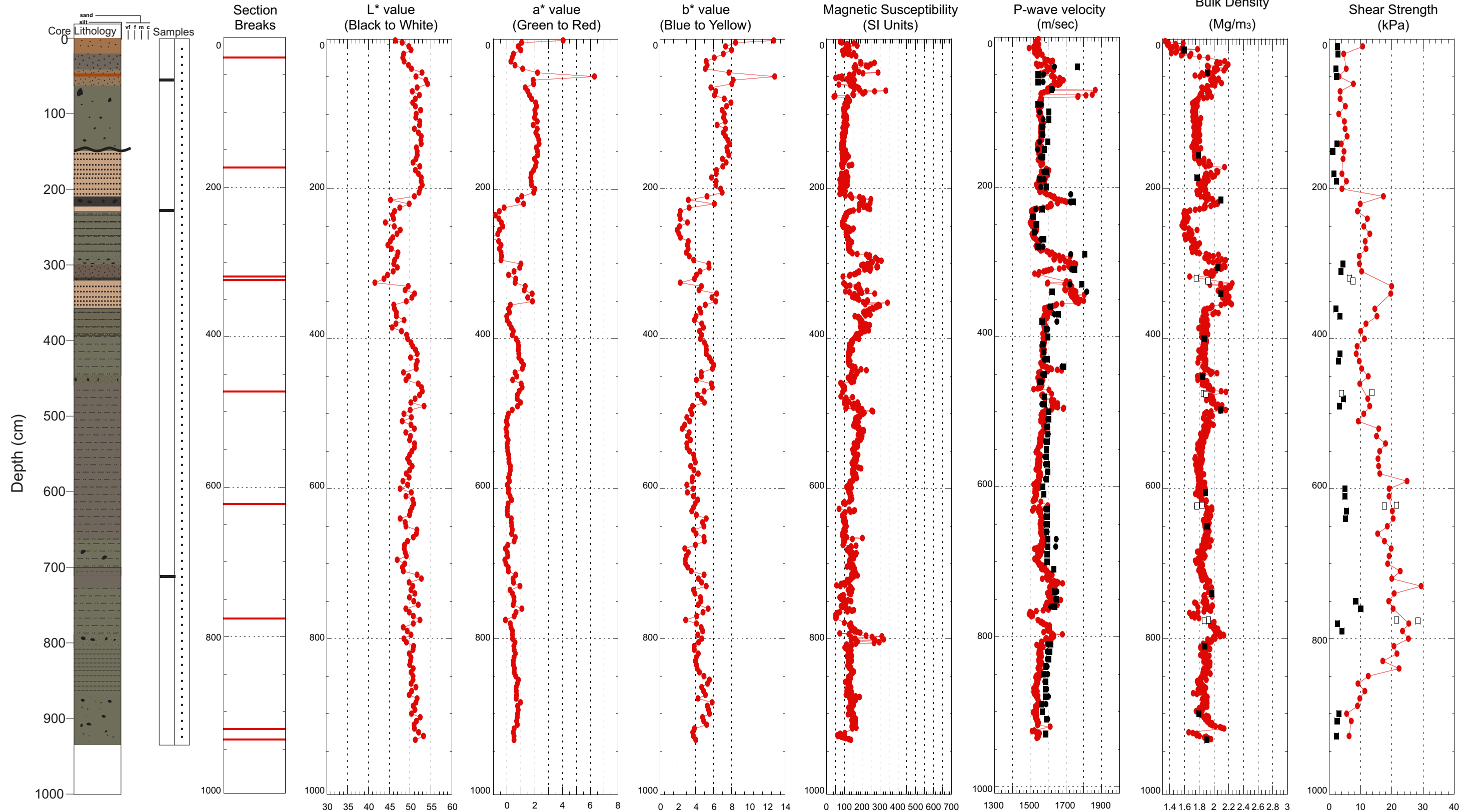
2008027 0021 PistonCore



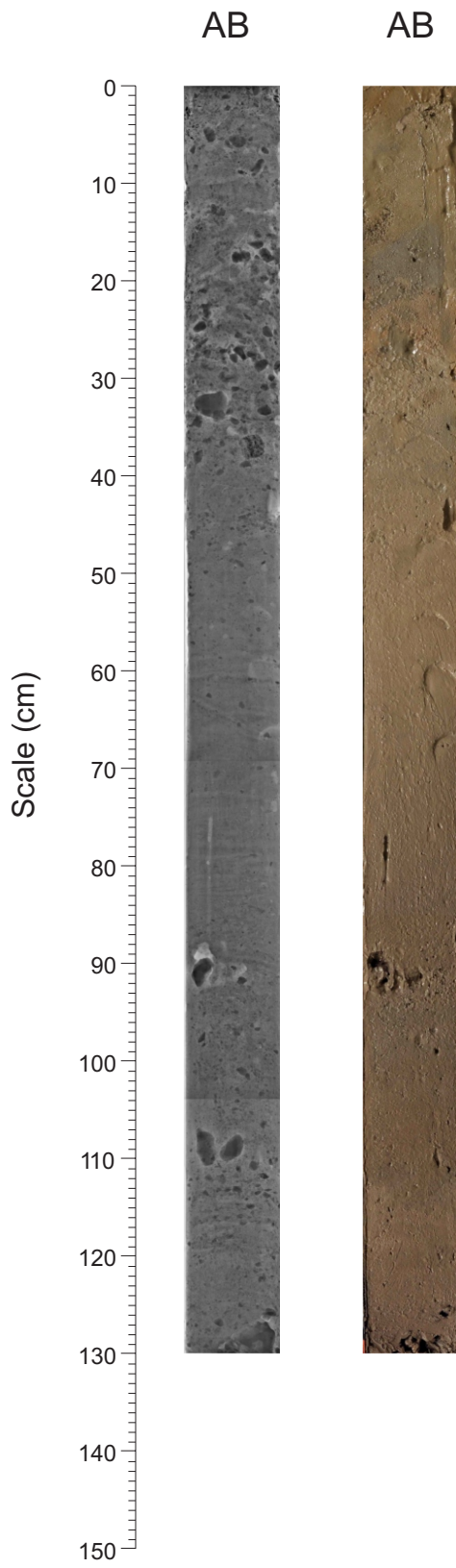
Hudson 2008027 Piston Core 0021

TD 938cm 59.557871° N -60123862° W Water depth 1223 m

- MST Velocity
- Discrete Longitudinal Velocity
- Discrete Transverse Velocity
- MST Bulk Density
- Discrete Bulk Density - split core
- Discrete Bulk Density - whole core
- Peak Shear Strength
- Remoulded Shear Strength
- Peak Shear Strength - whole core Torvane
- Peak Shear Strength - whole core Penetromet



2008027 0022 PistonCore



Hudson 2008027 Piston Core 0022

TD 130cm 59.44522° N -59.6557009° W Water depth 1627 m

